

PACIFIC EARTHQUAKE ENGINEERING RESEARCH CENTER

Low Seismic Damage Columns for Accelerated Bridge Construction

**Arpit Nema
José I. Restrepo**

**Department of Structural Engineering
University of California, San Diego**

PEER Report No. 2020/10

Pacific Earthquake Engineering Research Center
Headquarters at the University of California, Berkeley
December 2020

Disclaimer

The opinions, findings, and conclusions or recommendations expressed in this publication are those of the author(s) and do not necessarily reflect the views of the study sponsor(s), the Pacific Earthquake Engineering Research Center, or the Regents of the University of California.

Low Seismic Damage Columns for Accelerated Bridge Construction

Arpit Nema

José I. Restrepo

Department of Structural Engineering
University of California, San Diego

PEER Report 2020/10
Pacific Earthquake Engineering Research Center
Headquarters at the University of California, Berkeley

November 2020

ABSTRACT

This report describes the design, construction, and shaking table response and computation simulation of a Low Seismic-Damage Bridge Bent built using Accelerated Bridge Construction methods. The proposed bent combines precast post-tensioned columns with precast foundation and bent cap to simplify off- and on-site construction burdens and minimize earthquake-induced damage and associated repair costs. Each column consists of reinforced concrete cast inside a cylindrical steel shell, which acts as the formwork, and the confining and shear reinforcement. The column steel shell is engineered to facilitate the formation of a rocking interface for concentrating the deformation demands in the columns, thereby reducing earthquake-induced damage. The precast foundation and bent cap have corrugated-metal-duct lined sockets, where the columns will be placed and grouted on-site to form the column–beam joints. Large inelastic deformation demands in the structure are concentrated at the column–beam interfaces, which are designed to accommodate these demands with minimal structural damage. Longitudinal post-tensioned high-strength steel threaded bars, designed to respond elastically, ensure re-centering behavior. Internal mild steel reinforcing bars, debonded from the concrete at the interfaces, provide energy dissipation and impact mitigation.

ACKNOWLEDGMENTS

This work was sponsored and funded by the Pacific Earthquake Engineering Research Center (PEER). Any opinions, findings, and conclusions or recommendations expressed in this material are those of the authors and do not necessarily reflect those of the sponsoring agencies.

The participation of Yingjie Wu, doctoral student, and the work of the technical staff of PEER's Shaking Table Laboratory at the Richmond Field Station of the University of California, Berkeley, are thankfully acknowledged. We are also thankful to Overaa Construction, Richmond, California, and DSI America, Long Beach, California, for their assistance in bringing the experiment to fruition. Discussions with Professor Khalid Mosalam, Dr. Selim Gunay, and Yingjie Wu were invaluable for the specimen design and development of the numerical model.

CONTENTS

ABSTRACT	iii
ACKNOWLEDGMENTS	v
TABLE OF CONTENTS	vii
LIST OF TABLES	ix
LIST OF FIGURES	xi
1 INTRODUCTION.....	1
2 LITERATURE REVIEW	3
2.1 Hybrid Self-Centering Systems	3
2.2 Bridge Pier Socket Connections	4
3 PROTOTYPE BRIDGE STUDY	7
3.1 Hybrid System Model Development and Verification.....	7
3.2 Bridge Model	14
3.2.1 Bridge Description: Monolithic and Hybrid	14
3.2.2 Model Description	16
3.2.3 Input Ground Motions.....	17
3.2.4 Peak Responses.....	21
3.3 Prototype Modeling	23
4 DESIGN OF THE EXPERIMENT	25
4.1 Specimen Design and Construction.....	25
4.1.1 Scaling.....	25
4.1.2 Column.....	26
4.1.3 Foundation Strip.....	29
4.1.4 Bent Cap.....	30
4.1.5 Superstructure Mass.....	30
4.1.6 Specimen Assembly.....	30
4.2 Material Properties	37
4.2.1 Concrete	37
4.2.2 Infill Grout	38

4.2.3	Hysteretic Energy Dissipators.....	38
4.2.4	Prestressing Steel	38
4.2.5	Shell Steel	38
4.3	Instrumentation.....	40
4.4	Input Ground Motions	41
5	TESTING RESULTS.....	45
5.1	Lateral Response.....	45
5.2	Strain Measurements.....	53
5.3	Vertical Response.....	58
6	NUMERICAL MODEL CALIBRATION.....	65
6.1	Model Details.....	65
6.1.1	Column.....	65
6.1.2	Rocking Interface.....	67
6.1.3	Prestressing Bars.....	67
6.1.4	Energy Dissipators	67
6.2	Analysis Procedure	68
6.3	Model Improvement	68
6.4	Analytical Results.....	71
6.4.1	Lateral Force-Displacement Response	71
6.4.2	Prestressing Bar Stress History	72
7	SUMMARY AND CONCLUSIONS	81
	REFERENCES.....	83
APPENDIX A	CONSTRUCTION DRAWINGS	87
APPENDIX B	INSTRUMENTATION LAYOUT	115
APPENDIX C	INPUT TIME HISTORIES AND SPECTRAL RESPONSES	131

LIST OF TABLES

Table 3.1	Execution times (in seconds) for analytical models.	11
Table 3.2	Comparison of Λ_C and Λ_D values for different configurations.....	15
Table 3.3	Details of ground motions used for bridge parametric study.....	18
Table 4.1	Measured compressive strength of cementitious materials.	38
Table 4.2	Measured steel mechanical properties.	40
Table 4.3	Input ground-motion sequence for dynamic test.	42
Table 5.1	Summary of transverse drift and south column interface rotation response.....	50
Table 5.2	Summary of peak and residual prestressing ratios.....	52
Table 5.3	South column shell circumferential strain.	53
Table 6.1	Hysteretic energy comparison.....	72

LIST OF FIGURES

Figure 3.1	Hybrid recentering column analytical models.	8
Figure 3.2	Specimen drawings: (a) test setup; and (b) column base cross sections for Unit 1A (top) and Unit 1B (bottom).	9
Figure 3.3	Comparison of experimental and analytical results, Unit 1A: (a) Model 0, Guerrini [2014]; and (b) Model 1a and Model 1b.	12
Figure 3.4	Comparison of experimental and analytical results, Unit 1B: (a) Model 0, Guerrini [2014]; and (b) Model 1a and Model 1b.	13
Figure 3.5	MAOC elevation and plan.	16
Figure 3.6	MAOC typical bent.	15
Figure 3.7	Column sections for different configurations.	15
Figure 3.8	MAOC Bridge analytical model using OpenSees.	17
Figure 3.9	Abutment shear spring details.	17
Figure 3.10	Displacement response spectra of scaled ground motions imposed on MAOC bridge model.	19
Figure 3.11	Pseudo-acceleration response spectra of scaled ground motions imposed on MAOC bridge model.	20
Figure 3.12	Average peak and residual transverse drifts ratios of various bridge column configurations: (a) average of peak drifts; and (b) average of residual drifts.	22
Figure 3.13	Comparison of average peak PT stresses and average stress losses: (a) average of peak PT stresses; and (b) average of PT stress loss.	22
Figure 3.14	Typical hysteretic response, Bent #3 in MAOC bridge model, for various column configurations: (a) shell over the entire column; and (b) shell over ends only.	22
Figure 3.15	Comparison of axial loads in edge columns between Bent # 3 of the MAOC and the simplified two-column bent.	24
Figure 4.1	Specimen overview.	27
Figure 4.2	Column reinforcement details: (a) column steel shells; (b) weld beads at column ends; (c) column reinforcement cages; and (d) mild steel debonding details.	28
Figure 4.3	Column casting setup.	29

Figure 4.4	Foundation and bent cap reinforcement: (a) socket details in foundation; (b) socket reinforcements details in bent cage; and (c) assemblies reinforcement cage with bent cap.	32
Figure 4.5	Steel strip removal from columns: (a) removal of shell strip; and (b) strip removed.....	33
Figure 4.6	Column placement.	33
Figure 4.7	Grouting of columns in foundation socket.....	34
Figure 4.8	Bent cap placement.	34
Figure 4.9	Sealing bent cap socket bottom.....	35
Figure 4.10	Grouting bent cap socket.	35
Figure 4.11	Superstructure mass block installation.....	36
Figure 4.12	Finished specimen.....	36
Figure 4.13	Concrete material stress–strain response.	37
Figure 4.14	Mild steel material stress–strain response.....	39
Figure 4.15	Prestressing steel material stress–strain response.	39
Figure 4.16	Column steel shell material stress–strain response.....	40
Figure 4.17	Displacement response spectra of shaking table input ground motions	43
Figure 4.18	Pseudo-acceleration response spectra of shaking table input ground motions.....	44
Figure 5.1	Hysteretic responses on Day 1 of testing.	47
Figure 5.2	Hysteretic responses on Day 2 of testing.	48
Figure 5.3	Overlaid hysteretic responses.	49
Figure 5.4	Peak and residual transverse drifts.....	50
Figure 5.5	Peak and residual column interface rotations: (a) south column bottom; and (b) south column top.	51
Figure 5.6	Column base rotations seen in EQ08 and EQ09.....	52
Figure 5.7	Peak and residual prestress ratios: (a) north bar; and (b) south bar.	54
Figure 5.8	Stress–strain behavior of prestressing bars: (a) EQ08; and (b) EQ09.	55
Figure 5.9	EQ05 energy dissipator strain history.....	56
Figure 5.10	EQ09 prestressing bar strain history.....	56
Figure 5.11	EQ08 shell strain history, south column.	57

Figure 5.12	EQ09 corrugated metal pipe strain history.	57
Figure 5.13	EQ09 bent cap hanger reinforcement strain history.	57
Figure 5.14	Vertical acceleration vs. drift ratio.....	58
Figure 5.15	EQ05 vertical and horizontal response, and vertical acceleration time history.	59
Figure 5.16	EQ07 vertical and horizontal response, and vertical acceleration time history.	60
Figure 5.17	EQ05 specimen response at peak drifts: (a) south column interface, north face, $\Delta = 3.8\%$; (b) south column interface, south face, $\Delta = -3.5\%$; (c) south column, interface, north face, end of excitation; (d) south column interface, south face, end of excitation; (e) specimen deformation @ $\Delta = 3.8\%$; and (f) specimen deformation @ $\Delta = -3.5\%$	61
Figure 5.18	EQ07 specimen response at peak drifts: (a) south column interface, north face, $\Delta = 3.2\%$; (b) south column interface, south face, $\Delta = -4.5\%$; (c) south column, interface, north face, end of excitation; (d) south column interface, south face, end of excitation; (e) specimen deformation @ $\Delta = 3.2\%$; and (f) specimen deformation @ $\Delta = -4.5\%$	62
Figure 5.19	EQ08 specimen response at peak drifts: (a) south column interface, north face, $\Delta = 7.2\%$; (b) south column interface, south face, $\Delta = -4.5\%$; (c) south column, interface, north face, end of excitation; (d) south column interface, south face, end of excitation; (e) specimen deformation @ $\Delta = 7.2\%$; and (f) specimen deformation @ $\Delta = -4.5\%$	63
Figure 5.20	EQ09 specimen response at peak drifts: (a) south column interface north face, $\Delta = 5.4\%$; (b) south column interface, south face, $\Delta = -7.5\%$; (c) south column, interface, north face, end of excitation; (d) south column interface, south face, end of excitation; (e) specimen deformation @ $\Delta = -5.4\%$; and (f) specimen deformation @ $\Delta = -7.5\%$	64
Figure 6.1	Model overlaid over specimen.....	66
Figure 6.2	Confined concrete material properties used in analytical model.	69
Figure 6.3	Dissipator steel material properties used in analytical model.....	70
Figure 6.4	Prestressing steel material properties used in analytical model.....	70
Figure 6.5	Rayleigh damping model.	71
Figure 6.6	Numerical prediction of lateral force-displacement response.	73
Figure 6.7	Comparison of hysteretic energy dissipation over time.....	75

Figure 6.8	Comparison between the drifts as seen in the test and as predicted by numerical models: (a) peak drifts; and (b) residual drifts.....	78
Figure 6.9	Numerical prediction of peak stresses in the PT bars: (a) north bar; and (b) south bar.....	79
Figure 6.10	Numerical prediction of residual stresses in PT bars: (a) north bar; and (b) south bar.....	80
Figure C.1	EQ01 acceleration time histories.	133
Figure C.2	EQ01 spectral responses.	133
Figure C.3	EQ02 acceleration time histories.	134
Figure C.4	EQ02 spectral responses.	134
Figure C.5	EQ03 acceleration time histories.	135
Figure C.6	EQ03 spectral responses.	135
Figure C.7	EQ04 acceleration time histories.	136
Figure C.8	EQ04 spectral responses.	136
Figure C.9	EQ05 acceleration time histories.	137
Figure C.10	EQ05 spectral responses.	137
Figure C.11	EQ06 acceleration time histories.	138
Figure C.12	EQ06 spectral responses.	138
Figure C.13	EQ07 acceleration time histories.	139
Figure C.14	EQ07 spectral responses.	139
Figure C.15	EQ08 acceleration time histories.	140
Figure C.16	EQ08 spectral responses.	140
Figure C.17	EQ09 acceleration time histories.	141
Figure C.18	EQ09 spectral responses.	141
Figure C.19	EQ10 acceleration time histories.	142
Figure C.20	EQ10 spectral responses.	142
Figure C.21	EQ11 acceleration time histories.	143
Figure C.22	EQ11 spectral responses.	143
Figure C.23	EQ12 acceleration time histories.	144
Figure C.24	EQ12 spectral responses.	144

1 Introduction

This report presents the key features and seismic performance of a structural system designed and constructed around the aforementioned philosophies of Low Damage Structures and Accelerated Bridge Construction (ABC). Accelerated Bridge Construction is achieved by utilizing pre-cast columns and end beams connected using an innovative socket connection; the concept of resiliency is incorporated in the form of re-centering behavior of the columns [Guerrini and Restrepo 2011; Restrepo et al. 2011]. Re-centering columns are designed to display only minor damage localized at the column–beam interface under the same seismic demands that would cause extensive damage in conventional columns, with the goal of returning to their original position after the event through the use of unbonded post-tensioned elements. This results in a significant reduction in repair costs and downtime. The work presented here is an enhancement and a different outlook to earlier research [Guerrini et al. 2015]

The specimen presented in this report represents a 35%-scale, two-column bent cap based on an existing bridge located in a highly seismic region. The specimen was tested under dynamic loads arising from simulated ground motions produced by a shaking table. Under dynamic excitation, the specimen showed a flag-shaped nonlinear response typical of hybrid recentering systems, with rocking behavior occurring at the beam–column interfaces. Inertial forces were provided by the cap beam with six concrete blocks post-tensioned to it for a combined weight of 69 kips, thus simulating a portion of the bridge superstructure weighing 575 kips over two columns.

Test objectives included subjecting the specimen to two components of simulated ground motions, one horizontal and one vertical, with targeted lateral displacement demands as predicted by preliminary numerical simulations. The specimen’s dynamic response was monitored using a dense instrumentation setup. Verification of the system’s recentering capabilities and accuracy of the analysis methods were of primary interest. The specimen was subjected to a total of twelve earthquakes over two days at the University of California, Berkeley, shaking table, located off-campus at the Richmond Field Station Laboratory. The first nine tests formed a part of the primary test matrix, and their results also served as the benchmark for a blind prediction competition.

2 Literature Review

2.1 HYBRID SELF-CENTERING SYSTEMS

Re-centering structural systems, particularly those based on hybrid rocking behavior, have seen significant research in the past few decades. Excellent, low damage seismic performance demonstrated in subassembly tests, coupled with their suitability for fast and high-quality construction using precast concrete components, makes them a prime candidate for mitigating extensive damage, costly repairs, and associated downtimes to critical services that have occurred in recent earthquakes.

The earliest reported implementation of re-centering systems was in an industrial chimney at the airport at Christchurch, New Zealand [Sharpe and Skinner 1983]. Built in 1977, the chimney employed a passive rocking mechanism coupled with hysteretic dampers to meet architectural and engineering requirements. A similar system was implemented in the “stepping” railway bridge over the South Rangitikei River, New Zealand [Cormack 1988], where torsional hysteric energy dissipators were employed.

The PREcast Seismic Structural Systems (PRESSS) project was one of the earliest research program to explore experimentally and analytically the performance of hybrid rocking systems. The project itself started as a study into the seismic performance of precast systems [Priestley 1991]. The analytical work of Priestley and Tao [1993] began with the aim of preserving prestressing forces under large ductilities. To achieve that goal, they studied the behavior of partially unbonded prestressing tendons in precast moment frame connections. The behavior was studied experimentally by MacRae and Priestley [1994] and improved, in terms of energy dissipation, by incorporating mild steel reinforcement across joints; see Stone et al. [1995].

The promising results from these studies led to further analytical investigations into hybrid self-centering systems [El-Sheikh et al. 1999; Kurama et al. 1999] and culminated in the simulated seismic test of a 60%-scale, five-story structure [Nakaki et al. 1999; Priestley et al. 1999] that incorporated a hybrid coupled wall in one direction, and hybrid and emulative moment frames in the other direction as lateral force resisting systems.

The excellent results of this research have seen the concept of hybrid recentering systems being extended to steel moment frames [Christopoulos et al. 2002], masonry walls [Toranzo-Dianderas 2002], and tested in various precast concrete configurations [Holden et al. 2003; Perez et al. 2003]. Various energy-dissipation solutions have been explored by Restrepo and Rahman [2007] (milled bars in grouted ducts), Marriott et al. [2009] (viscous and mild steel external dissipators), Toranzo et al. [2009] (flexural external dissipators), and Eatherton and Hajjar [2014]

(steel plate fuses), while the behavior and effect of hybrid components has been explored experimentally by Belleri et al. [2014].

A pioneering study on the application of rocking systems to bridges was carried out by Mander and Cheng [1997] that included both theoretical development and experimental validation of hybrid bridge columns. Their work was followed by multiple analytical and experimental studies on hybrid bridge columns, exploration of construction methods, energy-dissipation solutions, and numerical simulation options. Hewes and Priestley [2002] studied experimentally and analytically the performance of segmented rocking bridge columns composed of only prestressing steel subjected to different levels of initial prestress and varying thickness steel jackets confining the plastic end regions of the columns. Kwan and Billington [2003a; b] and Ou et al. [2006] performed analytical studies on recentering columns using finite-element analysis. Sakai and Mahin [2004] and Hieber et al. [2005] studied hybrid bridge column behavior using fiber-based elements, with the former followed by shaking table tests [Jeong et al. 2008]. Palermo and Pampanin [2008] conducted analytical studies using lumped plasticity to model a prototype bridge, with supporting data from experiments comparing the performance of cantilevered monolithic and hybrid columns under monotonic and cyclic loading [Palermo et al. 2007]. Marriott et al. [2009; 2011] developed analytical models utilizing multiple springs to model the rocking interface and conducted uni- and bi-directional quasi-static cyclic tests on monolithic and hybrid columns, exploring different energy dissipation solutions. Guerrini et al. [2013; 2015] tested dual shell hybrid bridge columns under cyclic loading and shaking table excitation; their work explored options for external and internal energy dissipation and for improving PT bar deformability by addition of polyurethane pads. Thonstad et al. [2016] have tested a two-column, three-bent system with precast elements under shaking table excitation.

2.2 BRIDGE PIER SOCKET CONNECTIONS

Precast concrete elements offer an excellent means for reducing on-site construction work and have already been in use for some time in the construction of bridge girders, columns, and cap beams in regions with low seismicity. Yet, the construction of the bridge substructure in seismically active regions is done mostly using conventional cast-in-place methods. This trend primarily stems from limited research into the seismic performance of pre-cast connections. Considering the significant advantage precast systems display, there has been an upsurge in research into various methods for emulating cast-in-place connections, as well as into the development of non-emulative precast element connections like those used for re-centering systems.

Precast columns, hybrid or emulative, can be connected to the precast or cast-in-place foundations and bent caps through reinforcing bar couplers, grouted ducts, pockets, or sockets. The use of grouted ducts or reinforcing bar couplers typically involves prefabrication of the column over its clear height, with either the duct or the coupler embedded inside. The grouted duct connections are commonly used in hybrid bridge column studies and have been explored by Pang et al. [2010], Restrepo et al. [2011], and Tazarv and Saiidi [2015]. Couplers utilizing grouted splices have been studied by Ameli et al. [2015; 2016], while mechanical splices were explored in Haber et al. [2014]. Implementation of these connections in hybrid recentering columns requires

careful preparation of the bedding mortar layer at the rocking interface to develop the full strength of the column [Restrepo et al. 2011].

Pocket connections typically involve reinforcing bars extending out from the precast members, which need to be carefully meshed together before they are surrounded by either grout or concrete. This connection type has been explored in Restrepo et al. [2011]. Socketed connections allow the entire precast column to be embedded inside the end beam, which may be precast with a socket or may be cast on site by placing its reinforcing cage around the precast column. When used with precast cap beams or foundations, the socket connection presents a very easy to assemble system. This connection is particularly advantageous for hybrid recentering systems since no special preparation is needed for the rocking interface. A conservative design treatment of socket connections is present in some design codes [AIJ 1988; DIN 1045], while theoretical and experimental results for improved capacity calculation have been presented in Osanai et al. [1996], Blandon and Rodriguez [2005], and Fernandes Canha et al. [2007]. The application of this connection to hybrid bridge columns has been explored by Haraldsson et al. [2013], Mashal et al. [2012; 2013; 2015], Belleri and Riva [2012], and Thonstad et al. [2016].

3 Prototype Bridge Study

This chapter discusses the computational models developed in OpenSees in support of the shaking table test program. The computational work started from an existing model for recentering column systems. This model was optimized to increase computation speed and used to carry out a parametric analysis on a full 3D bridge model, which was used as a prototype to assist in the design of the test specimen.

3.1 HYBRID SYSTEM MODEL DEVELOPMENT AND VERIFICATION

The main elements of a hybrid rocking system are the rocking member, unbonded post-tensioning (PT) elements for improving recentering behavior and the energy-dissipating elements for controlling displacements. The rocking member typically has reinforced ends to withstand the large stresses arising during rocking and can be split into two subcomponents by function: the reinforced rocking interface and the central element, which largely stays elastic. Typically, the elastic limit of the unbonded post-tensioned elements controls the displacement capacity of the system.

A model incorporating these elements has been developed and validated by Guerrini et al. [2014; 2015], hereby called Model 0, using the analysis program OpenSees, where the specific behavior of each of these elements is explicitly modeled:

- The energy dissipators are modeled individually using displacement-based beam–column elements and material models to represent the energy dissipation method;
- The post-tensioned elements are modeled using nonlinear truss elements to account for any yielding, with fixity constraints to model anchorage points and an approximation of sliding constraints at the rocking interface;
- The rocking element is represented by elastic beam–column members split into multiple segments to model the point of connection to the energy dissipators; and
- The rocking interface is modeled using multiple compression-only, nonlinear truss elements, with appropriate material models representing the interface material.

The truss elements forming the rocking interface are connected via rigid members, with the elastic rocking element starting at their combined center. The energy dissipators and the PT elements are modeled at their physical locations and are connected to the elastic rocking element via rigid elements. The model has been validated against experimental data obtained from two cyclic tests, details of which will be presented in the next section.

While the model shows a good match with experimental data, the computational performance is slow. This is largely due to the modeling of individual fibers in the rocking interface: for each fiber, at least three degrees-of-freedom (DOFs) are added in the model. Considering that the execution times increase exponentially with the DOF count, this model is a poor choice for systems with multiple rocking interfaces, e.g., a complete bridge.

To improve the computational performance, first, the model is modified to use a single fiber-based beam-column element for the rocking interface and displacement-based beam-column elements to model the rocking element. This updated model, hereby called Model 1a, is again calibrated against the same tests. As a further optimization, the elements representing the individual dissipators are also combined together into a single fiber-based element. This model will be called Model 1b. A representation of the three models described above is shown in Figure 3.1.

The proposed models presented were validated against test results from two hybrid recentering systems tested by Guerrini et al. [2015] at the University of California, San Diego, Powell Structural Engineering Laboratories, where Unit 1A utilized external buckling restrained energy dissipators and Unit 1B utilized internal dowel bars. The same column was used for both the units: the column was flipped upside-down after testing Unit 1A and reused to test Unit 1B. This approach exploited the fact that only the bottom region of a cantilevered hybrid column experiences large strains and damage. Some drawings of the specimen are shown in Figure 3.2.

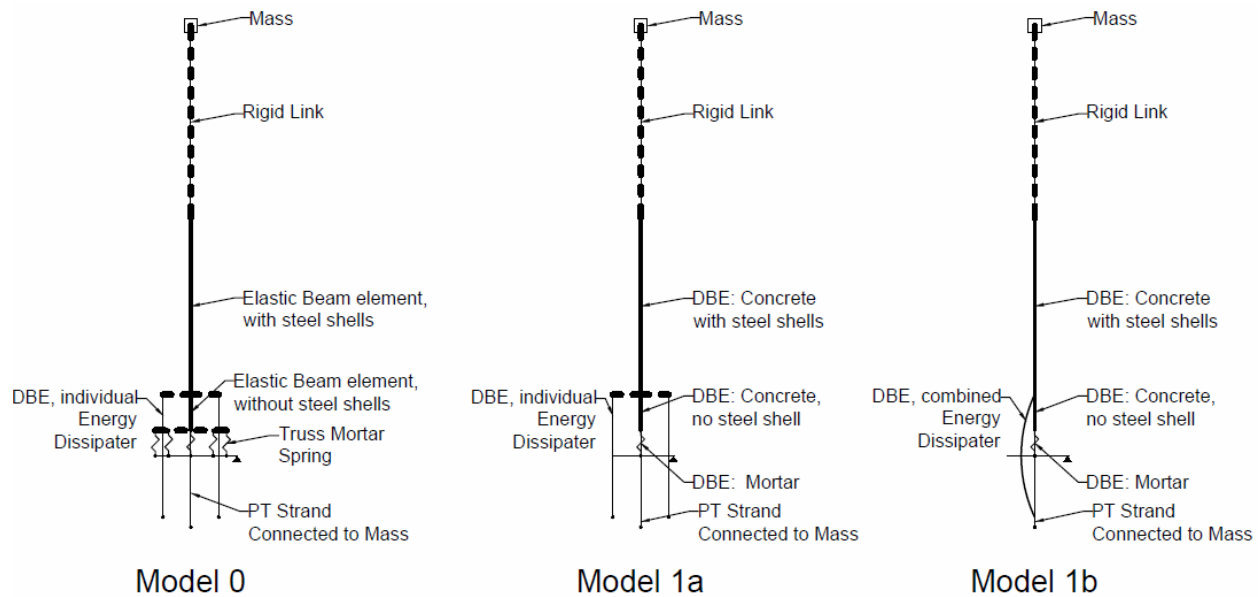


Figure 3.1 Hybrid recentering column analytical models.

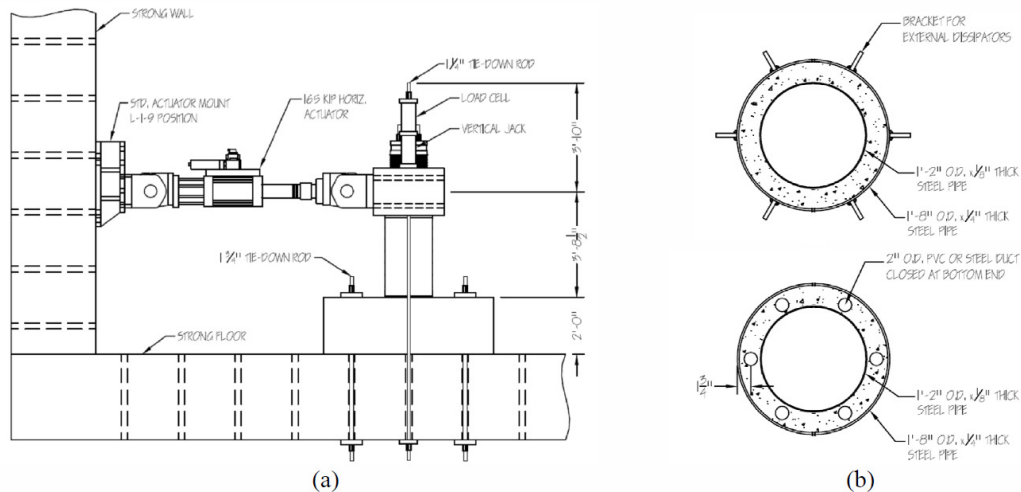


Figure 3.2 Specimen drawings: (a) test setup; and (b) column base cross sections for Unit 1A (top) and Unit 1B (bottom).

The tested column had an external diameter of 20 in. and a height of 33 in. The load was applied via a loading stub at an effective height of 44.5 in. The column was formed by casting high-strength normal weight concrete ($f'_c = 10.2$ ksi) between two A572 Gr 50 steel shells: an outer shell, 20 in. in diameter and 0.25 in. thick, and an internal shell, 14 in. in diameter and 0.125 in. thick. The inside of the internal shell was left hollow to reduce the column weight and facilitate the installation of PT steel, which was provided by four 1-3/8-in. diameter A722 Gr 150 DSI thread bars. The threaded bars were anchored into anchorage devices prearranged in the footing and seated on soft rubber pads on top of the loading stub. The rubber pads served to increase the displacement capacity of the column by delaying the yielding of the PT bars; their use was necessitated due by the low aspect ratio of the column. Each specimen was placed on a 0.5-in.-thick high-performance mortar layer ($f'_c = 7.7$ ksi) created on the foundation to compensate for lack of precision and aid in positioning and leveling of the specimen.

Unit 1A was provided with six radially distributed, external buckling restrained external energy dissipators, with a 6.5 in. region milled to 9/16 in. from 1-in.-diameter hot-rolled A576 Gr 1018 steel bars ($f_y = 48$ ksi, $f_u = 71$ ksi). These were welded to anchors installed in the foundation and to brackets on the column outer shell. A total effective PT force of 180 kips was applied, in addition to 63 kips of vertical load applied using two vertical jacks to simulate gravity.

Energy dissipation in Unit 1B was provided by six 316LN Gr 75 #4 internal dowels ($f_y = 108$ ksi, $f_u = 129$ ksi). The dowels were debonded over a length of 7 in. using duct tape and grouted inside pre-installed corrugated steel ducts inside the footing and the column, such that the middle of the debonded length was placed at the foundation level. The effective PT force and simulated gravity loads were 200 kips and 60 kips, respectively.

Both units were subjected to quasi-static reversed cyclic loading in the north-south direction. The loading began with three force-controlled cycles to ± 25 kips and three to ± 52 kips base shear, followed by displacement-controlled cycles: three to $\pm 0.5\%$ drift ratio and three to $\pm 0.75\%$ drift ratio. Subsequent cycles were composed of two large-amplitude cycles, followed by a lower one at a level corresponding to the previous large drift level: drift ratios of $\pm 1\%$, $\pm 1.5\%$, $\pm 2\%$, $\pm 3\%$, $\pm 5\%$, $\pm 7.5\%$, and $\pm 10\%$ were targeted.

In Model 0, the mortar was modeled using 36 circumferential \times 3 radial truss elements, the PT bars were modeled using truss elements, and the dual shell column was modeled using two elastic beam–column elements to account for the anchorage location of the energy dissipators. The energy dissipators were modeled individually using three displacement-based beam–column elements (DBE) per dissipator to model the varying dissipator section for Unit1A and a single DBE accounting for the effective unbonded length of each dissipator for Unit 1B.

The load was applied at the center of the load block, and the top node location of the PT bars accounted for the load cell height. The bar material accounted for the flexibility provided by the rubber bearing pads. Further details of the material models and fixity constraints used can be found in Guerrini [2014]. Note: the mortar crushing stress was increased from 1 ksi to 45% of peak stress (3.6 ksi for Unit1A and 3.8 ksi for Unit1B) to improve the model prediction at higher drifts.

For Models 1a and 1b, the mortar truss elements were replaced by a single two-integration point DBE, using the same mortar material and an equivalent fiber configuration. Both elastic beam–column elements between the mortar and load stub were replaced by an equivalent two-integration point DBE using fiber sections made of confined concrete derived from the concrete strength in the columns. The top element also included steel fibers representing the two enclosing steel shells. The model for the energy dissipators remained unchanged in Model 1a. In Model 1b, the energy dissipators for both units were modeled using a single three-integration point DBE, with an element length reflecting the total effective dissipator length. Compared to Model 0, the varying section was not modeled for Unit 1B. Attempts at varying the section resulted in larger base shears, which were possibly due to localization issues.

The results for Unit 1A from the three models are shown in Figure 3.3, while the results for Unit 1B are presented in Figure 3.4. All three models show a good agreement with the test results for Unit 1B; note that Model 0 gives higher forces for Unit 1A. Model 0 also shows higher initial stiffness when compared to Models 1a and 1b; this is due to constraints against horizontal displacement applied at the top of the mortar to ensure model stability. A lack of these constraints in Models 1a and 1b results in higher stresses and strains in the mortar, resulting in greater strength degradation at higher drifts.

The advantage of the modifications is clearly visible when comparing the execution times of the three models; see Table 3.1. Just switching to the fiber model for the mortar gains a speedup factor of 45 for Unit 1A and a factor of 56 for Unit 1B. Replacing the energy-dissipator trusses with a single fiber-based element results in a speedup factor of 98 for Unit 1A and a factor of 88 for Unit 1B. As stated earlier, this is due to the much larger number of DOFs in Model 0. For models involving multiple rocking interfaces, this number should be expected to increase nonlinearly. Simulation of a larger model can be made by doubling the number of mortar truss elements for two interfaces or quadrupling the number for four interfaces. The execution times for these simulations are also included in Table 3.1. From these values, it can be inferred that the execution time increases with an exponent of at least 1.3, with increasing exponent with the DOF count.

Table 3.1 **Execution times (in seconds) for analytical models.**

	Model 0: 36 × 3	Model 0: 36 × 6	Model 0: 72 × 6	Model 1a	Model 1b
Unit 1A	593	2894	16287	13	6
Unit 1B	1419	7535	54838	25	16

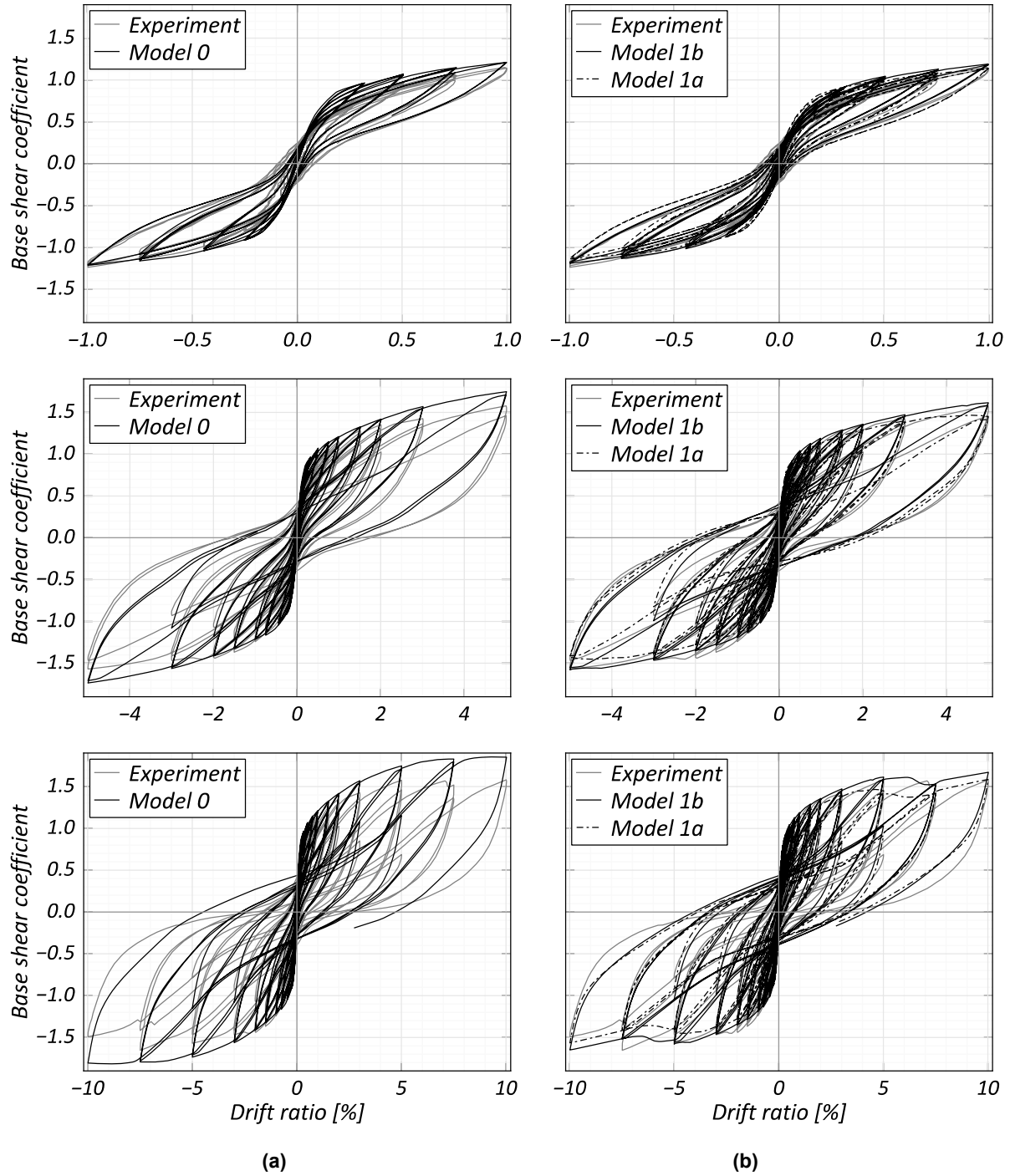


Figure 3.3 Comparison of experimental and analytical results, Unit 1A: (a) Model 0, Guerrini [2014]; and (b) Model 1a and Model 1b.

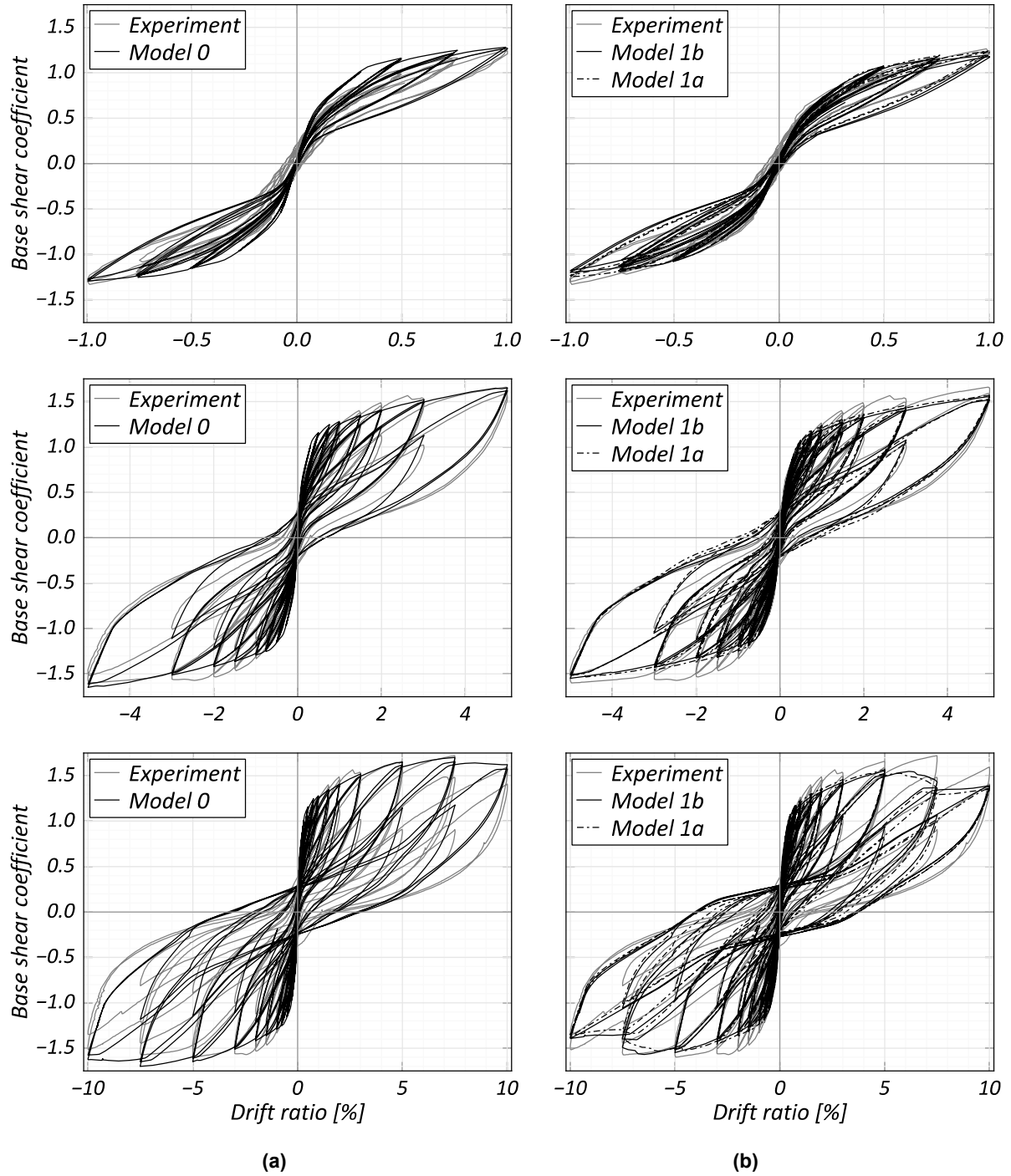


Figure 3.4 Comparison of experimental and analytical results, Unit 1B: (a) Model 0, Guerrini [2014]; and (b) Model 1a and Model 1b.

3.2 BRIDGE MODEL

The prototype was derived from an existing bridge: the Massachusetts Avenue Overcrossing (MAOC) located in San Bernardino, California, near the I215/HW210 Interchange in close proximity to the San Andreas fault. In order to better represent the bridge behavior in the test, the hybrid system model was incorporated into a three-dimensional (3D) model of the bridge, and the dynamic results from this model were used to decide upon the target behavior of the prototype, i.e., the ratio of energy dissipation to recentering capacity. To maintain similarity between the prototype and bridge behavior, the bridge model, in conjunction with a numerical model of the prototype, was also used for fine-tuning the column-to-column distance, a key parameter.

The 3D model for the as-built bridge was originally developed by Frank Beckwith¹, UC San Diego, for studying the seismic response with several types of shear keys. The data provided by the original model serves as benchmark result for comparing the performance of the hybrid system with a conventional cast-in-place system. This section focuses on the parametric studies conducted using the bridge model.

3.2.1 Bridge Description: Monolithic and Hybrid

The as-built bridge consisted of five asymmetric spans of lengths 49 ft, 92.5 ft, 92 ft, 100 ft, and 78 ft for a total bridge length of 415 ft. The four bent caps were skewed with respect to the bridge post-tensioned box girders to match the roadway underneath. Each bent cap was supported on four 4-ft circular columns reinforced using 22 #11 mild steel, with 2-ft-diameter shear keys between the columns and the foundation. The girder ends rested on isolated shear keys formed by bearing pads placed between the girders and the abutments. The bridge elevation and plan are shown in Figure 3.5; a typical bent is shown in Figure 3.6.

For the redesign of the bridge utilizing hybrid columns, one method is to use the conventional design as the base and replace a portion of the mild reinforcing steel with PT bars. In doing the replacement, the aim is to maintain similar strengths between the conventional and hybrid design, which is achieved by matching the nominal moment strength in both systems. A careful balance needs to be maintained between the mild and PT steel to have adequate re-centering capacity at the same time as adequate energy dissipation to limit maximum deflections. Guerrini et al. [2015] provides two equations to put limits on mild steel and PT steel amounts:

$$\Lambda_C = \frac{F_{ED,o}}{P_u + F_{PT,e}} \leq 1.0 \quad (3.1)$$

$$\Lambda_D = \frac{F_{ED,o}}{P_u + F_{PT,e} + F_{ED,o}} \geq 0.1 \quad (3.2)$$

Here, P_u is the design gravity load, $F_{PT,e}$ is the effective PT force, $F_{ED,o}$ is the total ultimate strength of the energy dissipators undergoing plastic deformations in the gap-opening portion of the column section. Λ_C is a recentering coefficient and gives a measure of the gap closing capability of the gravity and PT forces, with a value of 1.0 or less, indicating full recentering capacity. Λ_D is the energy-dissipation coefficient and should be limited as indicated to avoid large scatter on lateral displacement and acceleration demands. For circular sections, a reasonable value of $F_{ED,o}$ is the

¹ fbeckwit@eng.ucsd.edu

ultimate strength of half the energy dissipators since the dissipators inside the compression zone or close the neutral axis exhibit low tensile behavior.

Two designs were initially explored for the hybrid bridge columns. Type-1 configuration of the hybrid column follows the recommendations of Caltrans Recovery ERS Volume 1 [Bromenschenkel and Mahan 2014]: it contains a higher proportion of mild steel with 12 #11 Gr 60 bars and 4×4 -0.6 in. Gr 270 strands. Additionally, the strands are stressed variably with four strands stressed at 75%, 50%, 25%, and 10% of Guaranteed Ultimate Tensile Strength (GUTS) each (for an average initial stress of 40% GUTS). The proposed aim behind using different stress levels is to have additional stress capacities in reserve for different level events.

Type-5 configuration is based on the recommendations of Guerrini et al. [2015] and utilizes a smaller proportion of mild steel, with 8 #11 mild steel bars and 8×4 -0.6 in. Gr 270 strands stressed at 40% GUTS. The column section is taken to be an octagon circumscribing a 4-ft circle from precasting considerations.

For the final prototype, a configuration with Λ_c and Λ_D values between Type-1 and Type-5 configurations was selected. This configuration, termed Type-6, consisted of 10 #11 mild steel bars and 8×4 -0.6 in. Gr 270 strands stressed at 40% GUTS. The numerical value of the Λ_c and Λ_D for the three hybrid configurations is given in Table 3.2; the same gravity loading of 288 kips per column was used for all configurations, which was obtained from the average column axial load in Bent 3 in the conventional bridge model. A representation of the different sections is shown in Figure 3.7.

An effective mild steel debond length of 4 ft is used for the hybrid column configurations, equal to 20 in. applied debonding and additional 20 bar diameters (28 in.) to account for bar development on either side of the interface. The column toes were confined using 0.5-in.-thick steel jacket, assumed to be at least over the bottom 20 in., i.e., the region of mild steel debonding inside the column. The jacket thickness was selected to avoid permanent deformation or damage to the shell at the column toes. Guerrini et al. [2015] recommended a limit of $D_o/t_o \leq 100$ where D_o is the outer diameter and t_o the shell thickness. The clear column height was assumed to be precast, and the column-beam interface was assumed to be made of a 1-in.-thick layer of high-strength mortar. Finally, the effective PT strand debond was assumed to end 31 in. away from the column ends, which is the location of the center of gravity of the bent cap.

Table 3.2 Comparison of Λ_c and Λ_D values for different configurations.

Configuration	Mild steel, Gr 60	PT steel, Gr 270	Λ_c	Λ_D
Type 1	12 \times #11	16 \times 0.6 in.	1.34	0.57
Type 5	8 \times #11	32 \times 0.6 in.	0.57	0.36
Type 6	10 \times #11	32 \times 0.6 in.	0.71	0.42

In addition to the ratio of mild and recentering steel, the effect of jacketing the entire column with a steel shell was explored for the first two configurations. Using a steel shell over the entire column offers an alternative way for constructing the columns, which was especially suitable for rapid pre-cast construction of the hybrid system. This method was adopted for constructing the specimen and will be further explored in Chapter 4.

3.2.2 Model Description

In the 3D model developed in OpenSees, the post-tensioned box girder system was modeled using elastic elements along the spine of the bridge deck. Each girder elastic element was split into a number of equal length elements, with the number of elements determined such that all of them have similar lengths between different bridge spans. For the bent groups, the clear height of each bent column was modeled using a single force-based beam-column element with four integration points, so that the integration weights were roughly equal to the plastic hinge recommended by Caltrans. The columns are connected to the bridge spine through rigid links with vertical offsets to model the deck height and horizontal offsets to account for the column location within the bent.

The abutment model consists of several zero-length springs modeled both in series and in parallel to approximate the behavior of the bearing pads, gaps, shear keys, soil wedge, and embankment system. A representation of the bridge model is shown in Figure 3.8; details of the abutment are shown in Figure 3.9.

Since the incorporation of recentering columns calls for rocking at both ends, the original monolithic model was updated by removing the pin constraint at the foundations to provide a more accurate baseline. For the models utilizing hybrid columns, the single element monolithic columns were replaced with the hybrid column model utilizing nonlinear elements presented in the previous section. The strands were split into four groups, one group for each level of pre-stress for the Type-1 column and the pre-stress modeled using the *InitStrainMaterial* material in OpenSees. The strands were modeled using three-corotational elements for each strand to model the expected strand bending at each interface. Note: each strand was modeled at the column center since the strand physical location is important only for a hybrid cantilevered system and has no effect on a double-rocking system employed in the prototype bridge.

Based on initial model stiffness, 2% Rayleigh damping was used in Modes 1 and 30 to model damping in all models since in early analysis the damage-free models were found to be sensitive to damping in higher modes. Damping was modeled only in the beam-column elements, with no damping in the rocking interface elements. This was done to avoid unrealistic damping forces that arise due to large velocities seen during rocking [Charney 2008].

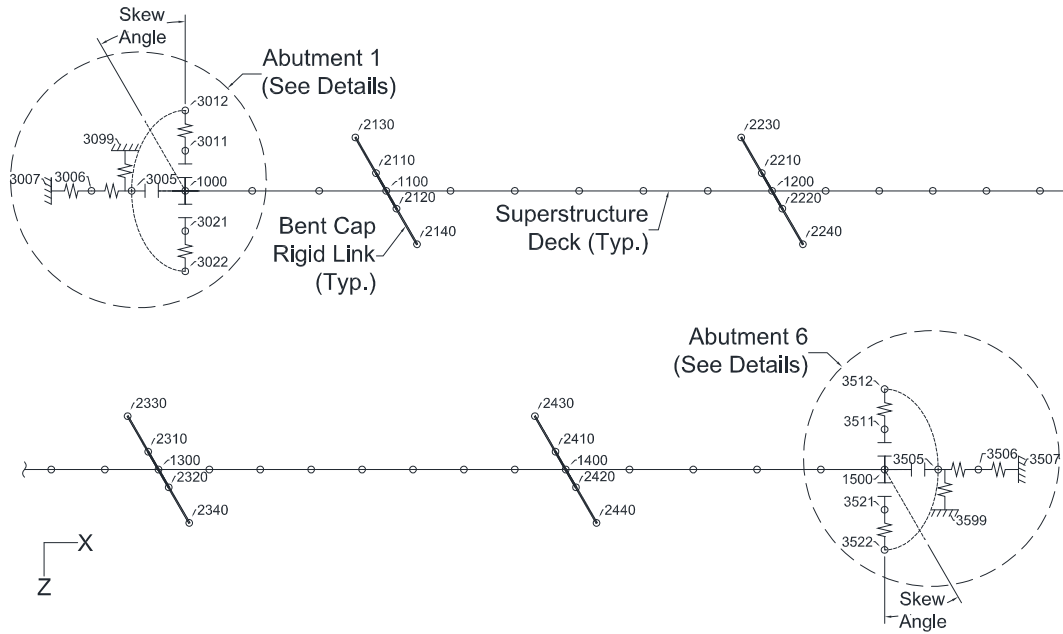


Figure 3.8 MAOC Bridge analytical model using OpenSees.

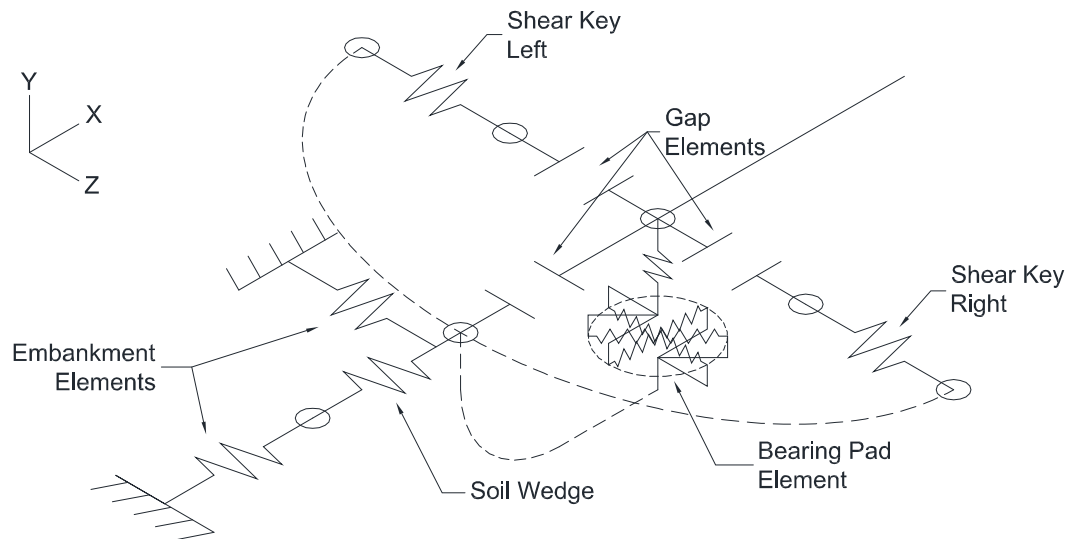


Figure 3.9 Abutment shear spring details.

3.2.3 Input Ground Motions

To compare the performance of different configurations listed above, the bridge model was subjected to three components of the ground motions listed in Table 3.3, with the fault-normal component being applied transverse to the bridge. The unscaled horizontal ground motions have been rotated to maximize the response transverse to the bridge, and the rotated ground-motion data was obtained from the work of Lu and Panagiotou [2013]. Ground motions were scaled to have a good match between the geometric mean of their fault-normal components and the SDC acceleration response spectrum (ARS) curve [2013] used for the original design of the bridge. To

account for the proximity of the San Andreas fault, the SDC ARS curve already includes modification for near-fault effects. The spectral responses of the three components of the ground motions can be seen in Figure 3.10 and Figure 3.11.

Table 3.3 Details of ground motions used for bridge parametric study.

Record ID	Earthquake	Year	Mw	Station	Fault type+	Scale factor	Unscaled PGA (g), fault normal
NZ002	Christchurch, NZ	2011	6.3	PRPC	OT	1.55	0.73
P0927	Northridge	1994	6.7	Newhall - Fire Station	BT	1.47	0.72
P1005	Northridge	1994	6.7	Rinaldi Receiving Station	BT	1.07	0.89
P1023	Northridge	1994	6.7	Sylmar - Converter Station	BT	1.46	0.59
P0934	Northridge	1994	6.7	Sylmar - Olive View Med FF	BT	1.53	0.73
P0770	Loma Prieta	1989	6.9	LGPC	SS	1.11	0.65
P1441	Chi-Chi, Taiwan	1999	7.6	TCU065	T/LLS	1.51	0.83

*OT=Oblique Thrust, BT=Blind Thrust, SS=Strike-Slip, T/LLS=Thrust/Left-Lateral Slip

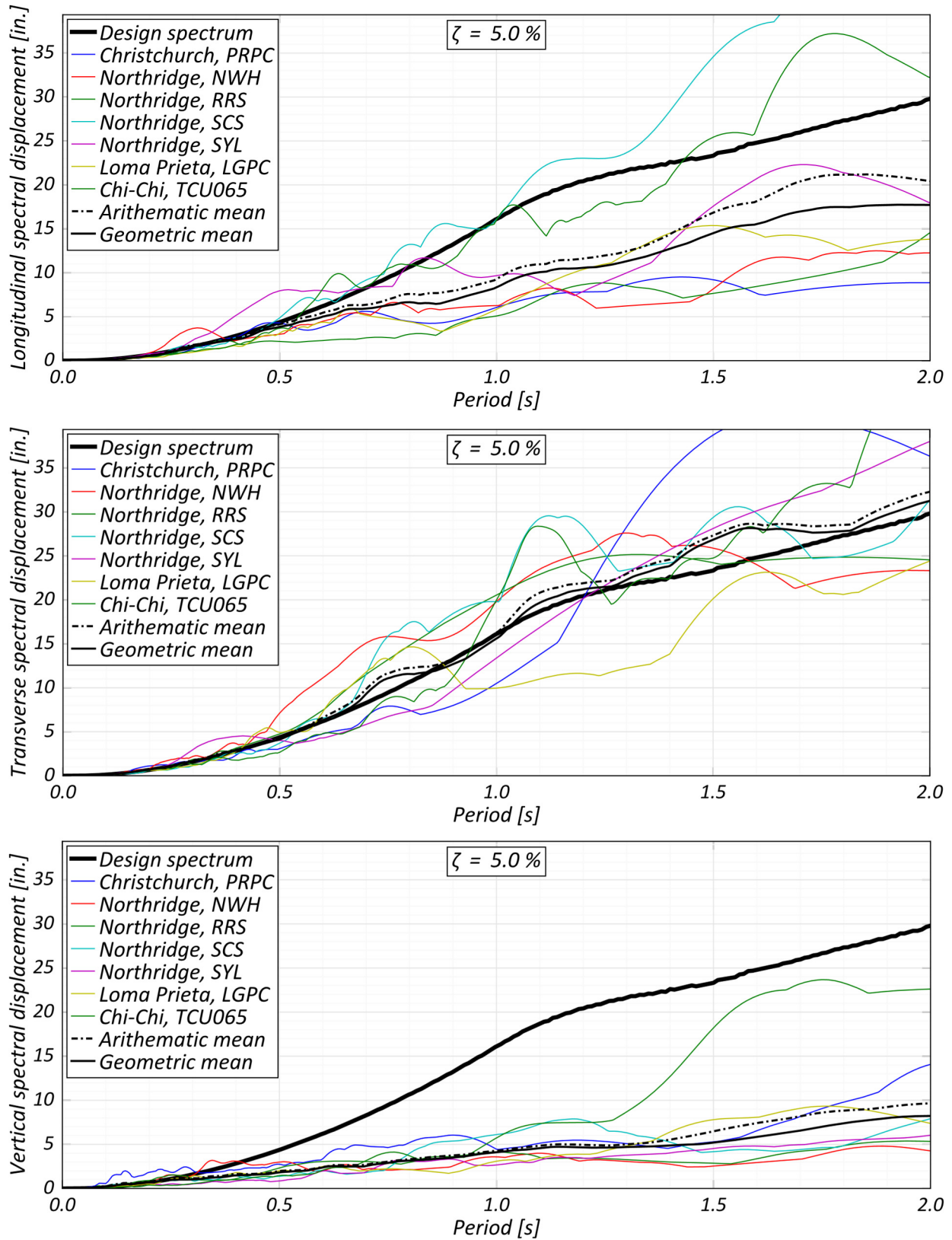


Figure 3.10 Displacement response spectra of scaled ground motions imposed on MAOC bridge model.

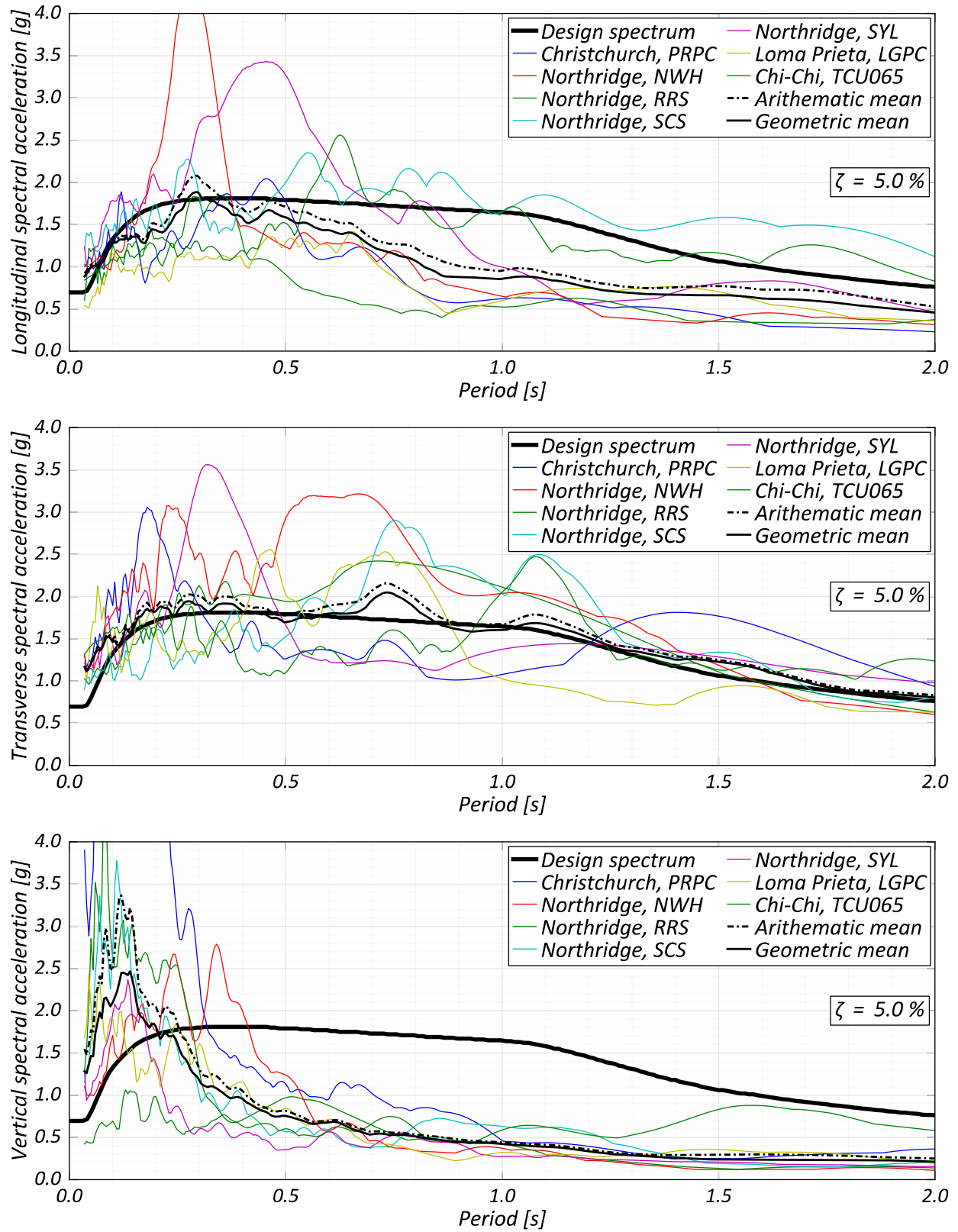


Figure 3.11 Pseudo-acceleration response spectra of scaled ground motions imposed on MAOC bridge model.

3.2.4 Peak Responses

The average peak and residual drifts observed in the various models are presented in Figure 3.12(a) and (b). The hybrid systems show larger peak drifts than the monolithic systems, while among hybrid configurations, peak drifts are seen to be slightly larger when only the column ends are jacketed. The Type-6 configuration typically shows the minimum peak drifts.

The advantage of hybrid columns is clearly seen in the residual drifts, which are much lower for the hybrid columns. A comparison among the different configurations of hybrid columns demonstrates that a high proportion of mild steel adversely affects the recentering capacity of the hybrid columns. The end-only jacket configurations are also seen to have larger residual drifts.

Figure 3.13(a) compares the average of the peak strand stresses among the different column configurations. Both variations of Type-1 columns were found to reach 90% GUTS of the strands on average as a direct result of the high initial stress of 75% GUTS in one group of strands in these configurations. Consequently, these configurations also show a significantly higher loss in strand prestress; see Figure 3.13(b). In contrast, The Type-5 and Type-6 configurations were limited to elastic strand behavior with very small losses in strand stresses. Additionally, configurations with end-only jackets experienced larger average stress losses compared to their fully jacketed counterparts.

A typical lateral force-drift response for the adequately confined columns is shown in Figure 3.14(a), while the same for end-only jacket models is shown in Figure 3.14(b). The superior recentering behavior of Type-5 configuration is seen in both figures. It can be observed that hybrid systems have smaller forces than the monolithic system at the same drift, although this can be a result of no damping being modeled at the rocking interface. Larger forces are seen with lower mild steel to PT steel ratio systems.

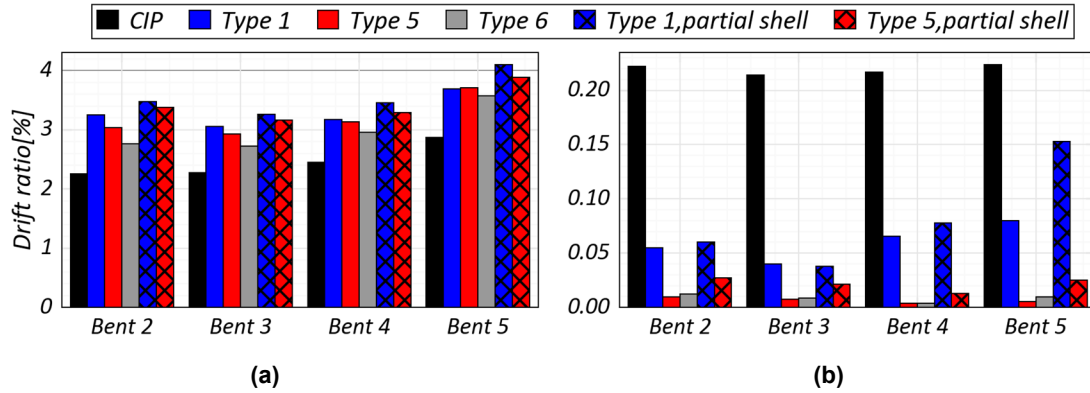


Figure 3.12 Average peak and residual transverse drifts ratios of various bridge column configurations: (a) average of peak drifts; and (b) average of residual drifts.

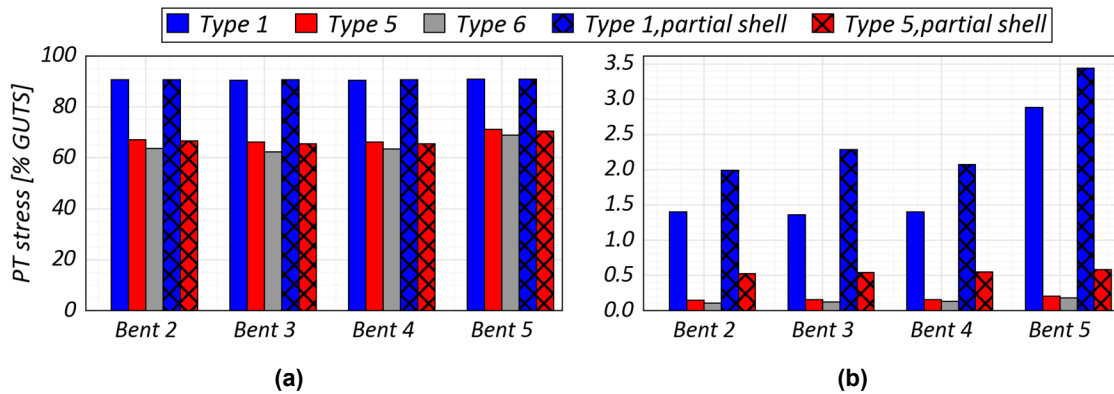


Figure 3.13 Comparison of average peak PT stresses and average stress losses: (a) average of peak PT stresses; and (b) average of PT stress loss.

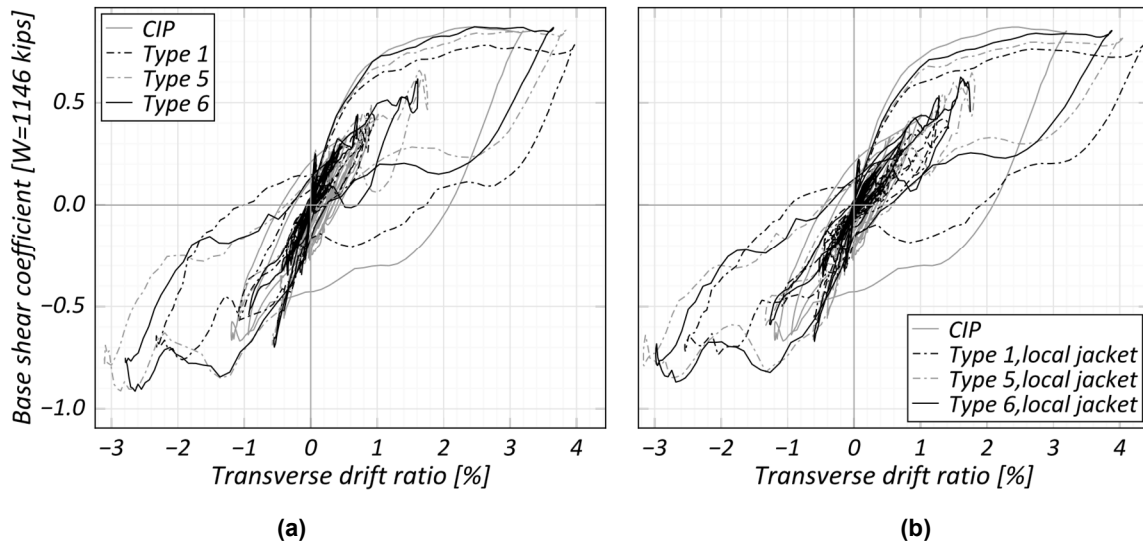


Figure 3.14 Typical hysteretic response, Bent #3 in MAOC bridge model, for various column configurations: (a) shell over the entire column; and (b) shell over ends only.

3.3 PROTOTYPE MODELING

With the details of the hybrid column established from the bridge model, a full-scale prototype was developed and tested on the shaking table. Unlike the actual bridge with four columns per bent, the prototype, derived from Bent #3 of the bridge, had two hybrid columns. This change was implemented to maximize the utilization of the shaking table in terms of force and displacement capacities, and optimize the economy of the experiment. The modification necessitated further changes in the prototype bent geometry; the distance between the columns was modified to improve similarity (in terms of column axial stresses) between the two columns in the prototype and the two edge columns in the bridge bent. The analytical model presented next assisted in tuning the column distance and aided in selecting the ground motion sequence to be used in the test.

The base prototype consisted of two columns separated by a distance of 30.2 ft, the same as the on-center distance between edge columns in the bridge bents. The columns were assumed to be precast, and the column–beam interface was assumed to be composed of a 1-in.-thick high-strength mortar layer. Post-tensioning was provided by unbonded 8×4 -0.6 in. Gr 270 strands with an initial prestress of 40% GUTS and assumed to be anchored a distance of 0.61 m from the column ends. Energy dissipation was provided through ten #11 Gr 60 reinforcing bars debonded from the concrete over a 20 in. length, which gave an effective unbonded dissipator length of 4 ft when coupled with assumed bond development over 10 bar diameters on each side of the rocking interface.

The foundation and cap-beam dimensions were assumed to be the same as those in the bridge, and effective inertial and gravity loads were inferred to be 573 kips for the prototype bent obtained from the column axial loads calculated during the analysis of the monolithic bridge. The prototype clear height between the foundation and cap beam was taken to be 31.5 ft, which was the average clear height in Bent #3 of the MAOC Bridge. The material properties of steel, concrete, and mortar were kept the same as those in the bridge: the effective concrete strength for the confined columns was taken as 9.6 ksi, the mortar strength was 14.5 ksi, and the mild steel yield stress was 65.8 ksi.

Two unavoidable—yet significant differences—were present in the prototype compared to the bridge: the bridge skew cannot be modeled, and any analyses/tests have to be done in the bridge's transverse direction. Both of these differences stem from the fact that the prototype contained only a single bent; no actual girders providing important constraints in the longitudinal direction were present. This results in any out-of-plane behavior in the prototype to be unrealistic compared to the bridge. To obtain comparable results from the numerical models of the prototype and the bridge, the bridge must be re-modeled with zero skew and under only transverse and vertical excitation.

The parametric study on the prototype column distance utilized the fault-normal and vertical components of the ground motion measured at the Sylmar–Olive View Medical Center station during the 1994 Northridge, California, earthquake. The axial loads in the prototype columns were compared to those in the outer columns of Bent #3 in the bridge for different column distances. The responses for a select few values are shown in Figure 3.15. On the basis of these results, a column center-to-center distance of 165.4 in. was selected for the final prototype.

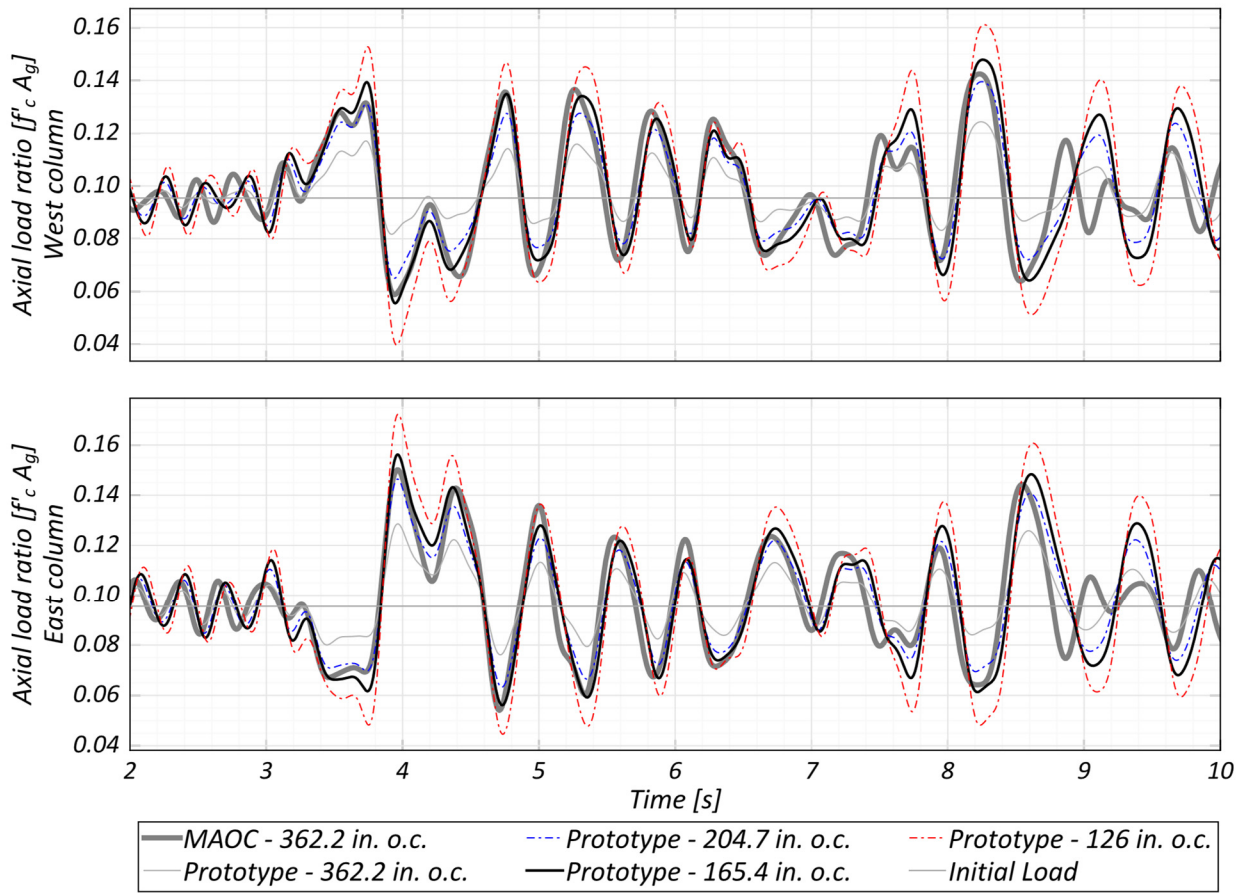


Figure 3.15 Comparison of axial loads in edge columns between Bent # 3 of the MAOC and the simplified two-column bent.

4 Design of the Experiment

4.1 SPECIMEN DESIGN AND CONSTRUCTION

Testing took place at the PEER shaking table laboratory located in the UC Berkeley Richmond Field Station campus. To limit expected forces and shaking table displacements, the prototype needed to be scaled down by a factor of $\lambda = 0.35$. An important objective was to maintain similarity in terms of stresses between the prototype and the specimen, which called for the provision of additional seismic mass in the specimen and required compression in time of the ground-motion histories to be applied. The seismic mass was provided by the bent cap and six concrete blocks post-tensioned to the bent cap representing the bridge superstructure. This splitting of the seismic mass was necessary so that the components could be safely picked up by the indoor crane in the laboratory.

The joints between the columns and the foundation/bent cap were formed using socket connections. This eliminated the need for a mortar layer at the rocking interface, which could be a limiting factor for the column response; see Restrepo et al. [2011]. Details of the scaling procedure and the design and construction of the columns, foundation, and bent cap are presented in the following sections.

4.1.1 Scaling

The specimen scaling procedure involved mass substitution in addition to geometrical scaling. The additional mass was required for similitude between stresses in the specimen and the prototype.

Scaling in the model space without mass substitution is derived from the length scale, defined as the ratio of the model unit length to the prototype unit length, as defined by Equation 4.1(a). The remaining scale factors were derived from the length-scale factor, assuming consistent mass density and mass material modulus between the prototype, and the specimen and are listed in Equations 4.1(b) to (g).

$$\text{Length} \quad S_l = \frac{l_m}{l_p} = 35\% \quad 4.1(a)$$

$$\text{Area} \quad S_A = \frac{A_m}{A_p} = \frac{l_m^2}{l_p^2} = S \frac{2}{l} \quad 4.1(b)$$

$$\text{Volume} \quad S_V = \frac{V_m}{V_p} = \frac{l_m^3}{l_p^3} = S_l^3 \quad 4.1(c)$$

$$\text{Mass} \quad S_M = \frac{M_m}{M_p} = \frac{\rho V_m}{\rho V_p} = S_l^3 \quad 4.1(d)$$

$$\text{Force} \quad S_F = \frac{F_m}{F_p} = \frac{M_m g}{M_p g} = S_l \quad 4.1(e)$$

$$\text{Stress} \quad S_\sigma = \frac{\sigma_m}{\sigma_p} = \frac{F_m/A_m}{F_p/A_p} = S_l \quad 4.1(f)$$

$$\text{Stiffness} \quad S_K = \frac{K_m}{K_p} = \frac{EA_m/l_m}{EA_p/l_p} = S_l \quad 4.1(g)$$

As can be noted from Equation [4.1(f)], the stresses in the model space are scaled by the factor S_l . To impose similitude in terms of stresses, additional mass was added to the system such that Equation [4.1(f)] with the total modified mass resulted in a scale factor of 1. The additional mass required can then be obtained from the total model space mass necessary for stress similitude. This relation is expressed in Equation [4.2(a)]. Finally, the scale time factor can be obtained using the masses and stiffnesses in the model and prototype space [Equation 4.2(b)].

$$S'_\sigma = 1 = \frac{M'_m g/A_m}{M_p g/A_p} \Rightarrow M'_m = M_p S_l^2 = \frac{M_m}{S_l} \quad 4.2(a)$$

$$\Delta M_m = M'_m - M_m = M_m \frac{(1 - S_l)}{S_l}$$

$$\text{Time} \quad S'_T = \frac{T_m^2}{T_p^2} = \frac{\sqrt{M'_m/K_m}}{\sqrt{M_p/K_p}} = \sqrt{S_l} \quad 4.2(b)$$

$$\text{Acceleration} \quad S'_a = \frac{l_m/T_m^2}{l_p/T_p^2} = 1 \quad 4.2(c)$$

4.1.2 Column

The column design was based on the scaled prototype column. Each column had an external diameter of 16 in. Ten #4 (1/2-in.-diameter) A706 Grade 60 reinforcing bars provided the longitudinal reinforcement; a 6-in. length of each reinforcing bar at the rocking interface was debonded from the surrounding concrete using duct tape to prevent large strains. Three separate #3 (3/8-in.-diameter) A706 Grade 60 spirals were used to hold the longitudinal reinforcement together; the splitting of the spiral was necessary to prevent the transverse spirals from contributing to energy dissipation by yielding at the rocking interface. The use of spirals was only for construction purposes since the column outer shell provided the majority of shear and confining reinforcement.

Due to the difficulty in sourcing 3/8-in.-diameter strands called for in the scaled prototype, and to aid in monitoring PT forces, the strands in the prototype were replaced by a single 1-3/8-

in.-diameter ASTM A722 Grade 150 threaded PT bar, which had a yield strength capacity equal to that of ten (10) 3/8-in.-diameter strands. The bar anchorage was embedded inside the column bottom before the pouring of concrete, and the PT bar itself was enclosed inside a 2-in.-ID PVC sleeve to debond it from the concrete. The PT bar was left inside the sleeve during the pouring of concrete to help keep the PVC sleeves aligned. The top end of the bar extended from the top of the column for the placement of a concentric load measuring cell resting on the bent cap. This extension also proved helpful in guiding the bent cap in place during assembly.

The use of a dry-socket connection to join the columns to the foundation and the bent cap allowed for an innovative construction method. The entirety of each column was formed by inserting the reinforcement cage inside a segmented steel shell assembled from 0.25-in.-thick ASTM A53 Grade B pipe, followed by the pouring of 6 ksi concrete. The steel pipe served as permanent formwork, provided a force transfer mechanism between the column and end beams, and served as confinement to ensure satisfactory rocking performance. To allow rocking to occur at the beam-column interface, the pipe was segmented into five sections: two end sections, to be embedded inside the socket connection were provided with weld beads outside and inside for developing composite action; one central section over the clear column height, and finally two thin removable open strips: one strip between the central section and each of the two end sections. The five segments were spot-welded together at a few locations to form the single pipe unit used for casting each column. These spot welds were grounded off, and the thin strip segments were removed to form the rocking interface in the assembled specimen. Photographs from the column construction process are shown in Figure 4.2 and Figure 4.3.

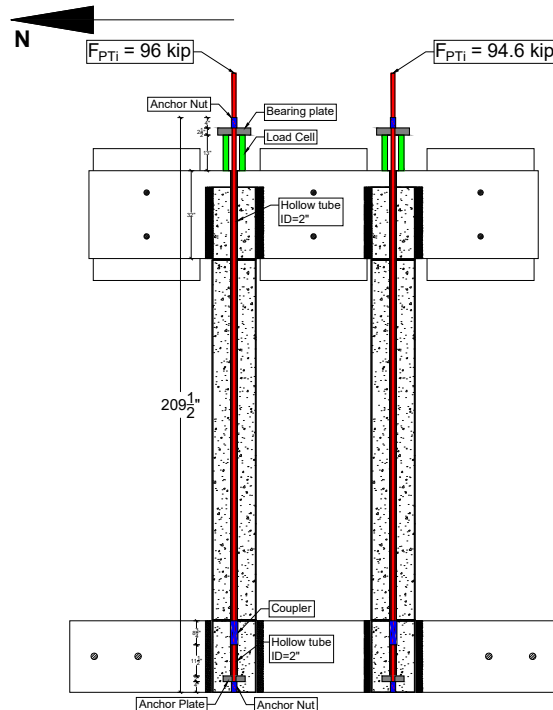


Figure 4.1 Specimen overview.



(a)



(b)



(c)



(d)

Figure 4.2 Column reinforcement details: (a) column steel shells; (b) weld beads at column ends; (c) column reinforcement cages; and (d) mild steel debonding details.



Figure 4.3 Column casting setup.

4.1.3 Foundation Strip

The foundation was designed around the socket connection. The socket for accommodating each column was formed out of 22-in. inner-diameter (ID) corrugated metal pipe (CMP). The foundation width was set to 38 in. to allow 8 in. of space on either side for placing reinforcement and provide cover. The foundation depth was set to 26 in. for bond development between the column and the foundation in the socket. Finally, a foundation length of 178 in. was selected to accommodate tie-downs for securing the foundation to the shaking table.

Primary reinforcement design was done following the strut-and-tie method as prescribed in § 5.6.3 of *AASHTO LRFD Bridge Design Specifications* [2012]. The column axial load was assumed to be transferred directly to the shaking table, while lateral loads were assumed to be transferred by lateral bearing at the top and bottom of the socket. The strut and tie model required

that the socket-type of joint include extra cross ties around the connection to prevent splitting of the foundation in the longitudinal direction due to the bearing forces arising from the transfer of column shears to the foundation. Additional staples were provided around the socket to prevent any splitting due to out-of-plane forces. This reinforcement, while not necessary for the specimen, is required in bridge foundations. A picture of the foundation reinforcement around the socket connection detail is shown in Figure 4.4(a).

4.1.4 Bent Cap

The bent-cap design, which was similar to the foundation, revolves around the socket connection. The socket was again formed from 22-in. ID and 26-in.-deep CMP; the beam width was kept the same at 38 in. Unlike the foundation, vertical loads need to be transferred from the bent cap to the columns. For this purpose, a 6-in.-thick layer of reinforced concrete was placed on top of the column sockets for a total bent cap depth of 32 in.; the contribution of the bond-development in the socket was ignored as a safety measure. The bent-cap length was set at 164 in. to accommodate the six concrete blocks needed to simulate the superstructure mass.

The reinforcement design was done using the strut-and-tie method, similar to the design of the foundation. The vertical load was transferred from the bent-cap to the column via bearing against the top layer of concrete, strengthened by straight- and bent-hanger reinforcement. As in the foundation, additional crossties and staples were provided to prevent the beam from splitting in the longitudinal and transverse direction.

A 2-in.-ID opening was allowed in the 6 in. top layer above each socket to allow the PT bars to pass through. Additional smaller openings were provided near the socket periphery to allow the pouring of the grout. Additional 2-in.-ID sleeves were provided through the vertical faces of the bent cap at three locations where the six concrete blocks were to be anchored. Photographs of the bent-cap reinforcement and the socket connection detail are shown in Figure 4.4(b) and (c).

4.1.5 Superstructure Mass

The superstructure mass in the specimen was provided by the bent cap and six concrete blocks measuring 48 in. \times 48 in. \times 39 in. This split in the superstructure mass was done to limit the weight of the bent cap and the blocks to within the lifting capability of the indoor crane at the shaking table. Each block had a weight of nearly 7800 lbf, and blocks were installed in pairs on each side of the bent cap at three locations. Minimum reinforcement was provided for each block and was distributed as skin reinforcement on each face of the blocks. The blocks were installed at mid-height on the bent cap to avoid introducing artificial rotational mass moment of inertia in the specimen.

4.1.6 Specimen Assembly

The precast columns, foundation, and bent cap were manufactured offsite by a precast concrete fabricator and delivered to the UC Berkeley shaking table for assembly and testing. Before starting the assembly, the 0.25 in. steel strips located at the column rocking interface were removed by grinding off the spot welds and prying apart the strips; see Figure 4.5. The PT bars extending out

from the top of the columns were covered with a few layers of duct tape to prevent any bonding to the grout in the sockets. At the same time, the foundation was installed on the shaking table on a bed of gypsum and tied down with a total force of 300 kips exerted through three tie-down bars. Once the foundation was installed, the shaking table was calibrated to the input ground motions for the faithful reproduction of the response spectra.

With the foundation installed and the shaking table calibrated, columns were leveled inside the foundation socket and anchored down to maintain their level; see Figure 4.6. Non-shrink grout was poured in the gap between each column and the CMP, thus forming the foundation socket; see Figure 4.7. The grout was then allowed to set for three days before beginning the placement of the bent cap on top. This time was spent creating the wooden formwork support for the bent cap.

In preparation of bent cap installation, 0.5-in. shim blocks were placed on top of the columns, and the column tops were covered with wet rags to ensure proper setting of the grout. The bent cap was then lifted above the columns and brought down carefully until it was lightly resting and centered on the columns; see Figure 4.8. The centering of the bent cap was aided by the PT bars extending out from the top of the columns. The bent cap was leveled on top of the columns by adjusting the wooden support, after which the supports were strengthened further by cross braces. With the bent cap in place and leveled, the bottoms of the sockets were sealed up (Figure 4.9), and grout was poured from the top; see Figure 4.10. Best practice was found to pour a thin layer of grout into each socket and let it harden for a day before completely filling the sockets with grout. This measure provides additional strength to the seal at the bottom of the socket and prevents any leaks due to the weight of the grout.

The grout in the bent cap was allowed to set for three days, after which the PT bars extending out from the top were moderately tensioned. The concrete blocks were post-tensioned to the bent cap with a total force of 100 kips for each set of two blocks, which was exerted through two 1-in. PT bars passing through the blocks and the bent cap; see Figure 4.11.

Since the specimen was designed to be tested under transverse and vertical shaking only, two restraint frames consisting of two A-frames connected together by a diagonal and horizontal W section for lateral stability were erected to limit any twisting or motion in the longitudinal (out-of-plane) direction; see Figure 4.12. The specimen was allowed to slide on a low-friction surface formed by greased wooden shims attached to the concrete blocks and the horizontal W-section beam connecting the A-frames. The frame installation was done concurrently with the installation of the concrete blocks. When the installation of the blocks and restraining frames was finished, the column PT bars were tensioned to the target stress of 40% GUTS, for a target force of 94.8 kips on each bar.



(a)



(b)



(c)

Figure 4.4 Foundation and bent cap reinforcement: (a) socket details in foundation; (b) socket reinforcements details in bent cage; and (c) assembles reinforcement cage with bent cap.



(a)



(b)

Figure 4.5 Steel strip removal from columns: (a) removal of shell strip; and (b) strip removed.



Figure 4.6 Column placement.



Figure 4.7 Grouting of columns in foundation socket.



Figure 4.8 Bent cap placement.



Figure 4.9 Sealing bent cap socket bottom.



Figure 4.10 Grouting bent cap socket.



Figure 4.11 Superstructure mass block installation.



Figure 4.12 Finished specimen.

4.2 MATERIAL PROPERTIES

4.2.1 Concrete

The specified strength of concrete for the foundation, bent cap, and the columns was 6 ksi. The compressive strength was measured using 6-in.-diameter and 12-in.-tall standard concrete cylinders. The foundation and bent cap were cast from the same batch of concrete, while the columns were cast together from a different batch. The same mix design was used for both concrete batches, with a large aggregate size of 1 in.

Before the testing of the specimen, six cylinders were tested two days prior to track the development of concrete strength. Additionally, on the first day of testing, six cylinders from each batch of concrete were tested using a compressometer to obtain their stress–strain profile in addition to crushing strength. The average strengths measured on each day of testing are listed in Table 4.1, and the average stress–strain responses from the compressometer tests are shown in Figure 4.13. Comparing the measured modulus of elasticity to the value calculated following equation 19.2.2.1.b, ACI 318-14, it can be seen that ACI equation underestimates Young’s modulus.

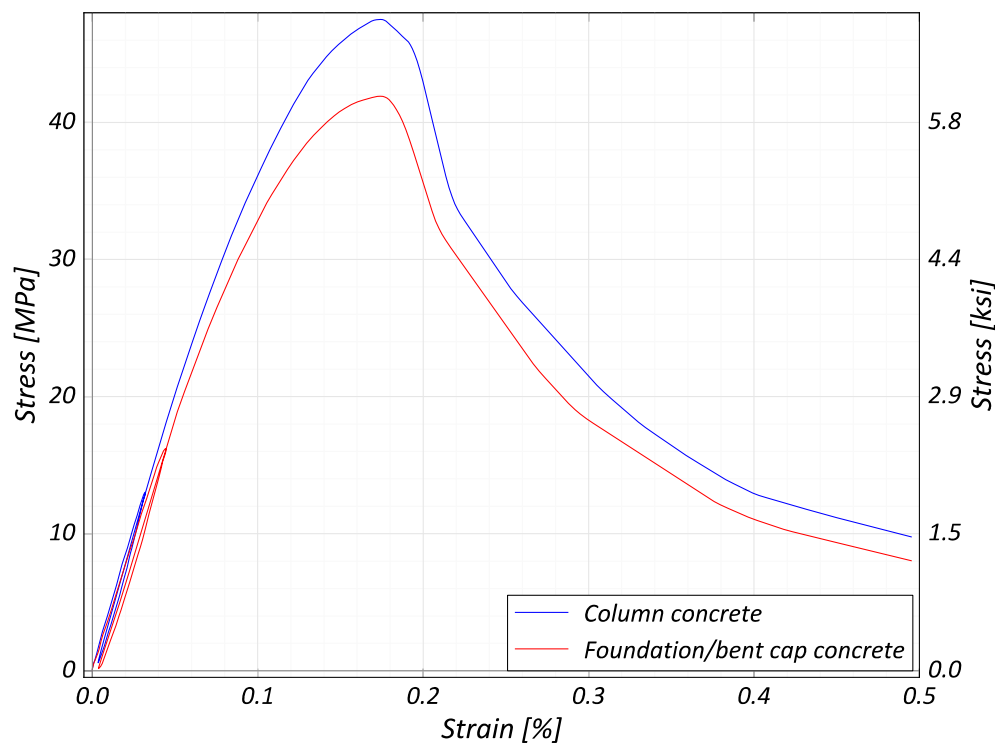


Figure 4.13 Concrete material stress–strain response.

4.2.2 Infill Grout

BASF MasterFlow® 928 non-shrink grout was mixed to a fluid consistency and used to grout the gap between the columns and the CMP socket walls. Compressive strengths were measured on the day of testing on 2-in.-diameter and 4-in.-tall standard cylinders. The average strength from three cylinders is reported in Table 4.1.

Table 4.1 Measured compressive strength of cementitious materials.

Material	Age (days)	Compressive strength		Young's modulus, measured		Young's modulus, ACI	
		(MPa)	(ksi)	(GPa)	(ksi)	(GPa)	(ksi)
Foundation / Bent-cap concrete	14	31.1	4.51	n/a		n/a	
	32	37.6	5.45				
	73 (DOT)	41.9	6.08	36.0	5220	30.6	4440
Column concrete	7	30.5	4.42	n/a		n/a	
	22	34.6	5.02				
	48 (DOT)	47.5	6.89	39.6	5750	32.6	4731
Infill grout	22 (DOT)	47.4	6.87	n/a		n/a	

4.2.3 Hysteretic Energy Dissipators

Three 18-in.-long A706 Grade 60 #4 bars used in the column reinforcement were tested under monotonic tension to characterize the material. The average properties of the three samples are reported in Table 4.2, and the full stress–strain relation is shown in Figure 4.14. Note that the uniform strain is taken as the minimum strain at peak stress from among the three samples.

4.2.4 Prestressing Steel

Three 24 in.-long ASTM A722 Grade 150 threaded bars used for post-tensioning the columns were tested under monotonic tension to characterize the material. The average properties of the three samples are reported in Table 4.2, and the full stress–strain relation is shown in Figure 4.15.

4.2.5 Shell Steel

Three samples obtained by straightening some of the 0.25 in. strips removed from the column outer steel shell at the rocking interface were tested under monotonic tension to characterize the material. The average properties of the three samples are reported in Table 4.2, and the full stress–strain relation is shown in Figure 4.16. For the strips, the strain recording was stopped at 1.8% strain, and only the ultimate strength was reported beyond that point.

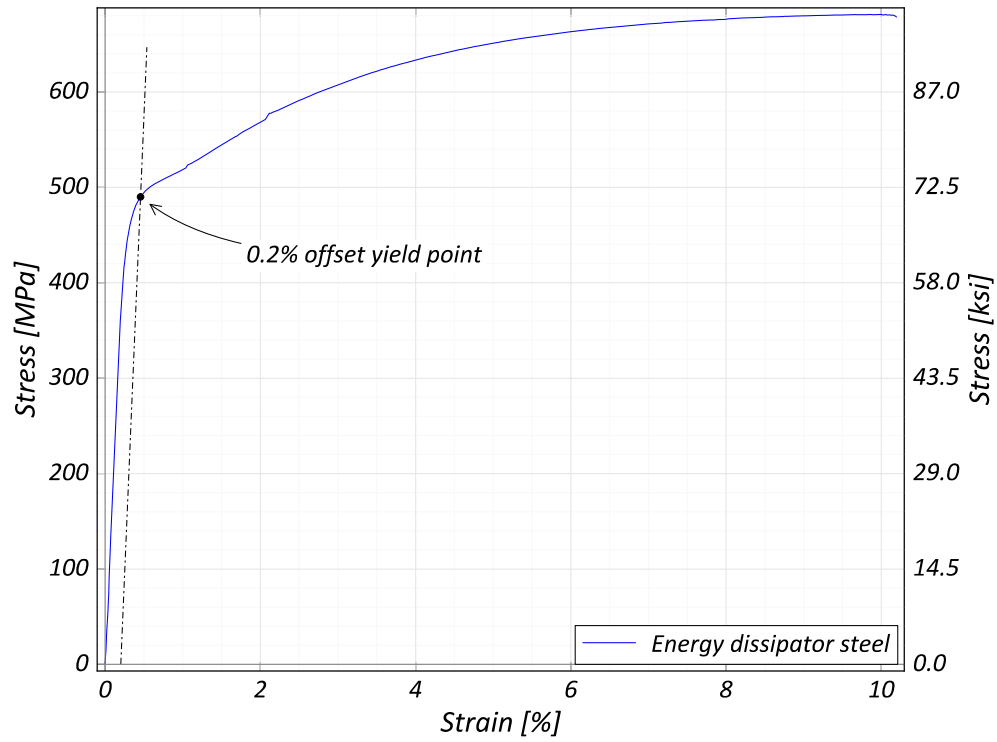


Figure 4.14 Mild steel material stress–strain response.

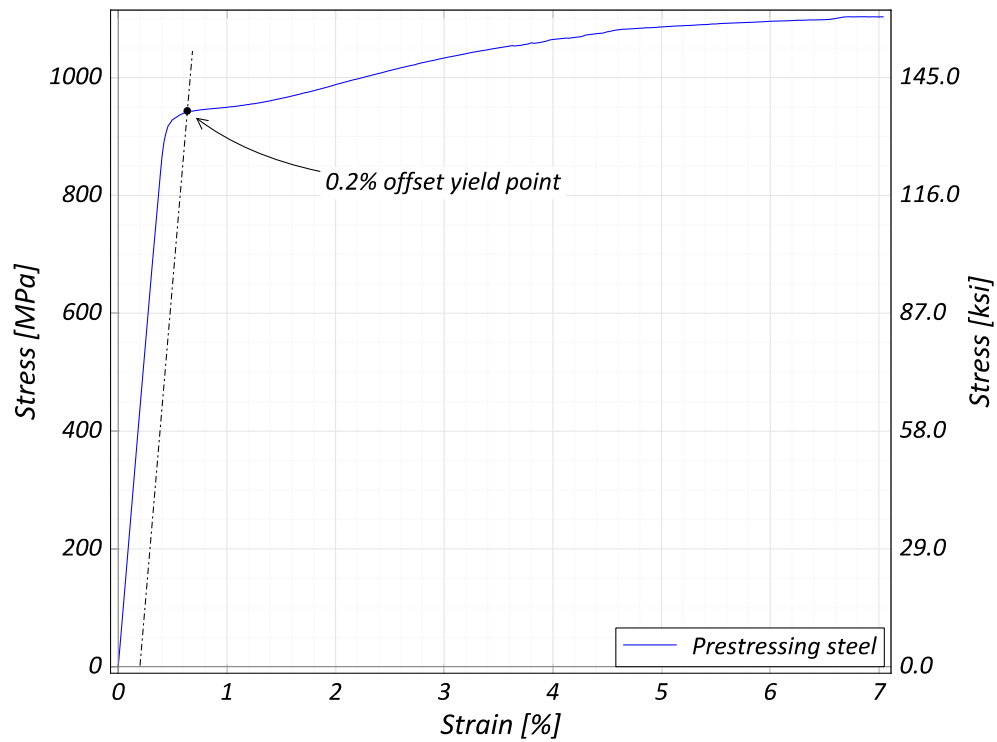


Figure 4.15 Prestressing steel material stress–strain response.

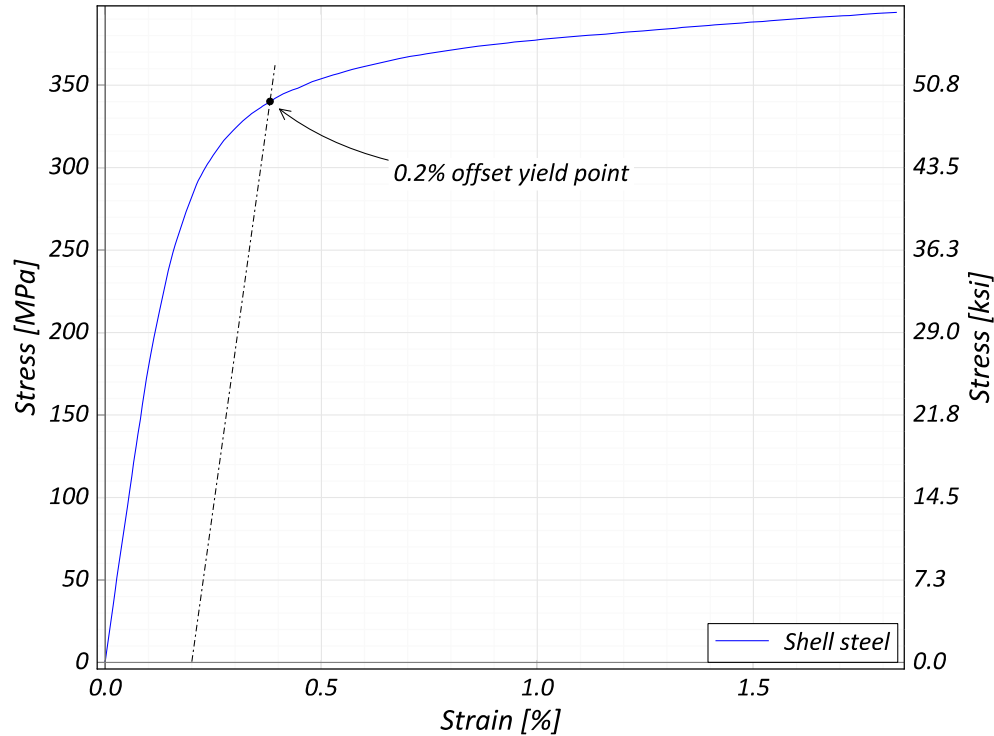


Figure 4.16 Column steel shell material stress–strain response.

Table 4.2 Measured steel mechanical properties.

Material	Elastic modulus		Yield stress		Yield strain (%)	Peak stress		Uniform strain (%)
	(MPa)	(ksi)	(MPa)	(ksi)		(MPa)	(ksi)	
A706	192,000	27,900	489	70.9	0.45	681	98.8	10
A722	217,000	31,400	939	136	0.63	1100	160	7.0
A53	188,000	27,200	339	49.2	0.38	461	66.9	n/a

4.3 INSTRUMENTATION

A wide array of instruments was installed to monitor the response of the specimen. All the sensor data was sampled at 200 Hz. Twelve (12) accelerometers installed on the shaking table and the foundation measured the input accelerations in three directions at the ends of the foundation. Twenty-six (26) accelerometers were placed on the bent cap, and the concrete blocks helped measure the inertia forces experienced in the specimen along all 6 DOFs.

Nine (9) string potentiometers were anchored at one end to frames located off the table and connected to the foundation and the bent cap at the other end to get a measure of absolute displacements. These, coupled with two curtains of two (2) diagonal and two (2) vertical string potentiometers, measuring relative displacement between the foundation and the bent cap, were used to give redundant measurements of relative displacements between the two. Four (4) linear potentiometers were installed at each rocking interface to measure the gap openings and end-

rotations in the columns. One last linear potentiometer was used to monitor the shaking table vertical displacement by suspending it from a stiff frame anchored to a location off the table.

Ten (10) strain gauges with a gauge length of 5 mm each were installed in the debonded lengths of three energy dissipators at each rocking interface and in each column to get a measure of strains experienced during shaking. Four (4) 5-mm strain gauges were installed in the CMP in each of the sockets, two (2) each at a location 8 in. from the top and the bottom of the socket along the direction of shaking, to measure the strains produced by transfer of axial forces between the columns and the end beams.

For the south column, the shell segments embedded inside the sockets were fitted with four (4) 5-mm rosette gauges at each end: one gauge at each point 2 in. from the end of the embedded segment and on diametrically opposite points along the shaking direction. Additional non-yielding gauges installed on this segment were in the specimen out-of-plane direction at each location corresponding to the strain gauges applied on the CMP. Four (4) strain gauges, measuring circumferential strains, were also installed 2 in. and 4 in. above each rocking interface in the same column, and along the direction of shaking, to get an indication of the steel shell behavior.

For each socket in the bent cap, a 5-mm strain gauge was installed in 45° segments of two hanger reinforcement bars, to measure the force transferred between the bent cap and the columns through bearing instead of socket shear. Two (2) strain gauges were installed in each of the PT bars, located on the portion of the bar above the bent cap and inside the load cells, which were installed to measure the PT bar forces.

In addition to the sensors, video recordings of the specimen response during the shaking were also made from various locations. Four (4) GoPro cameras recorded high-quality videos of the rocking interfaces at the foundation level for each of the two columns, while two additional GoPro cameras, and two Canon T5i DSLR cameras were used to record the specimen's overall response as seen from various locations off the table. The videos were synchronized to the sensor data using a system of LEDs set to blink at the beginning and end of the tests, with the input voltage being monitored at one of the data channels.

4.4 INPUT GROUND MOTIONS

The prototype model presented in Chapter 3 was modified by scaling down the member geometries and updating the material and PT properties to match the expected material properties as per Caltrans' *Seismic Design Criteria* [2013]. This model was then used to select a suite of near-fault earthquakes to be imposed on the specimen for dynamic testing.

The selection was made based on expected peak drift as calculated by the numerical model, in comparison with the design drift capacity of the system defined by the yielding of the PT bars and calculated to be 7%. The selected motions represent very mild (0.6% drift), mild (1.8% drift), moderate (4% drift) and large (>5% drift) events.

Nine earthquake simulations were planned in the initial loading protocol. To investigate the effects of lower intensity aftershocks, the test sequence was not conducted with continually increasing demands; instead, a larger motion was followed by smaller intensity of shaking until a peak drift of 4% was reached. The resulting protocol called for test with input motions capable of producing the following sequence of drifts: 0.6%, 0.6%, 1.8%, 0.6%, 4%, 1.8%, 4%, 5%, and 7%.

For larger drifts, ground-motion polarity was occasionally switched to avoid damaging the specimen in only one direction. A 2.5% RMS, 120-sec-long noise signal, bound by an upper frequency of 75 Hz, was applied in the horizontal excitation direction after each earthquake to monitor the dynamic properties of the specimen.

Significant structural integrity remained after the initially planned sequence, and the scope was expanded with three additional tests. Details of the ground motions are listed in Table 4.3 in the order they were imposed on the specimen; the displacement and pseudo acceleration response spectra for the two components are shown in Figure 4.17 and Figure 4.18.

Table 4.3 Input ground-motion sequence for dynamic test.

EQ #	Event name	Station name	Unscaled PGA (g)	Scale factor	Expected drift (%)
01	Landers, 1992	Lucerne	0.72	0.9	0.6
02	Landers, 1992	Lucerne	0.72	0.9	0.6
03	Tabas, 1978	Tabas	0.85	-0.9	1.8
04	Kocaeli, 1999	Yarimca	0.3	1	0.6
05	Northridge, 1994	RRS	0.85	0.81	4
06	Duzce, 1999	Duzce	0.51	1	1.8
07	Northridge, 1994	NFS	0.72	-1.2	4
08	Kobe, 1995	Takatori	0.76	-0.8	5
09	Kobe, 1995	Takatori	0.76	0.9	7
10	Tabas, 1978	Tabas	0.85	-0.9	-
11	Northridge, 1994	RRS	0.85	0.81	-
12	Kobe, 1995	Takatori	0.76	-0.8	-

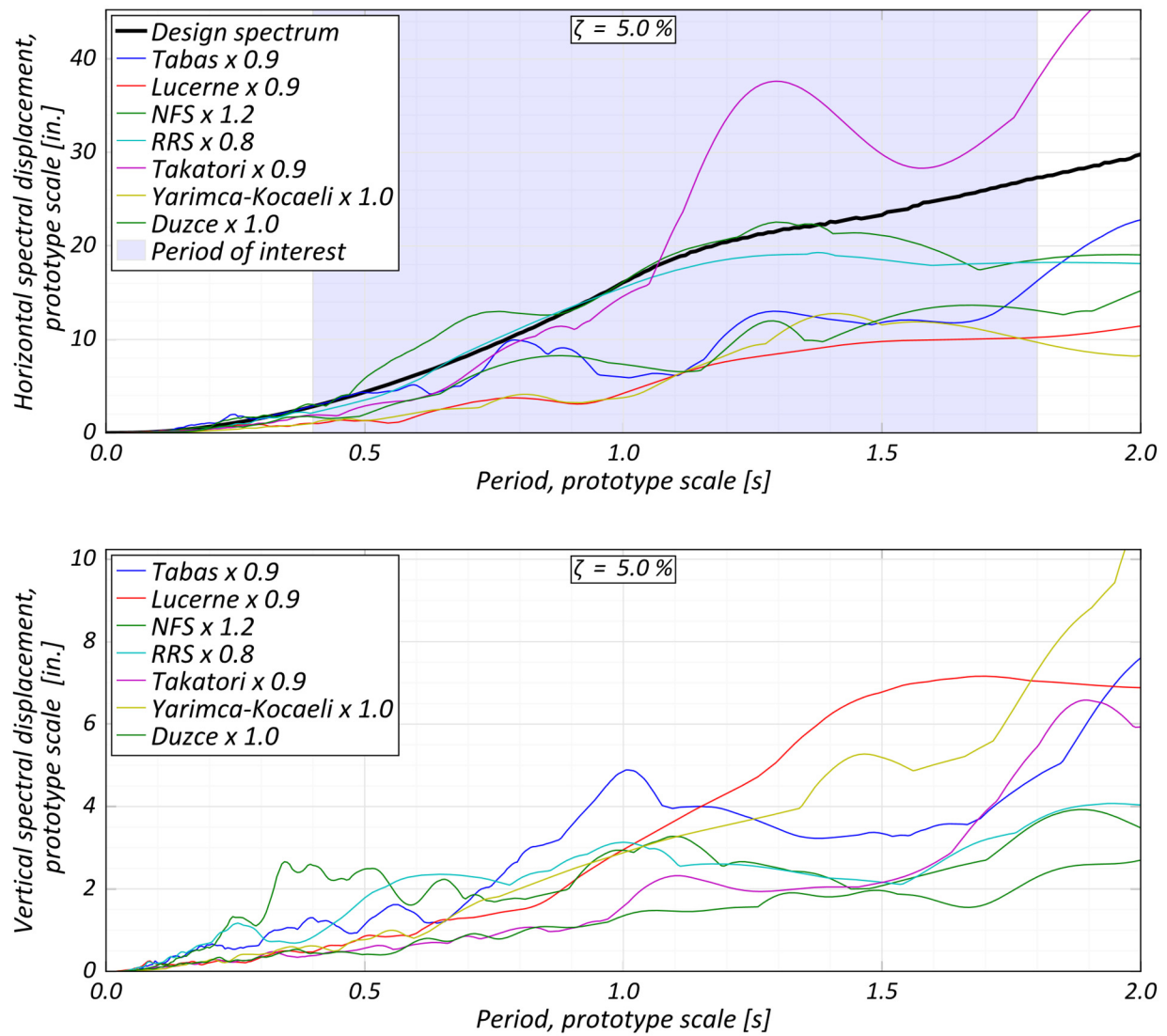


Figure 4.17 Displacement response spectra of shaking table input ground motions

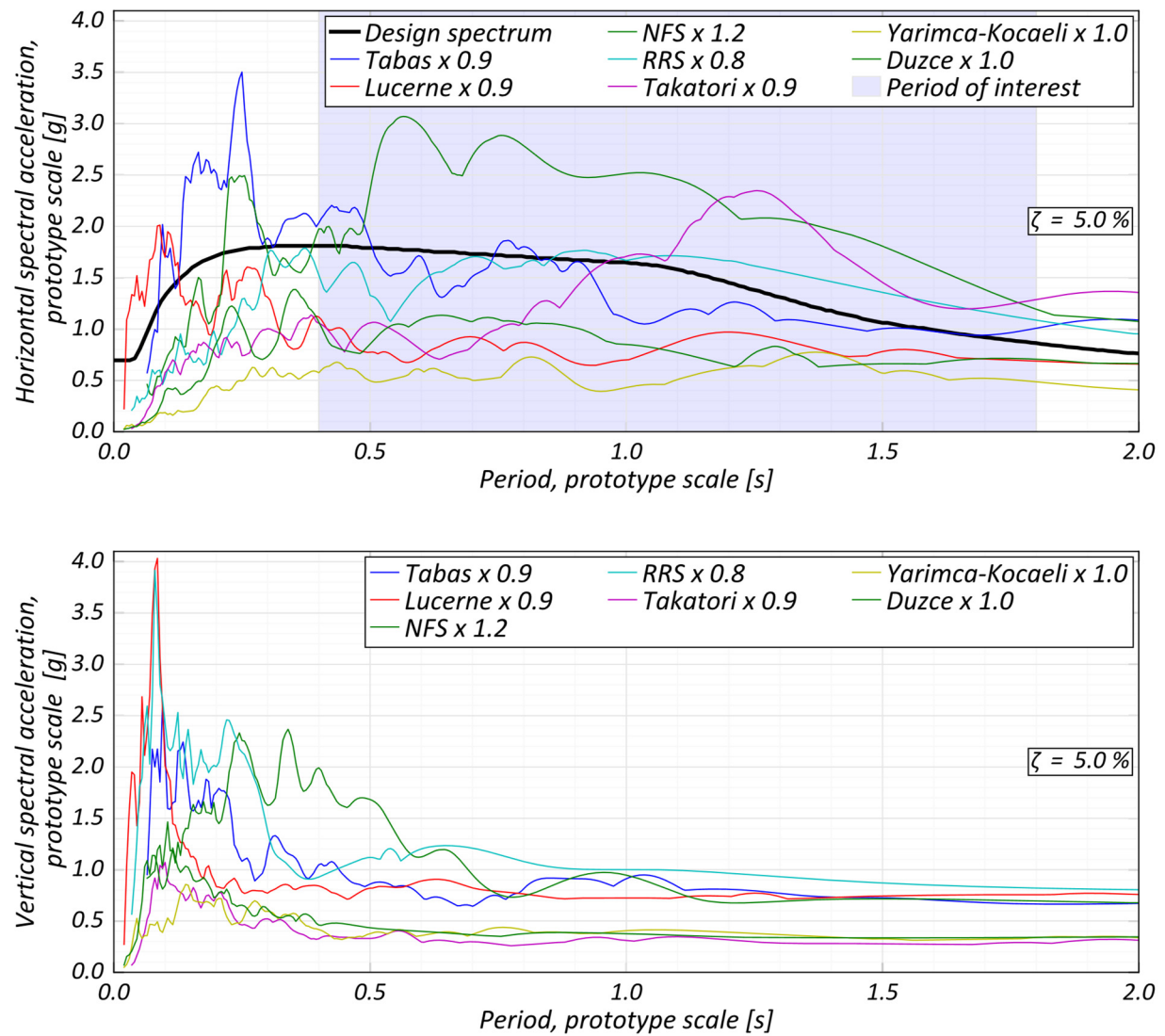


Figure 4.18 Pseudo-acceleration response spectra of shaking table input ground motions

5 Testing Results

In the test results presented below, lateral displacements have been normalized by the clear height of the columns and are expressed as drift ratios. Lateral forces have been normalized by the specimen superstructure weight, 68.1 kips, taken as the weight above half the clear height and are expressed as base-shear coefficients. Post-tensioning forces have been normalized by the ultimate force capacity of the bars (253 kips) and are expressed as a percentage of the measured ultimate stress in the prestressing bars (f_{pu} , 160 ksi). Any other non-normalized values have been scaled back to prototype space. Positive transverse drifts and accelerations are defined to be towards the south direction, whereas positive rotations are defined along the east direction.

All the results presented have been filtered through a high order (2000 point) low-pass filter with a cut-off frequency of 25 Hz. The testing took place over two days, with EQ01 to EQ04 being run on Day 1 and the remaining excitations taking place on Day 2.

5.1 LATERAL RESPONSE

The hysteretic responses seen during the tests are shown in Figure 5.1, Figure 5.2, and Figure 5.3. In each figure, a background plot in gray represents the specimen response to all the preceding excitations, and a red dot marks the specimen base shear and drift ratio at the end of the excitation.

EQ01 and EQ02 were repetitions of the same excitation, serving as a test run to check the correct behavior of the specimen and instrumentation, and to induce any settlements or cracking. This proved useful since during EQ01, the NW concrete block was found to be not seated properly and a slight twisting occurred. Additionally, the restraint frame was found to be bearing against the specimen and providing lateral resistance. Both these issues were corrected before conducting EQ02, by increasing the clamping force on the concrete mass blocks to 890 kN (200 kips) and pushing the restraint frames slightly away from the specimen. EQ02 can be seen to have a slightly softer response as compared to EQ01.

EQ03 represented an earthquake inducing mild drift demands on the specimen, with EQ04 acting as an aftershock. The hysteresis response shows a small amount of energy dissipation, indicating possible rocking at the base. From the hysteresis response of EQ03 and EQ04, it can be seen that the specimen response has softened, indicating that the concrete at the base has cracked.

EQ05 induced moderate drift demands on the specimen, with EQ06 serving as an aftershock with mild drift demands. The pinched shape of hysteresis seen in EQ05 is a characteristic of hybrid recentering systems, indicating rocking behavior under this excitation. As

expected, EQ06 and EQ03 exhibited mild ($\sim 1.8\%$) drift demands; however, comparing the responses under the two excitations shows reduced energy dissipation and softer response under EQ06.

EQ07, EQ08, and EQ09 formed the final three motions in the initial loading protocol, with increasingly greater demands. The direction of each excitation was carefully chosen to avoid larger drifts on only one side of the specimen. The response under EQ08 and EQ09 demonstrated that the specimen maintained its recentering behavior under the large demands imposed. The peak force seen under EQ09 was slightly smaller than that under EQ08, indicating a small loss in force capacity resulting from the yielding of the prestressing bars.

Since the specimen response under EQ09 suggested little damage, it was decided to impose additional ground motions until dissipator bar fracture was observed. EQ10, EQ11, and EQ12 were repetitions of EQ03, EQ05, and EQ08 with reversed polarities, and bar fractures were indicated by popping sounds heard during EQ11 and EQ12. The consequence of prestress loss and bar fracture is evident in the hysteretic response: the drifts in EQ10 and EQ11 are noticeably larger than EQ03 and EQ05, and while EQ12 has similar drifts to EQ08, the base shear is considerably smaller.

Table 5.1 lists the peak and residual drifts recorded during the different excitations. Figure 5.4 shows a graphical representation of these quantities. Table 5.1 also lists the rotations measured at the rocking interfaces of the south column, which are shown graphically in Figure 5.5(a) and (b). The recentering behavior of the system is evident in the residual drifts and rotations seen at the end of each motion. The rotations at the column top are slightly smaller than at the bottom; this can be attributed to the effect of the column self-weight, which resulted in higher shear and moment at the bottom. Additionally, the column base rotation time histories for EQ08 and EQ09 are shown in Figure 5.6: the rotation response closely follows the drift response, indicating that the column behaved nearly like a rigid body over the clear height.

The prestressing forces measured during the tests in each of the two bars are presented in Table 5.2 and Figure 5.7. Additionally, the stress-strain response measured during EQ08 and EQ09 are shown in Figure 5.8 (a) and (b), where the bar behaviors show light yielding. It is likely that the yielding is concentrated at the rocking interfaces, resulting from the potential development of “kinks” or yield curvatures at these locations.

The maximum and residual gap opening at the bottom interface of the south column at the north and south faces is shown in Figure 5.17, Figure 5.18, Figure 5.19, and Figure 5.20. Also shown below each face is the overall specimen deformation at the instance of maximum gap opening in that face, with the corresponding drift listed in the sub-caption. The rocking interface naturally forms at the location of the strip removed from the column outer shell, and the gap closes completely at the end of each excitation, with only minor spalling seen in EQ08.

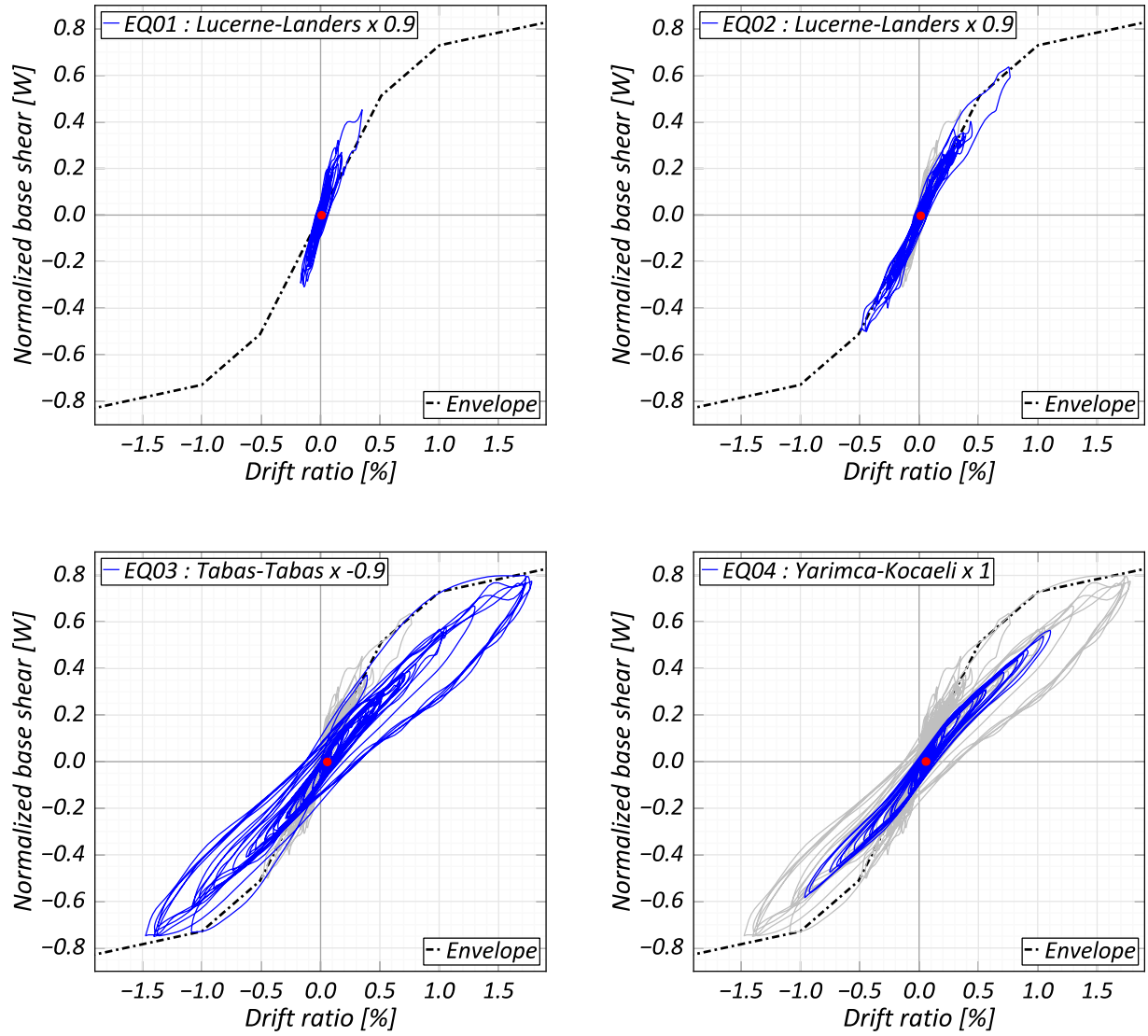


Figure 5.1 Hysteretic responses on Day 1 of testing.

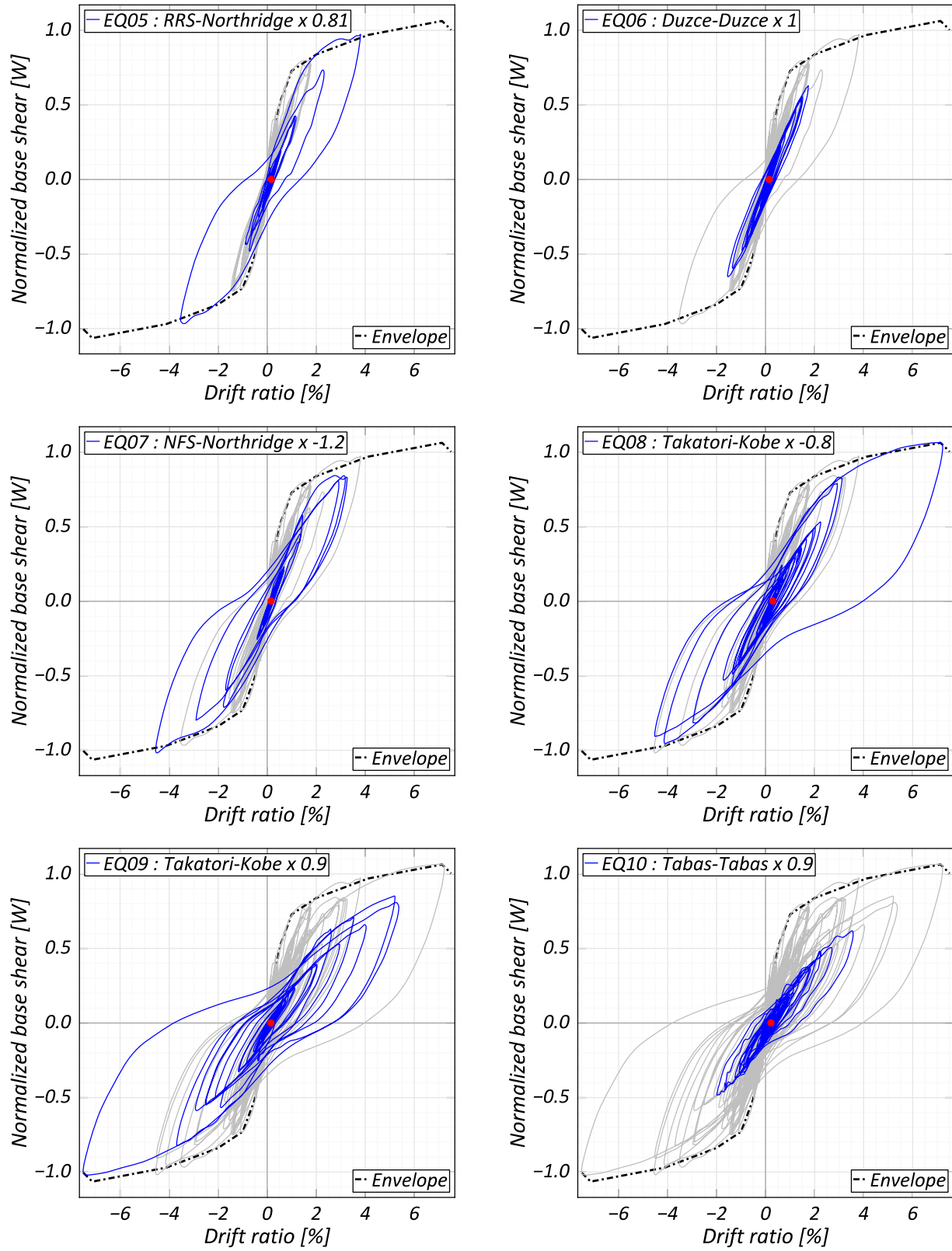


Figure 5.2 Hysteretic responses on Day 2 of testing.

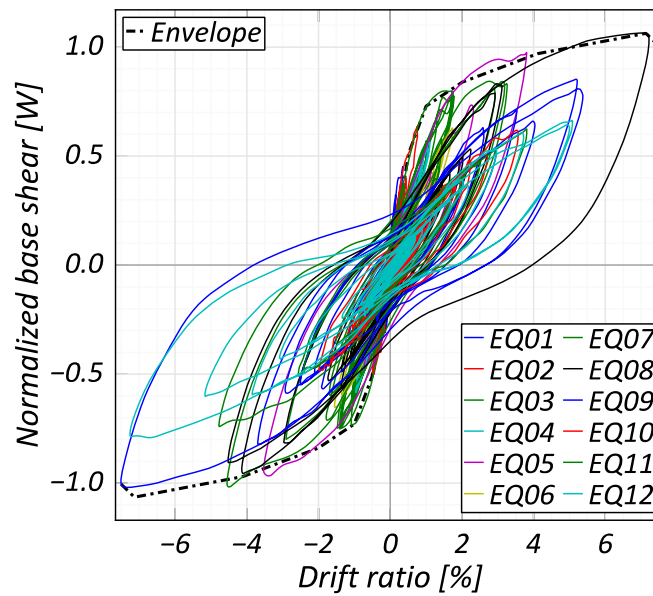
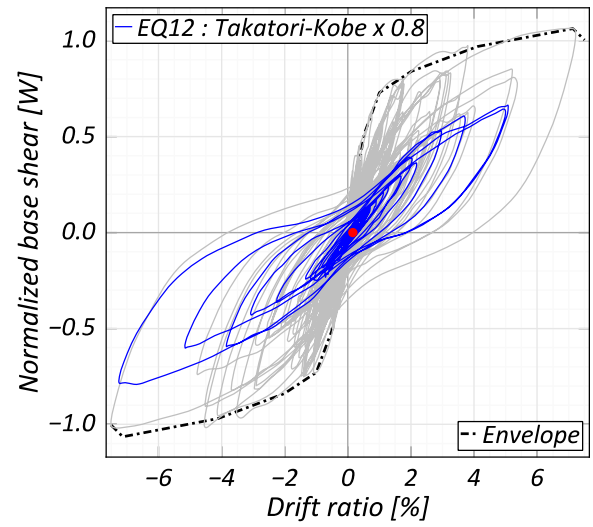
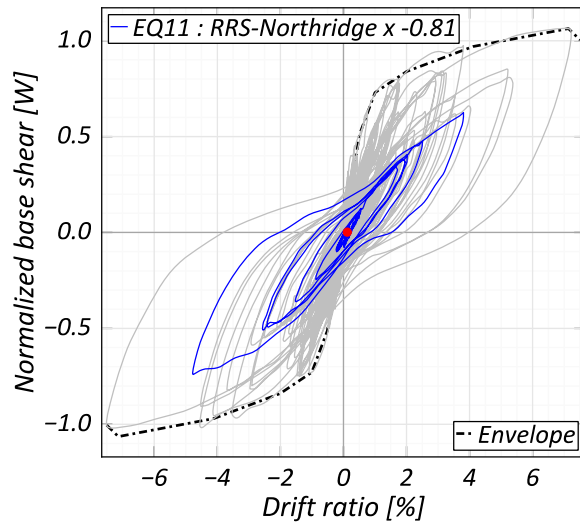


Figure 5.3 Overlaid hysteretic responses.

Table 5.1 Summary of transverse drift and south column interface rotation response.

Excitation	Drift ratio (%)		Bottom rotation (%)		Top rotation (%)	
	Peak	Residual	Peak	Residual	Peak	Residual
EQ01	0.35	0.01	0.26	0.007	0.25	0.006
EQ02	0.77	0.01	0.66	0.026	0.59	0.005
EQ03	1.78	0.06	1.60	0.068	1.45	0.028
EQ04	1.11	0.06	0.99	0.070	0.88	0.031
EQ05	3.81	0.16	3.51	0.160	3.28	0.114
EQ06	1.74	0.15	1.60	0.139	1.44	0.094
EQ07	4.55	0.15	4.29	0.135	4.16	0.104
EQ08	7.22	0.30	6.75	0.249	6.44	0.171
EQ09	7.51	0.15	7.16	0.111	7.00	0.055
EQ10	3.57	0.22	3.28	0.178	3.09	0.118
EQ11	4.78	0.12	4.57	0.083	4.39	0.032
EQ12	7.26	0.16	6.98	0.133	6.73	0.058

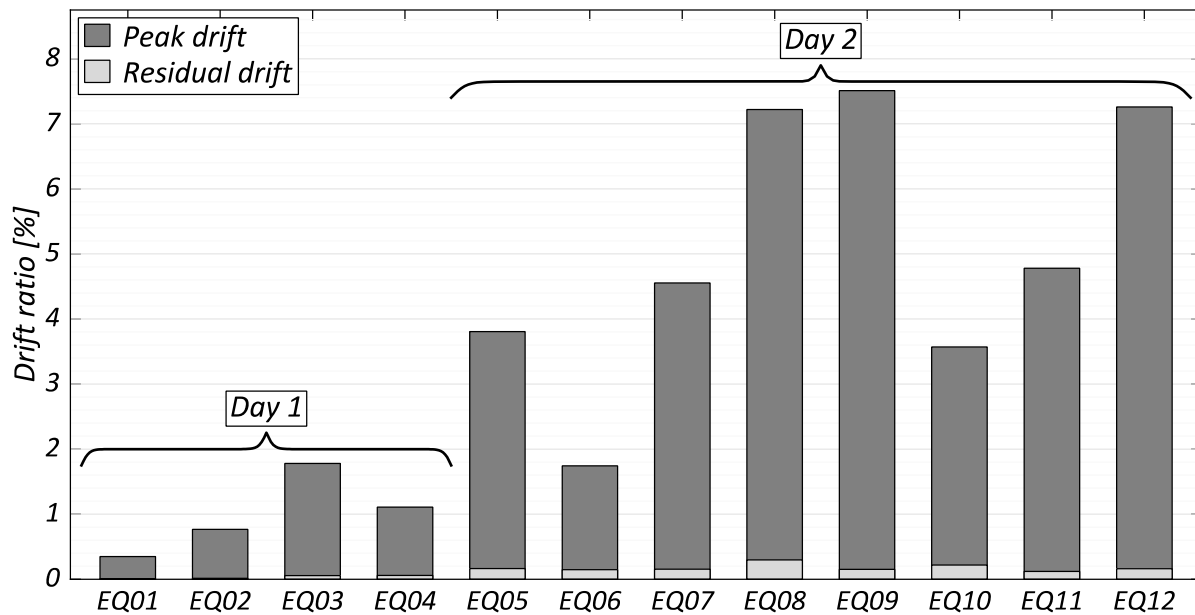
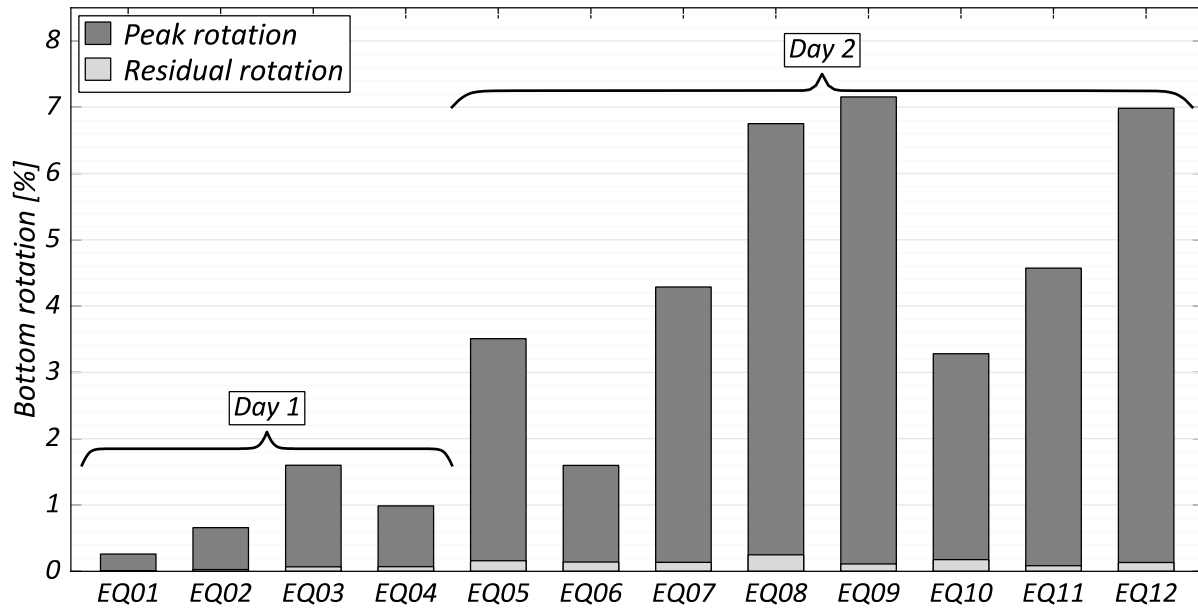
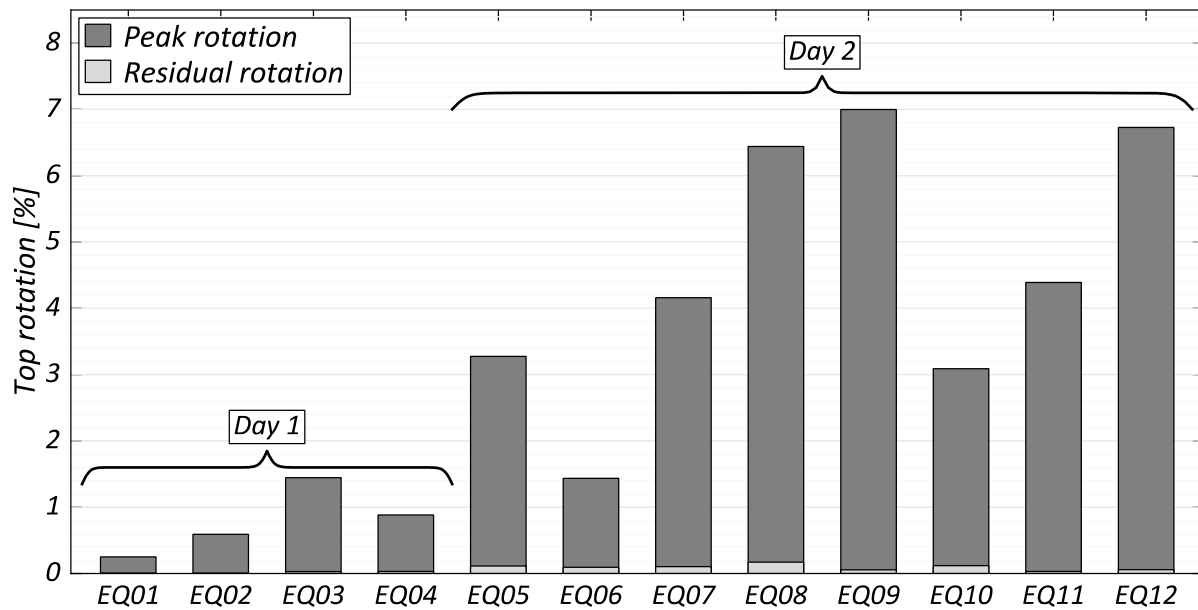


Figure 5.4 Peak and residual transverse drifts.



(a)



(b)

Figure 5.5 Peak and residual column interface rotations: (a) south column bottom; and (b) south column top.

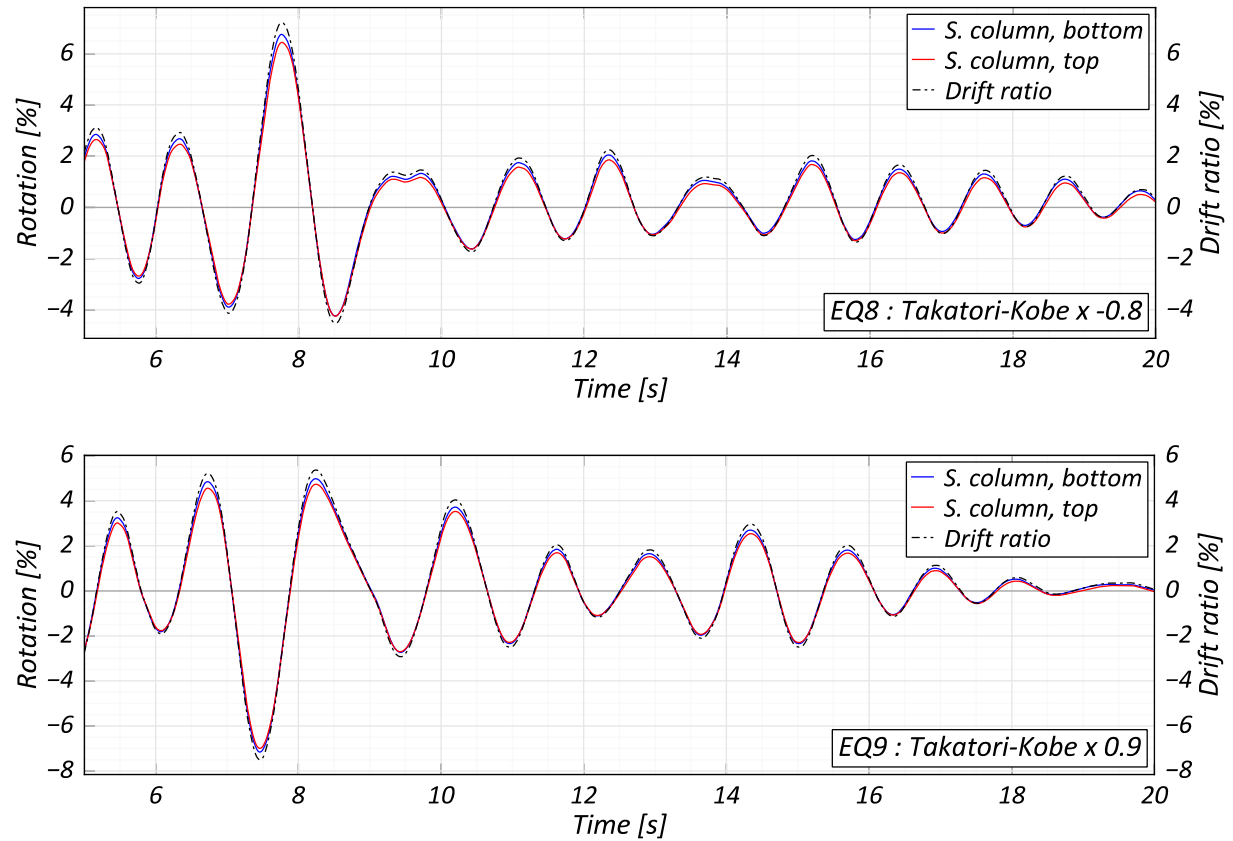


Figure 5.6 Column base rotations seen in EQ08 and EQ09.

Table 5.2 Summary of peak and residual prestressing ratios.

Excitation	Peak stress ($\%f_{pu}$)		Residual stress ($\%f_{pu}$)	
	North bar	South bar	North bar	South bar
EQ01	39.5	38.2	37.9	37.3
EQ02	42.2	40.0	37.8	37.1
EQ03	50.0	47.4	37.7	36.9
EQ04	44.5	43.3	37.7	36.8
EQ05	64.5	64.1	36.8	35.3
EQ06	47.5	46.8	36.7	35.1
EQ07	64.9	70.5	37.3	33.9
EQ08	84.2	70.0	30.9	31.1
EQ09	71.7	81.6	28.5	23.6
EQ10	50.8	37.5	28.5	23.4
EQ11	53.4	58.1	28.6	23.7
EQ12	65.1	76.1	28.2	22.8

5.2 STRAIN MEASUREMENTS

The strain time history measured during EQ05 from one dissipator bar in each of the two columns is shown in Figure 5.9. Also marked in the time history is the point of peak strain rate. Note: the strain rate value is given in specimen time since the strain rate plays an essential role in the modeling of the specimen and will be revisited in the next chapter. Strain data from the dissipators is not available beyond EQ05. The majority of the strain gauges installed on the dissipators ceased functioning at the end of Day 1 of testing, and the remaining strain gauges failed during EQ06. A similar strain history for the prestressing bars from EQ09 is presented in Figure 5.10.

The peak circumferential strains measured in the steel shell near the rocking interfaces of the south column are tabulated in Table 5.3. A comparison of the values to the stress-strain response seen for the shell material shows that the shell exhibited some local plastic deformations under EQ08. The strain history for this earthquake is presented in Figure 5.11. Note that the marked yield line corresponds to the 0.2% offset yield strain, while the nonlinear material response begins at a significantly smaller strain value of 1 milli-strain.

The longitudinal strain histories measured during EQ09 in the corrugated metal pipe forming the foundation socket of Column 1 are shown in Figure 5.12. The measured strain values are small and predominantly in compression. The compression measurements likely result from Poisson effects caused by the circumferential elongation of the CMP under increased column compression and socket compressive stresses.

The strain history from one of the hanger reinforcement bars in the bent cap is shown in Figure 5.13. From the small strain values seen, it can be concluded that this reinforcement is not necessary, and the CMP socket connection is likely sufficient for transferring the vertical forces.

Table 5.3 South column shell circumferential strain.

Excitation	North face strain (%)		South face strain (%)	
	Bottom	Top	Bottom	Top
EQ01	-0.014	0.017	-0.006	-0.017
EQ02	0.027	0.037	0.020	0.014
EQ03	0.064	0.067	0.075	-0.024
EQ04	0.056	0.041	0.054	-0.030
EQ05	0.120	0.178	0.138	-0.044
EQ06	0.081	0.115	0.085	0.023
EQ07	0.136	0.151	0.138	0.043
EQ08	0.127	0.403	0.315	0.062
EQ09	0.218	0.371	0.327	0.110
EQ10	0.135	0.322	0.276	0.078
EQ11	0.175	0.325	0.286	0.109
EQ12	0.211	0.347	0.320	0.148

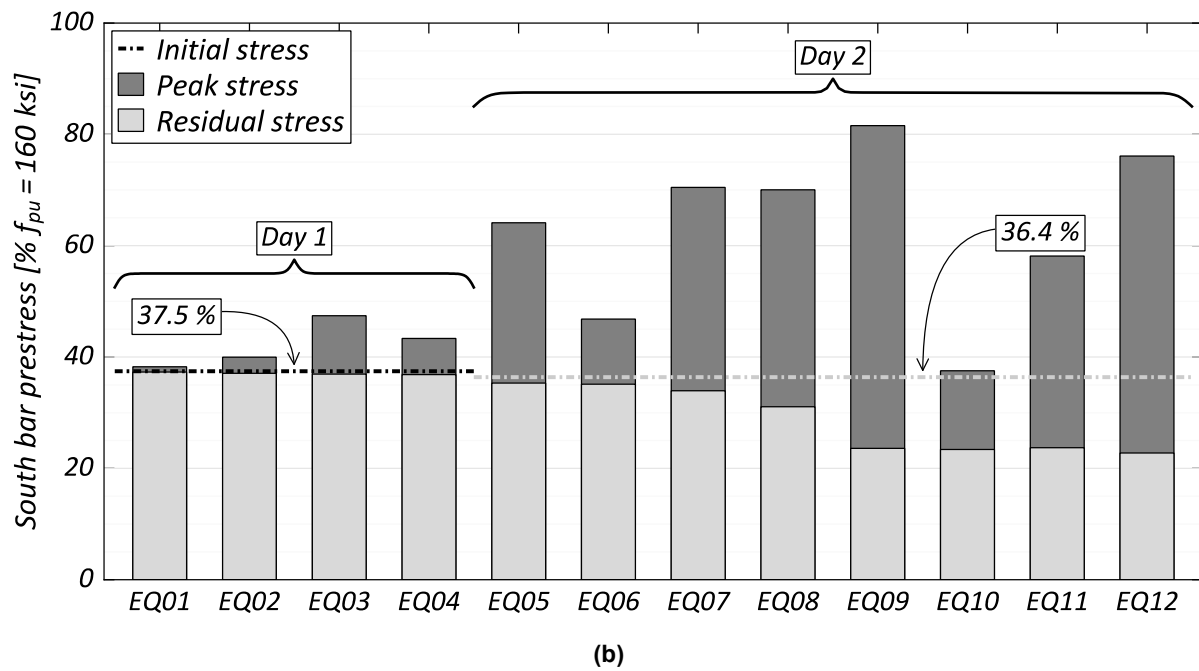
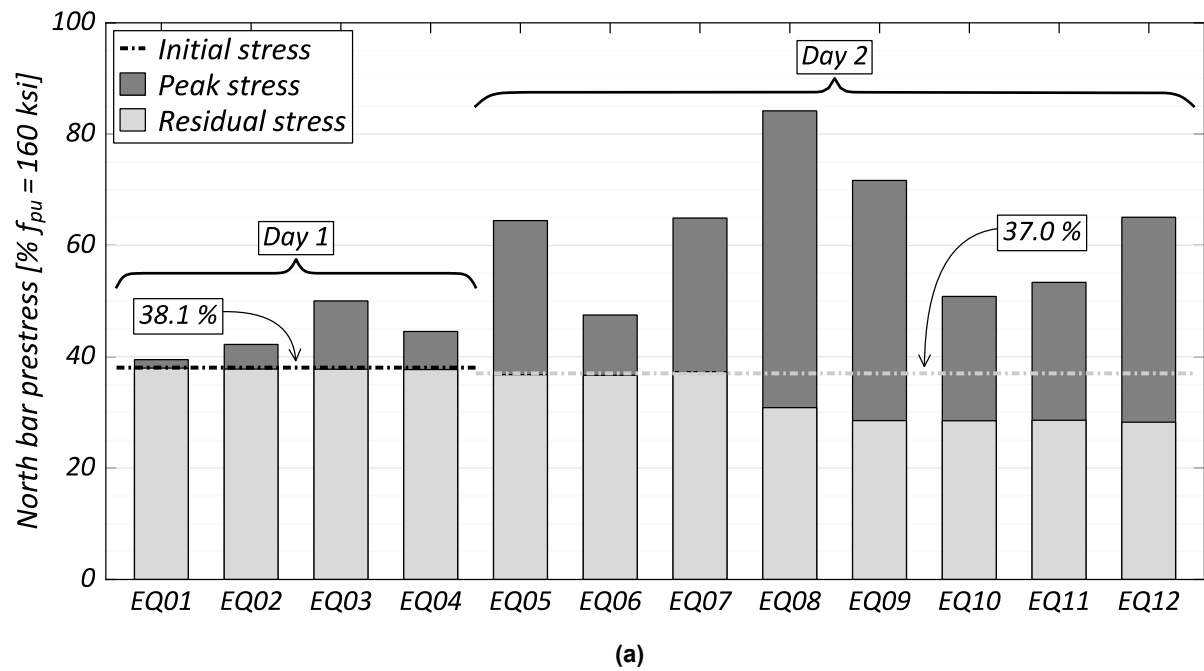
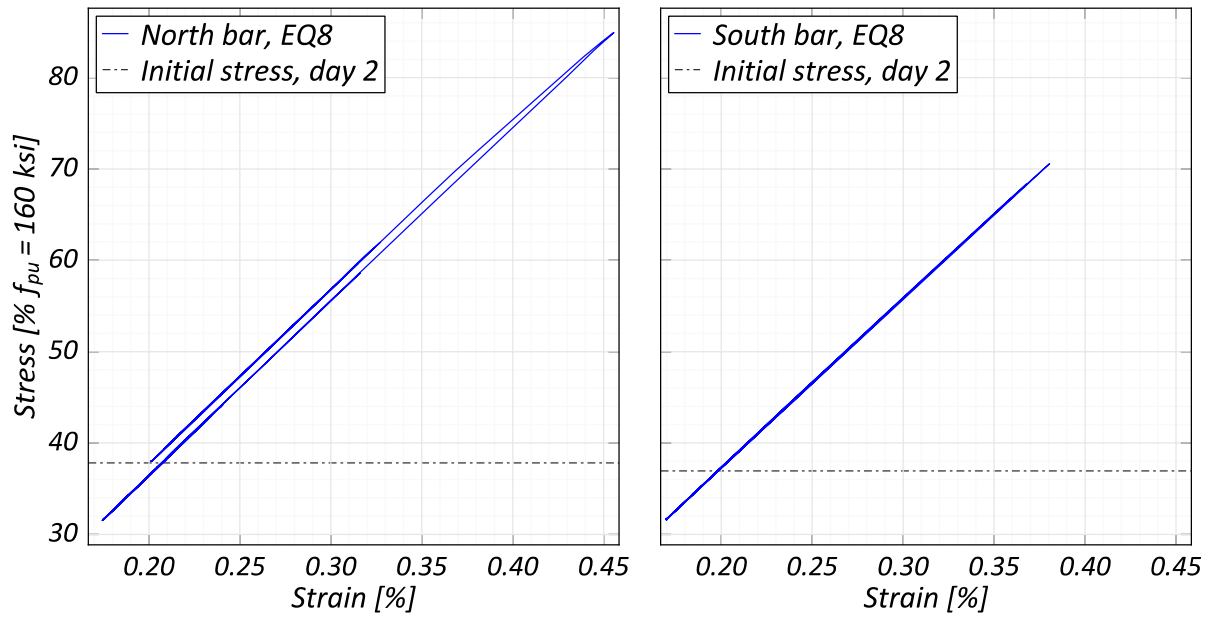
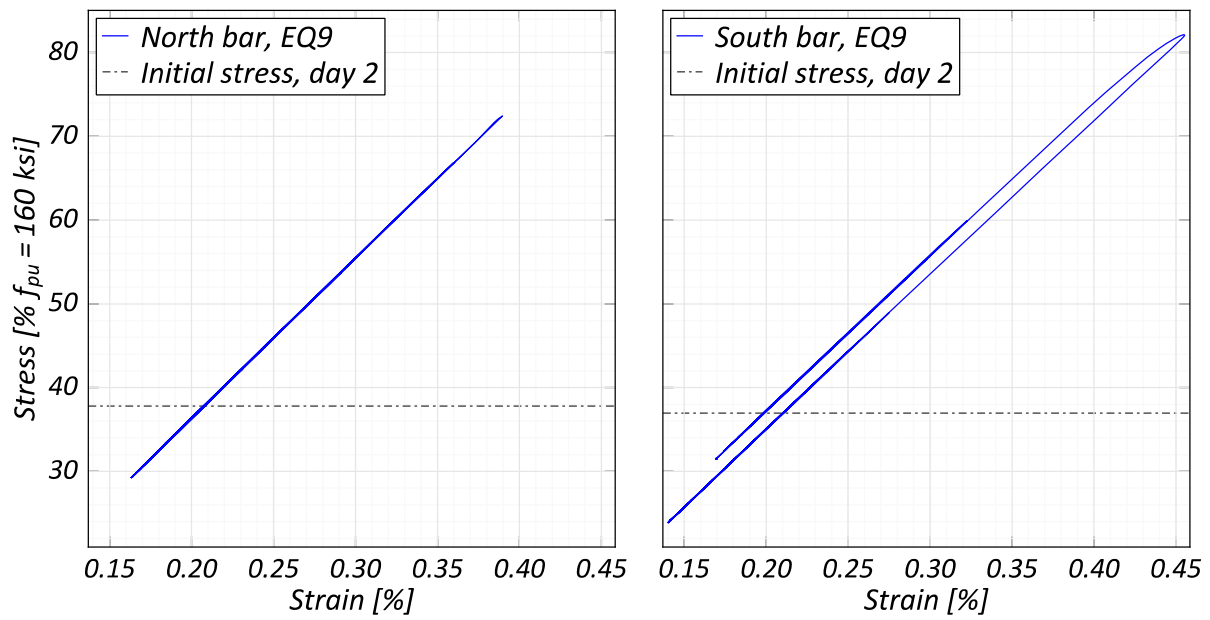


Figure 5.7 Peak and residual prestress ratios: (a) north bar; and (b) south bar.



(a)



(b)

Figure 5.8 Stress-strain behavior of prestressing bars: (a) EQ08; and (b) EQ09.

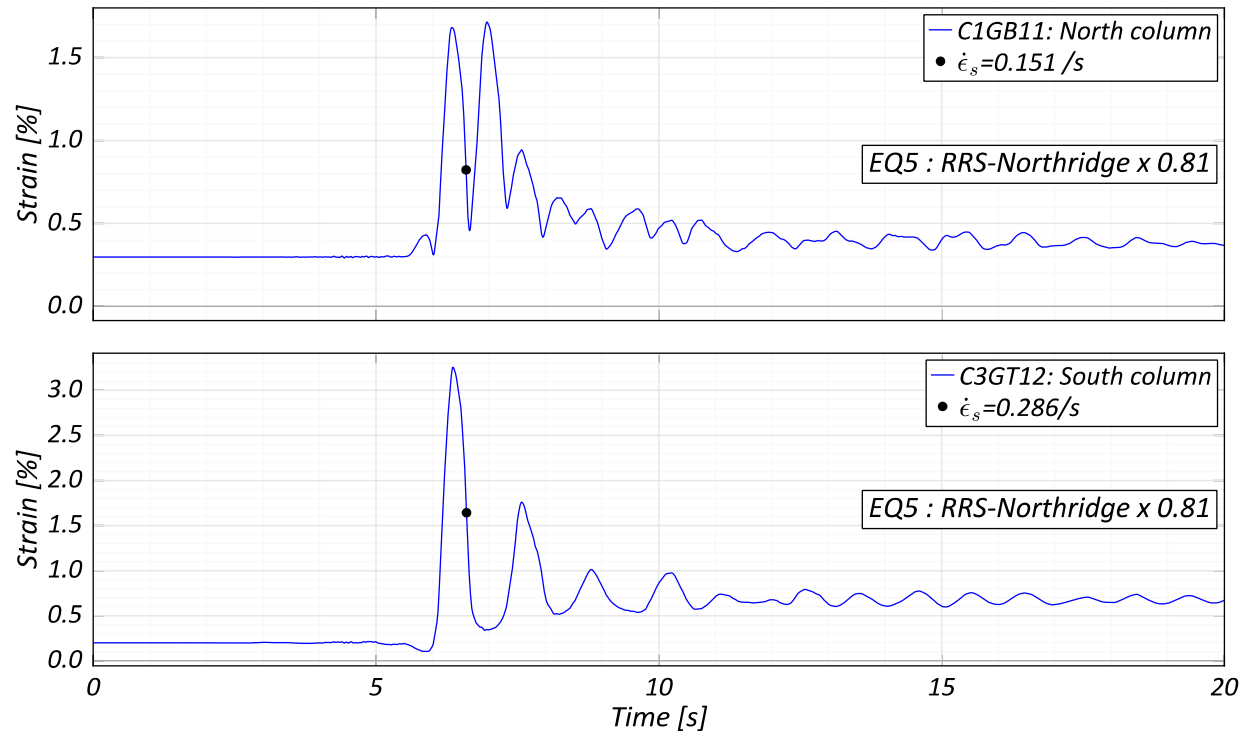


Figure 5.9 EQ5 energy dissipator strain history.

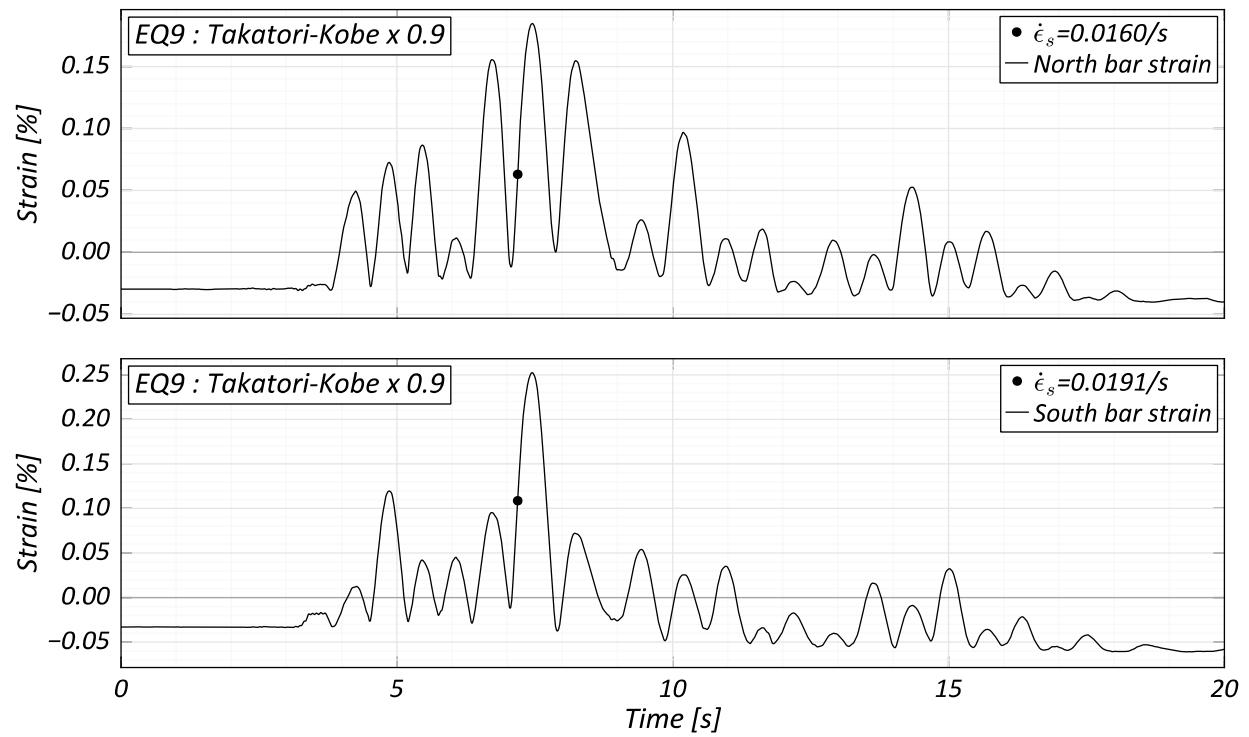


Figure 5.10 EQ9 prestressing bar strain history.

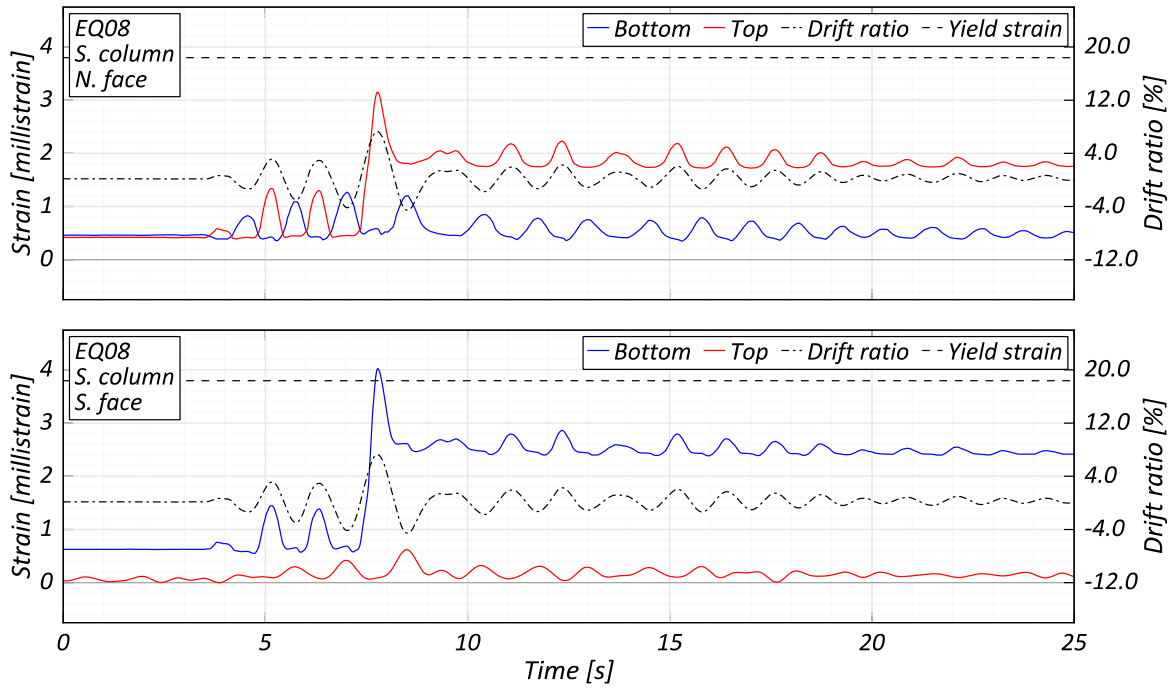


Figure 5.11 EQ08 shell strain history, south column.

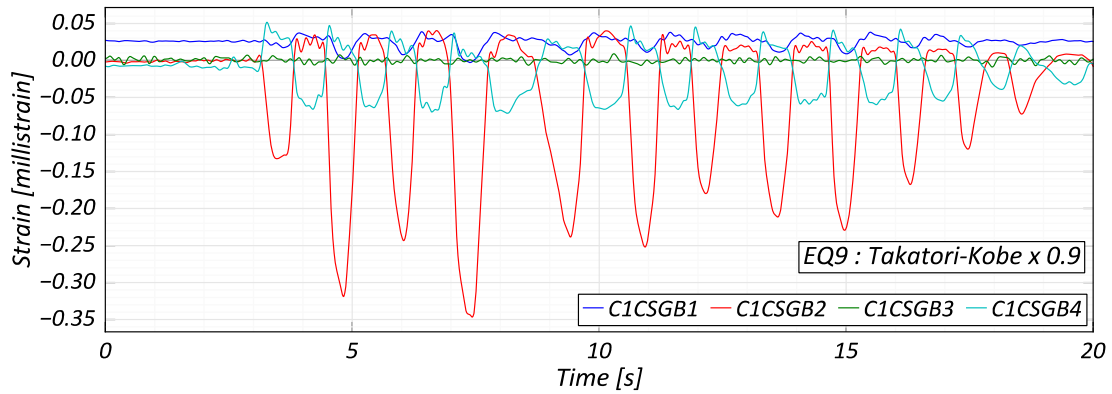


Figure 5.12 EQ09 corrugated metal pipe strain history.

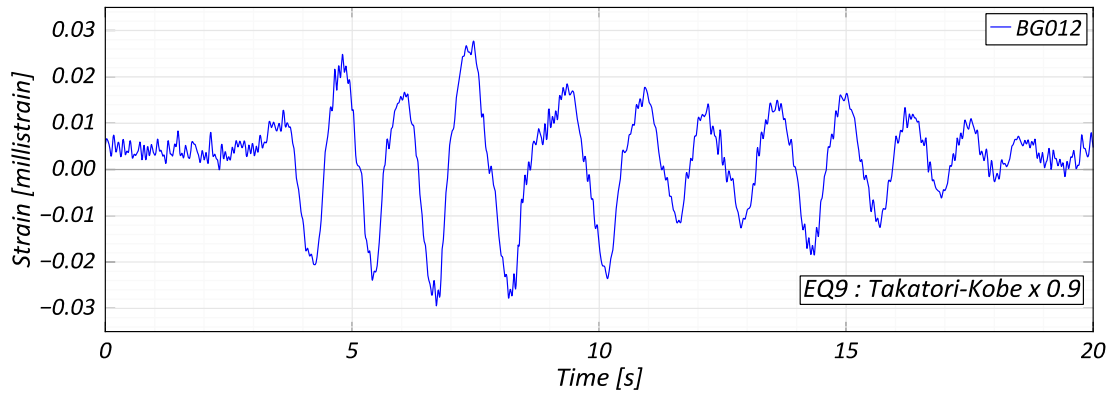


Figure 5.13 EQ09 bent cap hanger reinforcement strain history.

5.3 VERTICAL RESPONSE

A plot showing the vertical acceleration (measured positive upwards) vs. drift ratio for all the excitations is shown in Figure 5.14, where there is generally no correlation seen between the total vertical force and lateral drift in the system. EQ05 and EQ07 are the only two excitations that show peaks in vertical acceleration at larger drifts; their hysteretic response, vertical acceleration vs. drift and the vertical acceleration time histories at the foundation and cap beam are presented in Figure 5.15 and Figure 5.16, respectively. The point at the peak vertical acceleration (at large drifts) is marked in all responses for each excitation.

A comparison of the vertical and horizontal responses shows that such a peak in vertical acceleration occurs at the same time as a dip or a “kink” in the base-shear drift response caused by a sudden increase in the axial load and, hence, the P-delta forces in the specimen. Looking at the time histories of the vertical acceleration, it can be seen that such a peak is not caused by the peak input acceleration either: for EQ05, the noted peak occurs at input vertical accelerations, which are much smaller than the vertical peak ground acceleration (PGA). It is likely that such peaks occur as a result of the interplay between the frequency content of the input motion and the modal properties of the specimen.

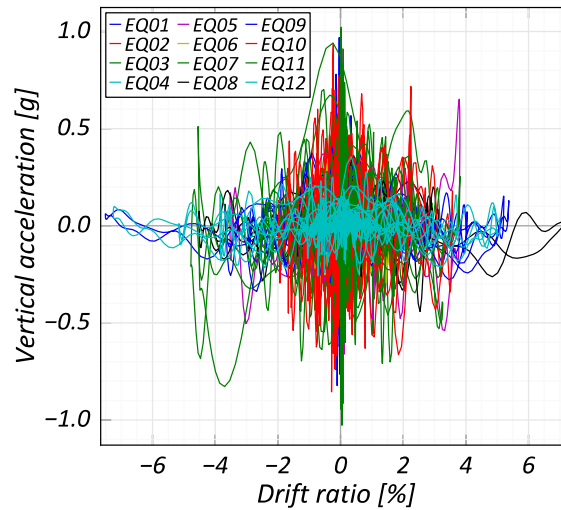


Figure 5.14 Vertical acceleration vs. drift ratio.

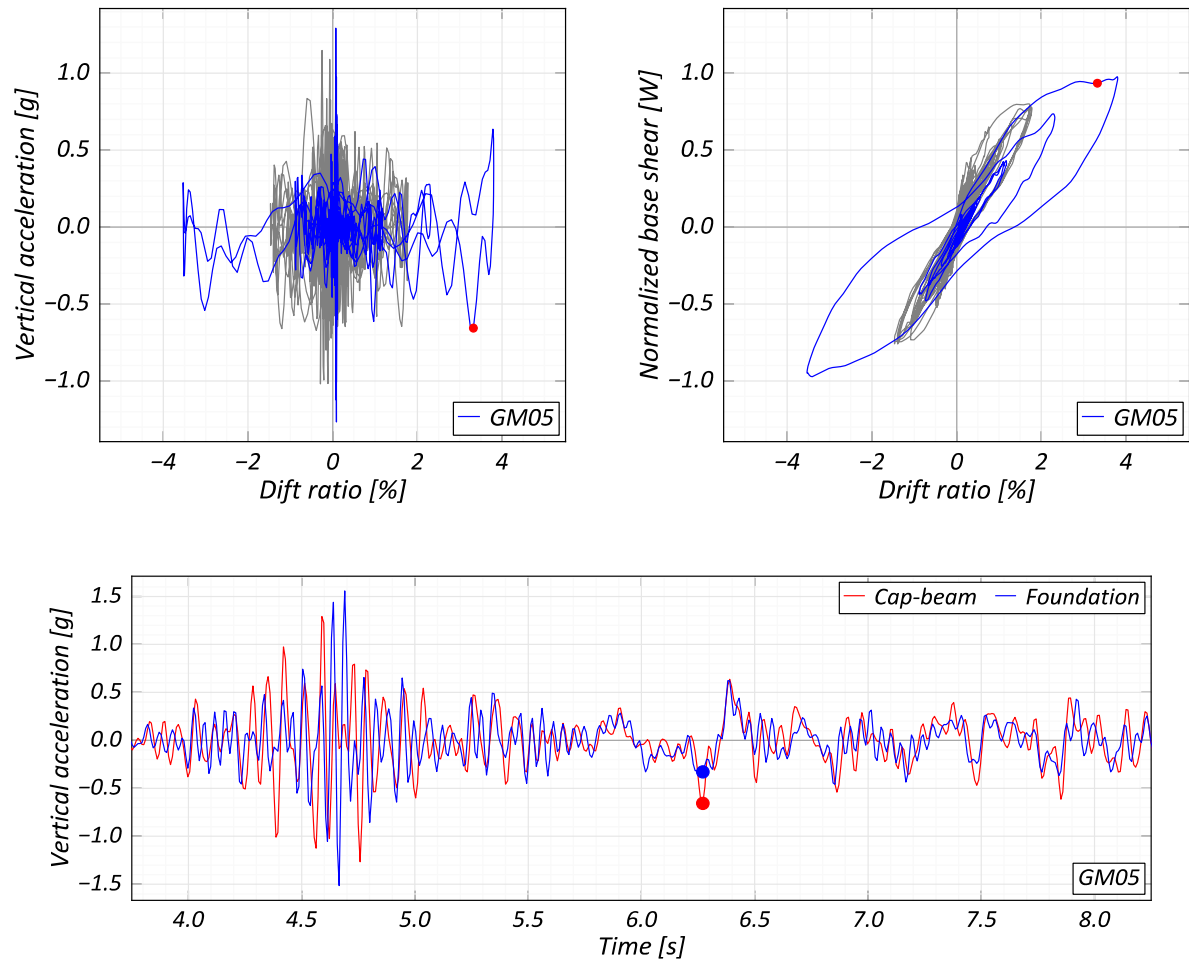


Figure 5.15 EQ05 vertical and horizontal response, and vertical acceleration time history.

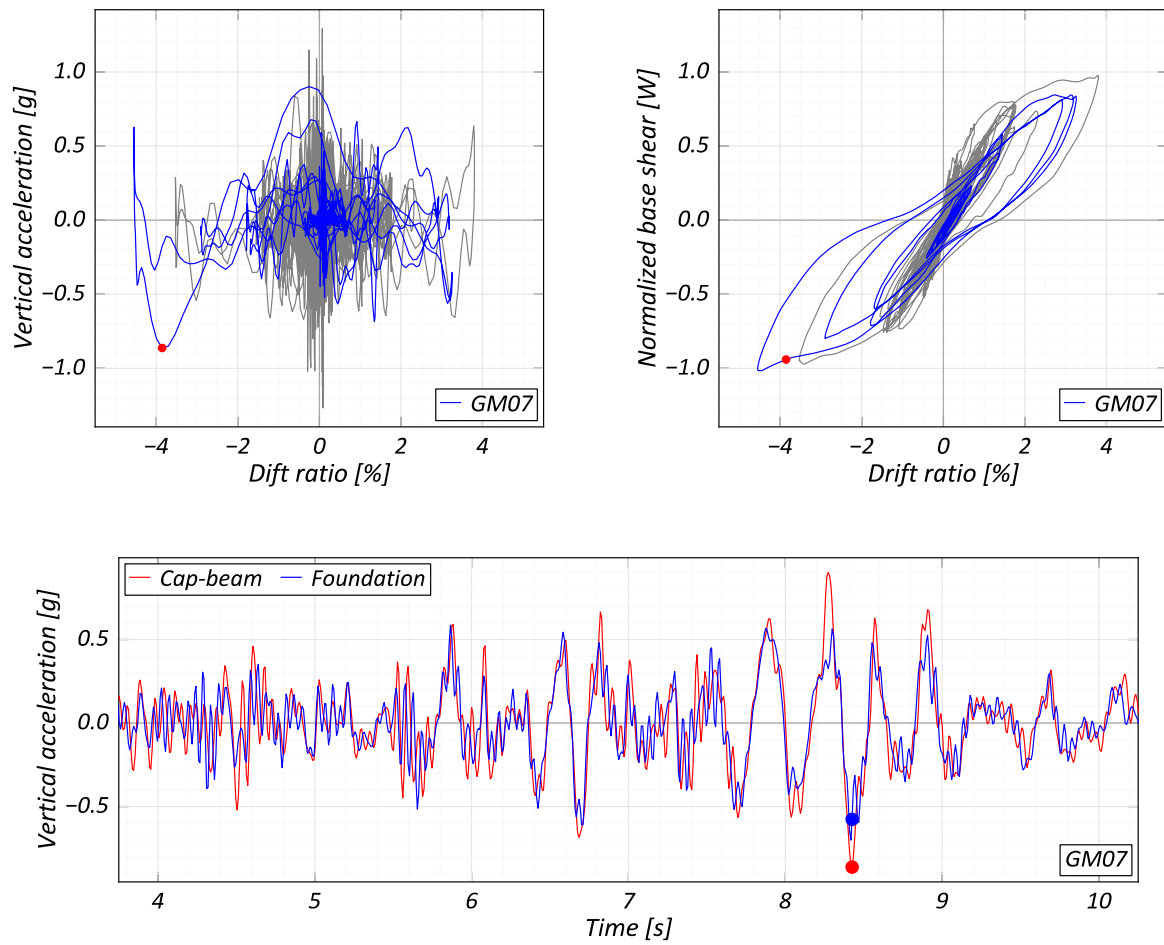


Figure 5.16 EQ07 vertical and horizontal response, and vertical acceleration time history.



(a)



(b)



(c)



(d)



(e)



(f)

Figure 5.17 EQ05 specimen response at peak drifts: (a) south column interface, north face, $\Delta = 3.8\%$; (b) south column interface, south face, $\Delta = -3.5\%$; (c) south column, interface, north face, end of excitation; (d) south column interface, south face, end of excitation; (e) specimen deformation @ $\Delta = 3.8\%$; and (f) specimen deformation @ $\Delta = -3.5\%$.



(a)



(b)



(c)



(d)



(e)



(f)

Figure 5.18 EQ07 specimen response at peak drifts: (a) south column interface, north face, $\Delta = 3.2\%$; (b) south column interface, south face, $\Delta = -4.5\%$; (c) south column, interface, north face, end of excitation; (d) south column interface, south face, end of excitation; (e) specimen deformation @ $\Delta = 3.2\%$; and (f) specimen deformation @ $\Delta = -4.5\%$.



(a)



(b)



(c)



(d)



(e)



(f)

Figure 5.19 EQ08 specimen response at peak drifts: (a) south column interface, north face, $\Delta = 7.2\%$; (b) south column interface, south face, $\Delta = -4.5\%$; (c) south column, interface, north face, end of excitation; (d) south column interface, south face, end of excitation; (e) specimen deformation @ $\Delta = 7.2\%$; and (f) specimen deformation @ $\Delta = -4.5\%$.



(a)



(b)



(c)



(d)



(e)



(f)

Figure 5.20 EQ09 specimen response at peak drifts: (a) south column interface north face, $\Delta = 5.4\%$; (b) south column interface, south face, $\Delta = -7.5\%$; (c) south column, interface, north face, end of excitation; (d) south column interface, south face, end of excitation; (e) specimen deformation @ $\Delta = -5.4\%$; and (f) specimen deformation @ $\Delta = -7.5\%$.

6 Numerical Model Calibration

Presented in this chapter are the details and results from two numerical models: the pre-test model, which is based on the prototype model used for determination of column-column on-center distance with updated as-measured monotonic material and geometric properties; and the post-test model, which includes additional updates based on the observed experimental results, e.g., utilization of dynamic material properties, modified damping, and improved modeling of prestressing bars. Both models were created in OpenSees [Mazzoni et al. 2007; McKenna et al. 2010].

6.1 MODEL DETAILS

A sketch of the main model components, overlaid on top of the specimen elevation view, is shown in Figure 6.1. The central height of each column was modeled using multiple beam-column elements in series, connected to displacement-based beam-column elements (DBE) at each end, which represent the rocking interfaces. The debonded dissipator bars were also modeled using DBE, with one element for modeling all the dissipators at each interface. Prestressing bars were modeled using nonlinear truss elements with applied initial stresses as measured at the beginning of the test. The ends of the rocking interface, energy dissipators, and the PT bars in the foundation were modeled as fixed ground nodes where their ends in the bent cap are connected, using stiff elastic elements modeling the bent cap, to a central point at half the bent-cap depth and equidistant from both columns.

6.1.1 Column

Each column was modeled using three beam-column elements connected in series. The central element, which was modeled using a four (4) integration point force-based beam-column element (FBE), represents the composite column section with the confined concrete, the bonded steel reinforcing bar, and the outer steel shell. The end elements represent the concrete between the rocking interface and the effective anchorage point of the debonded energy dissipators in the specimen clear height. These elements were modeled without any steel to represent the lack of bond between the concrete and either the dissipator or shell steel, and to represent the fact that the shell does not transfer any compression at the interface (resulting from the strip removed from the shell at the interface). The DBE with two integration points were used to model these elements to ensure stable performance: the concrete-only sections were found to lead to instabilities when using FBE due to the inherent lack of tensile strength.

The concrete was modeled using the *Concrete02* material model [Yassin 1994], with confined concrete behavior calculated based on the recommendations of Chang and Mander [1994]. The steel for the bonded reinforcement and the outer shell was modeled using the same *Steel02* material hysteretic rule [Filippou et al. 1983], based on the Giuffr -Menegotto-Pinto model [Mengotto and Pinto 1973], and calibrated against the measured material response of the mild steel reinforcing bars. The two material models are compared against the measured/calculated material response in Figure 6.2 and Figure 6.3.

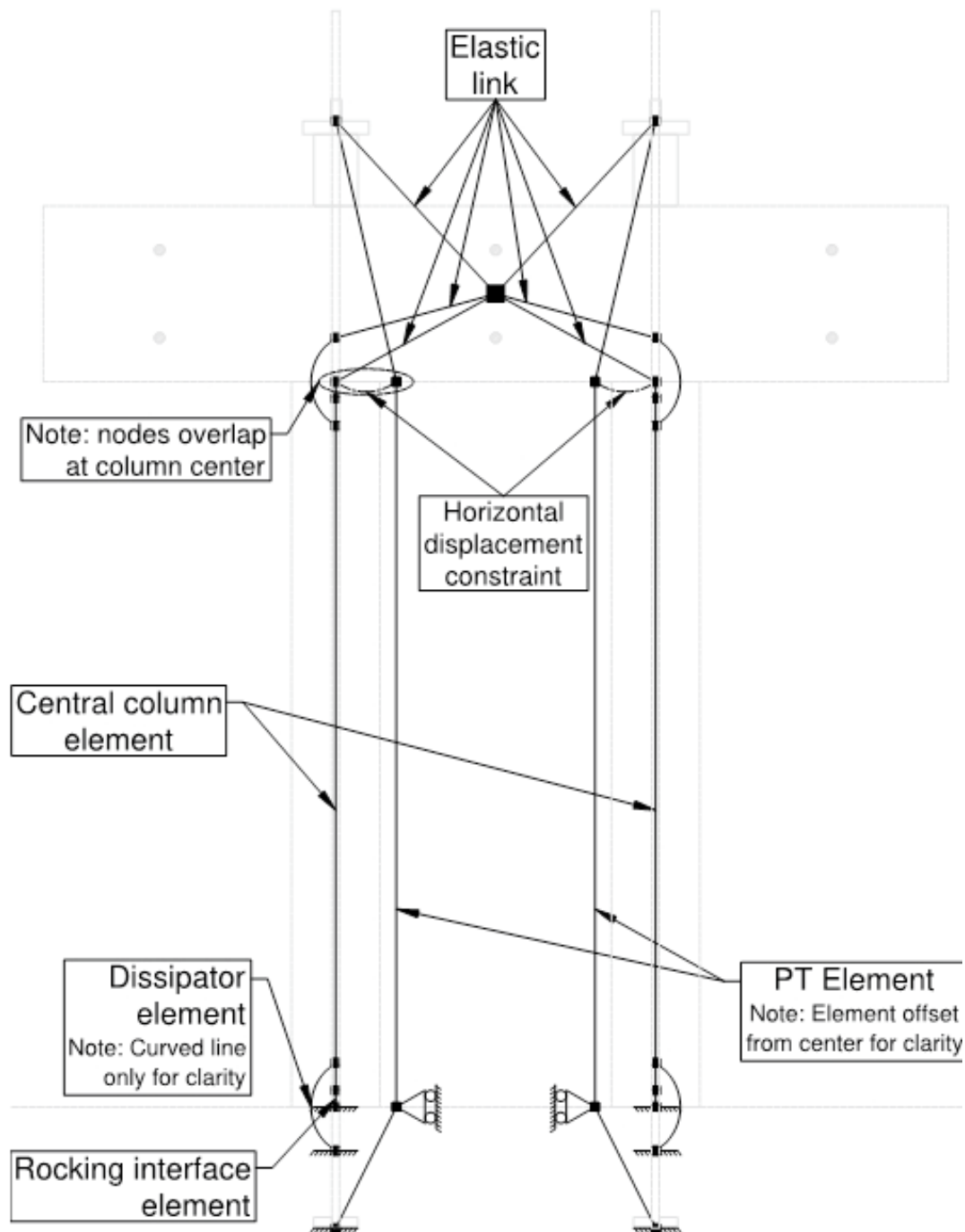


Figure 6.1 Model overlaid over specimen.

6.1.2 Rocking Interface

The rocking interfaces were modeled using DBE with two integration points, in accordance with the models presented in Chapter 3. The height of the element is set to be 2.0 in.; this height was selected to approximately model the spread of crack opening as seen during the test, e.g., in Figure 5.20(a) and (b).

Since the rocking interface was monolithic with the rest of the column, the material model used is similar to that of the confined concrete in the columns: the *Concrete02* rule was again used, with the concrete strength set to be the same as that for the column concrete; however, the strains were amplified by twice the ratio of the theoretical neutral axis depth (approximately 4 in., 0.25 times the column diameter) to the height of the element. This transformation was done to approximately capture the spread of inelastic behavior within the column, both above and below the interface, and assumed to extend uniformly for a length equal to the neutral axis depth from the interface [Restrepo and Rahman 2007].

6.1.3 Prestressing Bars

The prestressing bars were modeled using nonlinear corotational truss elements, connecting to a point located at the anchors inside the foundation and a point at the anchor location above the load cells on top of each column. The bars were split into three segments, with the end segments modeling the bars inside the foundation/bent cap, and the central segment modeling the bars inside the column. To approximately model the bar behavior expected at these locations, the nodes connecting the segments were restrained from having the same horizontal and rotational displacement as the closest rocking interface node.

The *Steel02* hysteretic rule was used to model the stress–strain behavior of the bars, with the material parameters calibrated against the measured bar response. The material behavior used for the PT bars is compared to the measured response in Figure 6.4. Initial stresses of 38% f_{pu} and 37.6% f_{pu} were applied to the north and south bars, respectively, to simulate the measured initial prestresses at the beginning of testing.

6.1.4 Energy Dissipators

Energy dissipators were modeled using a single, two integration point DBE for the ten (10) debonded reinforcement bars at each rocking interface. One end of these elements connects to the central element of the column, while the other end is either fixed to the ground or connected to the bent cap geometric center using stiff elastic element.

The length of these elements was selected to represent the debond length of 6 in. as well as the bar development length ($10d_b$, 5 in.) on either side of the interface to model bond-slip outside of the debonded portion of the reinforcing bars. Each element is located such that half its length is above and half below the interface. Finally, the material properties used for modeling of the bonded reinforcing bars inside the column were also used for modeling the debonded steel reinforcing bars constituting the dissipators. The material behavior used for the dissipator bars is compared to the measured response in Figure 6.3.

6.2 ANALYSIS PROCEDURE

The model analysis was performed in three stages. First, a nonlinear static analysis was performed in which the gravity loads were applied to the model. The Newton-Raphson algorithm was used to solve the equilibrium equations. At this point, the stress in the PT bars was checked to ensure correct initial conditions in the PT bars.

In the second stage, an Eigen analysis was performed to compute the “cracked” modal properties, which were then used to set the damping properties of the structure. Rayleigh damping, based on the initial, non-updating stiffness, was set in the model, with the coefficients calculated by assigning 1% damping to the first two calculated modal frequencies. The Rayleigh coefficients, normalized by the first-mode period of the specimen (0.247 sec), are $\alpha T_1 = 0.108$ and $\beta/T_1 = 0.000436$.

Dynamic, nonlinear time-history analysis (NL-THA) was performed in the third stage, using a time step size of 0.001 sec (in specimen time scale) and the Newmark constant average acceleration integration scheme. The foundation acceleration records in the horizontal and vertical direction as measured during the test are used for the NL-THA. The P-delta formulation was considered in all analyses to include nonlinear geometric effects arising due to the large drifts seen during the test.

6.3 MODEL IMPROVEMENT

Based on several studies done with the pre-test model as a base, several modifications were made to improve the match between the analytical model and experiment results. These changes were incorporated into the post-test model and are listed below:

- Energy dissipators and prestressing bars were modeled using an advanced material model based on the work of Carreño Vallejos [2018], which is an enhancement to the material rule presented in Dodd and Restrepo-Posada [1995];
- The prestressing bars were modeled using three force-based beam-column elements, with horizontal restraints at the rocking interfaces;
- The yield and ultimate stresses of the energy-dissipator steel model were increased by 7% to account for dynamic effects, as suggested by Restrepo-Posada et al. [1994]; and
- The damping ratio used for calculating the Rayleigh coefficients was reduced to 0.5%, resulting in updated values of $\alpha T_1 = 0.889$ and $\beta/T_1 = 0.000218$. The Rayleigh damping response for the two models is compared in Figure 6.5

Among these changes, the changes in the modeling of PT bars and the updated damping model were the most effective in improving the prediction of the analytical model. The use of FBE for modeling the PT bars helped account for the flexural yielding expected at the rocking interfaces and prevented large PT losses. On the other hand, updating the damping model prevented excessive damping in large periods, which were the predominant mode of response during EQ08

and EQ09 due to the yielding of the PT bars; this allowed the model to reach drifts comparable to the test. A comparison of the material properties is shown in Figure 6.2, Figure 6.3, and Figure 6.4.

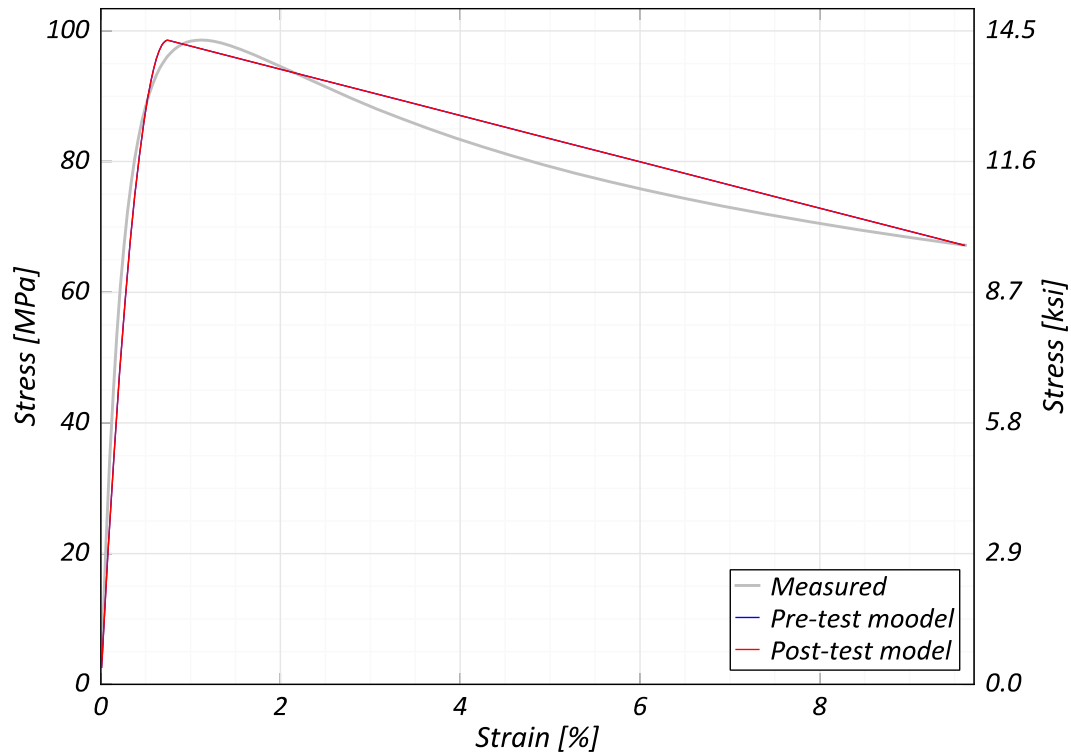


Figure 6.2 Confined concrete material properties used in analytical model.

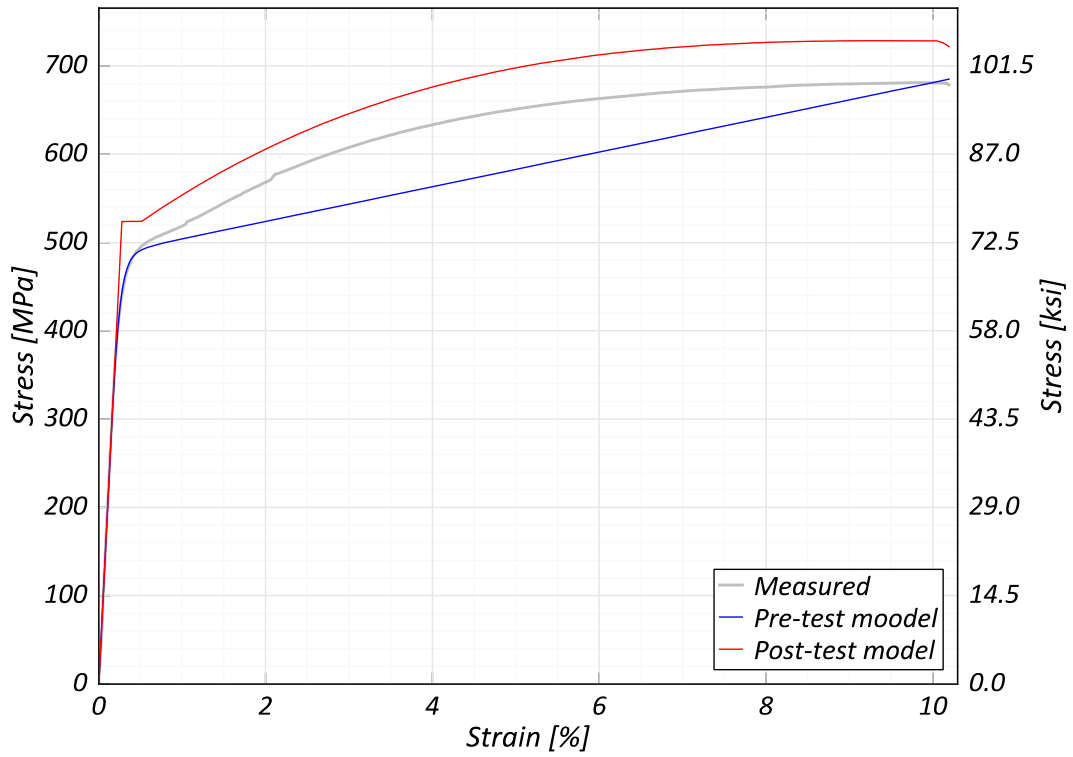


Figure 6.3 Dissipator steel material properties used in analytical model.

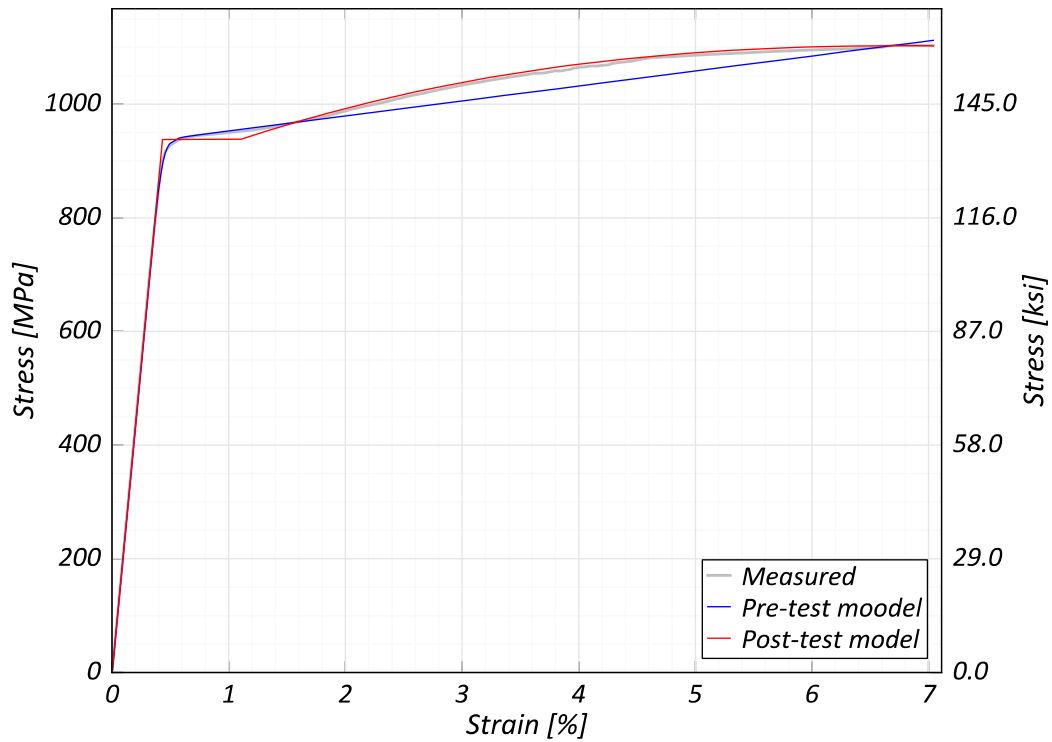


Figure 6.4 Prestressing steel material properties used in analytical model.

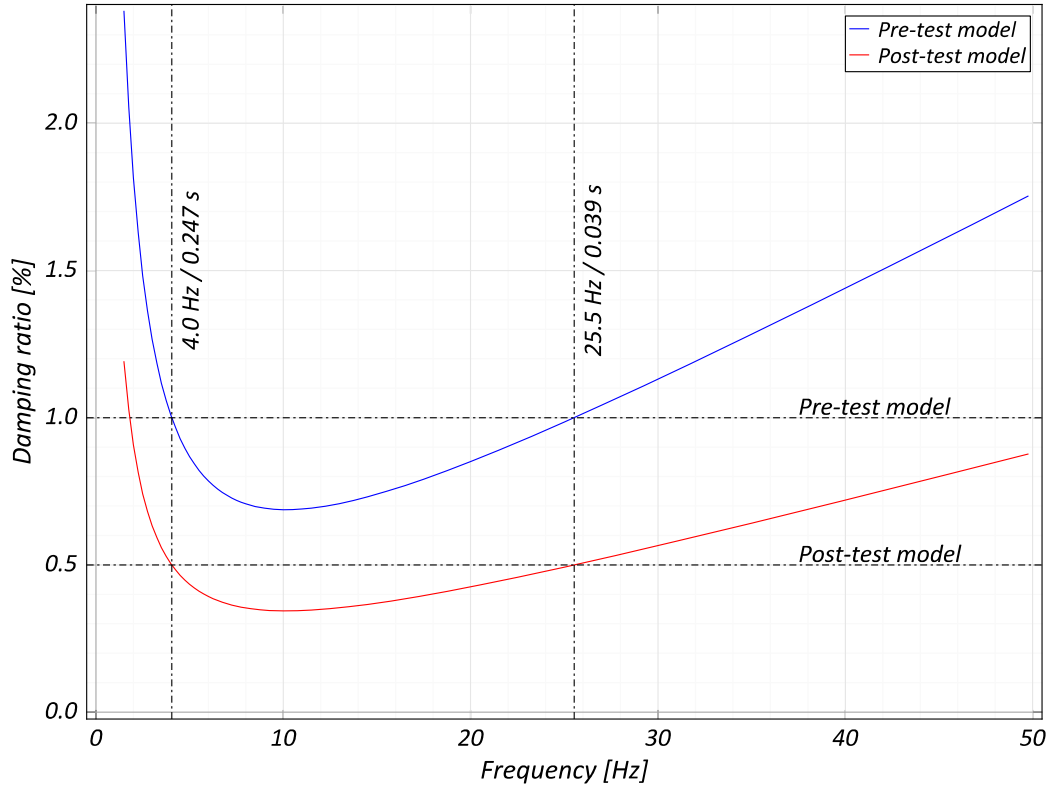


Figure 6.5 Rayleigh damping model.

6.4 ANALYTICAL RESULTS

6.4.1 Lateral Force-Displacement Response

Figure 6.6 compares the hysteretic responses of the two models with the test results. For the first motion, both models show a softer response compared to the test: this is likely a result of the friction between the restraint frames and the specimen, which was eliminated before the start of EQ02. For the remaining excitations on Day 1, a reasonable match is seen between the models and the test results, although the models show a slightly stiffer response for very small drifts ($<0.8\%$). The normalized hysteretic energy (normalized by the product of the specimen weight and the clear height) for the test and the two models is listed in Table 6.1, and a comparison of the hysteretic energy dissipated over time is presented in Figure 6.7.

For Day 2 of testing, results from the models typically compare well with the experimental results in terms of hysteretic behavior, except for EQ08, where the pre-test model significantly underpredicted the drifts. Note: in the aftermath of EQ09, the pre-test model shows significant softening and numerical instabilities. The reason for this becomes apparent when comparing the behavior of the prestressing bars: the pre-test model predicts significantly larger stresses than seen in the experiment, which resulted in a large loss in prestressing force starting from EQ08. By the end of EQ09, the residual stresses are nearly zero, which results in soft behavior.

Compared to the pre-test model, the post-test model predicts slightly smaller base shears for drifts < 5%. Otherwise, the predictions from the post-test model show a better agreement with the experiment, up to the point of bar fracture in EQ11, which has not been modeled. A comparison of the peak and residual drifts between the test results and the model predictions is shown in Figure 6.8(a) and (b). Note that while the peak drifts are well predicted, the prediction of residual drifts is significantly optimistic when compared to the test results.

The hysteretic energy dissipation predicted by the analytical models is generally smaller than the measured values but follows a similar trend over time. For the large-intensity earthquakes, this discrepancy is largely a result of greater “pinching” in the analytical models. The smaller pinching seen in the test specimen response is possibly due to the accumulation of loose concrete debris at the rocking interface, which is not accounted for in the material model of concrete used. For smaller intensity earthquakes, the discrepancy is significantly larger and is likely a result of the low system damping used in the analytical model. The calibrated analytical model shows a better agreement with the experimental values.

6.4.2 Prestressing Bar Stress History

Figure 6.9 and Figure 6.10 compare the observed and predicted stresses in the two PT bars. The over prediction of PT stresses as well as the resultant early stress loss in the pre-test model is well highlighted here. It can also be seen that the post-test model better predicts both the peak and the residual stresses. It should be noted that the residual stresses in south bar show losses between EQ05 and EQ07; these losses, possibly caused by localized slipping during the test, are not modeled and could be a potential reason behind the remaining discrepancies with the predictions of the post-test model.

Table 6.1 Hysteretic energy comparison.

Excitation	Experiment	Pre-test model	Post-test model
EQ01	0.0035	0.0025	0.0018
EQ02	0.0074	0.0010	0.0017
EQ03	0.0564	0.0474	0.0447
EQ04	0.0123	0.0047	0.0085
EQ05	0.0516	0.0441	0.0450
EQ06	0.0214	0.0208	0.0191
EQ07	0.0857	0.0543	0.0723
EQ08	0.1640	0.1119	0.1316
EQ09	0.2029	0.1635	0.1672
EQ10	0.0458	0.0385	0.0381
EQ11	0.0578	0.0473	0.0539
EQ12	0.1271	0.1097	0.1250

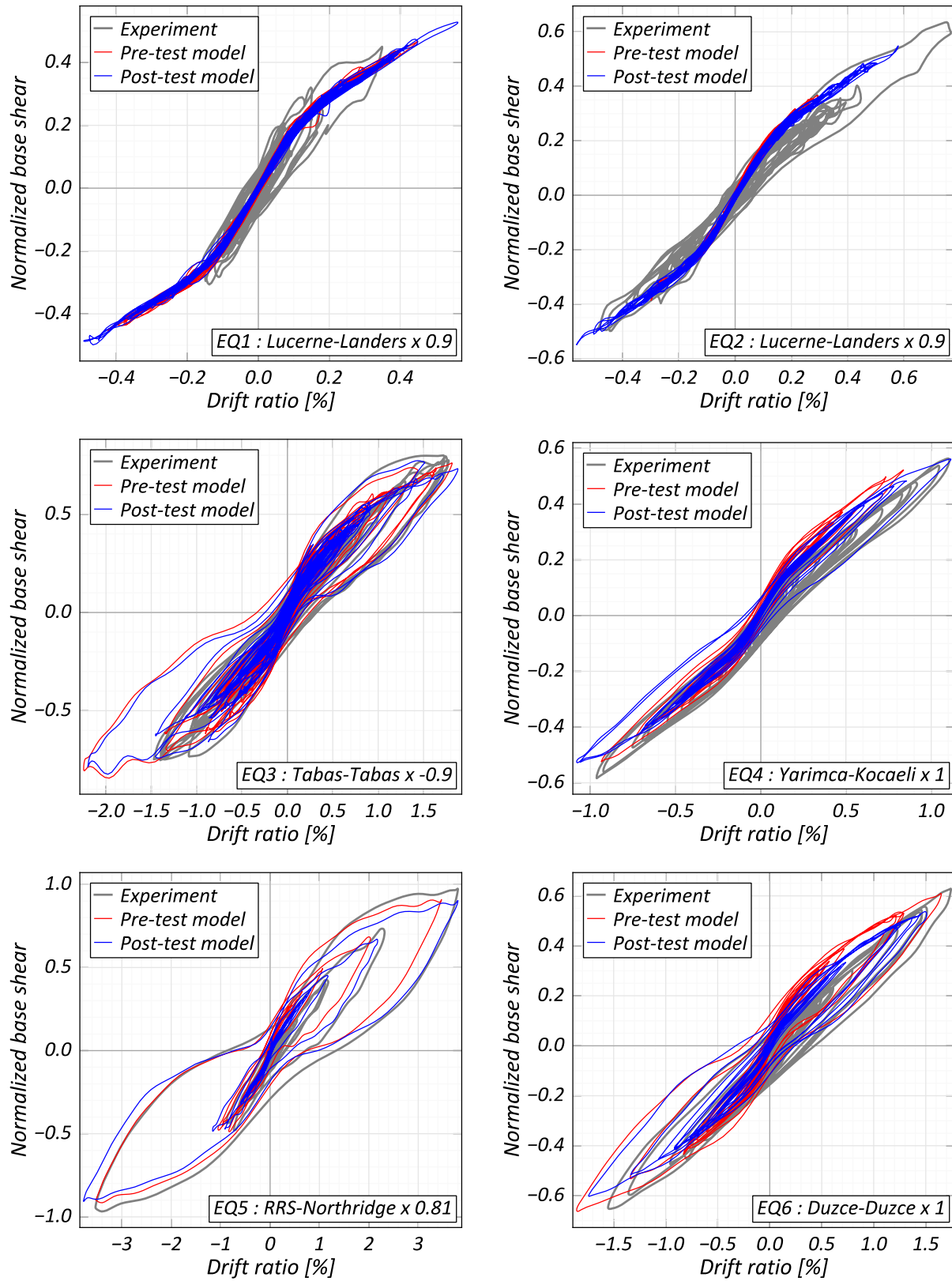


Figure 6.6 Numerical prediction of lateral force-displacement response.

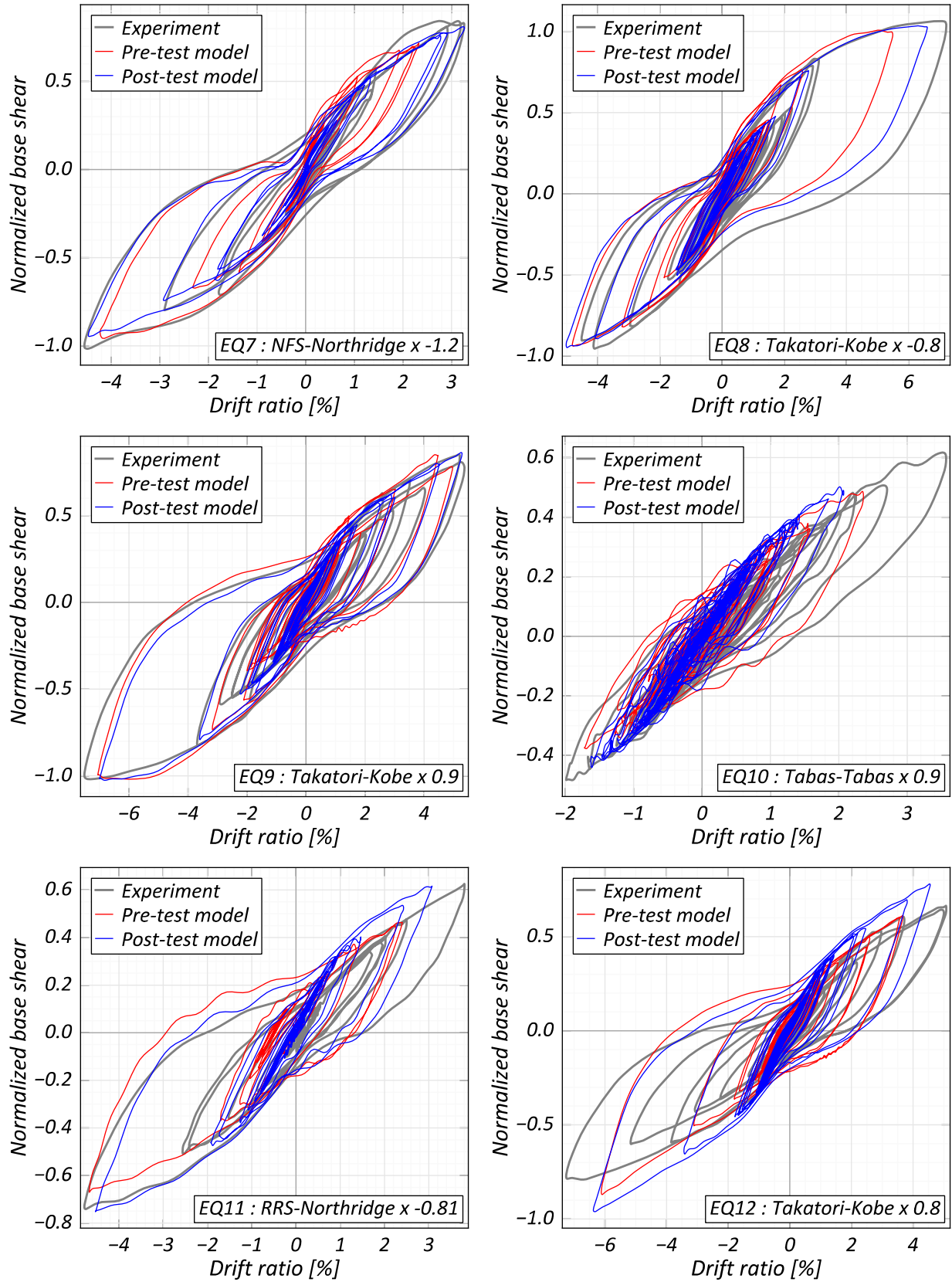


Figure 6.6 (continued).

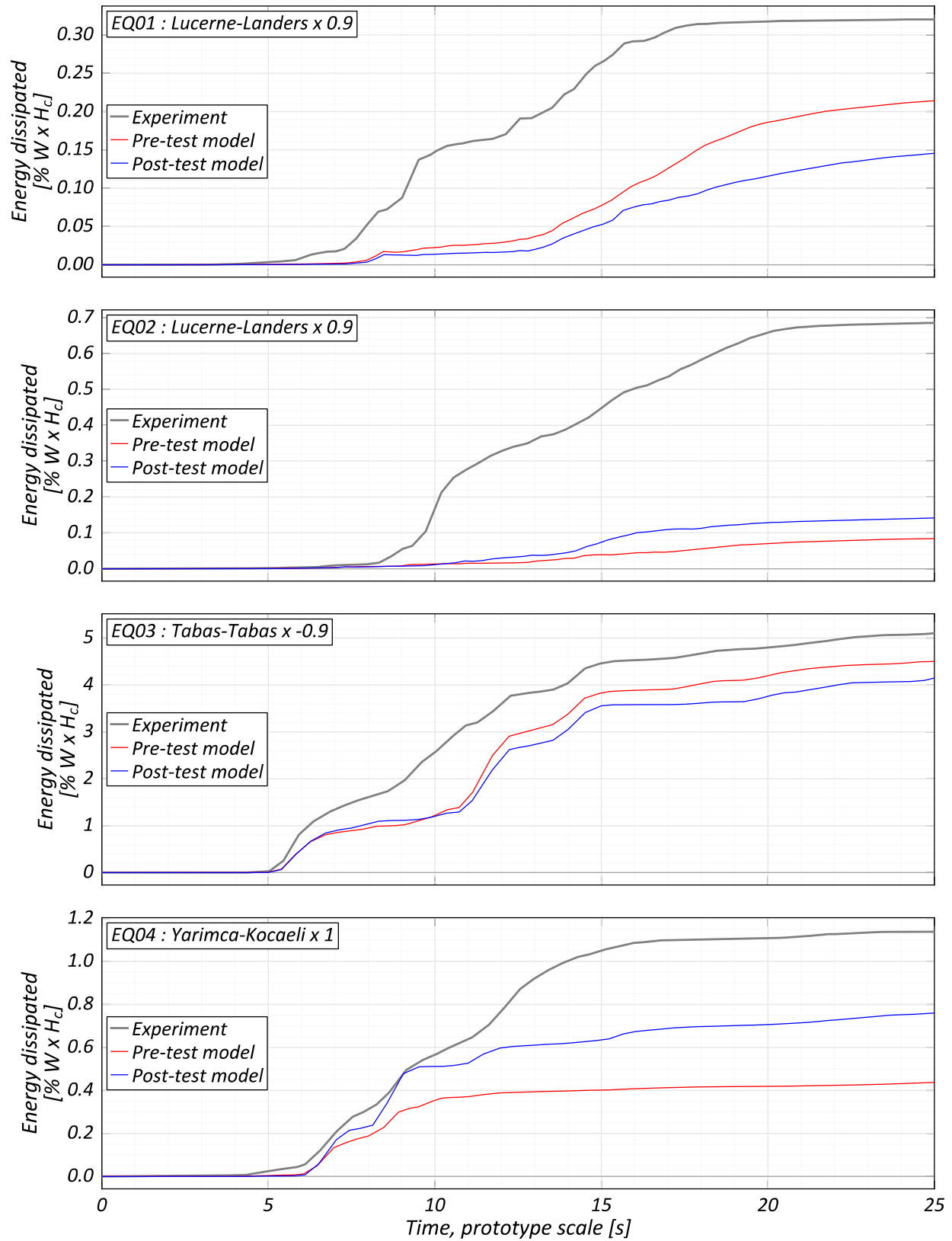


Figure 6.7 Comparison of hysteretic energy dissipation over time.

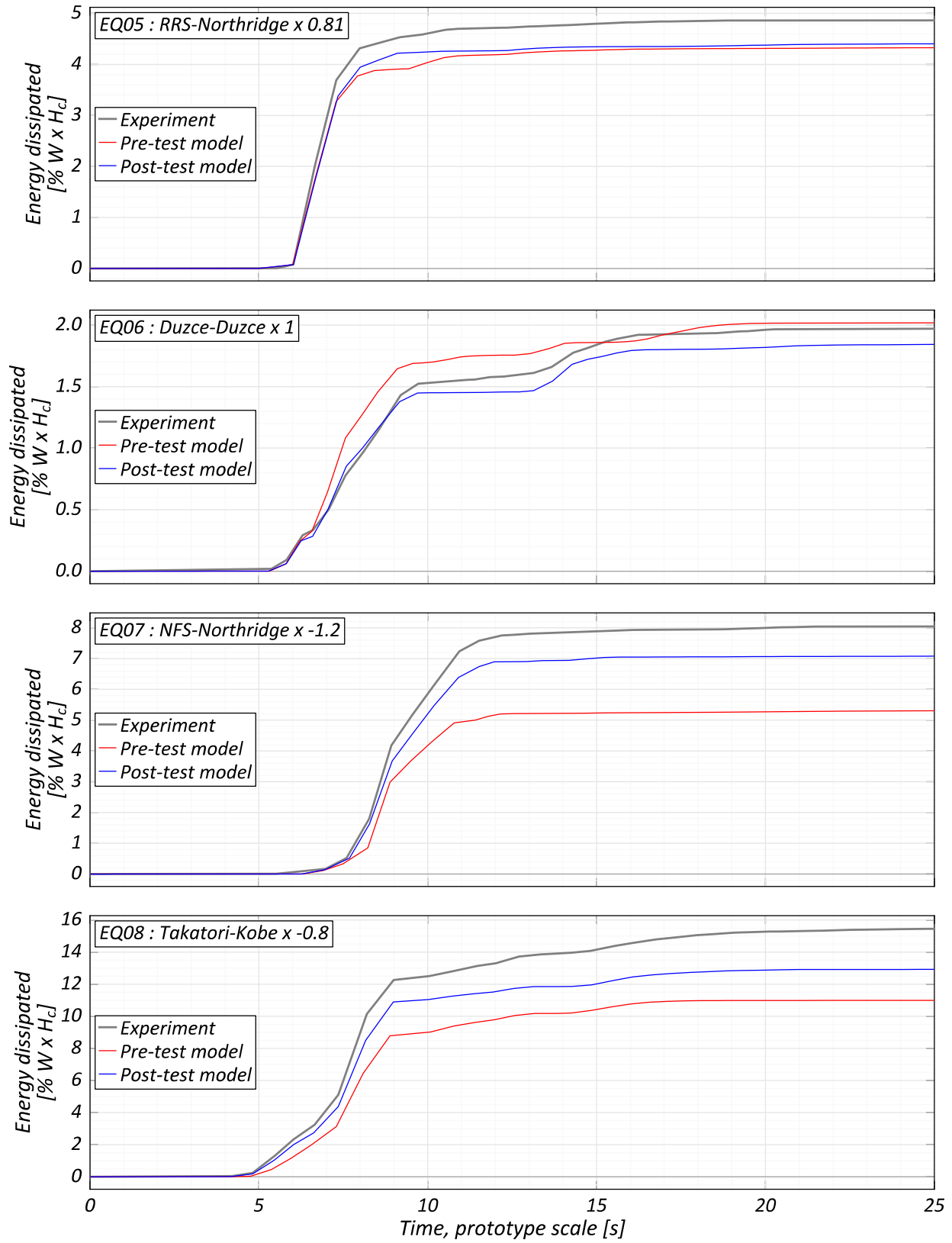


Figure 6.7 (continued).

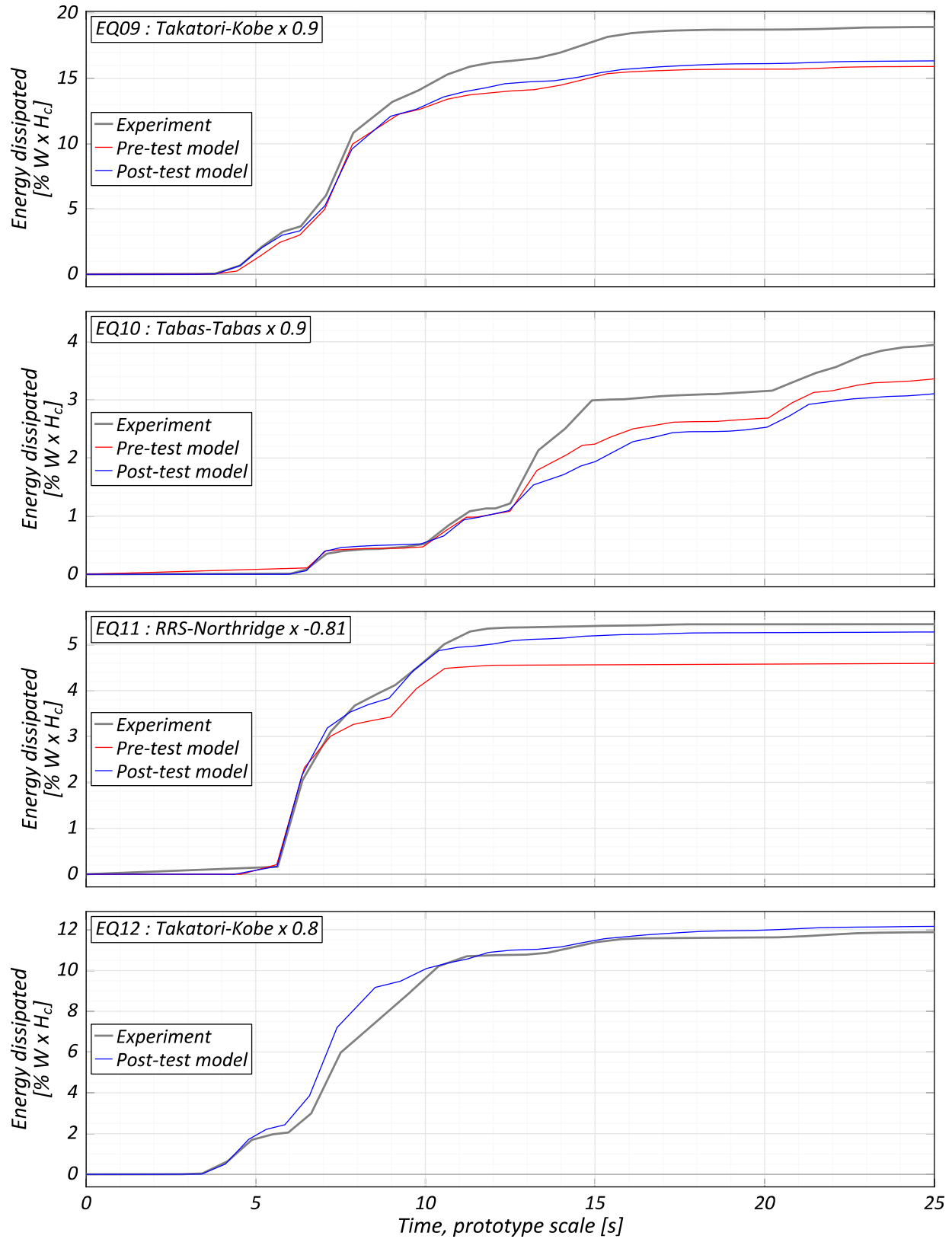
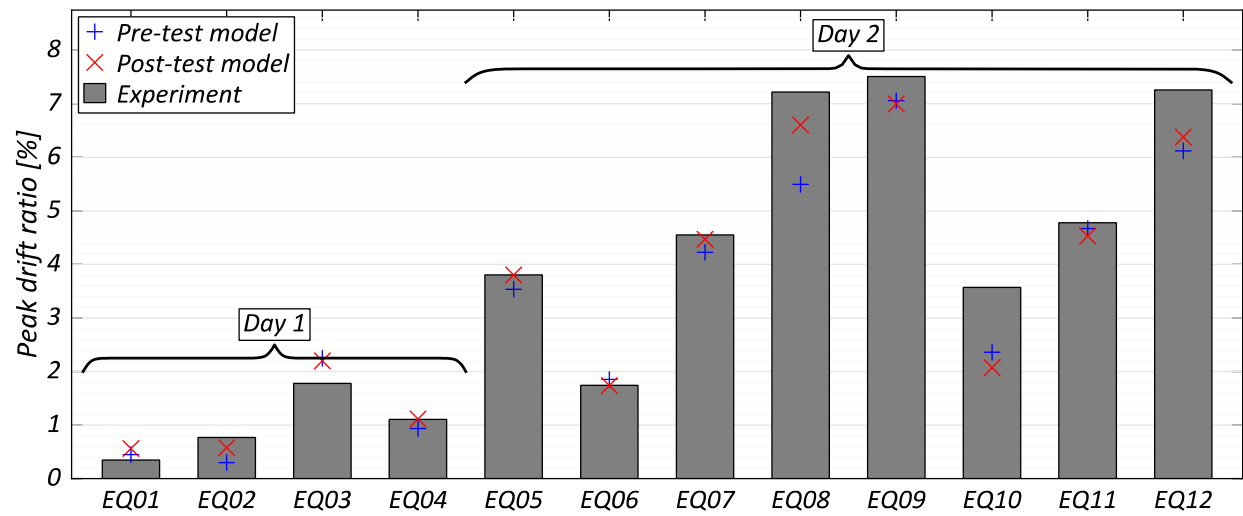
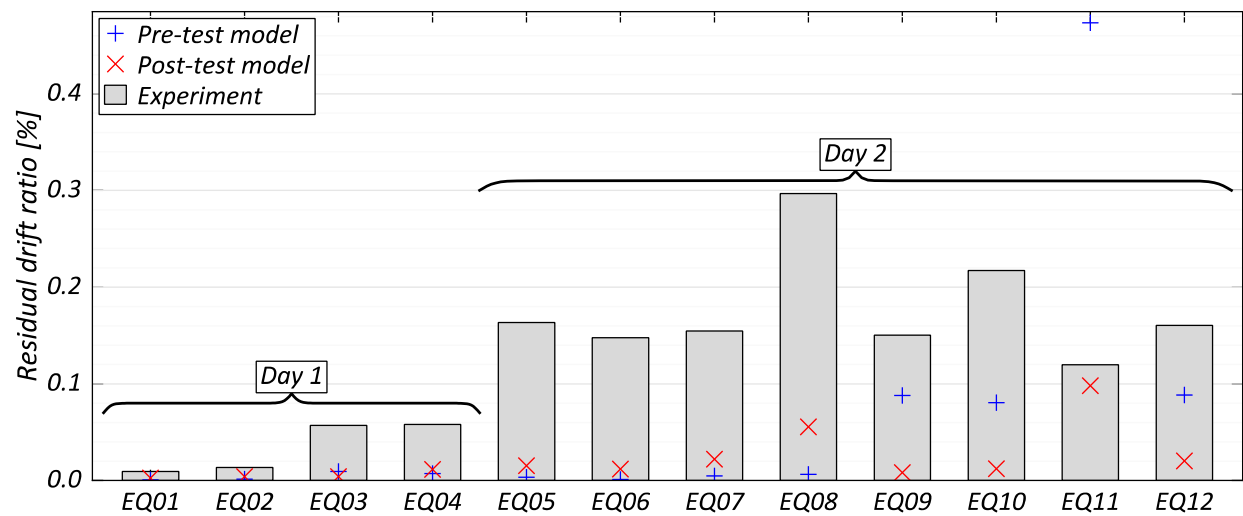


Figure 6.7 (continued).

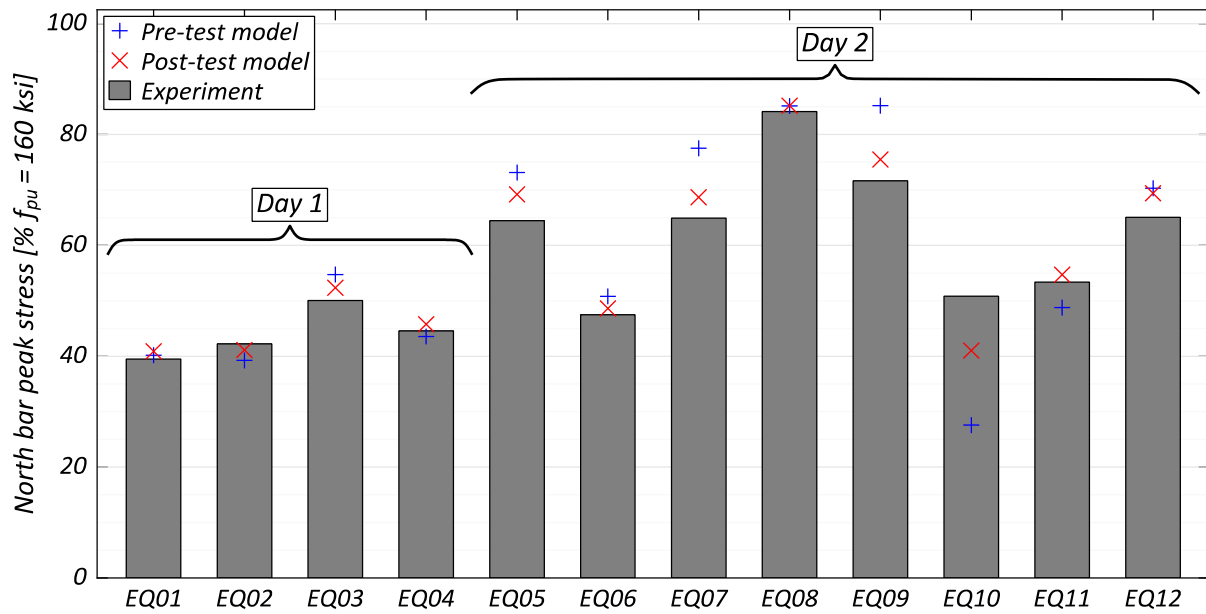


(a)

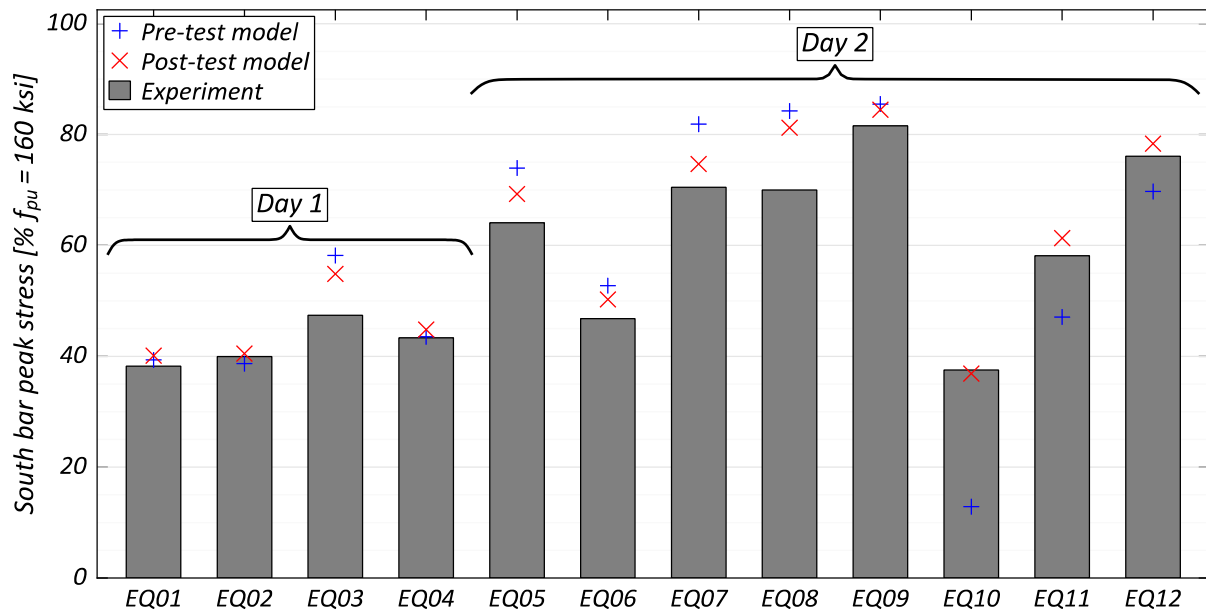


(b)

Figure 6.8 Comparison between the drifts as seen in the test and as predicted by numerical models: (a) peak drifts; and (b) residual drifts.

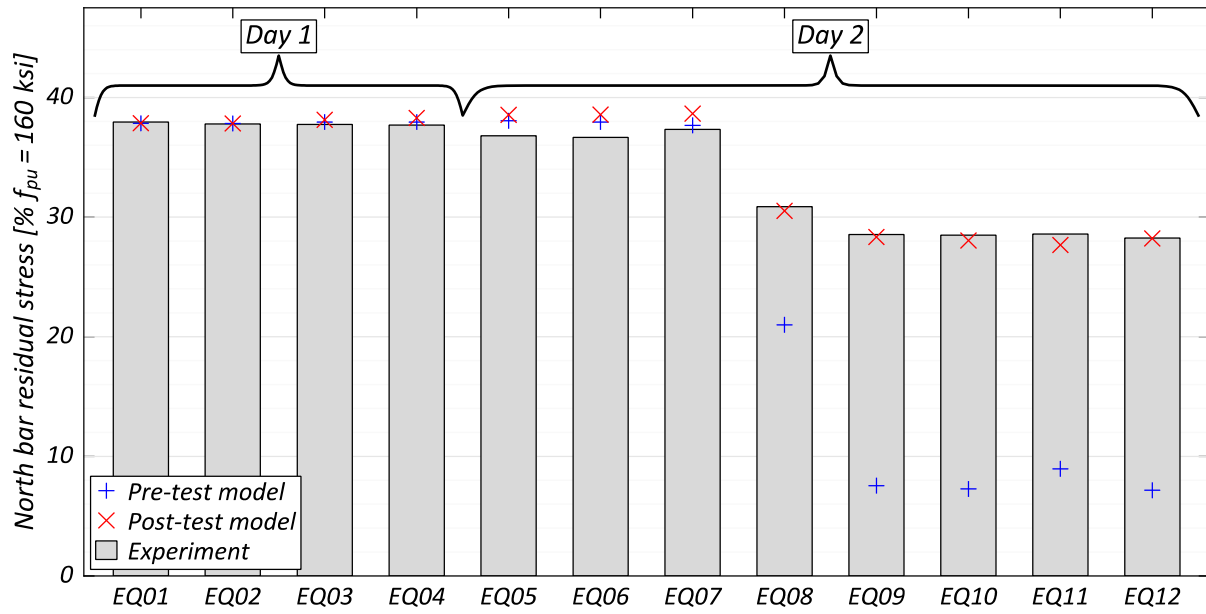


(a)

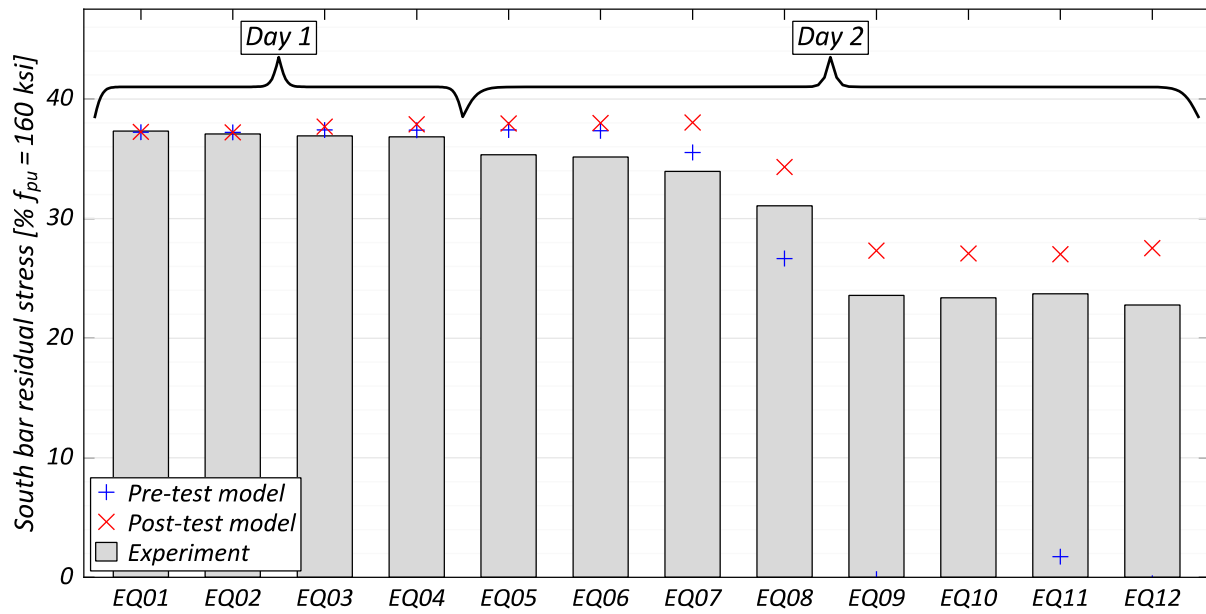


(b)

Figure 6.9 Numerical prediction of peak stresses in the PT bars: (a) north bar; and (b) south bar.



(a)



(b)

Figure 6.10 Numerical prediction of residual stresses in PT bars: (a) north bar; and (b) south bar.

7 Summary and Conclusions

This report has presented the design process, experimental performance, and numerical simulations of the hybrid recentering column technology as applied to a two-column bridge bent system. The recentering column design was rationally derived from that of an existing monolithic bridge, and the final configuration was selected on the basis of parametric analysis performed on a three-dimensional model of the prototype bridge. To aid in the numerical analysis, a computationally fast model was developed for hybrid recentering columns and verified against cyclic test data. The final scaled test specimen was designed to emulate the behavior of the full bridge with hybrid recentering columns as predicted by the analytical model while maintaining the economy of the experiment.

The specimen fabrication was done following the principles of Accelerated Bridge Construction and utilized readily available technologies. The use of a socket connection allows for the simultaneous fabrication of all the subcomponents at a dedicated precast facility, resulting in higher quality construction. The construction is further simplified by the proposed use of an external shell, specially engineered around rocking behavior, to serve as both the formwork and the transverse reinforcement in the bridge columns. As an added benefit, this technology eliminates the need for a mortar bed at the column base, commonly used to accommodate construction tolerances in systems with precast columns over the clear height, which can limit the optimal performance of the hybrid system.

The specimen was subjected to a suite of 12 seismic excitations in the horizontal (transverse to the bridge) and vertical directions, targeting increasing drift demands and representing near-fault earthquakes and their aftershocks. The columns showed no external signs of damage, primarily thanks to the confinement provided by the encasing steel shell, and the specimen maintained its strength until a drift ratio of 7%. At drifts approaching 7%, the PT bars and the steel shells near the column toes showed signs of minor yielding. Yet repeating the excitation which caused this drift showed only a minor loss in strength and stiffness. Significant strength reduction was not seen until bar fracture in the internal mild steel reinforcement, which took place under repeat imposition of drifts greater than 4%.

The tests were simulated using OpenSees for all the imposed motions, using the model developed for the design of the specimen and the measured material properties. A good match was obtained for moderate drifts, less than 4%; however, this model showed significantly larger PT bar stresses, larger prestress loss, and smaller drifts for larger excitations.

An improved model, with more realistic modeling of the PT bars, and using an advanced steel material model, was developed to improve the predictions. This improved model, with

reduced damping, was found to give improved predictions for the PT bar stresses and the specimen drifts. Neither the bar fracture in mild steel reinforcement, nor the stress-relaxation in the PT bars seen during the test was modeled, which could be the cause behind the remainder of the discrepancies between the analytical prediction and the experimental results. Considering the uncertainties in construction, the predictions obtained from the model proved adequate for use in the seismic design and analysis of such systems.

REFERENCES

- AASHTO (2012). *AASHTO LRFD Bridge Design Specifications*, 7th ed., The American Association of State Highway and Transportation Officials, Washington DC.
- AIJ (1998). *AIJ Standard for Structural Design of Reinforced Concrete Boxed-Shaped Wall Structures*, Architectural Institute of Japan, Tokyo, Japan.
- Ameli M.J., Pantelides C.P. (2016). Seismic analysis of precast concrete bridge columns connected with grouted splice sleeve connectors, ASCE, *J. Struct. Eng.*, 143(2): 04016176.
- Ameli M.J., Parks J.N., Brown D., Pantelides C.P. (2015). Seismic evaluation of grouted splice sleeve connections for reinforced precast concrete column-to-cap beam joints in accelerated bridge construction, *PCI J.*, 60: 80–103.
- Belleri A., Riva P. (2012). Seismic performance and retrofit of precast concrete grouted sleeve connections, *PCI J.*, 57, 97–109.
- Belleri A., Schoettler M.J., Restrepo J.I., Fleischman R.B. (2014). Dynamic behavior of rocking and hybrid cantilever walls in a precast concrete building, *Struct. J.*, 111(3): 661–672.
- Blandon J.J., Rodriguez M.E. (2005). Behavior of connections and floor diaphragms in seismic-resisting precast concrete buildings, *PCI J.*, 50(2): 56–75.
- Bromenschenkel R., Mahan M. (2014). *Recovery Earthquake Resisting Systems, Volume I*, California Department of Transportation, Sacramento, CA.
- Caltrans. (2013). *Seismic Design Criteria, v. 1.7*, California Department of Transportation, Sacramento, CA.
- Carreno Vallejos R. (2018). *Characterization of Large Diameter Reinforcement Under Large Strain Cyclic Reversals*, Ph.D. thesis, Department of Structural Engineering, University of California, San Diego, CA.
- Chang G.A., Mander J.B. (1994). Seismic energy based fatigue damage analysis of bridge columns: Part I-evaluation of seismic capacity, *NCEER-94-0006*, University at Buffalo, State University of New York, Buffalo, NY.
- Charney F.A. (2008). Unintended consequences of modeling damping in structures, ASCE, *J. Struct. Eng.*, 134(4): 581–592.
- Christopoulos C., Filiatrault A., Uang C.-M., Folz B. (2002). Posttensioned energy dissipating connections for moment-resisting steel frames, ASCE, *J. Struct. Eng.*, 128(9): 1111–1120.
- Cormack L. (1988). The design and construction of the major bridges on the Mangaweka rail deviation, *Trans. Inst. Eng. N.Z.*, 15(1): 17–23.
- DIN (2008). *DIN 1045: Plain, reinforced and prestressed concrete structures*. Deutsches Institut für Normung E.V. (DIN), Berlin, Germany.
- Dodd L.L., Restrepo-Posada J. I. (1995). Model for predicting cyclic behavior of reinforcing steel, ASCE, *J. Struct. Eng.*, 121(3): 433–445.
- Eatherton M.R., Hajjar J.F. (2014). Hybrid simulation testing of a self-centering rocking steel braced frame system, *Earthq. Eng. Struct. Dyn.*, 43(11): 1725–1742.
- El-Sheikh M.T., Sause R., Pessiki S., Lu L.-W. (1999). Seismic behavior and design of unbonded post-tensioned precast concrete frames, *PCI J.*, 44(3): 54–71.
- Canha R.M., de Cresce El Debs A.L.H., El Debs M. K. (2007). Design model for socket base connections adjusted from experimental results, *Struct. Concr.*, 8(1): 3–10.
- Filippou F.C., Bertero V.V., Popov E.P. (1983). Effects of bond deterioration on hysteretic behavior of reinforced concrete joints, *UCB/EERC-83/19*, Earthquake Engineering Research Center, University of California, Berkeley, CA.
- Guerrini G. (2014). *Seismic Performance of Precast Concrete Dual-Shell Steel Columns for Accelerated Bridge Construction*, Ph.D. thesis, Department of Structural Engineering, University of California, San Diego, CA.

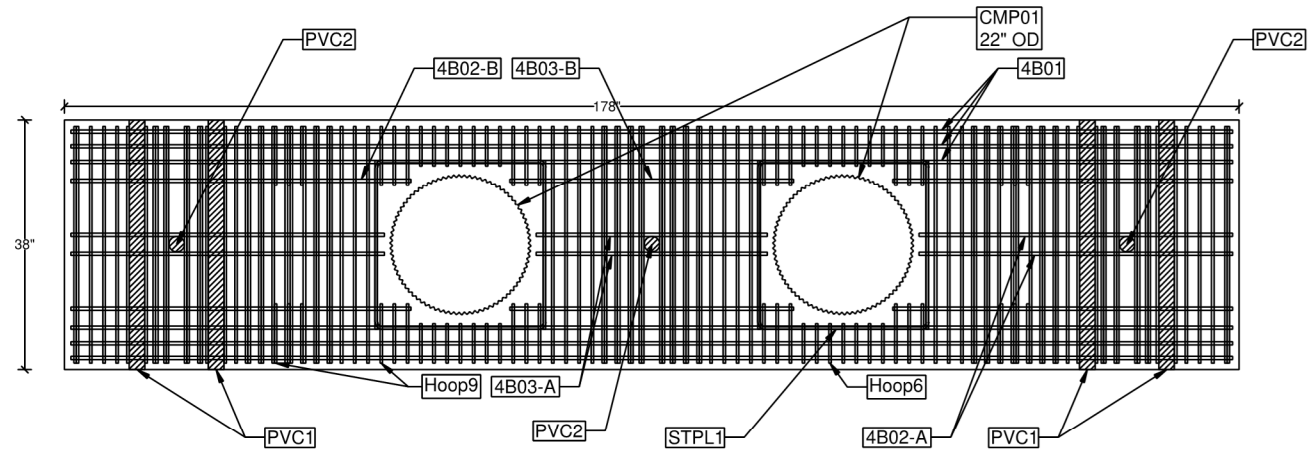
- Guerrini G., Restrepo J.I. (2011). Advanced precast concrete dual-shell steel columns, *Proceedings, 8th International Conference on Urban Earthquake Engineering*, 1: 1125–1129, Tokyo, Japan.
- Guerrini G., Restrepo J.I. (2013). Seismic response of composite concrete-dual steel shell columns for accelerated bridge construction, *Proceedings, 7th National Seismic Conference on Bridges and Highways*, Oakland, CA.
- Guerrini G., Restrepo J.I., Vervelidis A., Massari M. (2015). Self-centering precast concrete dual-steel-shell columns for accelerated bridge construction: seismic, performance, analysis, *PEER Report No. 2015/13*, Pacific Earthquake Engineering Research Center, University of California, Berkeley, CA.
- Haber Z.B., Saiidi M.S., Sanders D.H. (2014). Seismic performance of precast columns with mechanically spliced column-footing connections, *Struct. J.*, 111(3): 639–650.
- Haraldsson O.S., Janes T.M., Eberhard M.O., Stanton J.F. (2013). Seismic resistance of socket connection between footing and precast column, *ASCE, J. Bridge Eng.*, 18(9): 910–919.
- Hewes J.T., Priestley M.J.N. (2002). *Seismic Design and Performance of Precast Concrete Segmental Bridge Columns*, Department of Structural Engineering, University of California, San Diego, CA.
- Hieber D.G., Wacker J.M., Eberhard M.O., Stanton J.F. (2005). Precast concrete pier systems for rapid construction of bridges in seismic regions, *Washington State Transportation Center Task 53*, University of Washington, Seattle, WA, 308 pgs.
- Holden T., Restrepo J., Mander J.B. (2003). Seismic performance of precast reinforced and prestressed concrete walls, *ASCE, J. Struct. Eng.*, 129(3): 286–296.
- Jeong H.I., Sakai J., Mahin S.A. (2008). Shaking table tests and numerical investigation of self-centering reinforced concrete bridge columns, *PEER Report No. 2008/06*, Pacific Earthquake Engineering Research Center, University of California, Berkeley, CA.
- Kurama Y., Pessiki S., Sause R., Lu L.-W. (1999). Seismic behavior and design of unbonded post-tensioned precast concrete walls, *PCI J.*, 44(3): 72–89.
- Kwan W.-P., Billington S.L. (2003a). Unbonded post-tensioned concrete bridge piers. I: Monotonic and cyclic analyses, *ASCE, J. Bridge Eng.*, 8(2): 92–101.
- Kwan W.-P., Billington S.L. (2003b). Unbonded posttensioned concrete bridge piers. II: Seismic analyses, *ASCE, J. Bridge Eng.*, 8(2): 102–111.
- Lu Y., Panagiotou M. (2013). Characterization and representation of near-fault ground motions using cumulative pulse extraction with wavelet analysis, *Bull. Seismol. Soc. Am.*, 104(1): 410–426.
- Mander J.B., Cheng C.-T. (1997). Seismic resistance of bridge piers based on damage avoidance design, *NCEER-97-0014*, University at Buffalo, State University of New York, Buffalo, NY.
- Marriott D., Pampanin S., Palermo A. (2009). Quasi-static and pseudo-dynamic testing of unbonded post-tensioned rocking bridge piers with external replaceable dissipators, *Earthq. Eng. Struct. Dyn.*, 38(3): 331–354.
- Marriott D., Pampanin S., Palermo A. (2011). Biaxial testing of unbonded post-tensioned rocking bridge piers with external replaceable dissipators, *Earthq. Eng. Struct. Dyn.*, 40(15): 1723–1741.
- Mashal M., Palermo A. (2015). High-damage and low-damage seismic design technologies for accelerated bridge construction, *Proceedings, Structures Congress*, Portland, OR.
- Mashal M., White S., Palermo A. (2013). Quasi-static cyclic tests of emulative precast segmental bridge piers (E-PSBP), *Proceedings, 2013 New Zealand Society for Earthquake Engineering*, Wellington, NZ.
- Mazzoni S., McKenna F., Scott M.H., Fenves G. L. (2006). *OpenSees Command Language Manual*, University of California, Berkeley, CA, <https://opensees.berkeley.edu/OpenSees/manuals/usermanual/OpenSeesCommandLanguageManualJune2006.pdf>.
- McKenna F., Scott M.H., Fenves G.L. (2010). Nonlinear finite-element analysis software architecture using object composition, *J. Comp. Civil Eng.*, 24(1): 95–107.

- Mengotto M., Pinto P.E. (1973). Method of analysis for cyclically loaded RC plane frames including changes in geometry and non-elastic behavior of elements under combined normal force and bending, *Proceedings, IABSE Symposium on Resistance and Ultimate Deformability of Structures Acted On by Well Defined Repeated Loads*, Lisbon, Portugal, pp. 15–22.
- Nakaki S.D., Stanton J.F., Sritharan S. (1999). An overview of the PRESSS five-story precast test building, *PCI J.*, 44(2): 26–39.
- Osanai Y., Watanabe F., Okamoto S. (1996). Stress transfer mechanism of socket base connections with precast concrete columns, *Struct. J.*, 93(3): 266–276.
- Ou Y.-C., Chiewanichakorn M., Ahn I.-S., Aref A., Chen S., Filiatrault A., Lee G. (2006). “Cyclic performance of precast concrete segmental bridge columns: Simplified analytical and finite element studies, *Trans. Res. Record*, 1976: 66–74.
- Palermo A., Mashal M. (2012). Accelerated bridge construction (ABC) and seismic damage resistant technology: a New Zealand challenge, *Bull. N.Z. Soc. Earthq. Eng.*, 45(3): 123–134.
- Palermo A., Pampanin S. (2008). Enhanced seismic performance of hybrid bridge systems: comparison with traditional monolithic solutions, *J. Earthq. Eng.*, 12(8): 1267–1295.
- Palermo A., Pampanin S., Marriott D. (2007). Design, modeling, and experimental response of seismic resistant bridge piers with posttensioned dissipating connections, *ASCE, J. Struct. Eng.*, 133(11): 1648–1661.
- Pang J.B.K., Eberhard M.O., Stanton J.F. (2010). Large-bar connection for precast bridge bents in seismic regions, *ASCE, J. Bridge Eng.*, 15(3): 231–239.
- Perez F.J., Pessiki S., Sause R., Lu L.-W. (2003). Lateral load tests of unbonded post-tensioned precast concrete walls, American Concrete Institute, *Special Publication*, 211: 161–182.
- Priestley M.J.N. (1991). Overview of PRESSS research program, *PCI J.*, 36(4): 50–57.
- Priestley M.J.N., MacRae G. (1994). Seismic tests of precast post-tensioned ungrouted concrete beam-column subassembly tests, *Report No. PRESSS 94/01*, Department of Applied Mechanics and Engineering Sciences, University of California, San Diego, CA, 124 pgs.
- Priestley M.J.N., Sritharan S., Conley J.R., Pampanin S. (1999). Preliminary results and conclusions from the PRESSS five-story precast concrete test building, *PCI J.*, 44(6): 42–67.
- Priestley M.J.N., Tao J.R. (1993). Seismic response of precast prestressed concrete frames with partially debonded tendons, *PCI J.*, 38(1): 58–69.
- Restrepo J.I., Rahman A. (2007). Seismic performance of self-centering structural walls incorporating energy dissipators, *ASCE, J. Struct. Eng.*, 133(11): 1560–1570.
- Restrepo J.I., Tobolski M.J., Matsumoto E.E. (2011). Development of a precast bent cap system for seismic regions, *NCHRP Report 681*, National Academies Press, Washington, D.C.
- Restrepo-Posada, J. I., Dodd, L. L., Park, R., and Cooke, N. (1994). “Variables affecting cyclic behavior of reinforcing steel.” *ASCE, J. Struct. Eng.*, 120(11): 3178–3196.
- Sakai J., Mahin S.A. (2004). Analytical investigations of new methods for reducing residual displacements of reinforced concrete bridge columns, *PEER Report No. 2004/02*, Pacific Earthquake Engineering Research Center, University of California, Berkeley, CA.
- Sharpe R.D., Skinner R.I. (1983). “The seismic design of an industrial chimney with rocking base, *Bull. N.Z. Soc. Earthq. Eng.*, 16(2): 98–106.
- Stone W.C., Cheok G.S., Stanton J.F. (1995). Performance of hybrid moment-resisting precast beam-column concrete connections subjected to cyclic loading, *Struct. J.*, 92(2): 229–249.
- Tazarv M., Saiidi M.S. (2015). Low-damage precast columns for accelerated bridge construction in high seismic zones, *ASCE, J. Bridge Eng.*, 21(3): 04015056.
- Thonstad T., Mantawy I.M., Stanton J.F., Eberhard M.O., Sanders D.H. (2016). Shaking table performance of a new bridge system with pretensioned rocking columns, *ASCE, J. Bridge Eng.*, 21(4): 04015079.

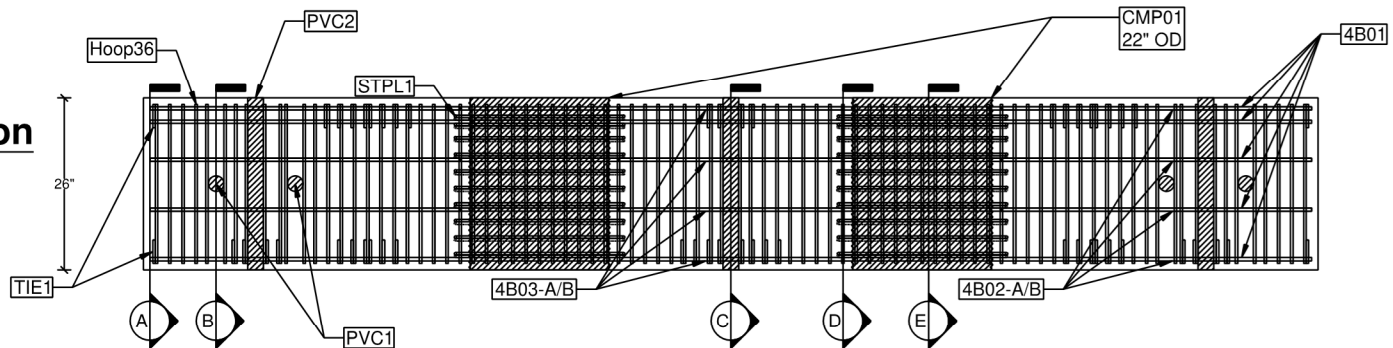
- Toranzo L.A., Restrepo J.I., Mander J.B., Carr, A. J. (2009). Shake-table tests of confined-masonry rocking walls with supplementary hysteretic damping, *J. Earthq. Eng.*, 13(6): 882–898.
- Toranzo-Dianderas L.A. (2002). *The Use of Rocking Walls in Confined Masonry Structures: A Performance-Based Approach*, PhD Thesis, Department of Civil and Natural Resources Engineering, University of Canterbury, Christchurch, New Zealand.
- Yassin M.H.M. (1994). *Nonlinear Analysis of Prestressed Concrete Structures under Monotonic and Cyclic Loads*, Ph.D., Department of Civil and Environmental Engineering, University of California, Berkeley, CA.

Appendix A Construction Drawings

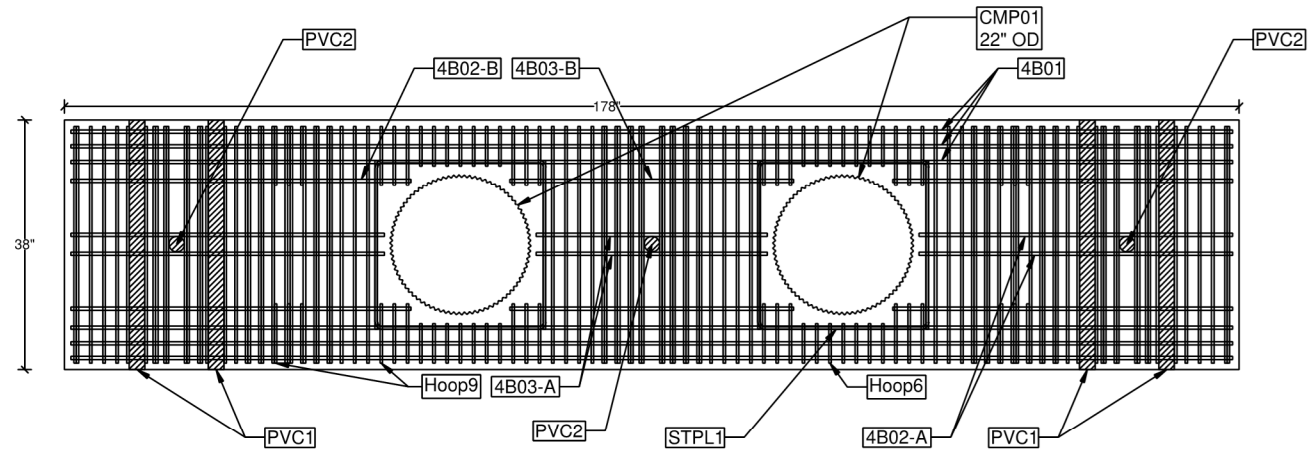
Plan



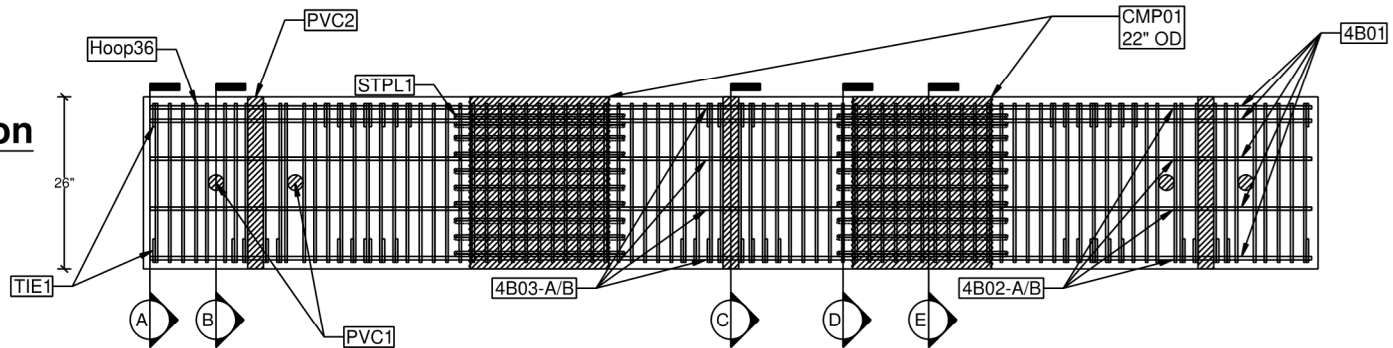
Elevation



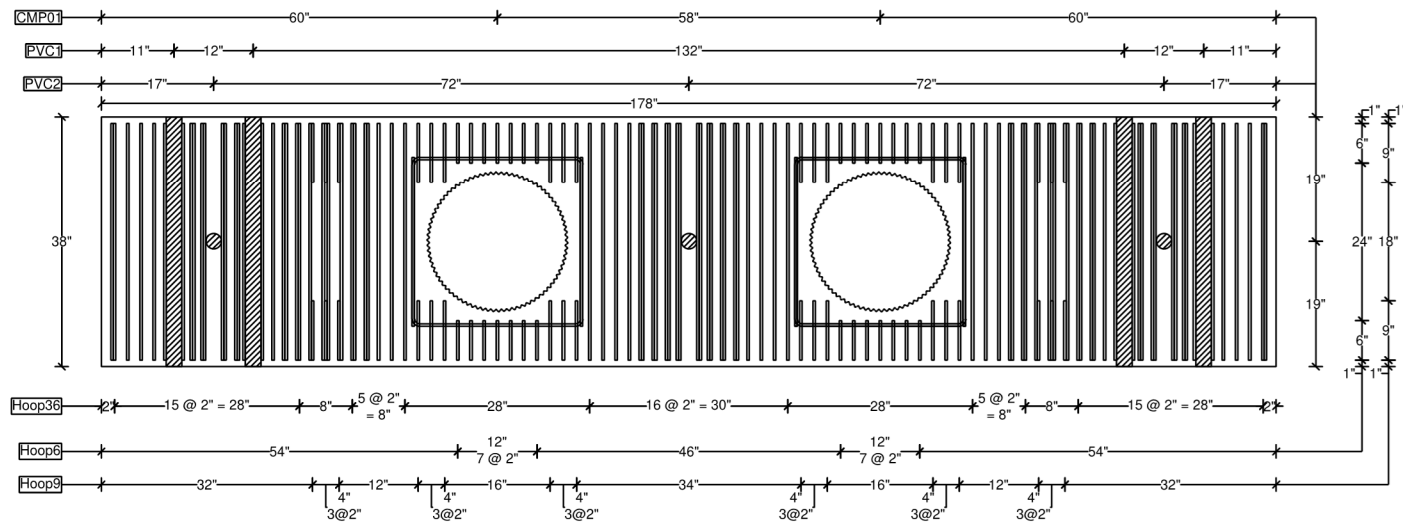
Plan



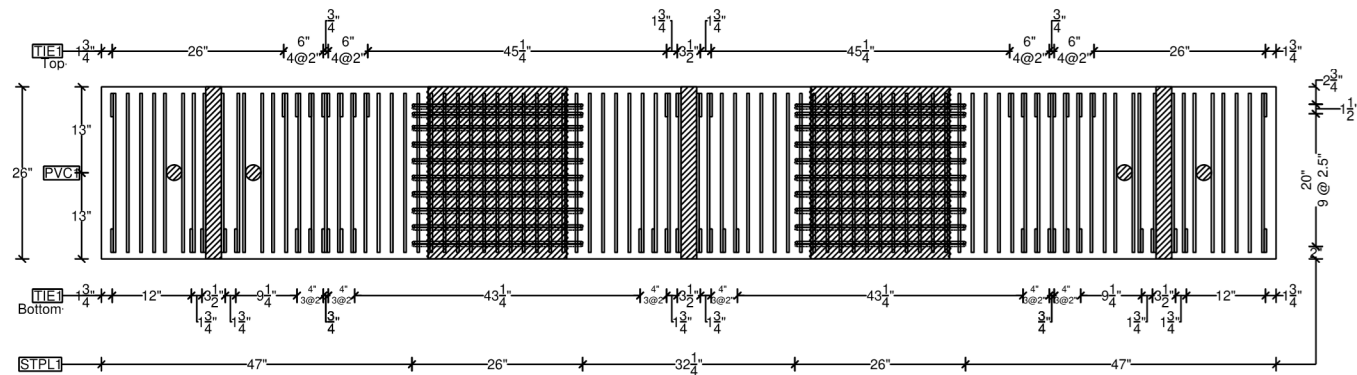
Elevation



Plan



Elevation



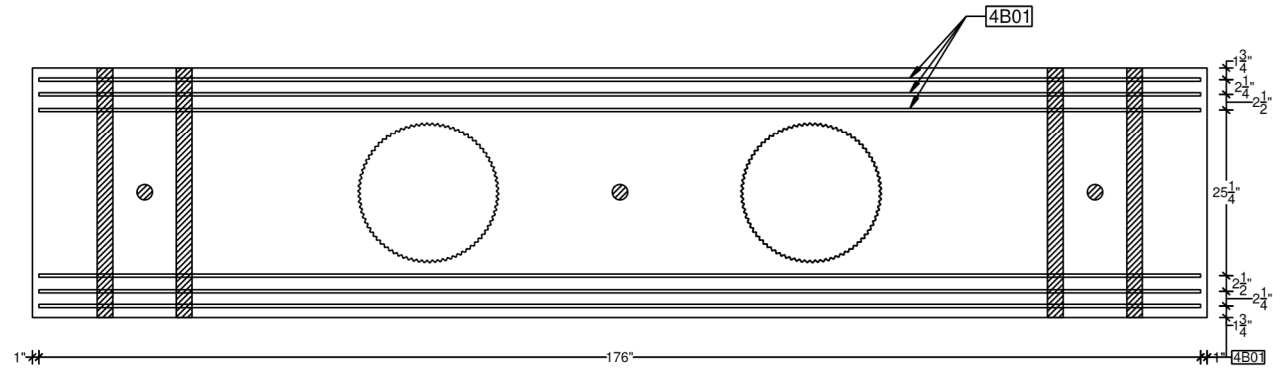
PEER Resilient Bridge Column Test

Foundation Details: Transverse Reinf., Openings

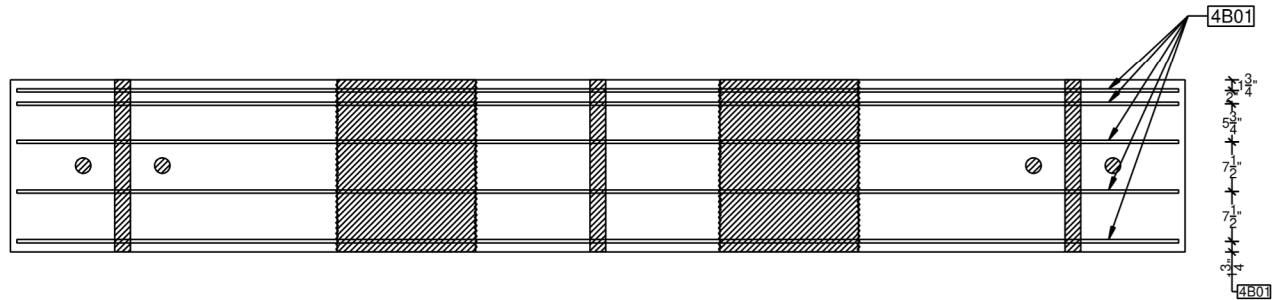
BY: AN CHK: Date: 05/12/2017 Scale: 1"=25"

Sheet
2 of 8

Plan



Elevation

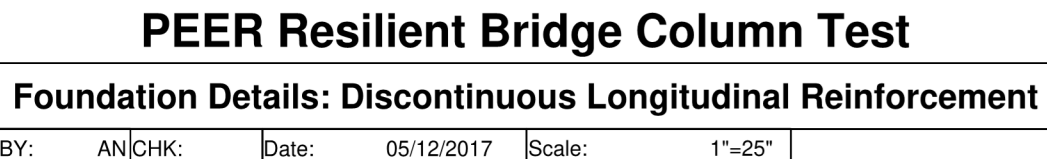


PEER Resilient Bridge Column Test

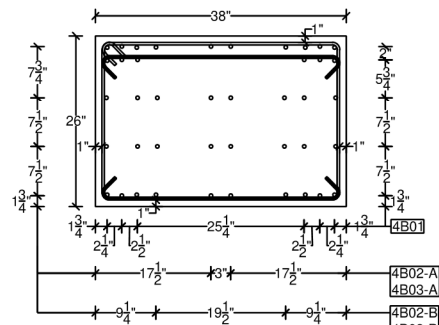
Foundation Details: Continuous Longitudinal Reinforcement

BY: AN CHK: Date: 05/12/2017 Scale: 1"=25"

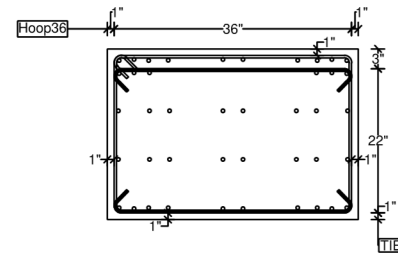
**Sheet
3 of 8**



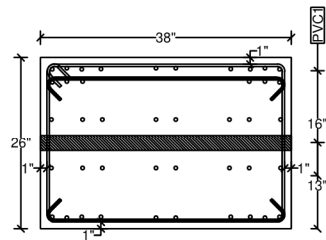
93



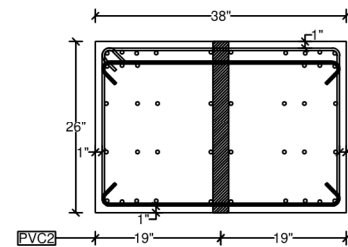
Section A
Longitudinal Reinforcement



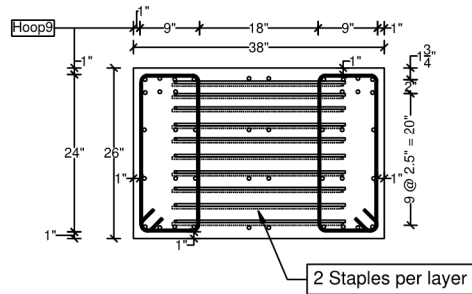
Section A
Transverse Reinforcement



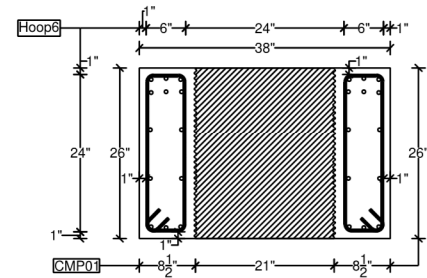
Section B



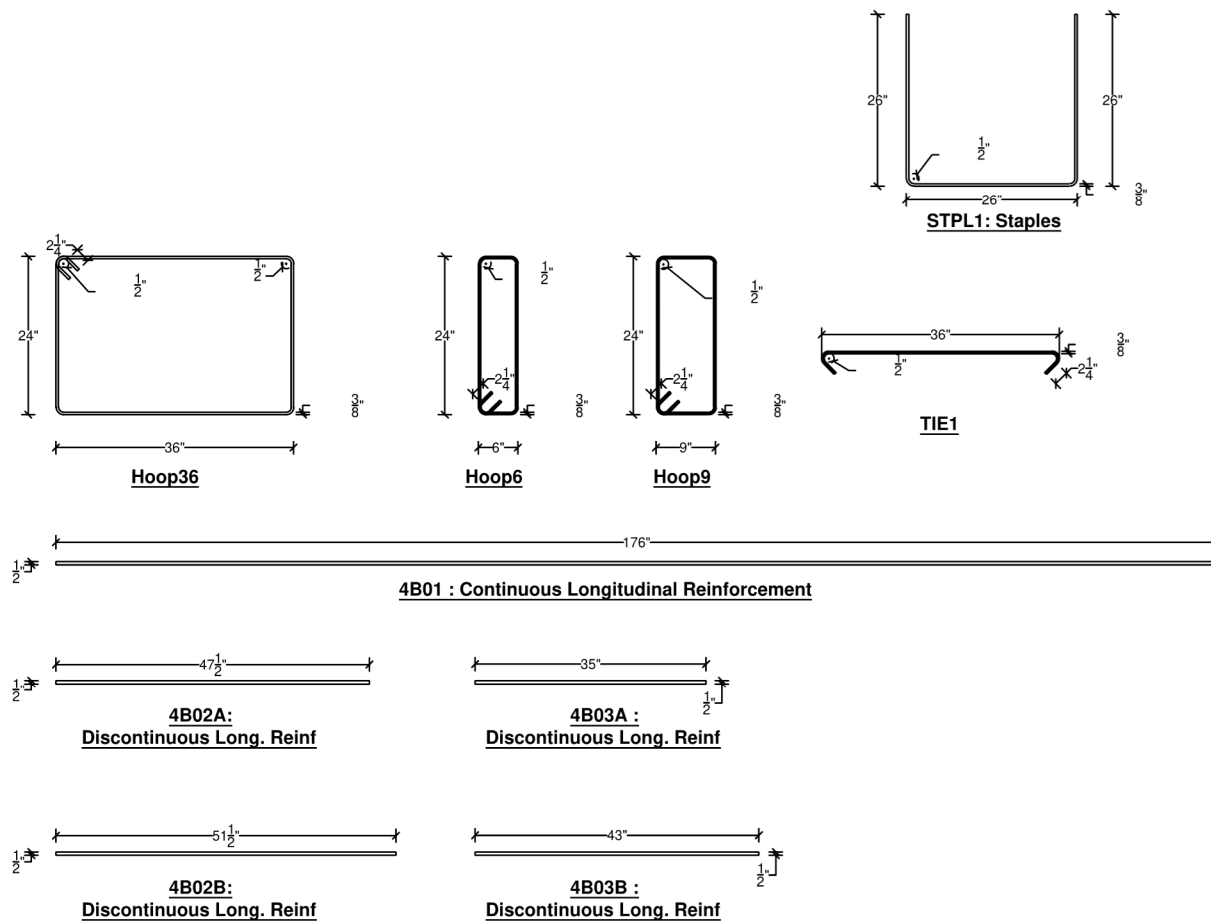
Section C



Section D




Section E



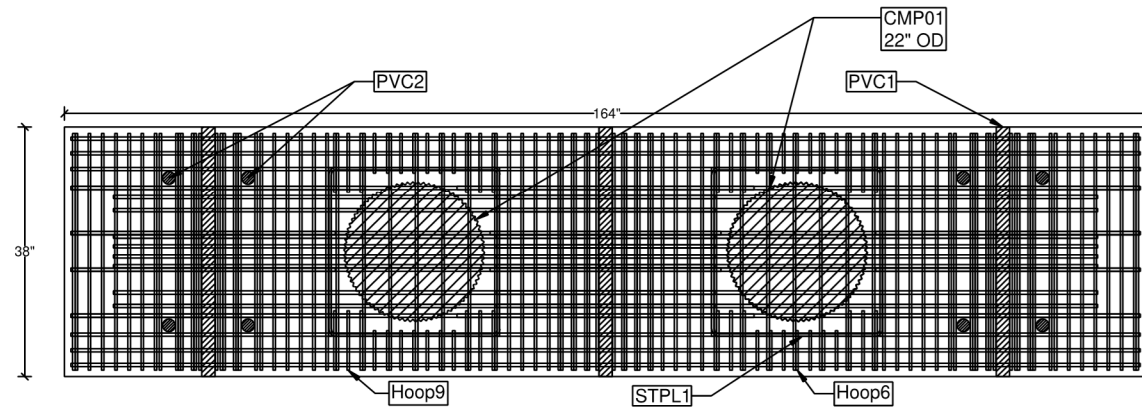
Reinforcement Schedule		
Mark	Quantity	Description
4B01	26	#4 ASTM A615 G60
4B02-A	16	#4 ASTM A615 G60
4B02-B	16	#4 ASTM A615 G60
4B03-A	8	#4 ASTM A615 G60
4B03-B	8	#4 ASTM A615 G60
TIE1	52	#3 ASTM A615 G60, Ties
Hoop6	28	#3 ASTM A615 G60, Hoops
Hoop9	36	#3 ASTM A615 G60, Hoops
Hoop36	56	#3 ASTM A615 G60, Hoops
STPL1	40	#3 ASTM A615 G60, Staples

Bill of Materials		
PVC1	4	38" long x 2" ID x PVC duct
PVC2	3	32" long x 2" ID x PVC duct
CMP01	2	21" Nominal ID, 26" tall Helical-Corrugated Metal Pipe, ASTM A760/A760M

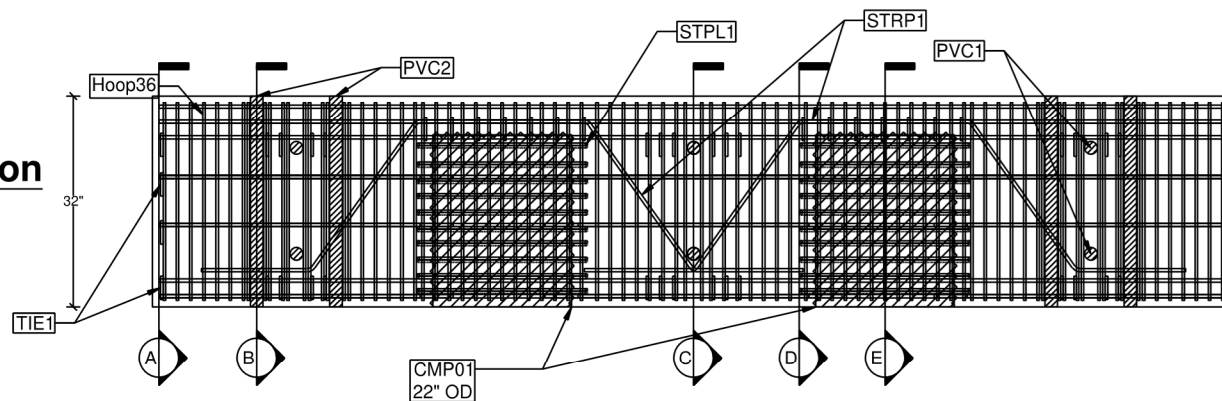
Concrete Specifications			
Mix Design	Unit Weight (P.C.F)	Volume (CU.YD.)	f' _c (P.S.I.)
-	150	3.7	6000

	PEER Resilient Bridge Column Test					Sheet 8 of 8
	Foundation Details: Materials					
	BY: AN	CHK:	Date: 05/12/2017	Scale: -		

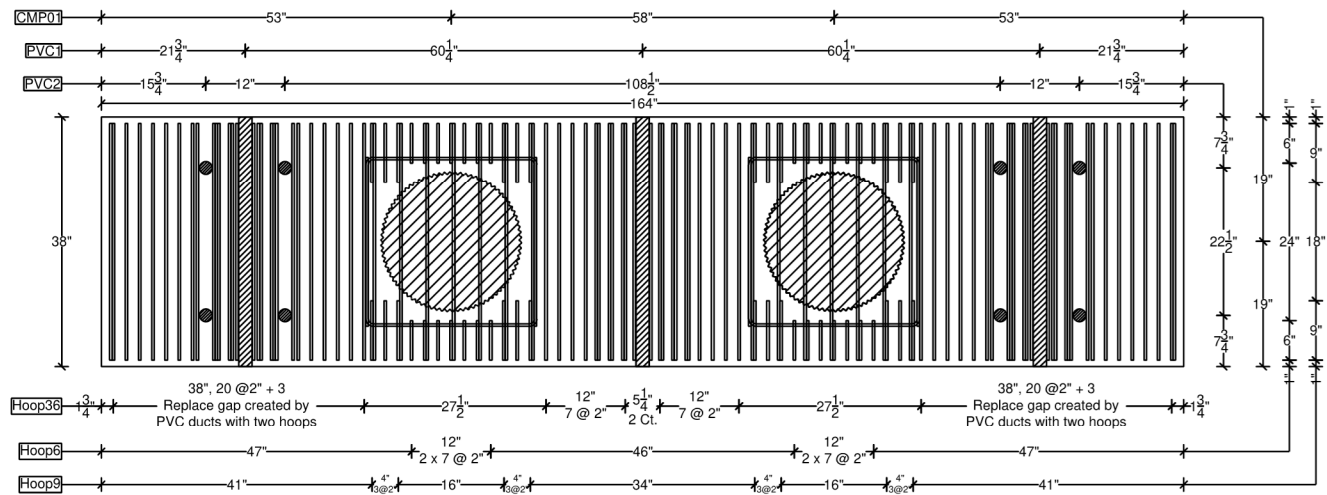
Plan



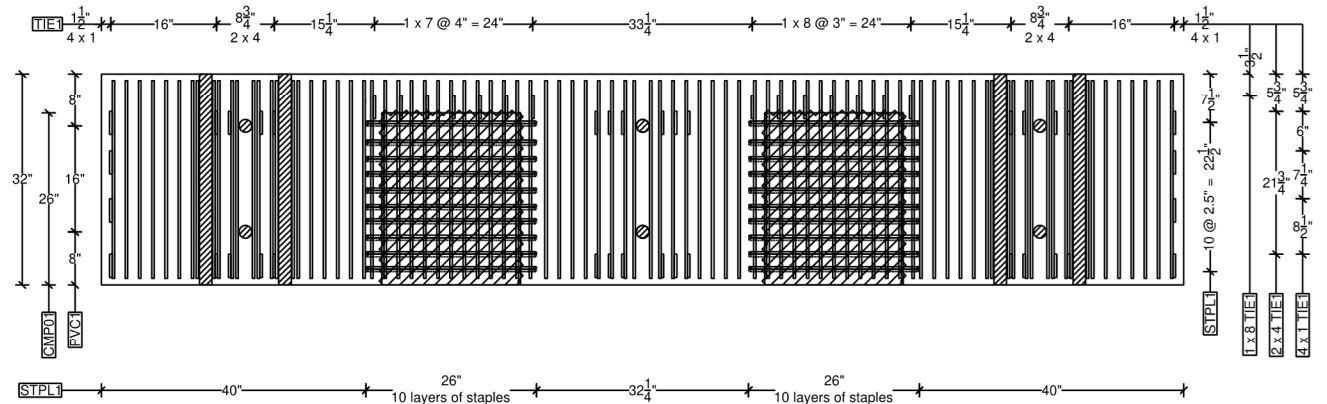
Elevation



Plan



Elevation



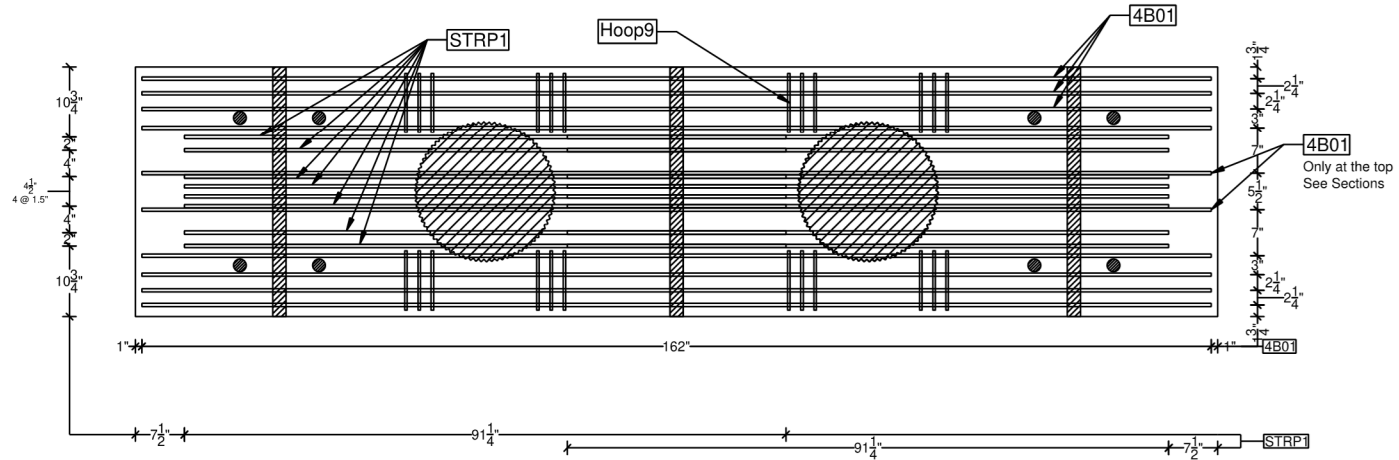
PEER Resilient Bridge Column Test

Bent Cap Details: Transverse Reinf., Openings

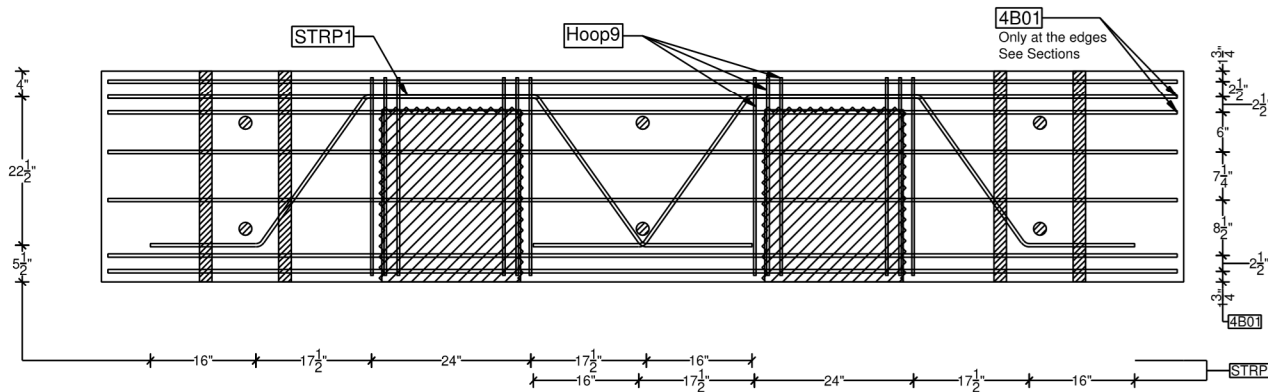
BY: AN CHK: Date: 05/12/2017 Scale: 1"=25"

Sheet
2 of 8

Plan



Elevation



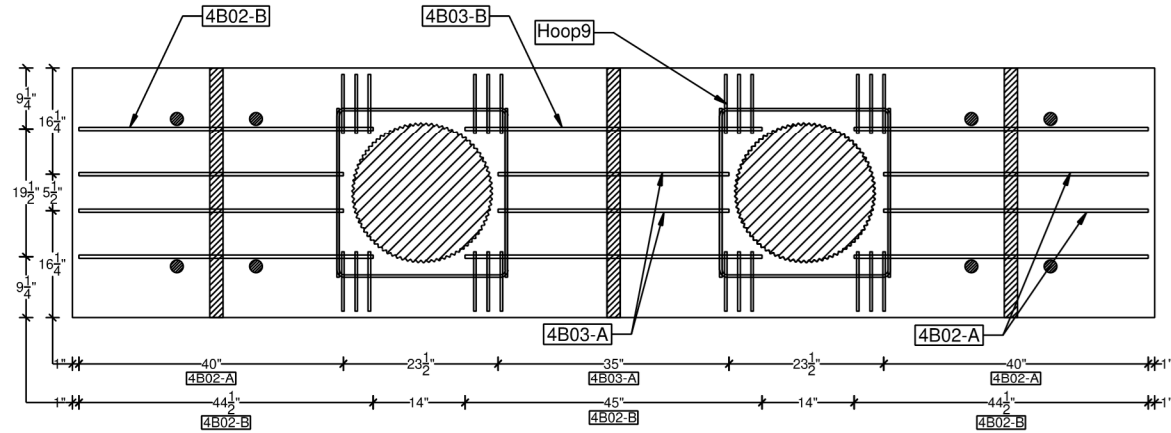
PEER Resilient Bridge Column Test

Bent Cap Details: Continuous Longitudinal Reinforcement

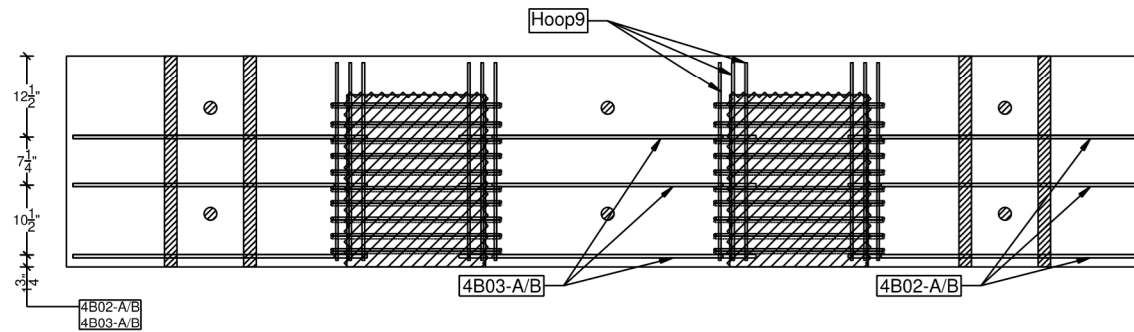
BY: AN CHK: Date: 05/12/2017 Scale: 1"=25"

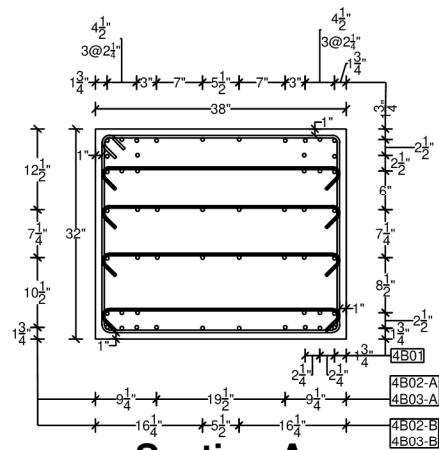
**Sheet
3 of 8**

Plan

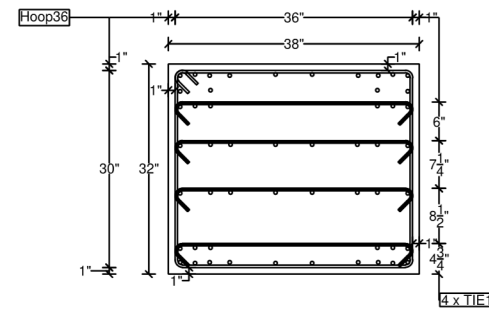


Elevation

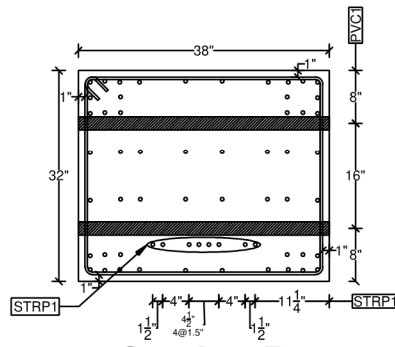




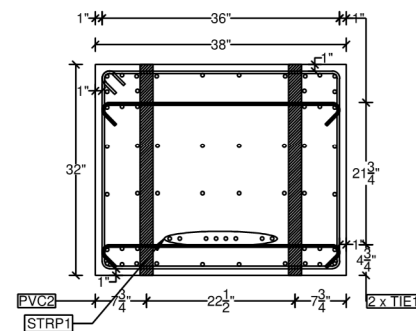
Section A
Longitudinal Reinforcement



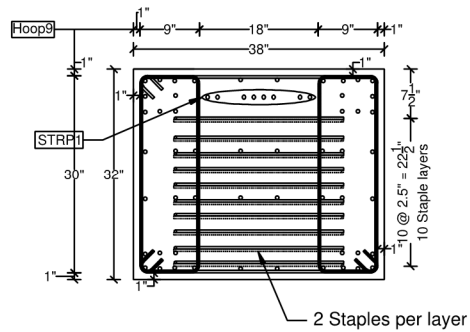
Section A
Transverse Reinforcement



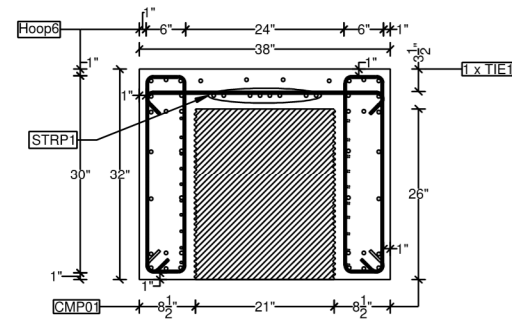
Section B



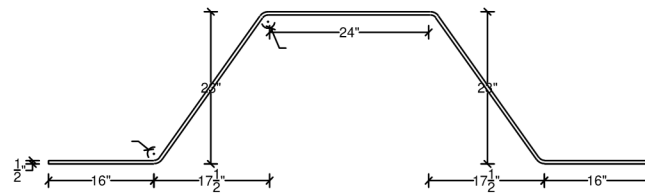
Section C



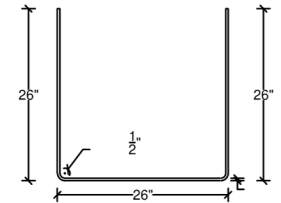
Section D



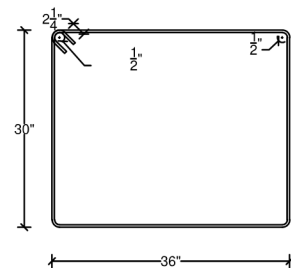
Section E



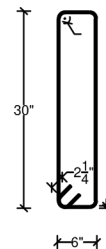
STRP1: Bent Stirrups



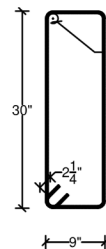
STPL1: Staples



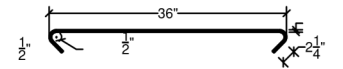
Hoop36



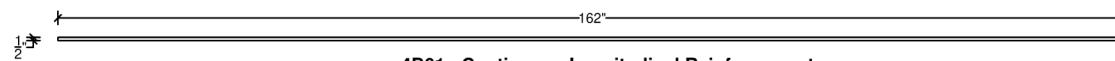
Hoop6



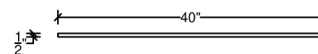
Hoop9



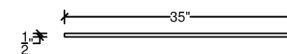
TIE1



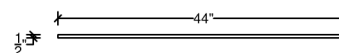
4B01 : Continuous Longitudinal Reinforcement



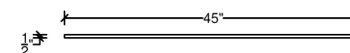
4B02-A



4B03-A



4B02-B




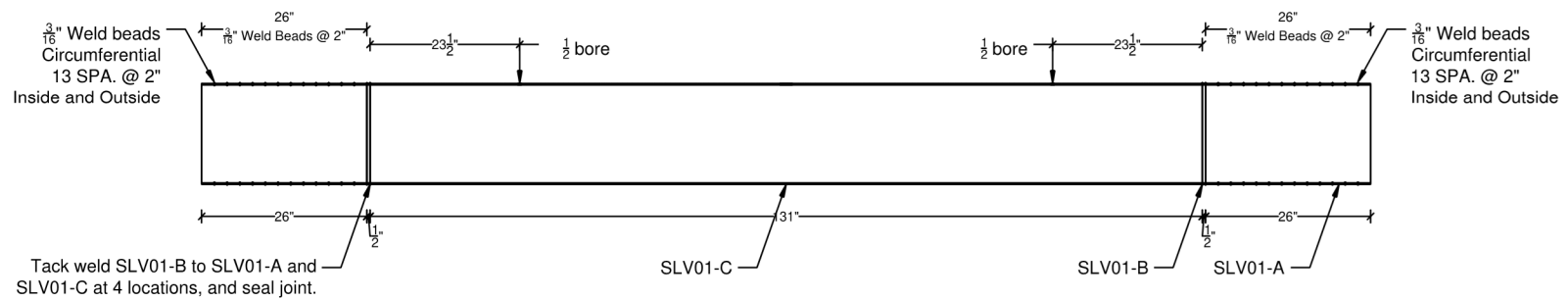
4B03-B

Reinforcement Schedule		
Mark	Quantity	Description
4B01	40	#4 ASTM A615 G60
4B02-A	12	#4 ASTM A615 G60
4B02-B	12	#4 ASTM A615 G60
4B03-A	6	#4 ASTM A615 G60
4B03-B	6	#4 ASTM A615 G60
STRP1	16	#4 ASTM A615 G60, Stirrups
TIE1	52	#3 ASTM A615 G60, Ties
Hoop6	28	#3 ASTM A615 G60, Hoops
Hoop9	24	#3 ASTM A615 G60, Hoops
Hoop36	62	#3 ASTM A615 G60, Hoops
STPL1	40	#3 ASTM A615 G60, Staples

Bill of Materials		
PVC1	6	38" long x 2" ID PVC sleeve. Tie location for weights
PVC2	8	32" long x 2" ID PVC sleeve
CMP01	2	21" Nominal ID, 26" tall Helical-Corrugated Metal Pipe, ASTM A760/A760M

Concrete Specifications			
Mix Design	Unit Weight (P.C.F)	Volume (CU.YD.)	f' _c (P.S.I.)
-	150	4.3	6000

	PEER Resilient Bridge Column Test					Sheet 8 of 8
	Bent Cap Details: Materials					
	BY: AN	CHK:	Date: 05/12/2017	Scale: -		



IMPORTANT: Tack welds on SLV01-B to allow for removal before testing



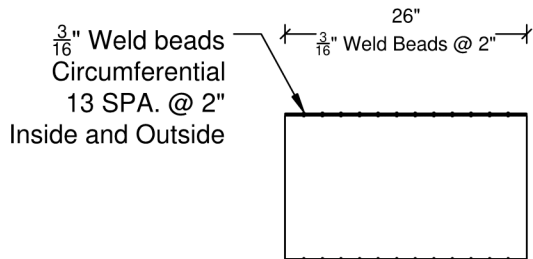
Revisions		
07-20-2017	Modify SLV01-B and SLV01-C length	
07-20-2017	Modify SLV01-B production method	
07-20-2017	Change debonding method in PT Anchor ASQ101	
07-20-2017	4 bore to SLV01-C for instrumentation	

PEER Resilient Bridge Column Test

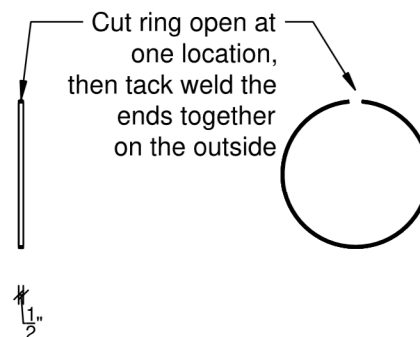
Pre-cast column: SLV01 Assembly

BY: AN CHK: Date: 07/15/2017 Scale: 1"=25"

Sheet
2 of 6

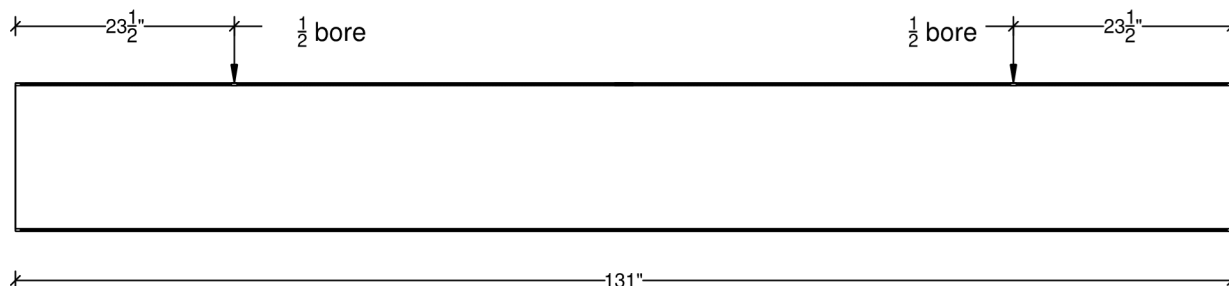


SLV01-A: 2 Count



SLV01-B : 2 Count

Cut $\frac{1}{2}$ " ring at one location,
then tack weld to form easy
to remove strip



SLV01-C



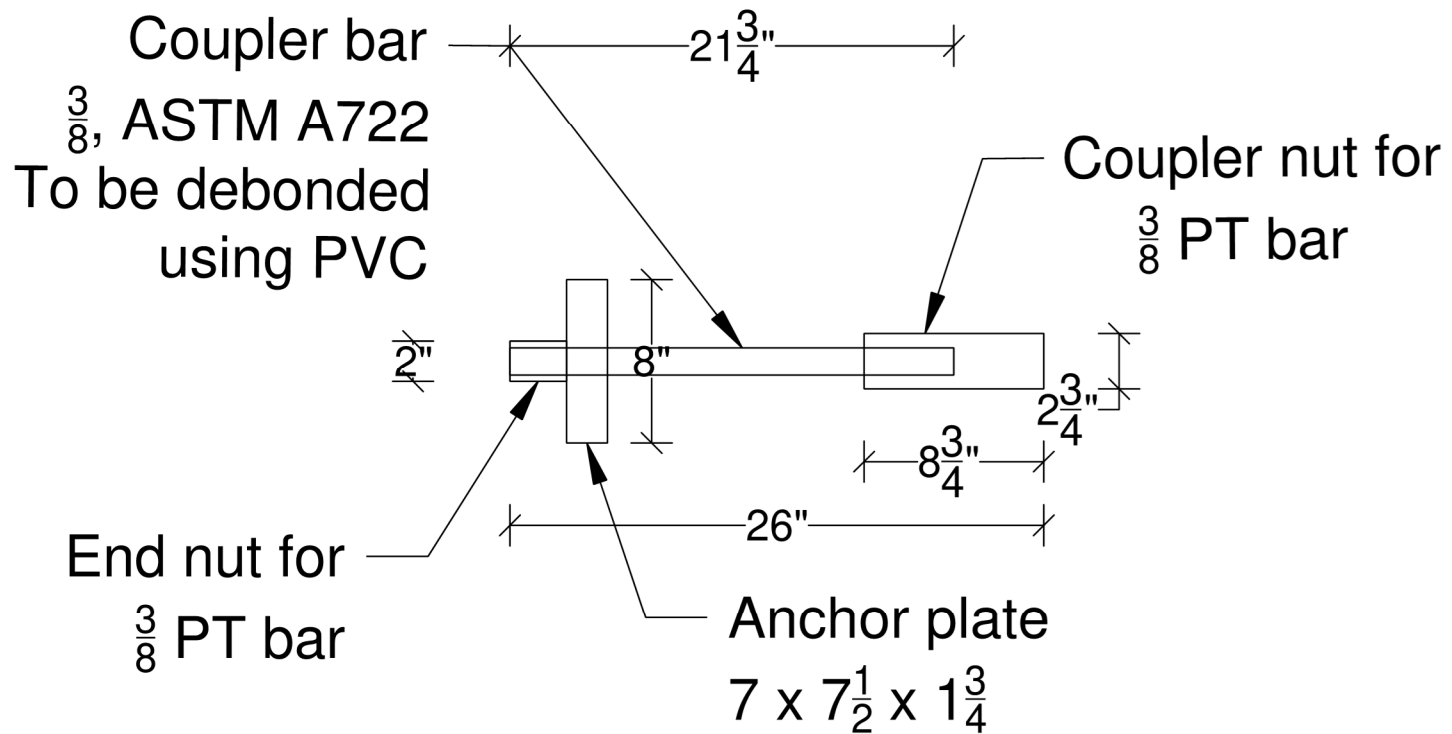
Revisions	
07-20-2017	Modify SLV01-B and SLV01-C length
07-20-2017	Modify SLV01-B production method
07-20-2017	Change debonding method in PT Anchor ASQ201
07-20-2017	4 bore to SLV01-C for instrumentation

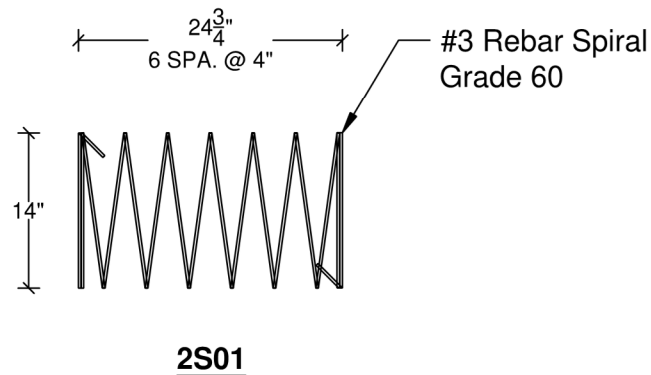
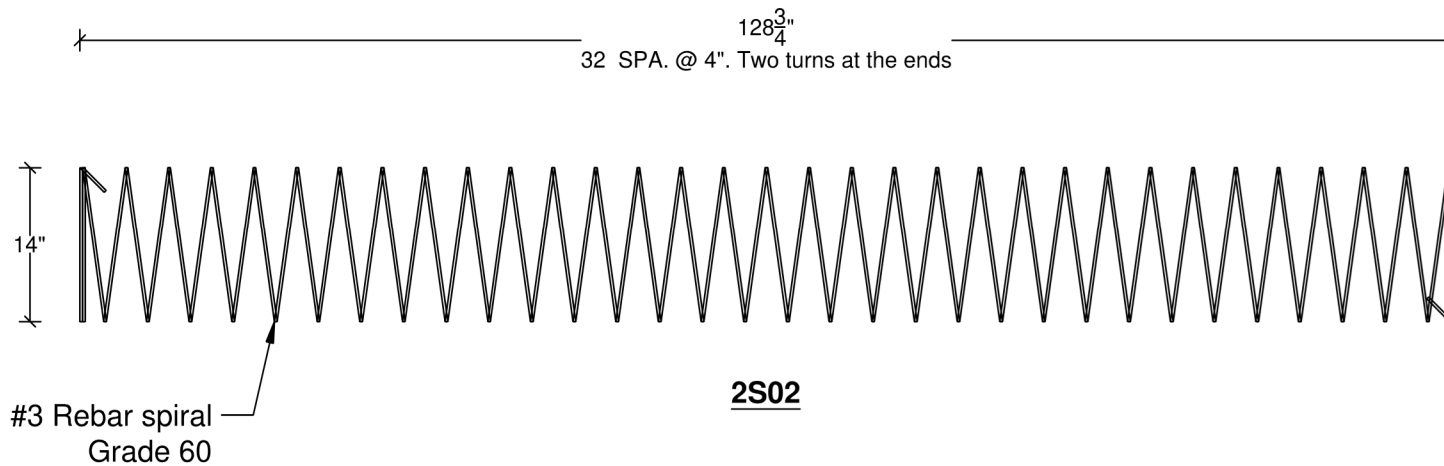
PEER Resilient Bridge Column Test

Pre-cast column: SLV01 Sub-components

BY: AN CHK: Date: 07/15/2017 Scale: 2"=35"

**Sheet
3 of 6**






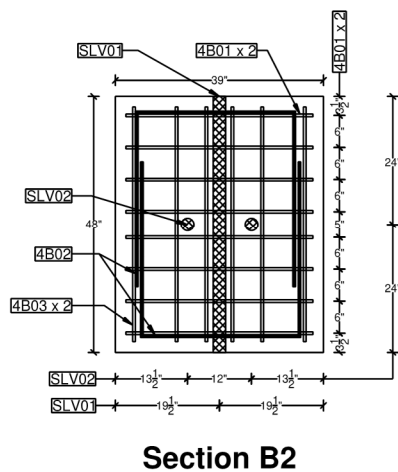
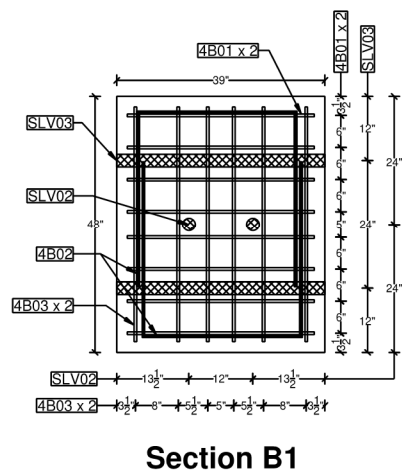
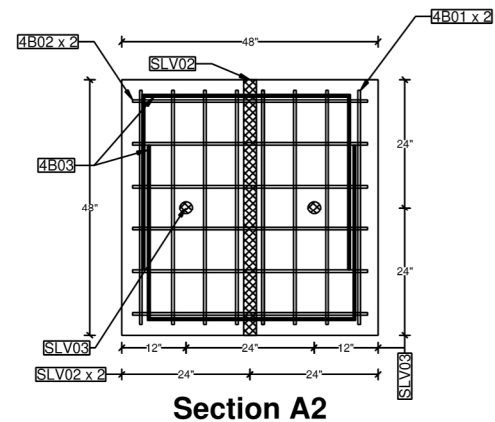
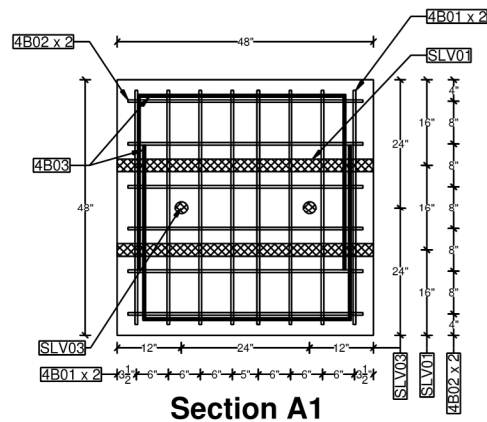
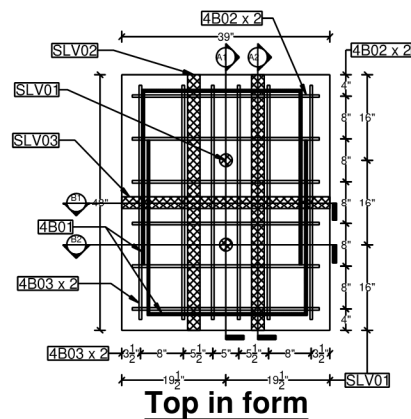
Reinforcing Schedule			
Mark	Quantity		Description
	PC	Total	
4B01	10	42	#4 ASTM A706 Grade 60 184" long straight bar Two (2) extra for material testing
ANCH01	1	4	$\frac{3}{8}$ " ASTM A722 PT bar
2S01	2	8	#3 Spiral, ASTM A615 Grade 60 OD=14", pitch=4", 6 turns + Two closing turns at each end Rebar length=38' (per mark) / 304' (Total)
2S02	1	4	#3 Spiral, ASTM A615 Grade 60 OD=14", pitch=4", 32 turns + Two closing turns at each end Rebar length=135' (per mark) / 540' (Total)
SLV01	1	4	$\frac{1}{4}$ " thick steel pipe, 184" length, O.D=16" <u>See detail, Sheets 2 & 3</u>


Bill of Materials			
Mark	Quantity		Description
	PC	Total	
SLV03	1	4	158" long , 2" ID PVC for $\frac{3}{8}$ PT bar

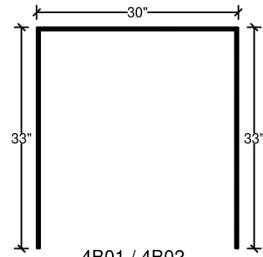
Concrete Specifications			
Mix Design	Unit Weight (P.C.F)	Volume (CU.YD.)	f' _C (P.S.I.)
-	150	1.0	6000

No. Required: 4

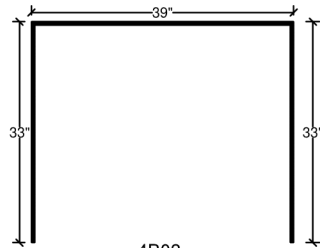
	Revisions		PEER Resilient Bridge Column Test				Sheet 6 of 6
	07-20-2017	Modify SLV01-B and SLV01-C length					
	07-20-2017	Modify SLV01-B production method	Pre-cast column: Bill of Materials				
	07-20-2017	Change bonding method in PT Anchor ANCH01					
	07-20-2017	4 bore to SLV01-C for instrumentation					
		BY: AN	CHK:	Date: 07/15/2017	Scale: -		



	PEER Resilient Bridge Column Test					Sheet 1 of 2
	Inertial Mass Blocks					
	BY:	AN	CHK:	Date:	05/12/2017	



4B01 / 4B02



4B03

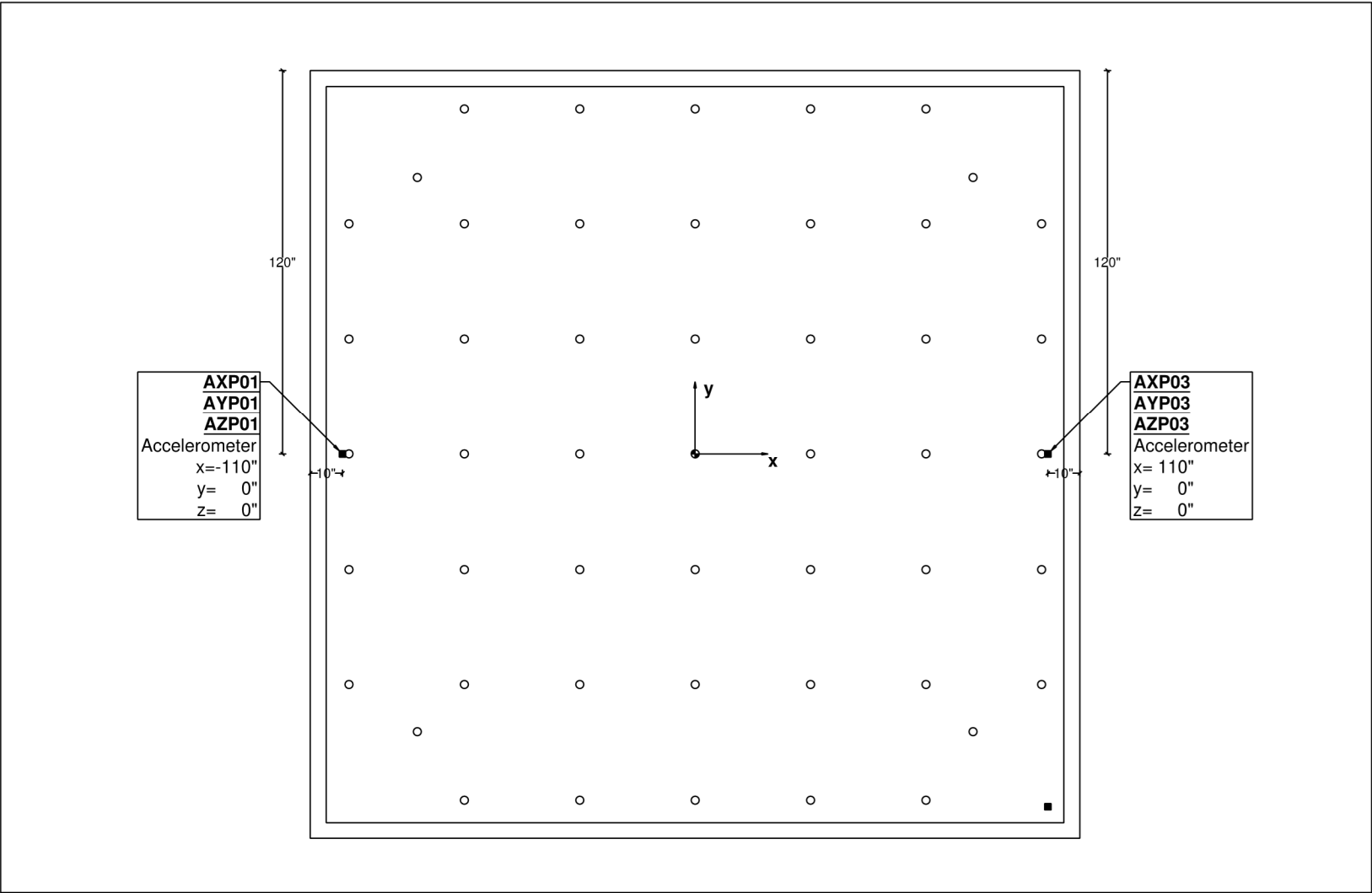
Reinforcing Schedule			
Mark	Quantity		Description
	PC	Total	
4B01	16	96	#4 ASTM A615 G60
4B02	12	72	#4 ASTM A615 G60
4B03	12	72	#4 ASTM A615 G60


Bill of Materials			
Mark	Quantity		Description
	PC	Total	
SLV01	2	12	48" long, 2" ID PVC duct
SLV02	2	12	48" long, 2" ID PVC duct
SLV03	2	12	39" long, 2" ID PVC duct

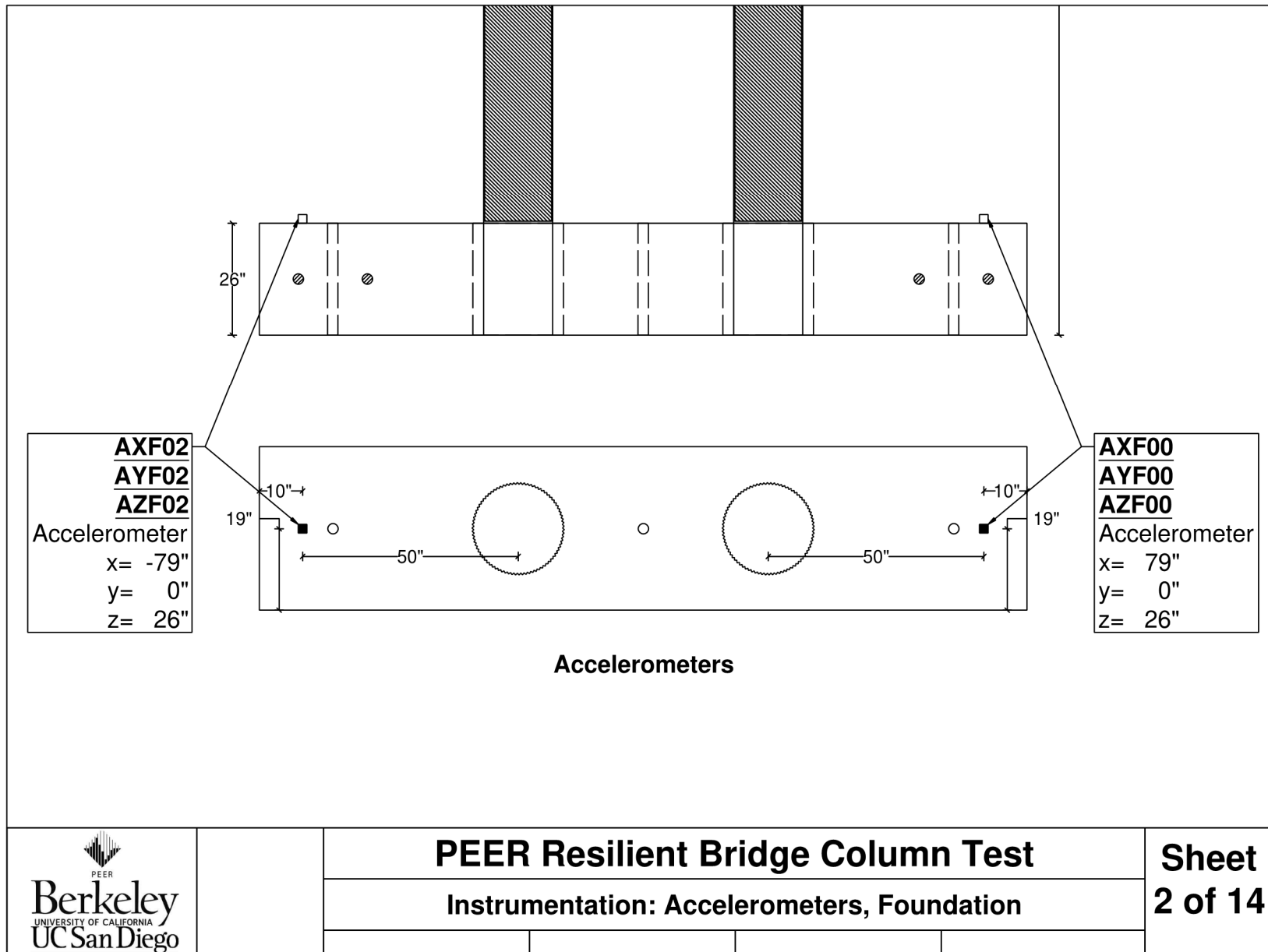
Concrete Specifications			
Mix Design	Unit Weight (P.C.F)	Volume (CU.YD.)	f' _c (P.S.I.)
-	150	1.9	4000

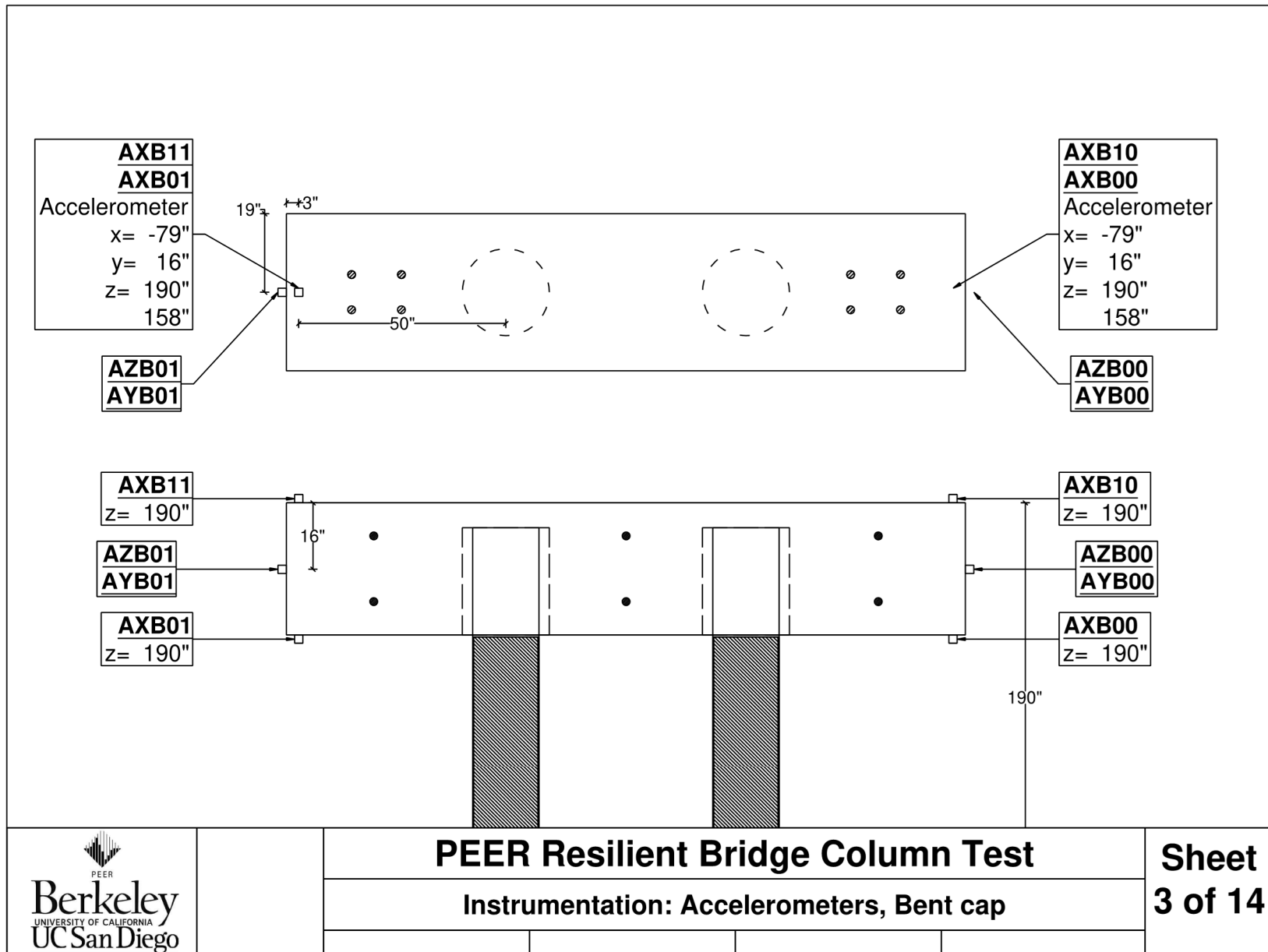
No. Required: 6

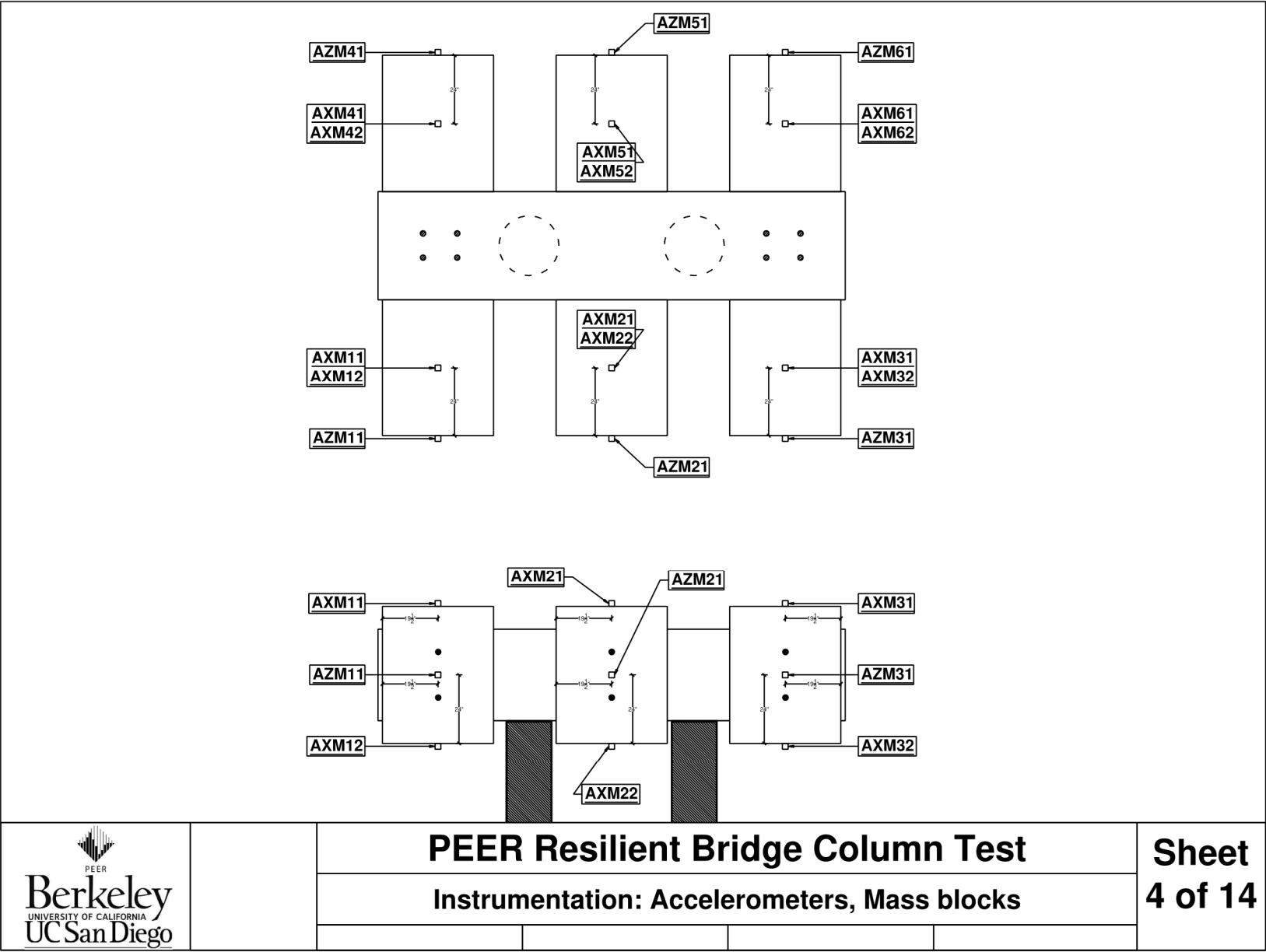
Appendix B Instrumentation Layout

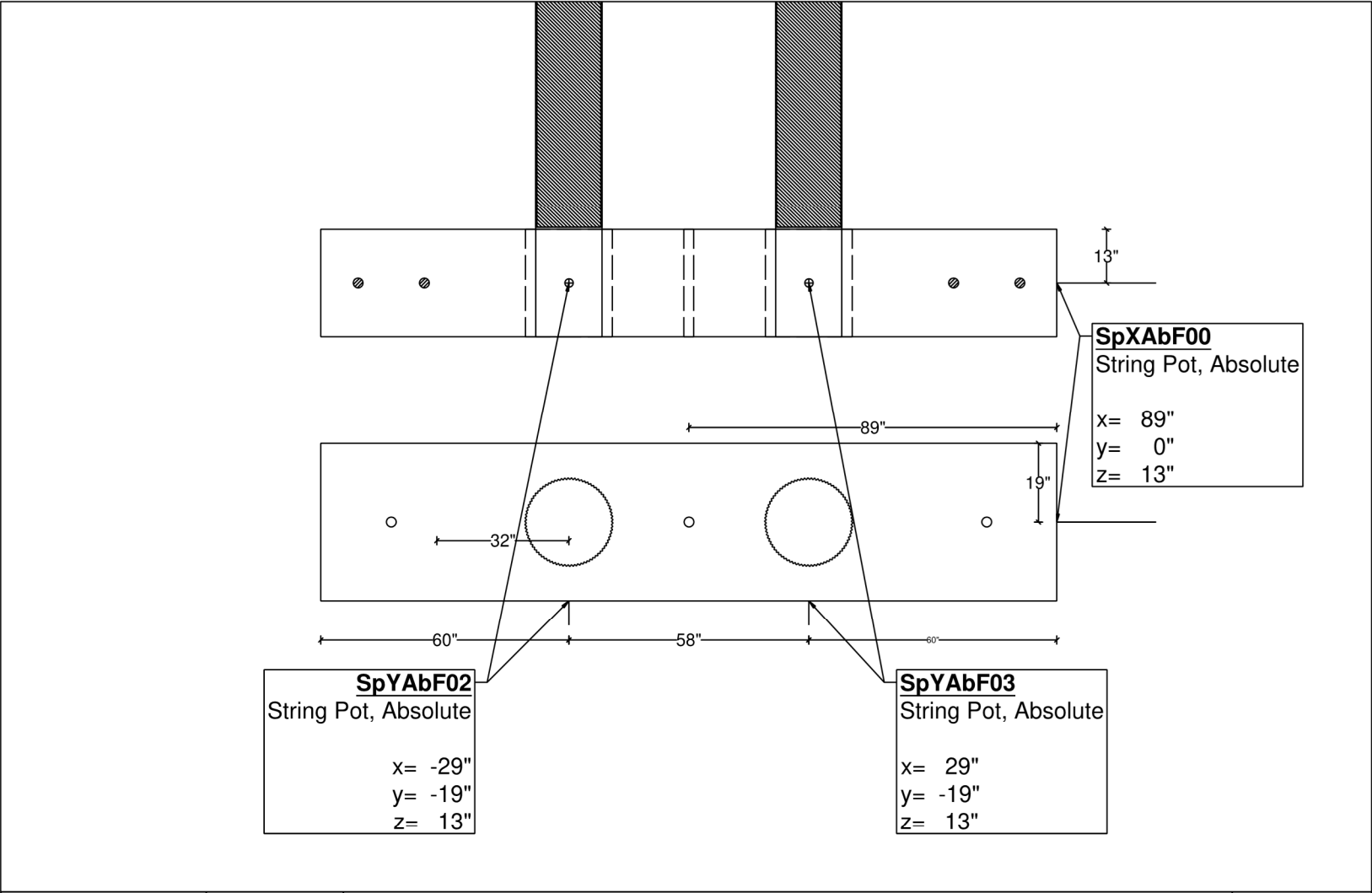



	PEER Resilient Bridge Column Test				Sheet 1 of 14
	Accelerometers: Platen				

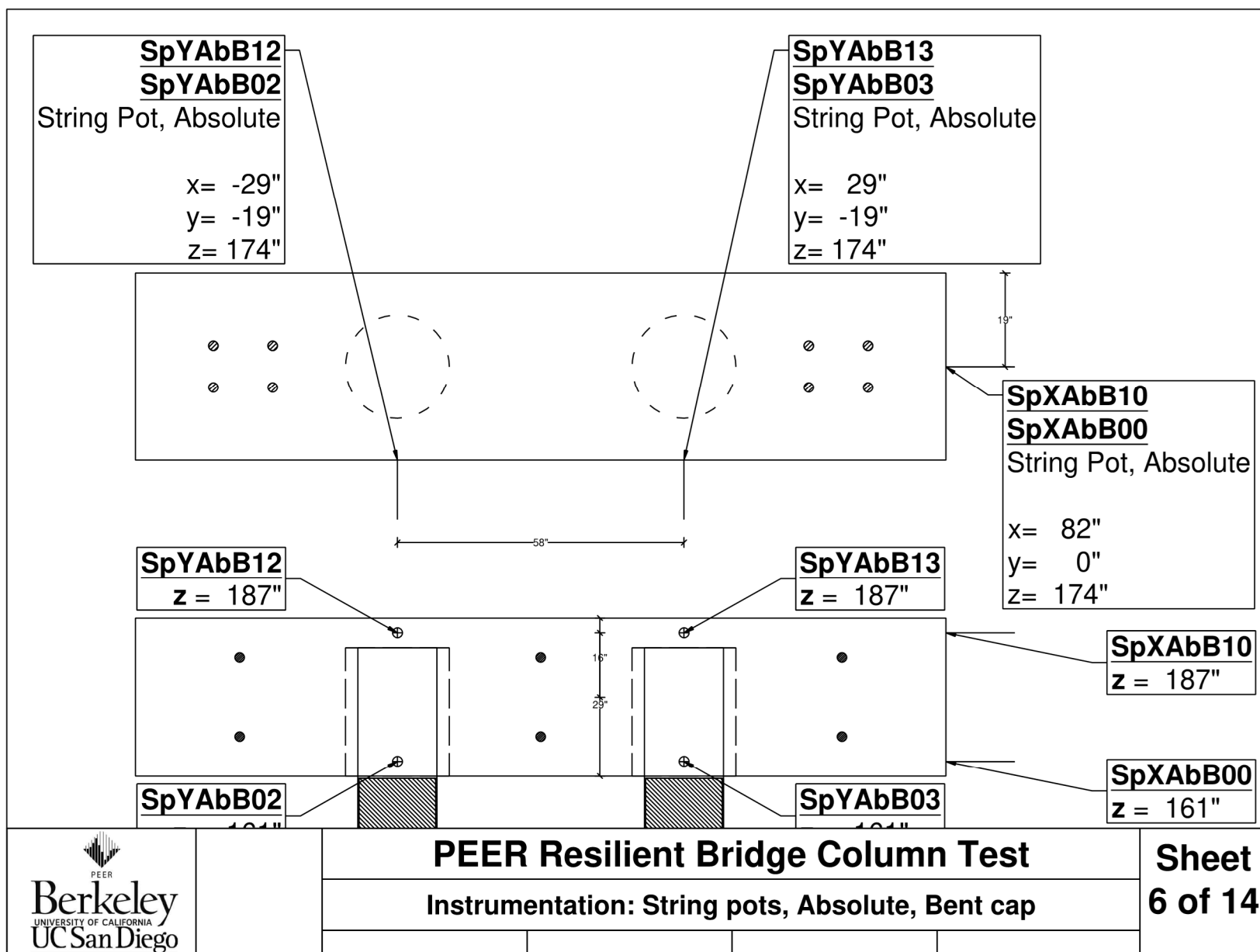


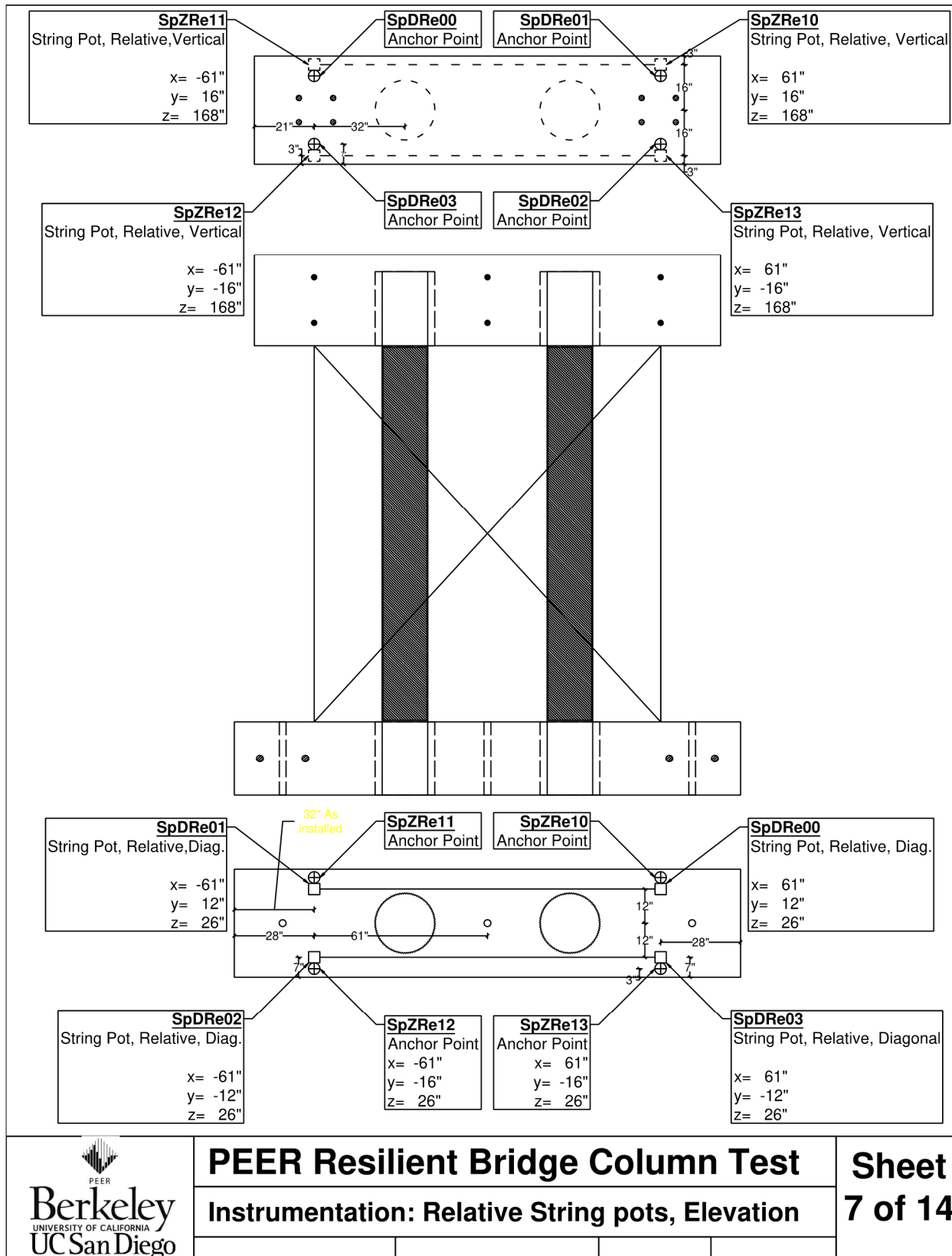


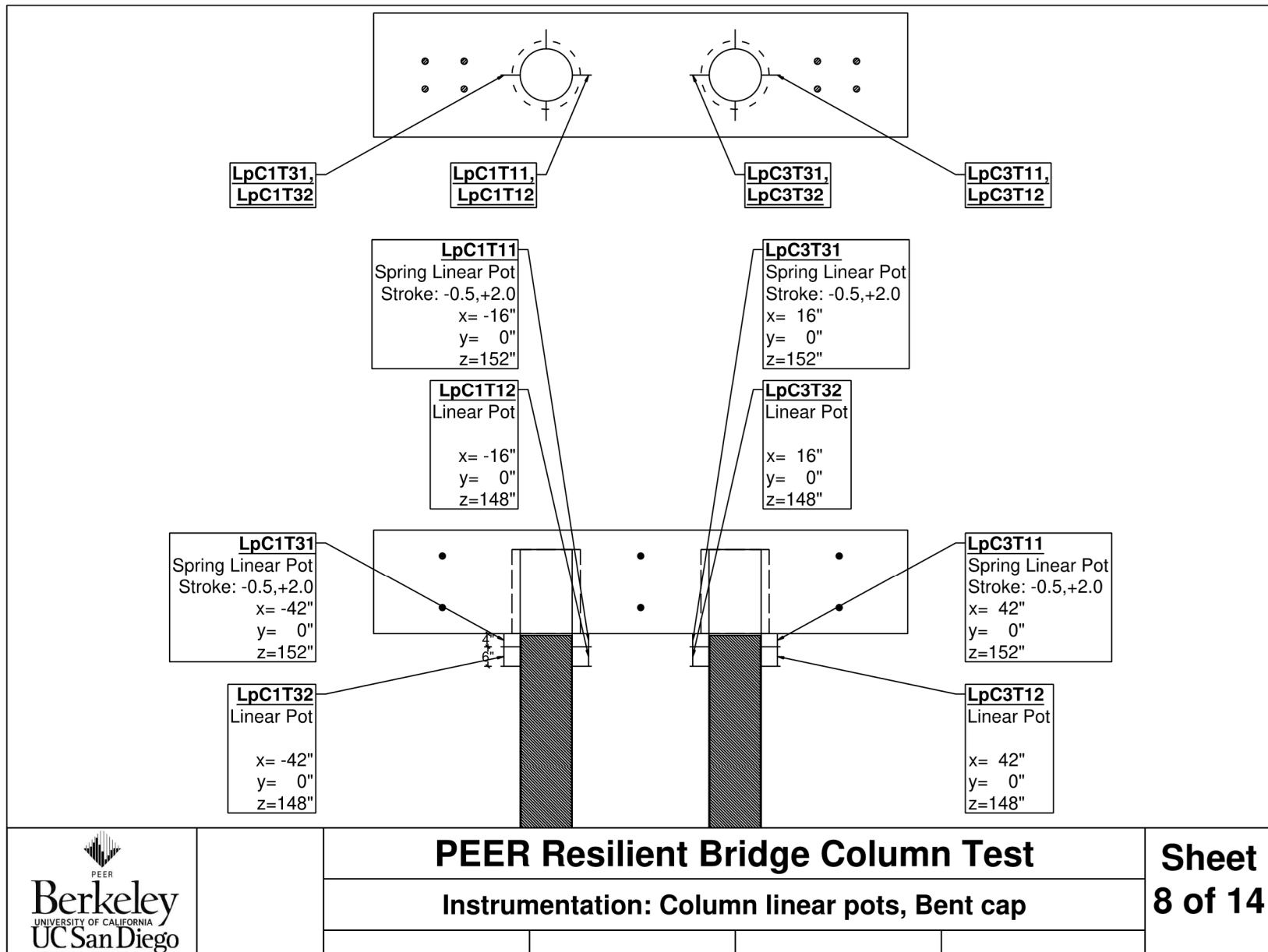


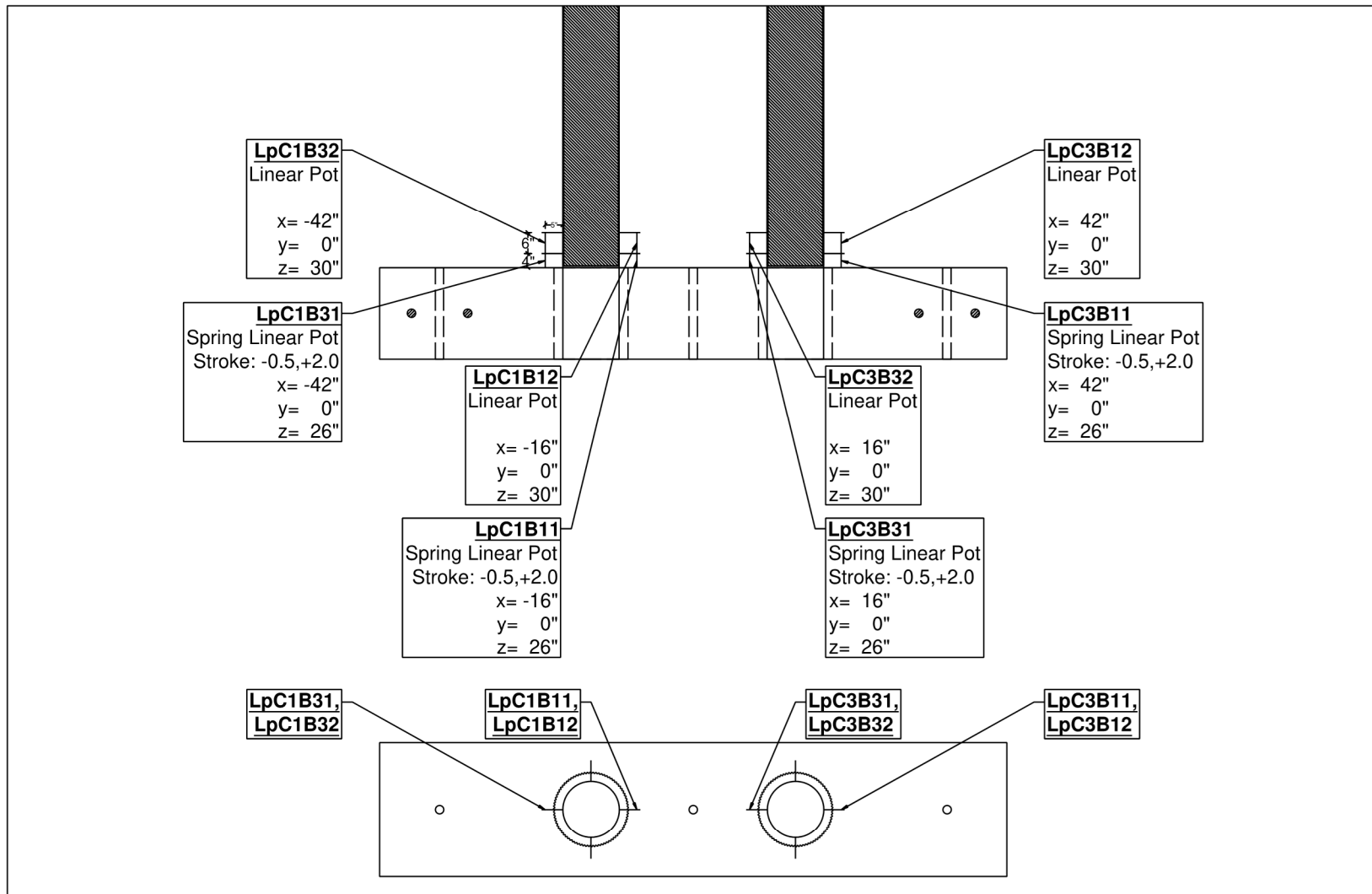


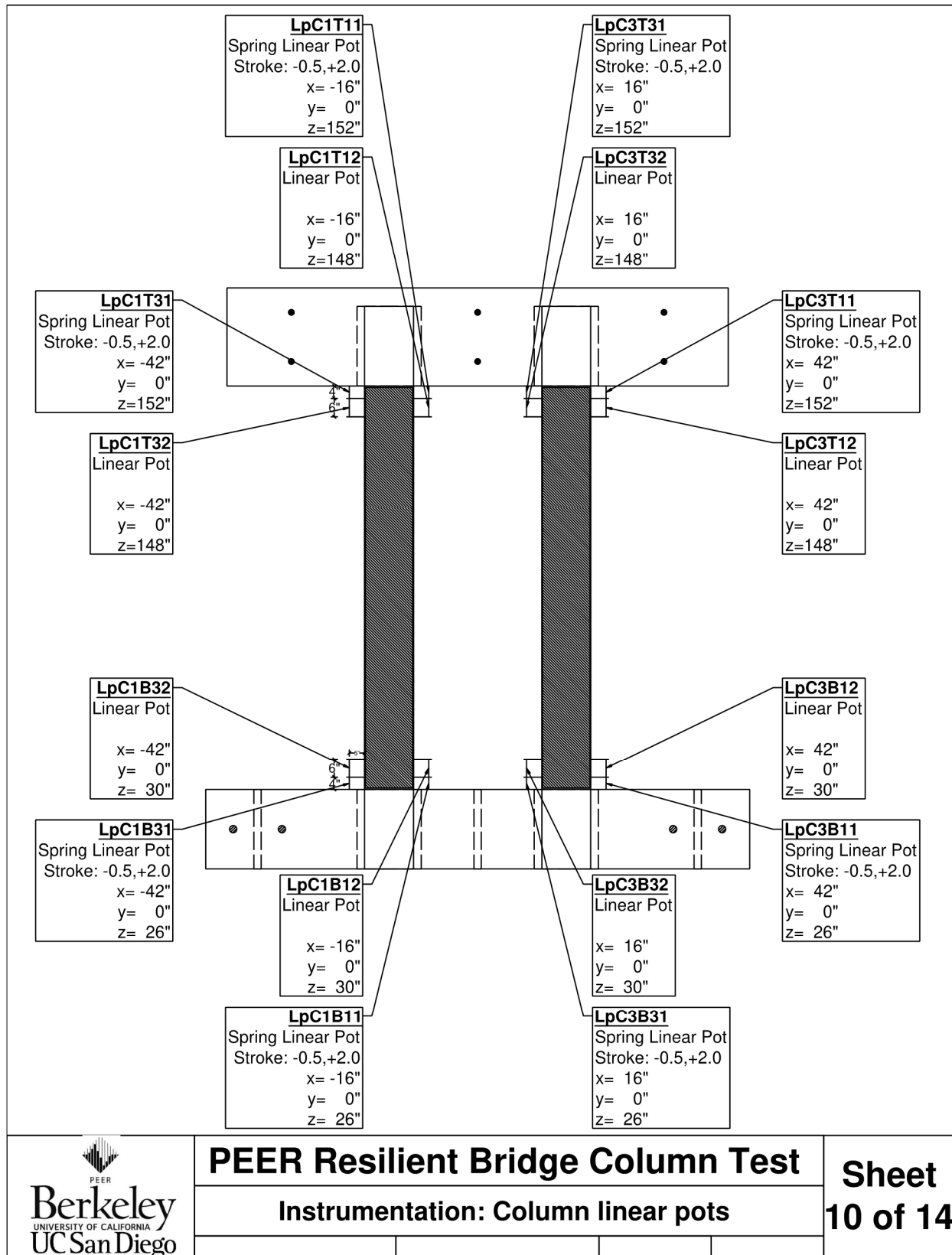
	PEER Resilient Bridge Column Test				Sheet 5 of 14
	Instrumentation: String pots, Absolute, Foundation				

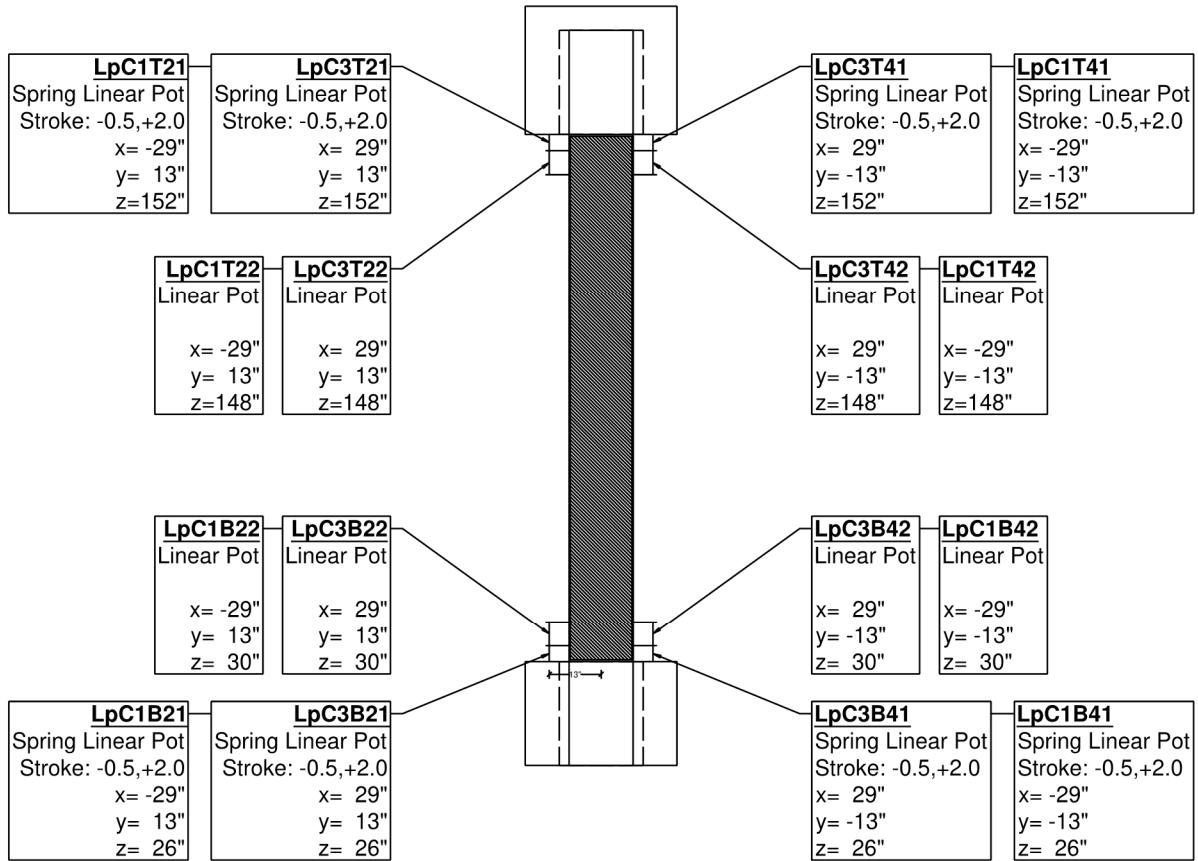


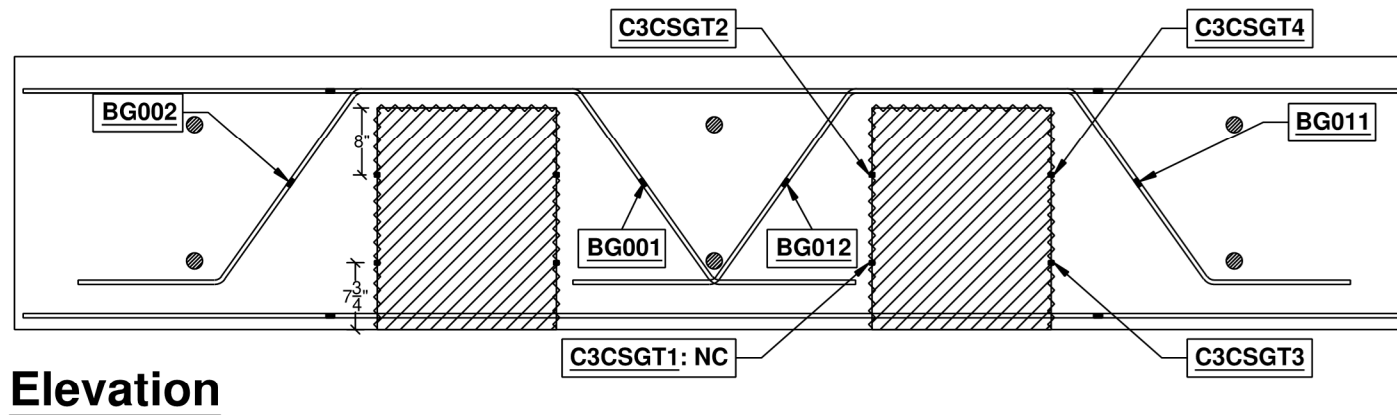
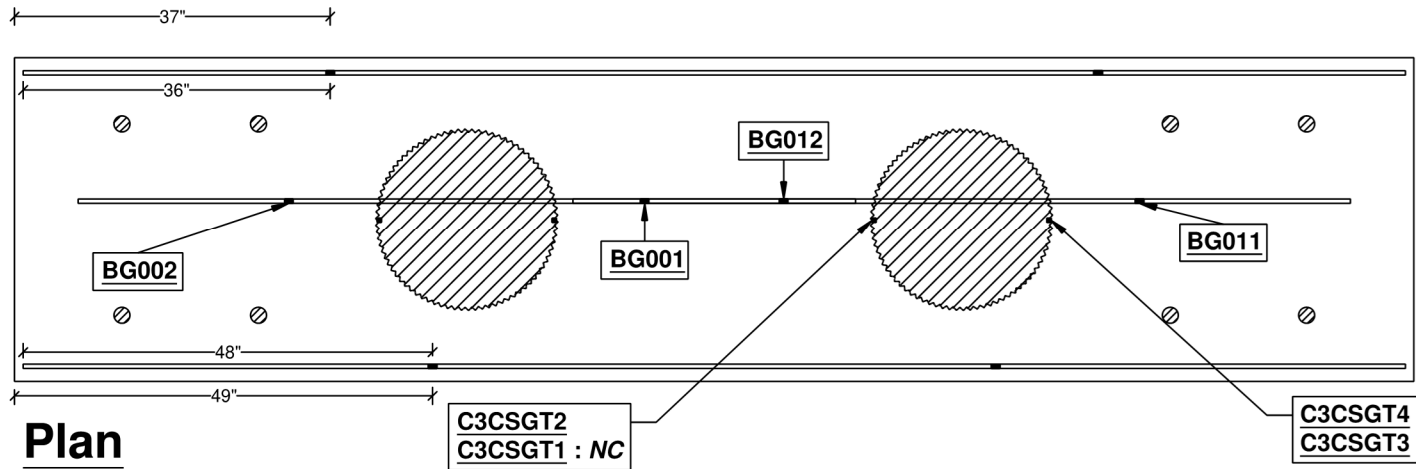


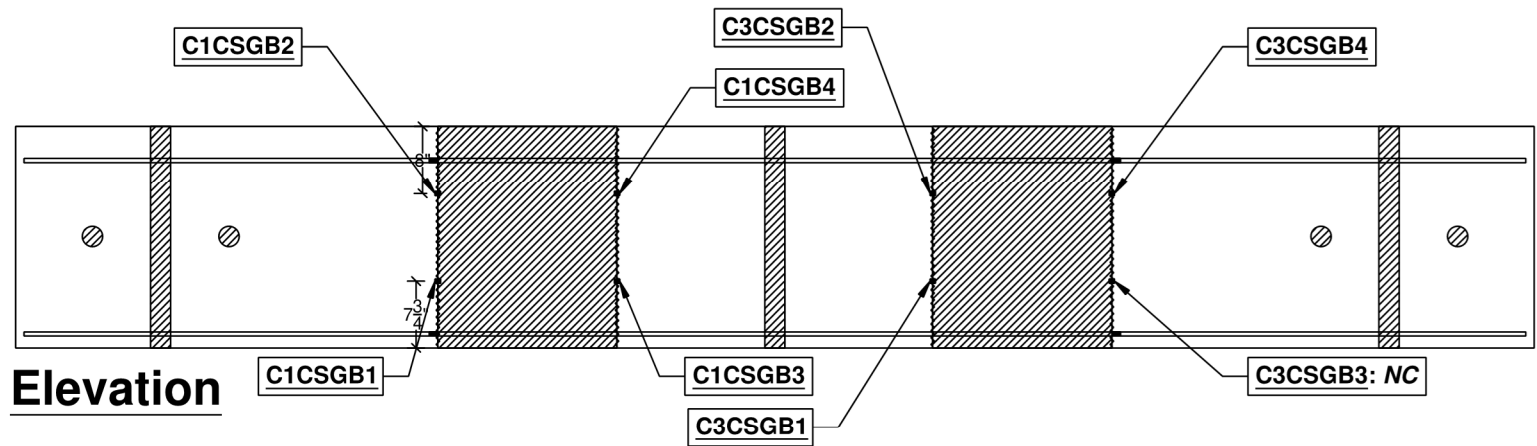
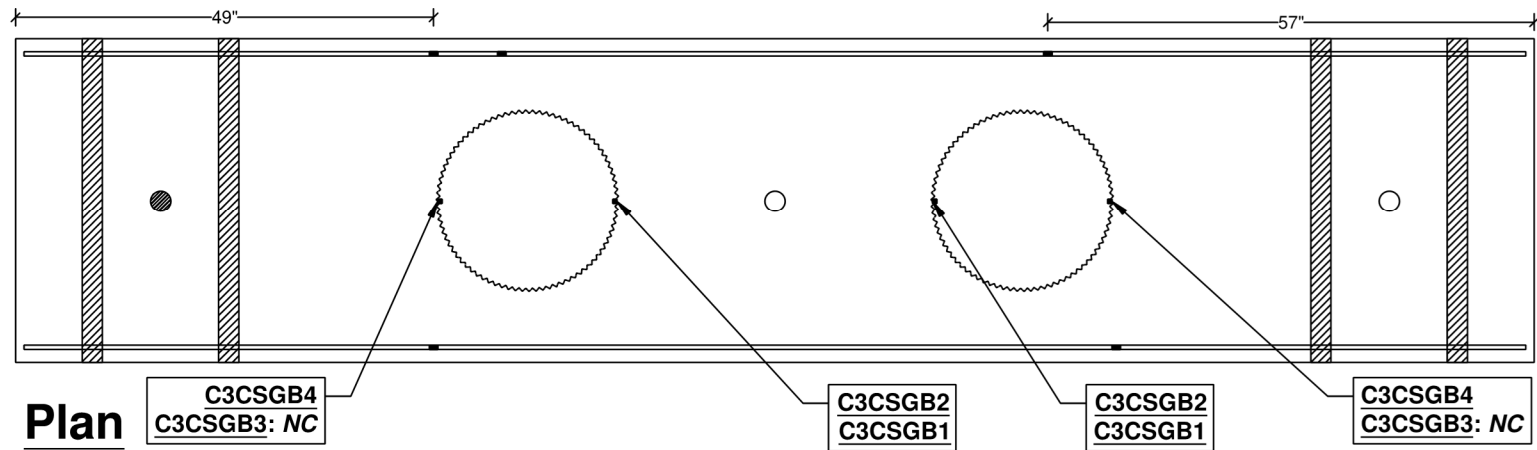


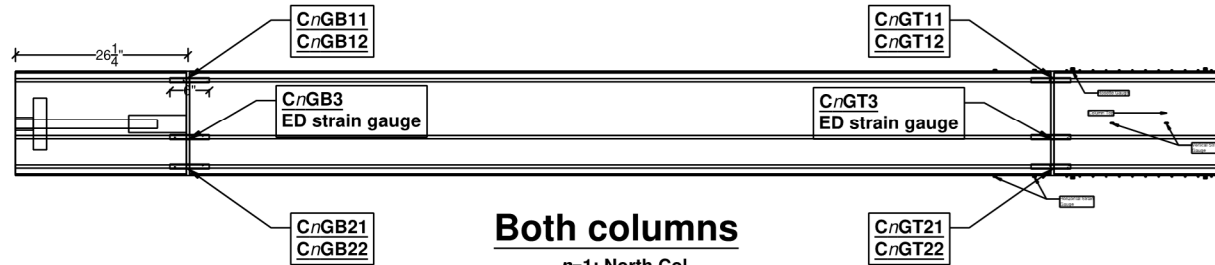






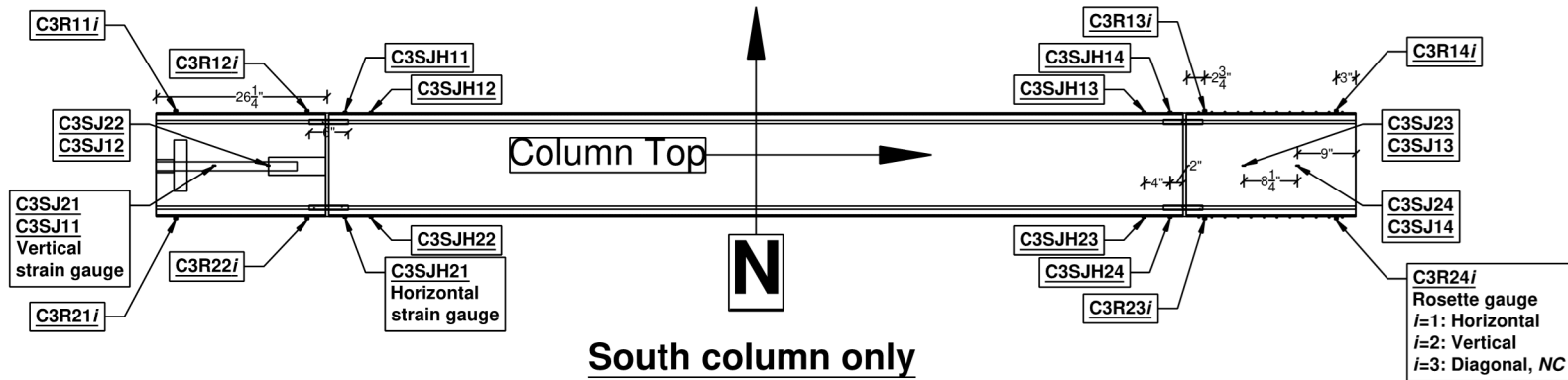






Both columns

*n=1: North Col.
n=3: South Col.*



South column only

Appendix C Input Time Histories and Spectral Responses

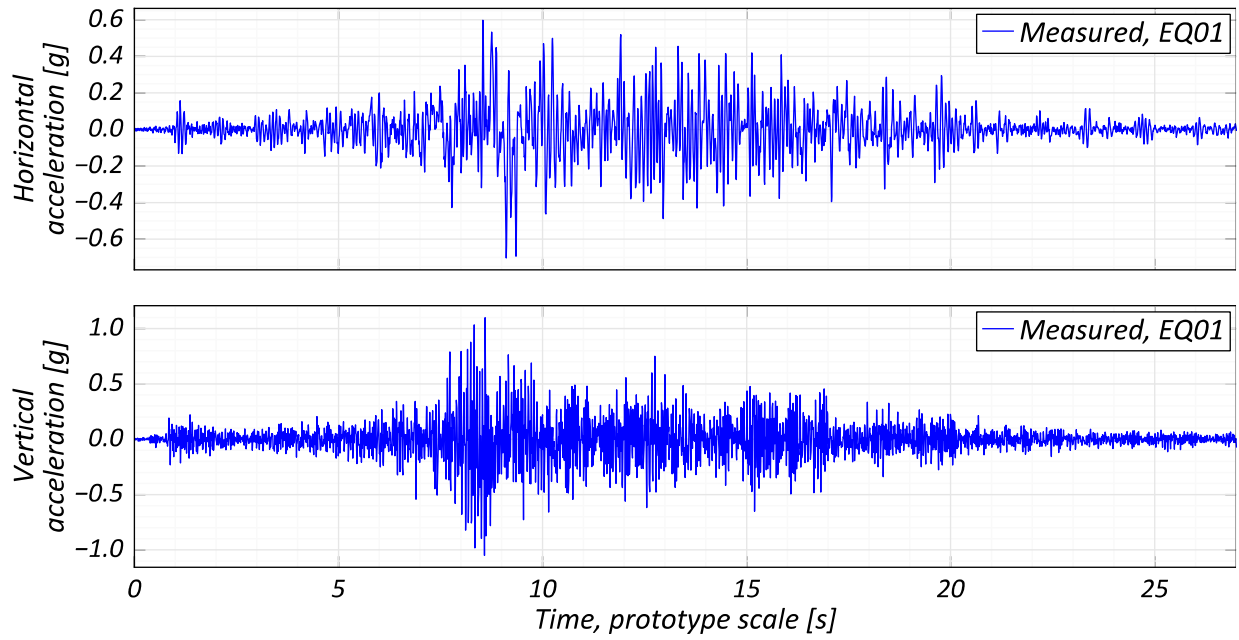


Figure C.1 EQ01 acceleration time histories.

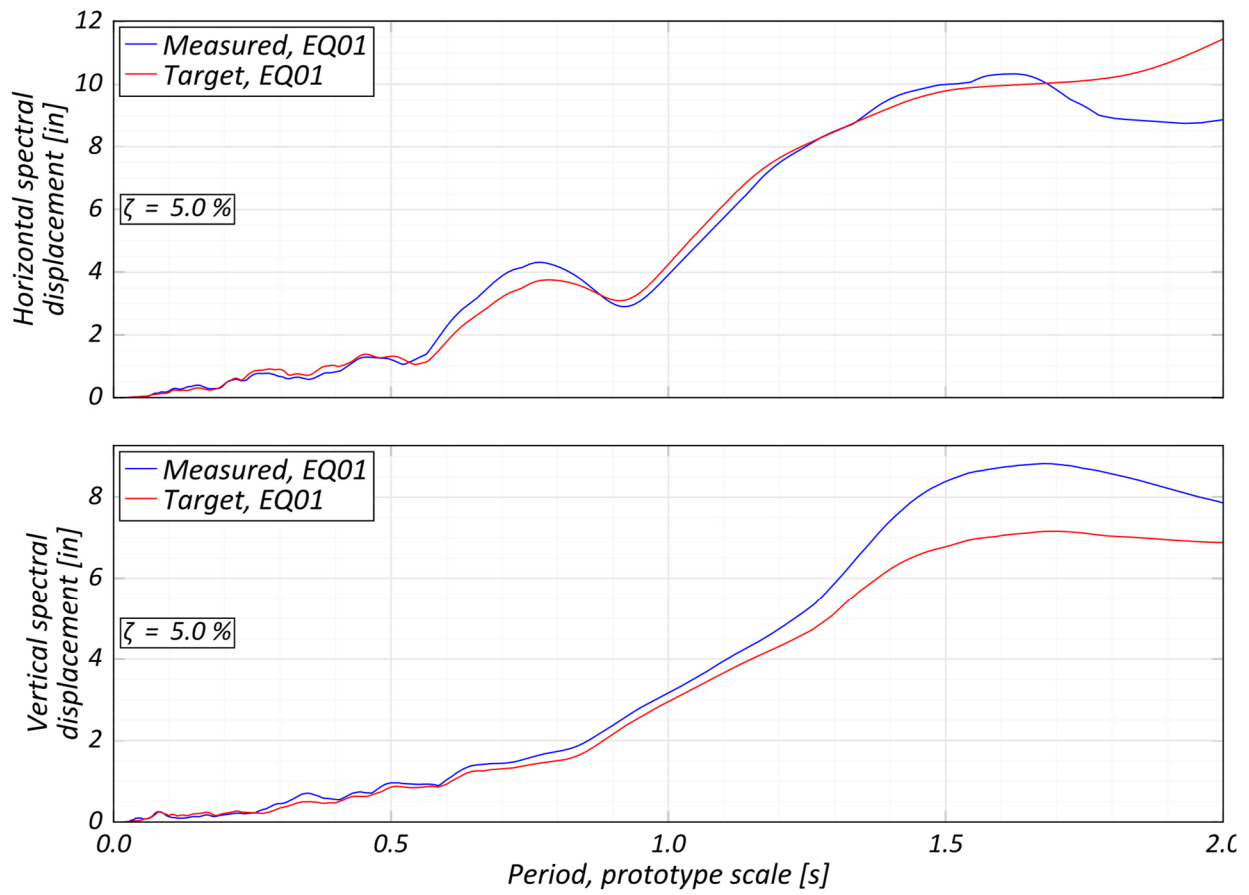


Figure C.2 EQ01 spectral responses.

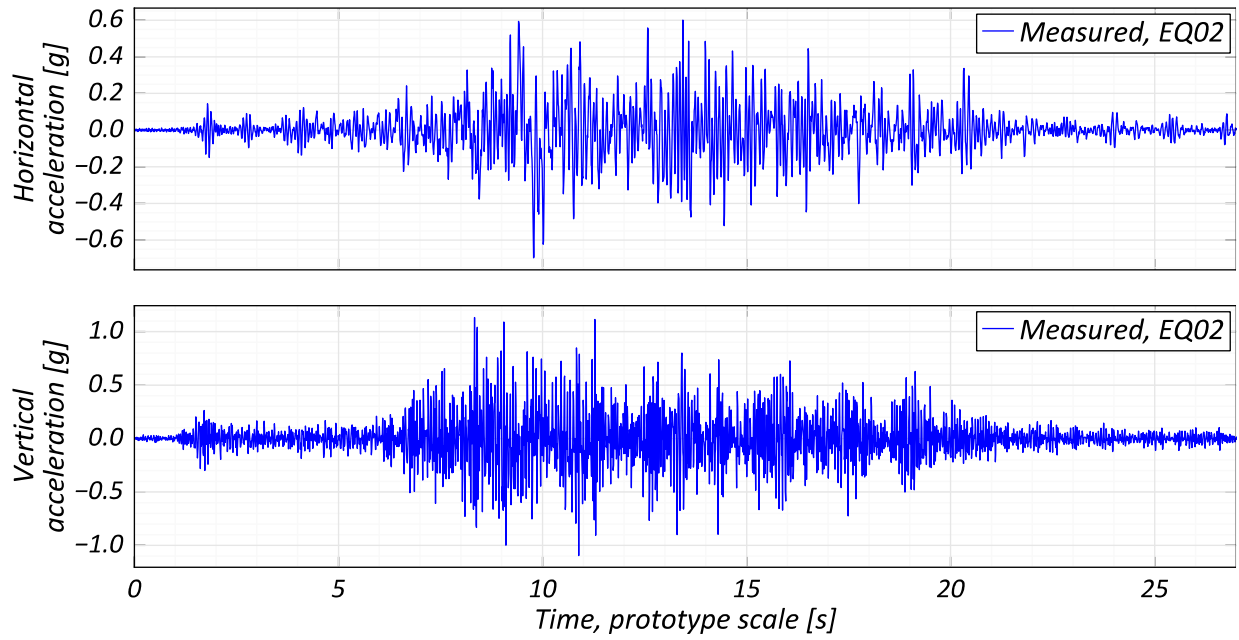


Figure C.3 EQ02 acceleration time histories.

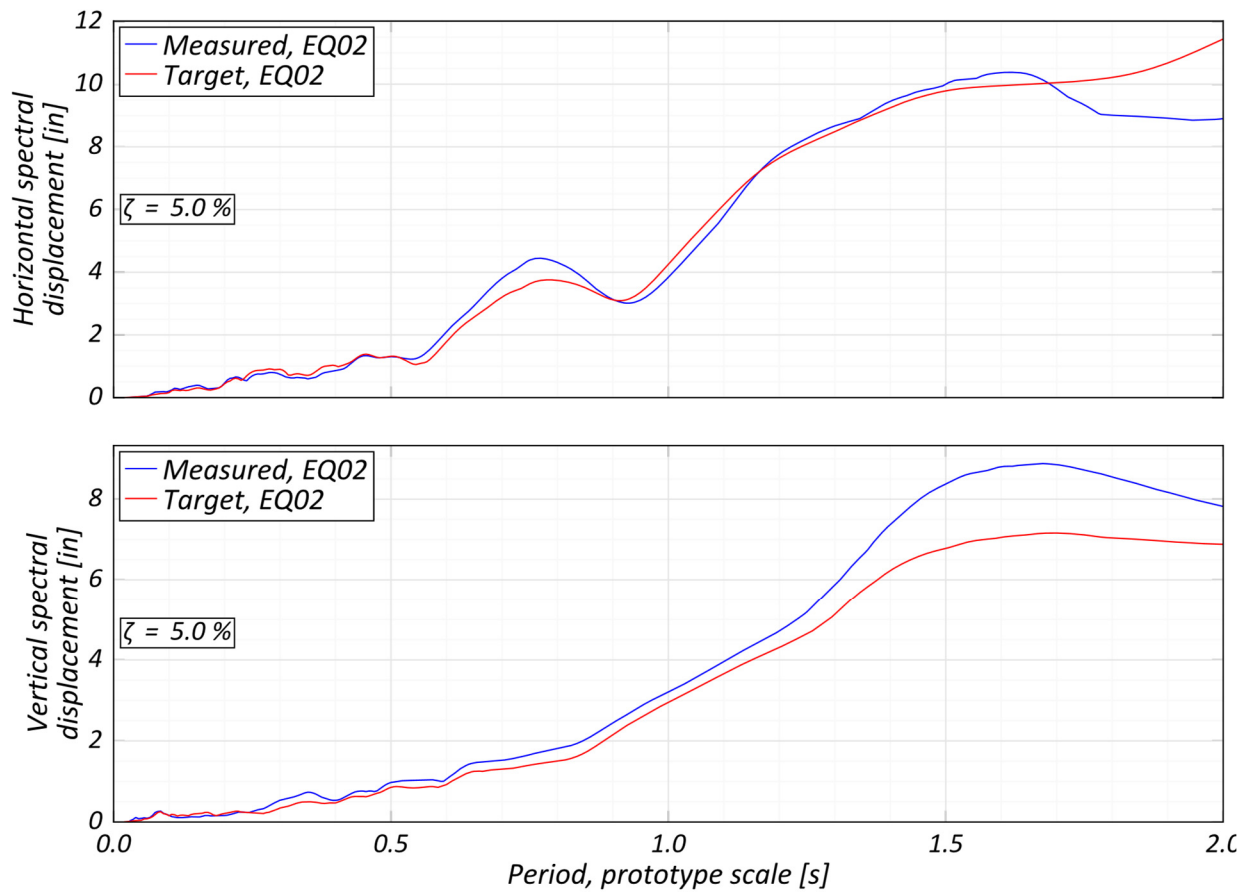


Figure C.4 EQ02 spectral responses.

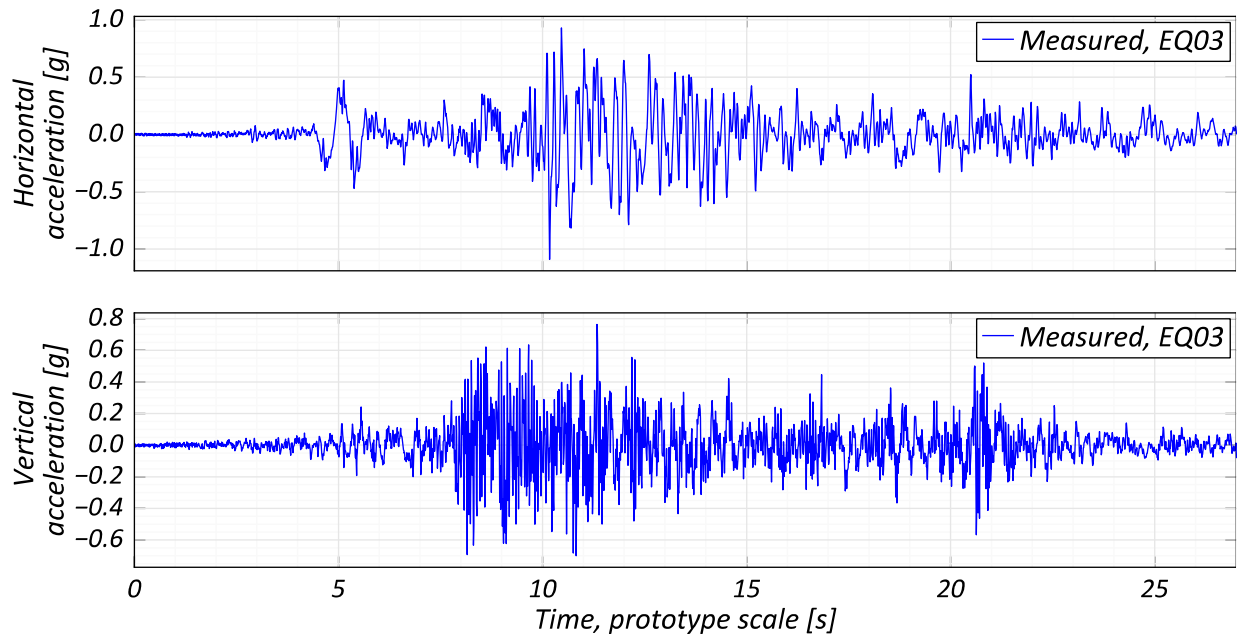


Figure C.5 EQ03 acceleration time histories.

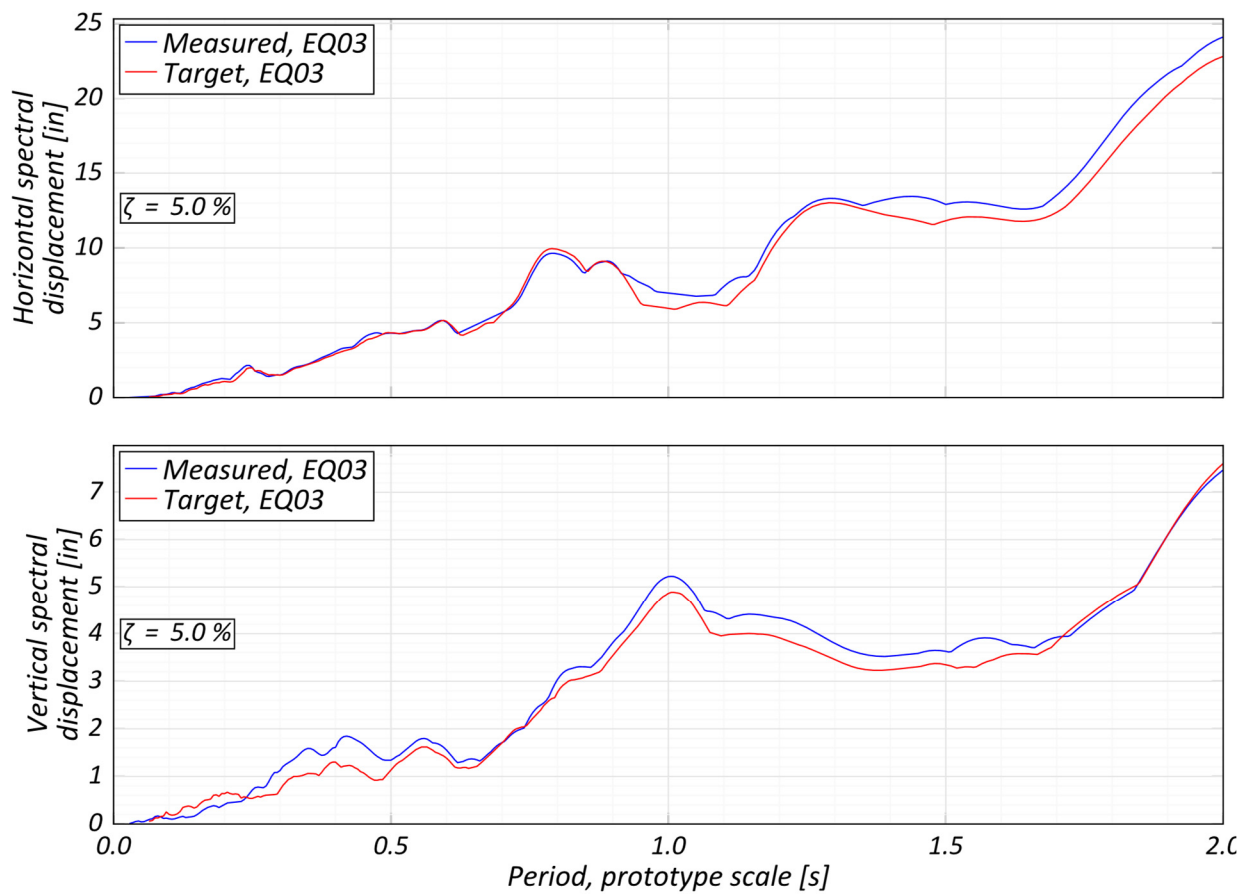


Figure C.6 EQ03 spectral responses.

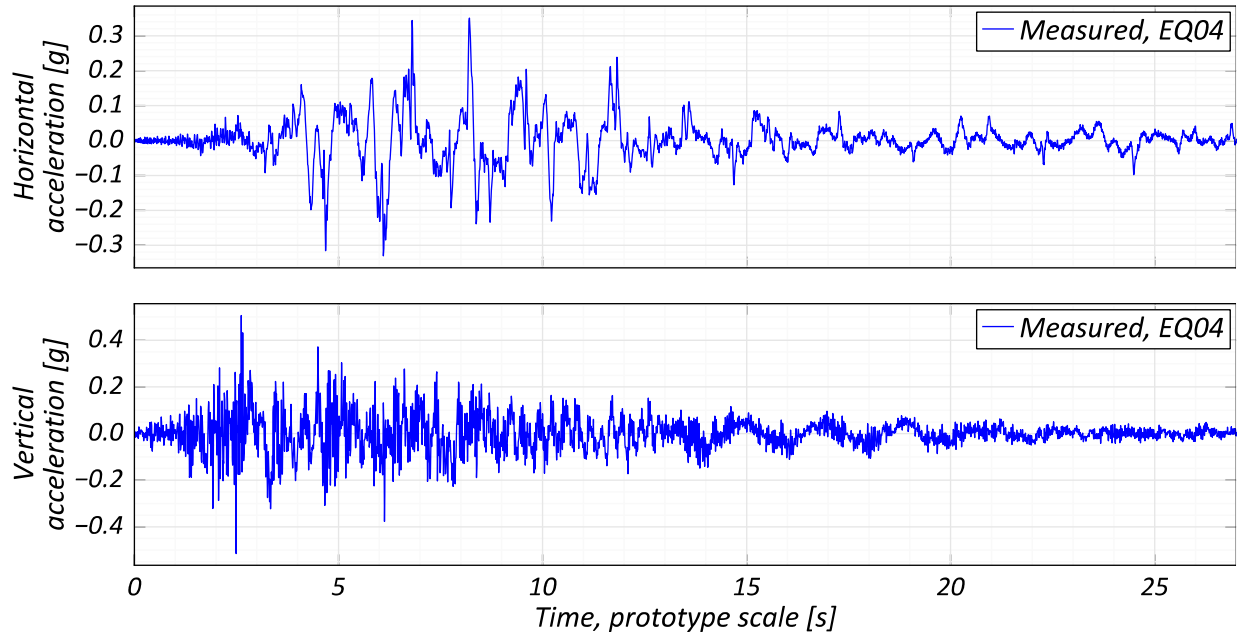


Figure C.7 EQ04 acceleration time histories.

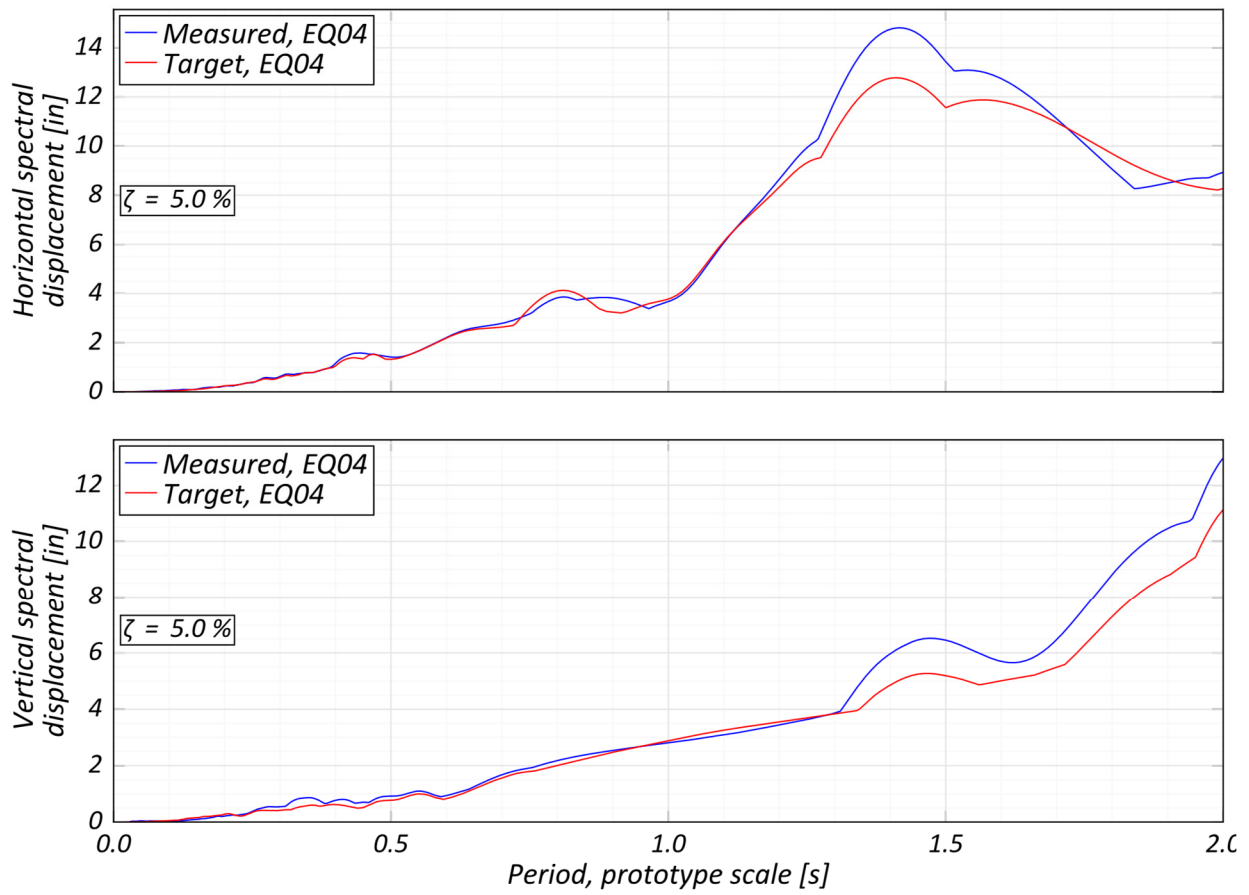


Figure C.8 EQ04 spectral responses.

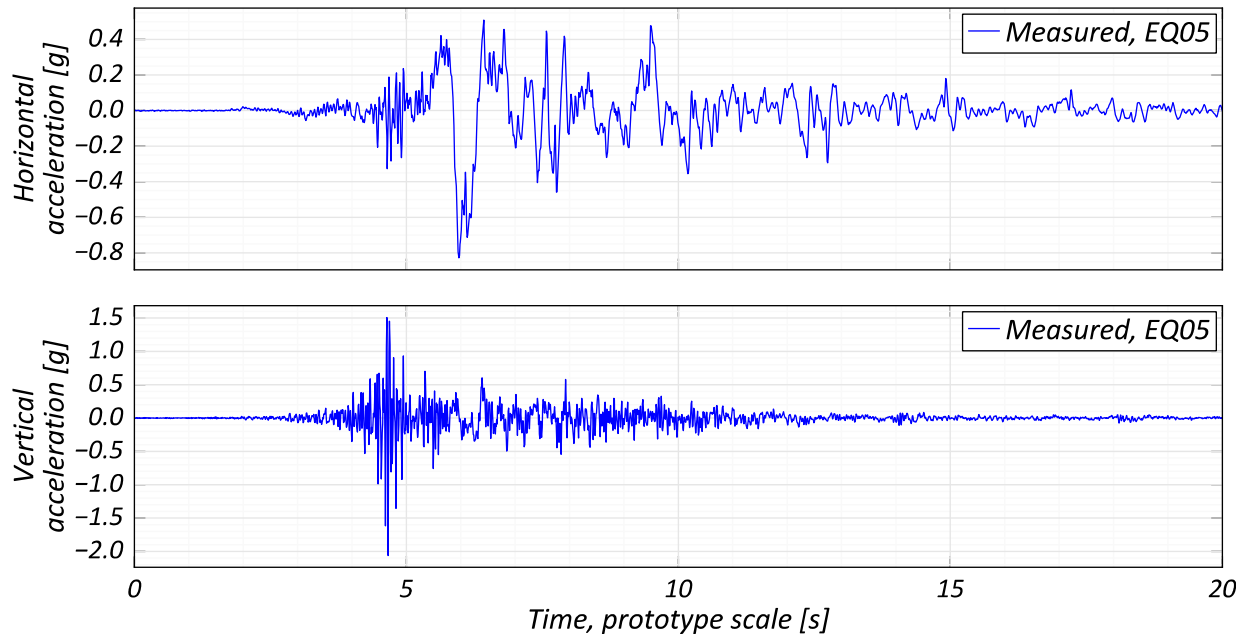


Figure C.9 EQ05 acceleration time histories.

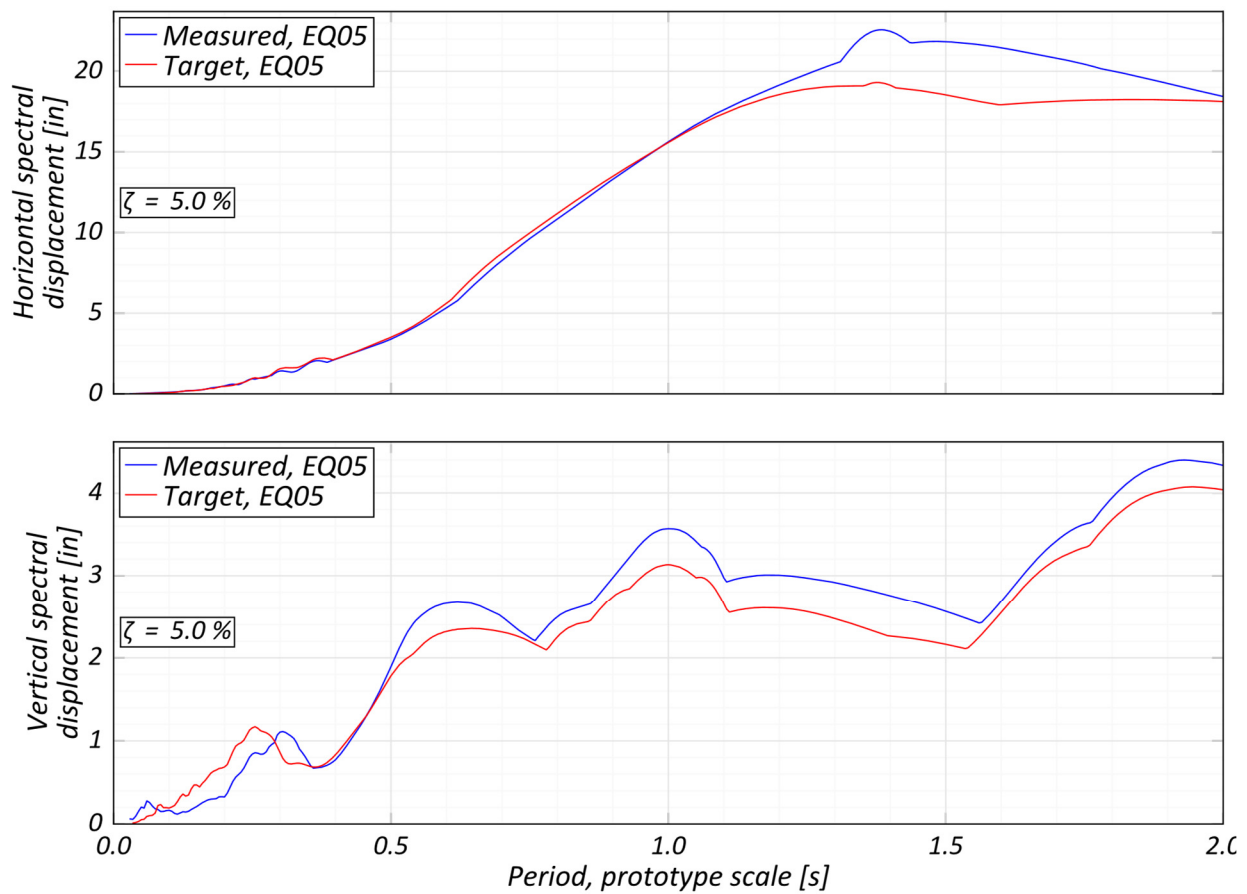


Figure C.10 EQ05 spectral responses.

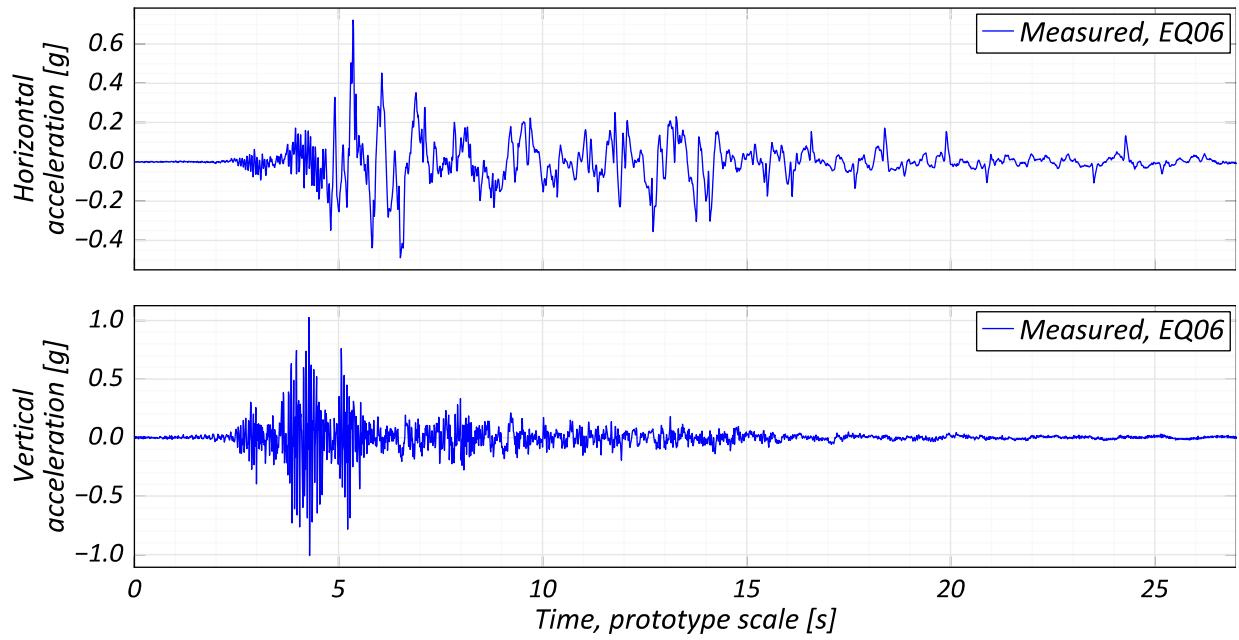


Figure C.11 EQ06 acceleration time histories.

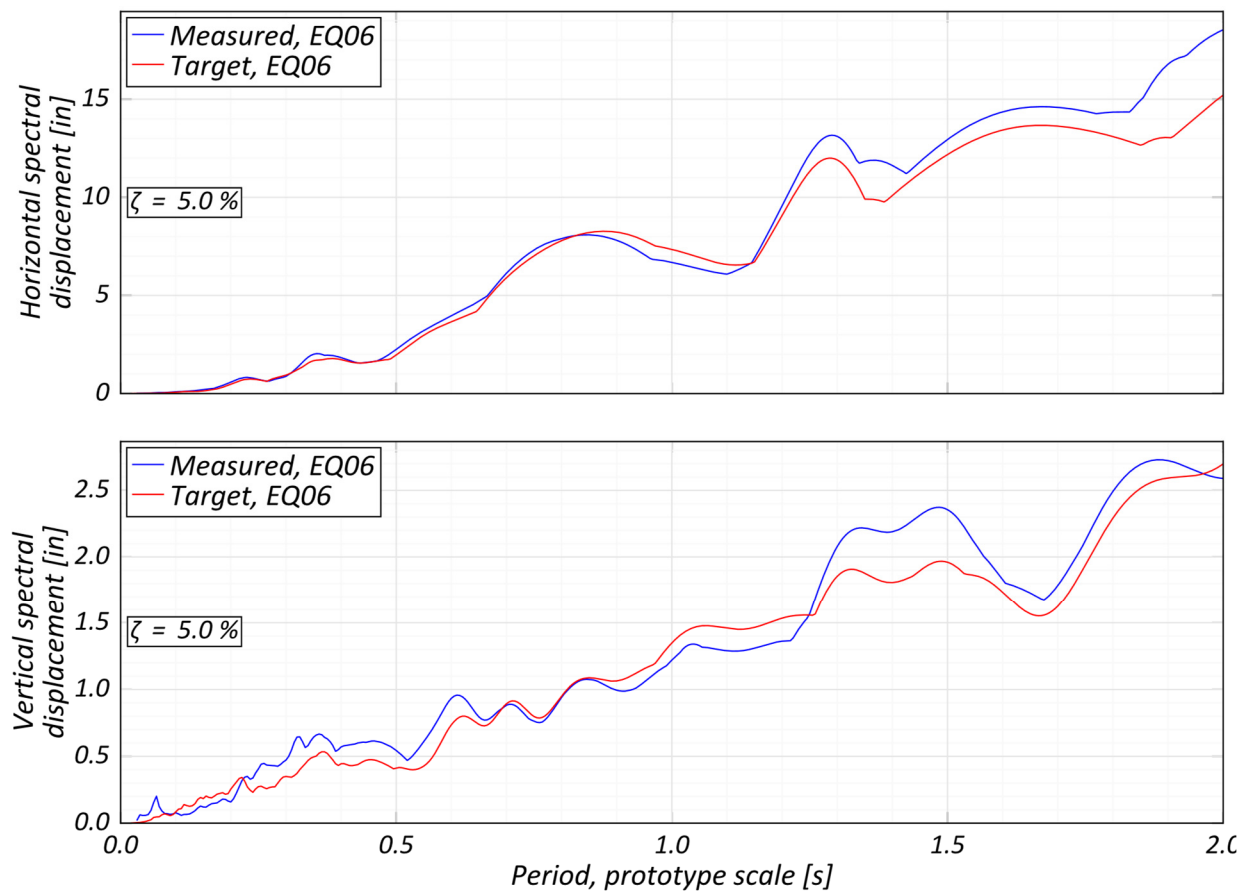


Figure C.12 EQ06 spectral responses.

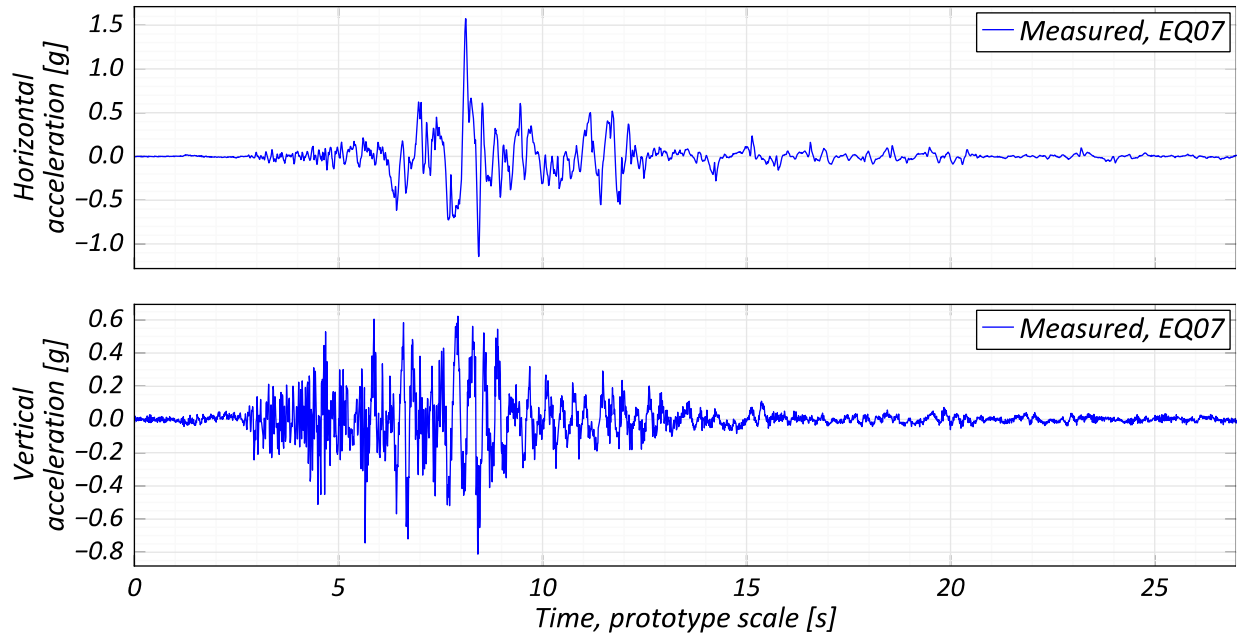


Figure C.13 EQ07 acceleration time histories.

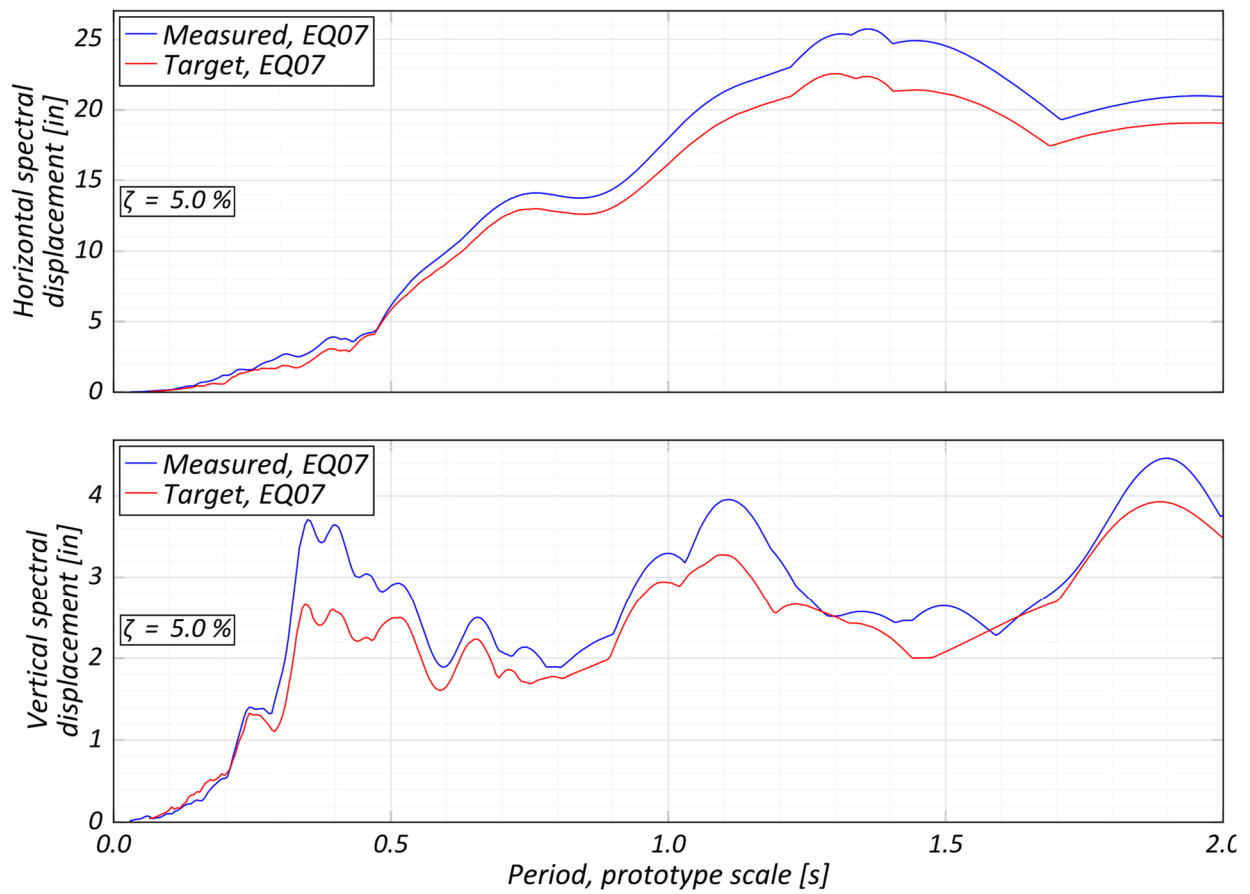


Figure C.14 EQ07 spectral responses.

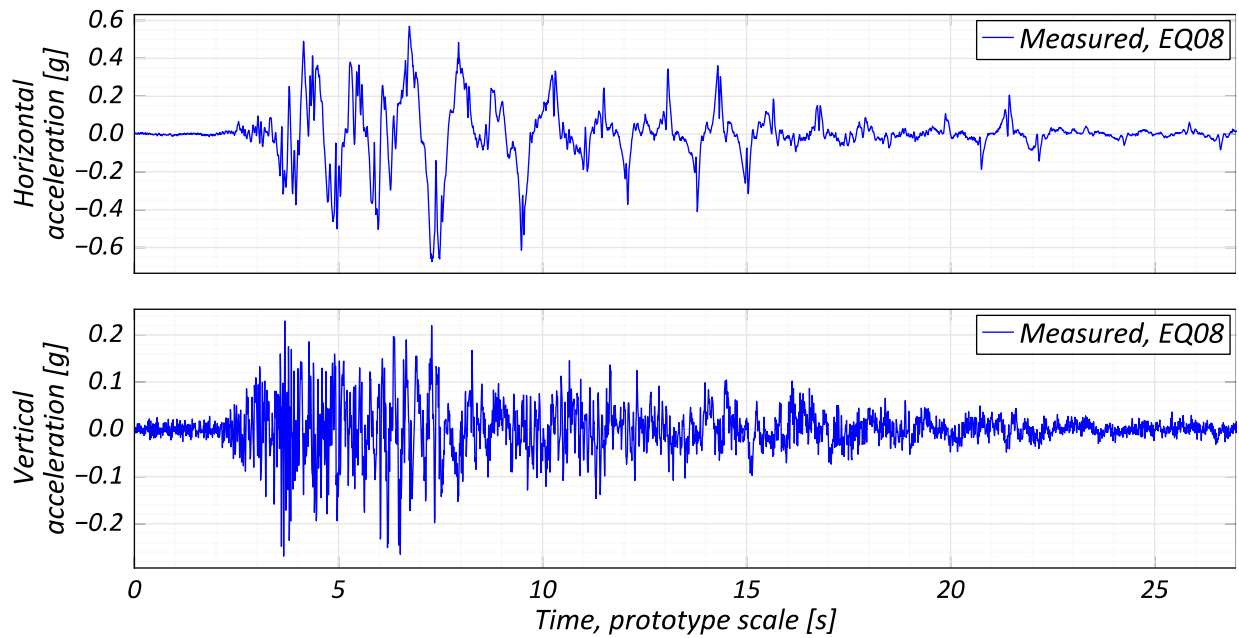


Figure C.15 EQ08 acceleration time histories.

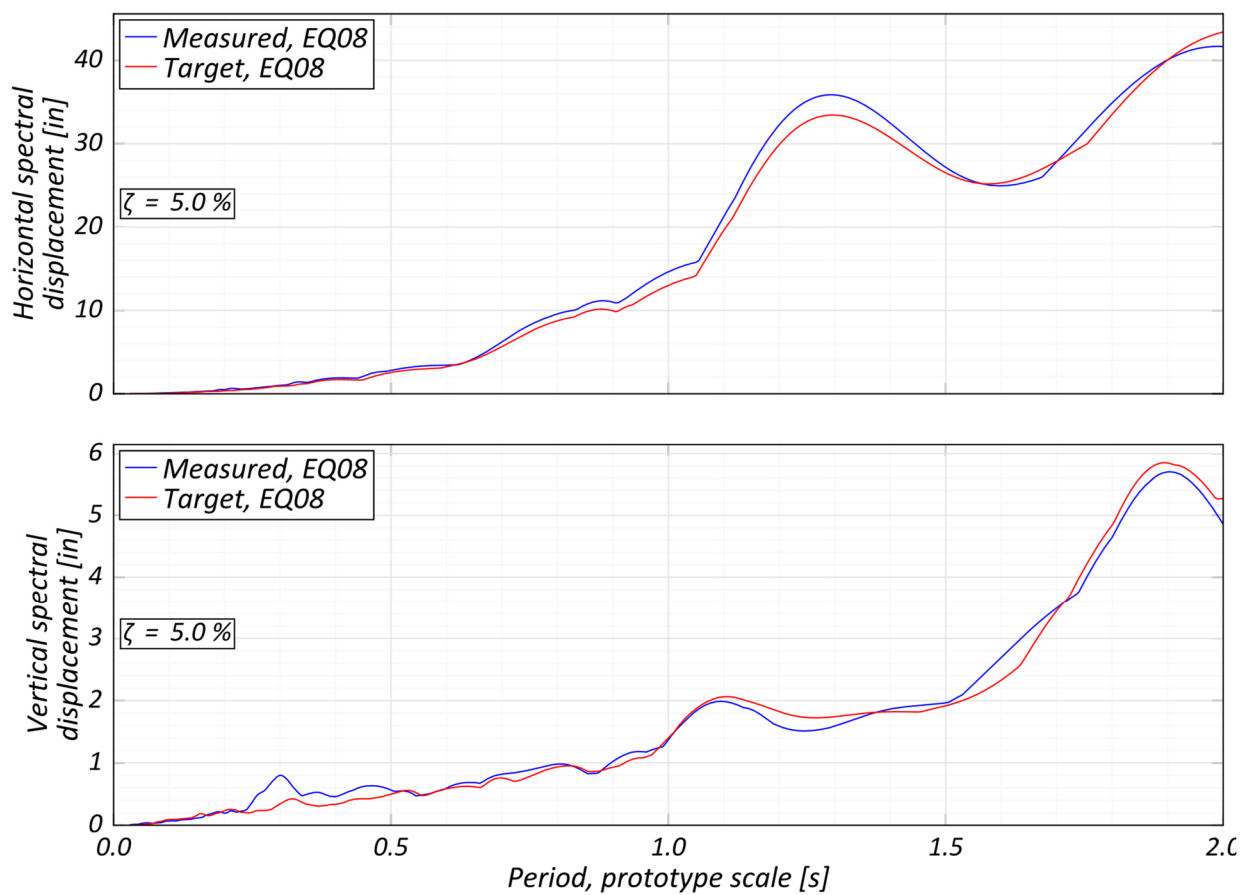


Figure C.16 EQ08 spectral responses.

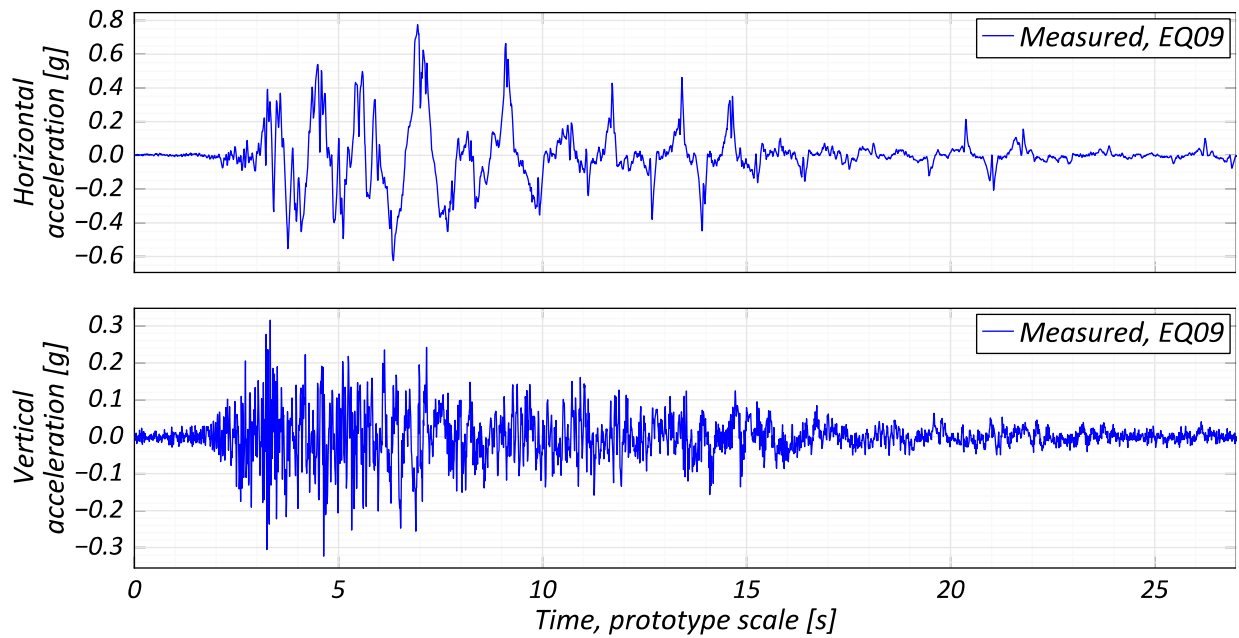


Figure C.17 EQ09 acceleration time histories.

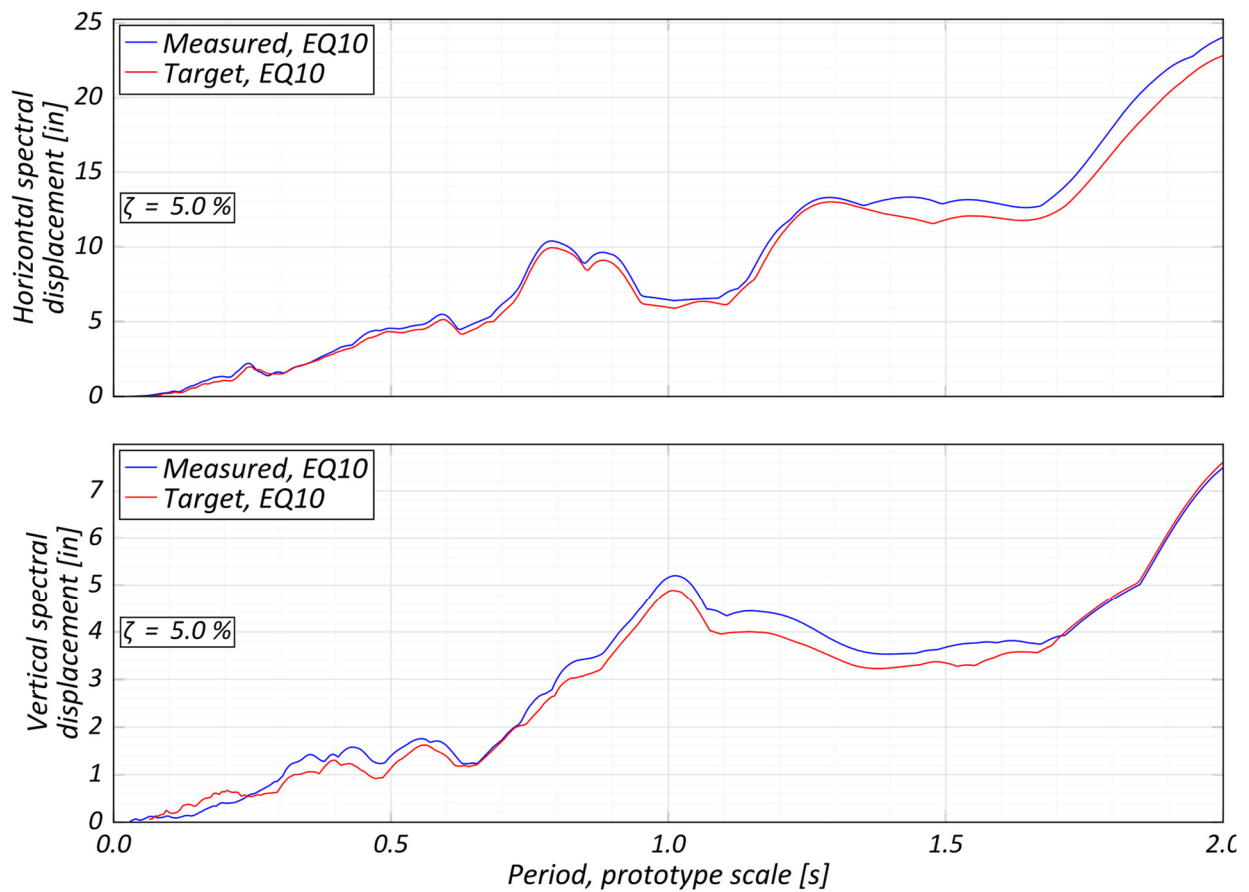


Figure C.18 EQ09 spectral responses.

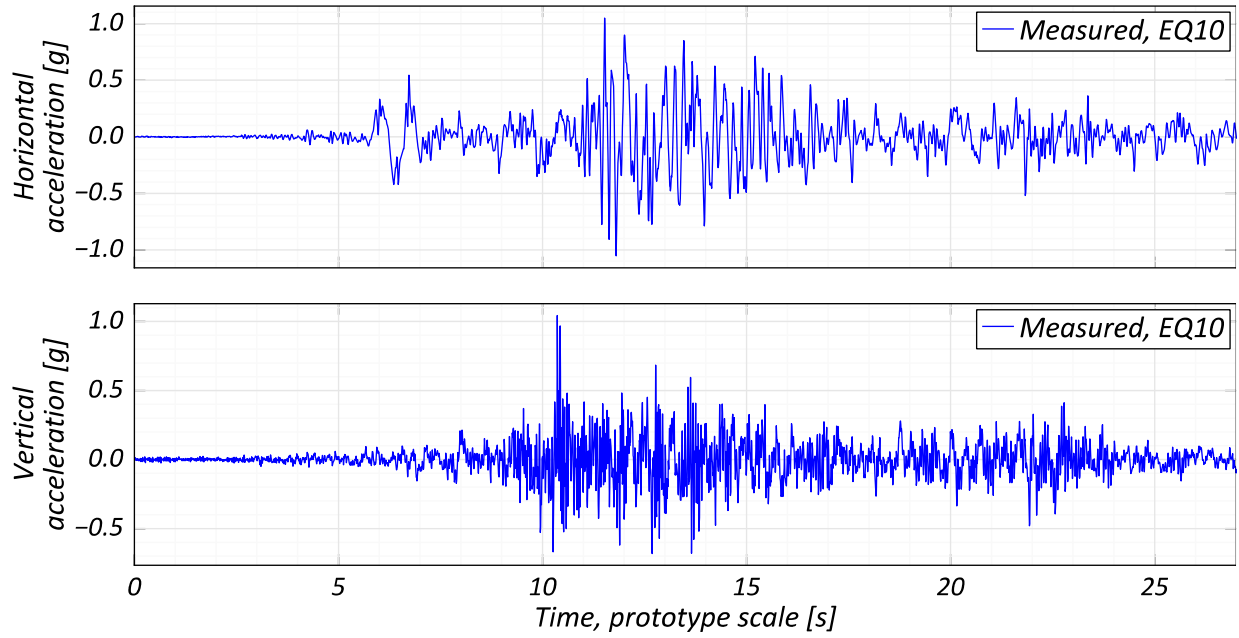


Figure C.19 EQ10 acceleration time histories.

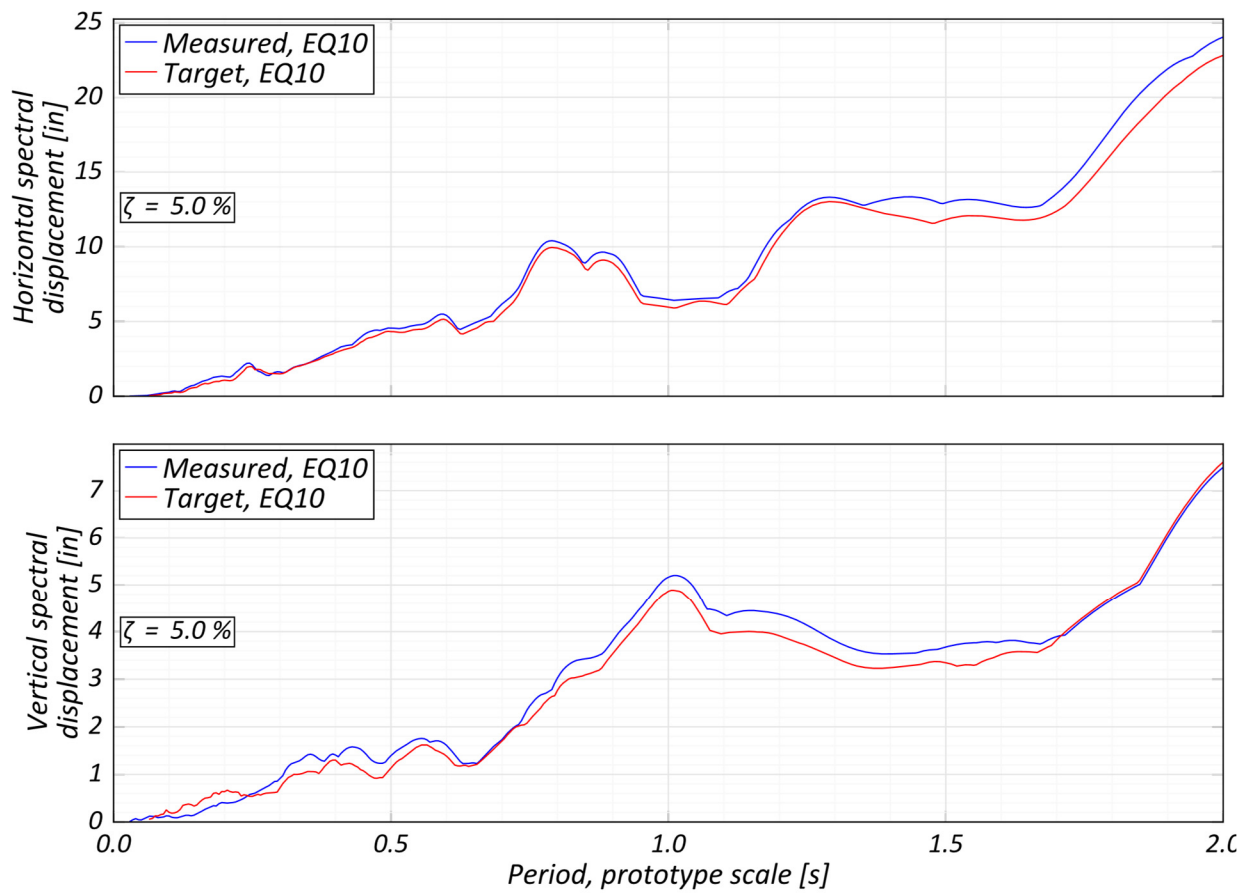


Figure C.20 EQ10 spectral responses.

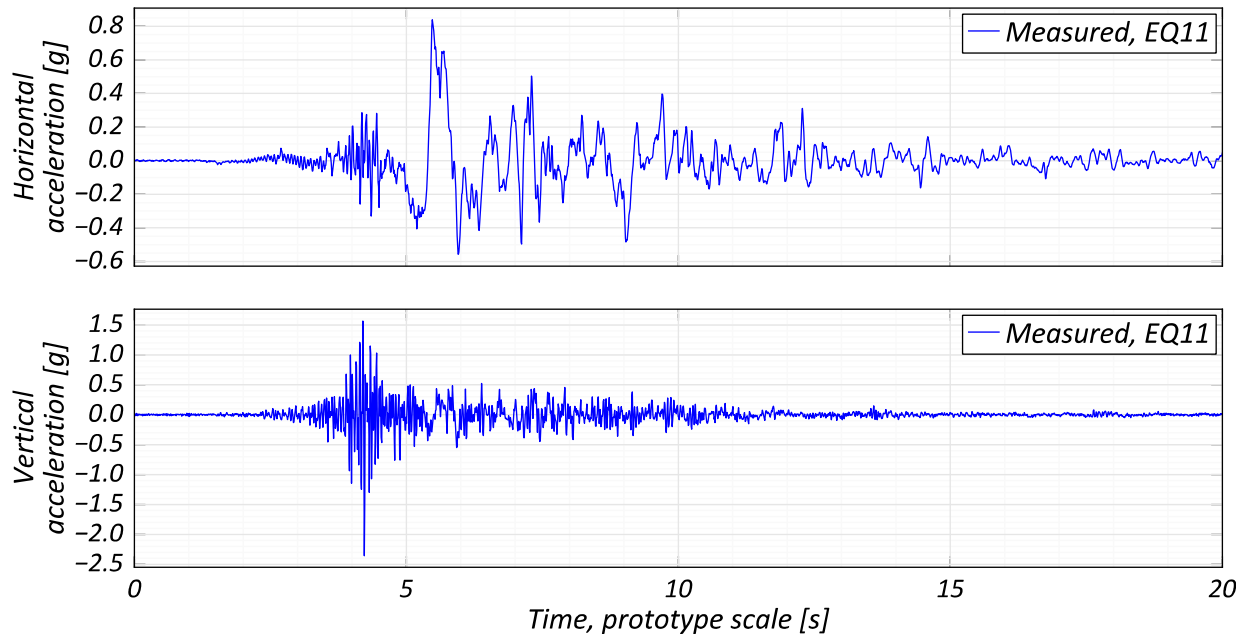


Figure C.21 EQ11 acceleration time histories.

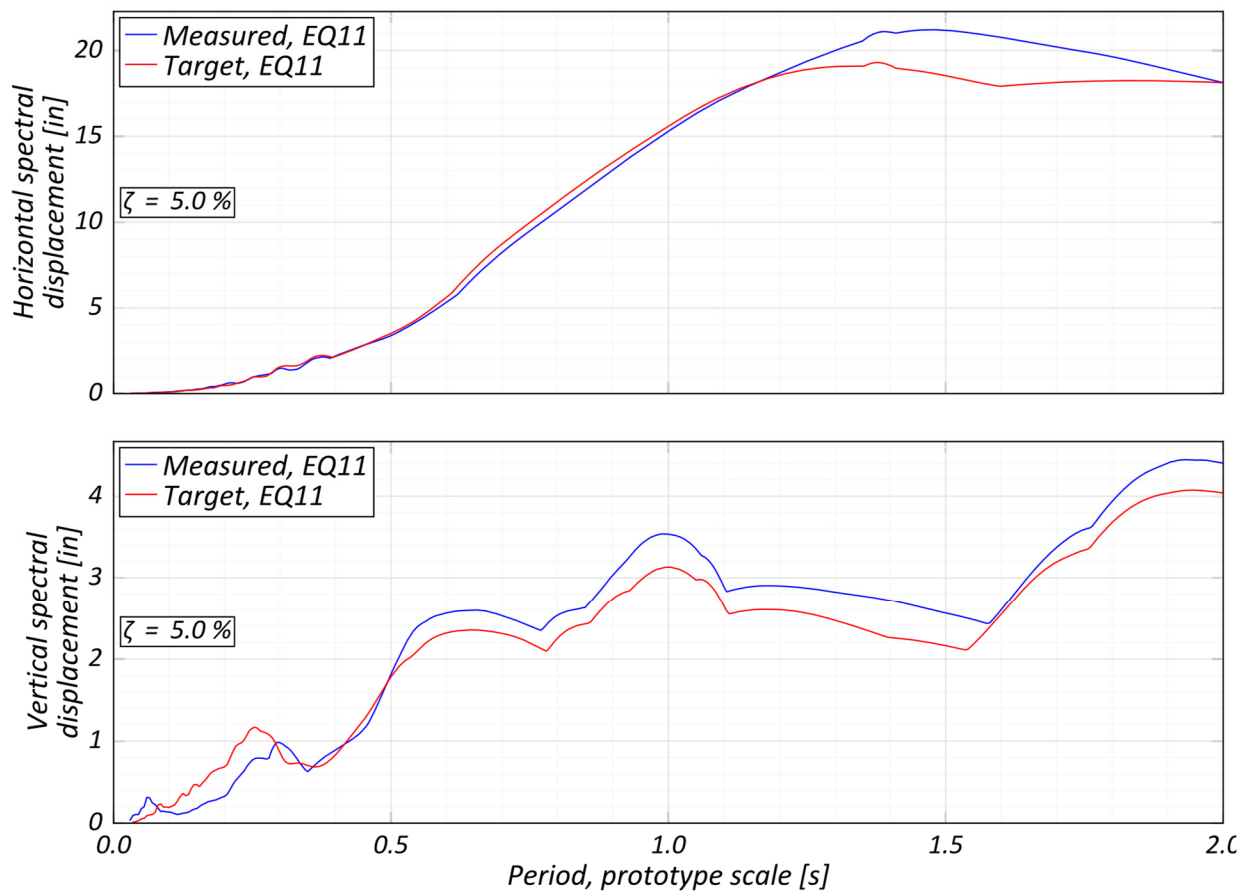


Figure C.22 EQ11 spectral responses.

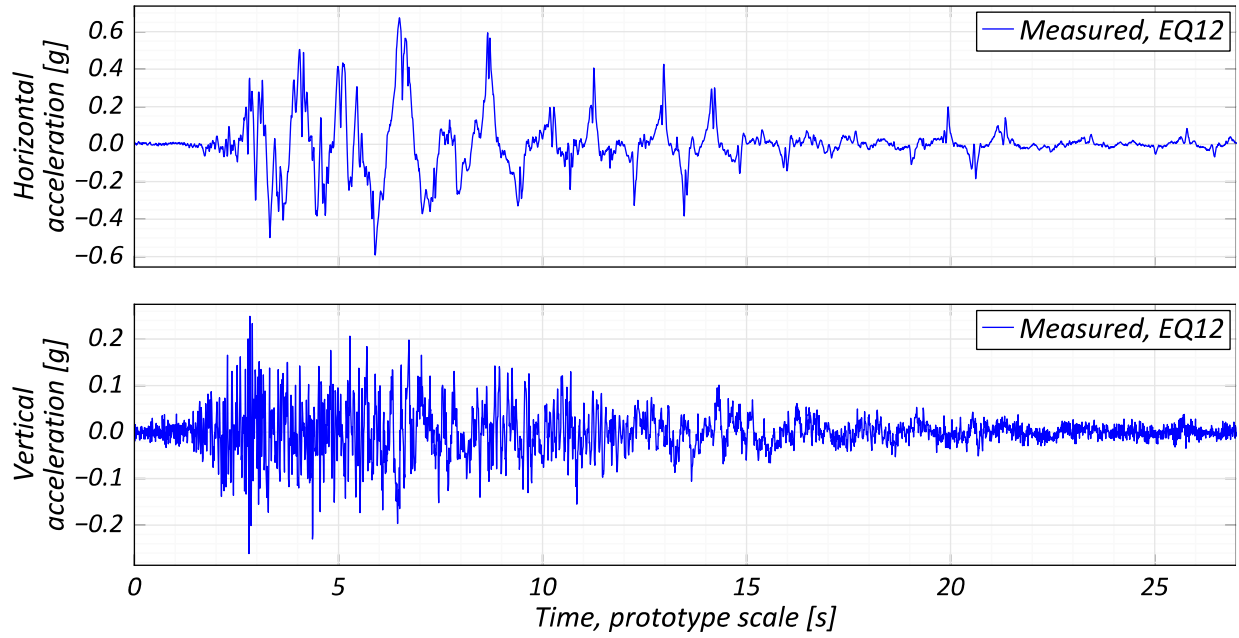


Figure C.23 EQ12 acceleration time histories.

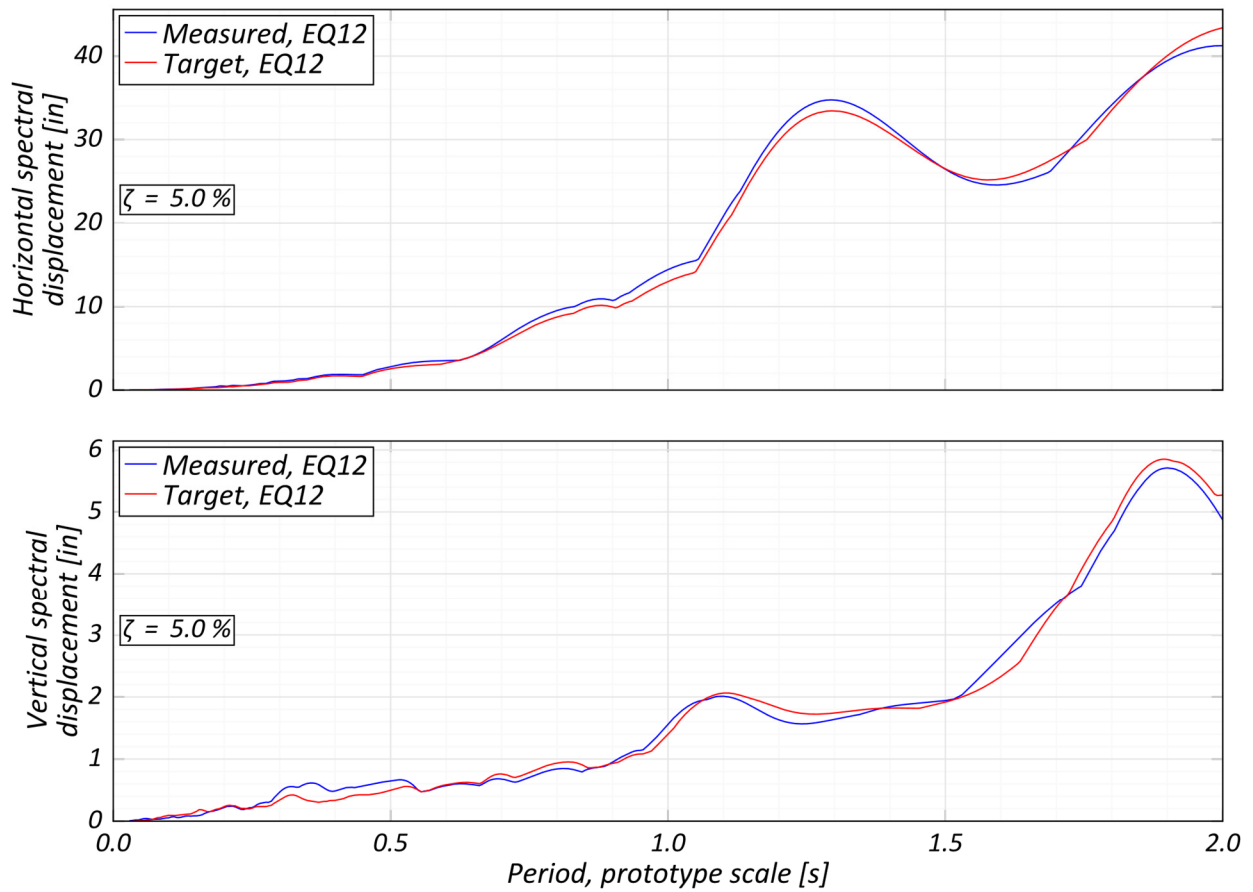


Figure C.24 EQ12 spectral responses.

PEER REPORTS

PEER reports are available as a free PDF download from <https://peer.berkeley.edu/peer-reports>. In addition, printed hard copies of PEER reports can be ordered directly from our printer by following the instructions at <https://peer.berkeley.edu/peer-reports>. For other related questions about the PEER Report Series, contact the Pacific Earthquake Engineering Research Center, 325 Davis Hall, Mail Code 1792, Berkeley, CA 94720. Tel.: (510) 642-3437; and Email: peer_center@berkeley.edu.

- PEER 2020/09** *Blind Prediction of Shaking Table Tests of a New Bridge Ben Design.* Selim Gunay, Fan Hu, Khalid Mosalam, Arpit Nema, Jose Restrepo, Adam Zsarnoczay, and Jack Baker, November 2020.
- PEER 2020/08** *PEER Activities Report 2018_2020.* Khalid M. Mosalam and Amarnath Kasalanati, November 2020.
- PEER 2020/07** *Comparison of NGA-Sub Ground-Motion Models.* Nicholas Gregor, Kofi Addo, Linda Al Atik, David M. Boore, Yousef Bozorgnia, Kenneth W. Campbell, Brian S.-J. Chou, Zeynep Gülerce, Behzad Hassani, Tadahiro Kishida, Nico Kuehn, Saburoh Midorikawa, Silvia Mazzoni, Grace A. Parker, Hongjun Si, Jonathan P. Stewart, and Robert R. Youngs. November 2020.
- PEER 2020/06** *Development of NGA-Sub Ground-Motion Model of 5%-Damped Pseudo-Spectral Acceleration based on Database for Subduction Earthquakes in Japan.* Hongjun Si, Saburoh Midorikawa, and Tadahiro Kishida. November 2020.
- PEER 2020/05** *Conditional Ground-Motion Model for Peak Ground Velocity for Active Crustal Regions.* Norman A. Abrahamson and Sarabjot Bhasin. October 2020.
- PEER 2020/05** *Conditional Ground-Motion Model for Peak Ground Velocity for Active Crustal Regions.* Norman A. Abrahamson and Sarabjot Bhasin. October 2020.
- PEER 2020/04** *Partially Non-Ergodic Ground-Motion Model for Subduction Regions using the NGA-Subduction Database.* Nicolas Kuehn, Yousef Bozorgnia, Kenneth W. Campbell, and Nicholas Gregor. September 2020.
- PEER 2020/03** *NGA-Subduction Global Ground-Motion Models with Regional Adjustment Factors.* Grace A. Parker, Jonathan P. Stewart, David M. Boore, Gail M. Atkinson, and Behzad Hassani. September 2020.
- PEER 2020/02** *Data Resources for NGA-Subduction Project.* Yousef Bozorgnia (PI) and Jonathan P. Stewart (Editor). March 2020.
- PEER 2020/01** *Modeling Viscous Damping in Nonlinear Response History Analysis for Steel Moment-Frame Buildings.* Xin Qian, Anil K. Chopra, and Frank McKenna. June 2020.
- PEER 2019/09** *Seismic Behavior of Special Concentric Braced Frames under Short- and Long-Duration Ground Motions.* Ali Hammad and Mohamed A. Moustafa. December 2019.
- PEER 2019/08** *Influence of Vertical Ground Motion on Bridges Isolated with Spherical Sliding Bearings.* Rushil Mojidra and Keri L. Ryan. December 2019.
- PEER 2019/07** *PEER Hub ImageNet (φ-Net): A Large-Scale Multi-Attribute Benchmark Dataset of Structural Images.* Yuqing Gao, and Khalid. M. Mosalam. November 2019.
- PEER 2019/06** *Fluid-Structure Interaction and Python-Scripting Capabilities in OpenSees.* Minjie Zhu and Michael H. Scott. August 2019.
- PEER 2019/05** *Expected Earthquake Performance of Buildings Designed to the California Building Code (California Alfred E. Alquist Seismic Safety Publication 19-01).* Grace S. Kang, Sifat Muin, Jorge Archbold, Bitanoosh Woods, and Khalid Mosalam. July 2019.
- PEER 2019/04** *Aftershock Seismic Vulnerability and Time-Dependent Risk Assessment of Bridges.* Sujith Mangalathu, Mehrdad Shokrabadi, and Henry V. Burton. May 2019.
- PEER 2019/03** *Ground-Motion Directivity Modeling for Seismic Hazard Applications.* Jennifer L. Donahue, Jonathan P. Stewart, Nicholas Gregor, and Yousef Bozorgnia. Review Panel: Jonathan D. Bray, Stephen A. Mahin, I. M. Idriss, Robert W. Graves, and Tom Shantz. May 2019.
- PEER 2019/02** *Direct-Finite-Element Method for Nonlinear Earthquake Analysis of Concrete Dams Including Dam–Water–Foundation Rock Interaction.* Arnkjell Løkke and Anil K. Chopra. March 2019.
- PEER 2019/01** *Flow-Failure Case History of the Las Palmas, Chile, Tailings Dam.* R. E. S. Moss, T. R. Gebhart, D. J. Frost, and C. Ledezma. January 2019.
- PEER 2018/08** *Central and Eastern North America Ground-Motion Characterization: NGA-East Final Report.* Christine Goulet, Yousef Bozorgnia, Norman Abrahamson, Nicolas Kuehn, Linda Al Atik, Robert Youngs, Robert Graves, and Gail Atkinson. December 2018.

- PEER 2018/07** *An Empirical Model for Fourier Amplitude Spectra using the NGA-West2 Database.* Jeff Bayless, and Norman A. Abrahamson. December 2018.
- PEER 2018/06** *Estimation of Shear Demands on Rock-Socketed Drilled Shafts subjected to Lateral Loading.* Pedro Arduino, Long Chen, and Christopher R. McGann. December 2018.
- PEER 2018/05** *Selection of Random Vibration Procedures for the NGA-East Project.* Albert Kottke, Norman A. Abrahamson, David M. Boore, Yousef Bozorgnia, Christine Goulet, Justin Hollenback, Tadahiro Kishida, Armen Der Kiureghian, Olga-Joan Ktenidou, Nicolas Kuehn, Ellen M. Rathje, Walter J. Silva, Eric Thompson, and Xiaoyue Wang. December 2018.
- PEER 2018/04** *Capturing Directivity Effects in the Mean and Aleatory Variability of the NGA-West 2 Ground Motion Prediction Equations.* Jennie A. Watson-Lamprey. November 2018.
- PEER 2018/03** *Probabilistic Seismic Hazard Analysis Code Verification.* Christie Hale, Norman Abrahamson, and Yousef Bozorgnia. July 2018.
- PEER 2018/02** *Update of the BChydro Subduction Ground-Motion Model using the NGA-Subduction Dataset.* Norman Abrahamson, Nicolas Kuehn, Zeynep Gulerce, Nicholas Gregor, Yousef Bozorgnia, Grace Parker, Jonathan Stewart, Brian Chiou, I. M. Idriss, Kenneth Campbell, and Robert Youngs. June 2018.
- PEER 2018/01** *PEER Annual Report 2017–2018.* Khalid Mosalam, Amarnath Kasalanati, and Selim Günay. June 2018.
- PEER 2017/12** *Experimental Investigation of the Behavior of Vintage and Retrofit Concentrically Braced Steel Frames under Cyclic Loading.* Barbara G. Simpson, Stephen A. Mahin, and Jiun-Wei Lai, December 2017.
- PEER 2017/11** *Preliminary Studies on the Dynamic Response of a Seismically Isolated Prototype Gen-IV Sodium-Cooled Fast Reactor (PGSFR).* Benshun Shao, Andreas H. Schellenberg, Matthew J. Schoettler, and Stephen A. Mahin. December 2017.
- PEER 2017/10** *Development of Time Histories for IEEE693 Testing and Analysis (including Seismically Isolated Equipment).* Shakhzod M. Takhirov, Eric Fujisaki, Leon Kempner, Michael Riley, and Brian Low. December 2017.
- PEER 2017/09** *“R” Package for Computation of Earthquake Ground-Motion Response Spectra.* Pengfei Wang, Jonathan P. Stewart, Yousef Bozorgnia, David M. Boore, and Tadahiro Kishida. December 2017.
- PEER 2017/08** *Influence of Kinematic SSI on Foundation Input Motions for Bridges on Deep Foundations.* Benjamin J. Turner, Scott J. Brandenburg, and Jonathan P. Stewart. November 2017.
- PEER 2017/07** *A Nonlinear Kinetic Model for Multi-Stage Friction Pendulum Systems.* Paul L. Drazin and Sanjay Govindjee. September 2017.
- PEER 2017/06** *Guidelines for Performance-Based Seismic Design of Tall Buildings, Version 2.02.* TBI Working Group led by co-chairs Ron Hamburger and Jack Moehle: Jack Baker, Jonathan Bray, C.B. Crouse, Greg Deierlein, John Hooper, Marshall Lew, Joe Maffei, Stephen Mahin, James Malley, Farzad Naeim, Jonathan Stewart, and John Wallace. May 2017.
- PEER 2017/05** *Recommendations for Ergodic Nonlinear Site Amplification in Central and Eastern North America.* Youssef M.A. Hashash, Joseph A. Harmon, Okan Ilhan, Grace A. Parker, and Jonathan P. Stewart. March 2017.
- PEER 2017/04** *Expert Panel Recommendations for Ergodic Site Amplification in Central and Eastern North America.* Jonathan P. Stewart, Grace A. Parker, Joseph P. Harmon, Gail M. Atkinson, David M. Boore, Robert B. Darragh, Walter J. Silva, and Youssef M.A. Hashash. March 2017.
- PEER 2017/03** *NGA-East Ground-Motion Models for the U.S. Geological Survey National Seismic Hazard Maps.* Christine A. Goulet, Yousef Bozorgnia, Nicolas Kuehn, Linda Al Atik, Robert R. Youngs, Robert W. Graves, and Gail M. Atkinson. March 2017.
- PEER 2017/02** *U.S.–New Zealand–Japan Workshop: Liquefaction-Induced Ground Movements Effects, University of California, Berkeley, California, 2–4 November 2016.* Jonathan D. Bray, Ross W. Boulanger, Misko Cubrinovski, Kohji Tokimatsu, Steven L. Kramer, Thomas O’Rourke, Ellen Rathje, Russell A. Green, Peter K. Robinson, and Christine Z. Beyzaei. March 2017.
- PEER 2017/01** *2016 PEER Annual Report.* Khalid M. Mosalam, Amarnath Kasalanati, and Grace Kang. March 2017.
- PEER 2016/10** *Performance-Based Robust Nonlinear Seismic Analysis with Application to Reinforced Concrete Bridge Systems.* Xiao Ling and Khalid M. Mosalam. December 2016.
- PEER 2017/09** *Detailing Requirements for Column Plastic Hinges subjected to Combined Flexural, Axial, and Torsional Seismic Loading.* Gabriel Hurtado and Jack P. Moehle. December 2016.
- PEER 2016/08** *Resilience of Critical Structures, Infrastructure, and Communities.* Gian Paolo Cimellaro, Ali Zamani-Noori, Omar Kamouh, Vesna Terzic, and Stephen A. Mahin. December 2016.

- PEER 2016/07** *Hybrid Simulation Theory for a Classical Nonlinear Dynamical System.* Paul L. Drazin and Sanjay Govindjee. September 2016.
- PEER 2016/06** *California Earthquake Early Warning System Benefit Study.* Laurie A. Johnson, Sharyl Rabinovici, Grace S. Kang, and Stephen A. Mahin. July 2006.
- PEER 2016/05** *Ground-Motion Prediction Equations for Arias Intensity Consistent with the NGA-West2 Ground-Motion Models.* Charlotte Abrahamson, Hao-Jun Michael Shi, and Brian Yang. July 2016.
- PEER 2016/04** *The M_w 6.0 South Napa Earthquake of August 24, 2014: A Wake-Up Call for Renewed Investment in Seismic Resilience Across California.* Prepared for the California Seismic Safety Commission, Laurie A. Johnson and Stephen A. Mahin. May 2016.
- PEER 2016/03** *Simulation Confidence in Tsunami-Driven Overland Flow.* Patrick Lynett. May 2016.
- PEER 2016/02** *Semi-Automated Procedure for Windowing time Series and Computing Fourier Amplitude Spectra for the NGA-West2 Database.* Tadahiro Kishida, Olga-Joan Ktenidou, Robert B. Darragh, and Walter J. Silva. May 2016.
- PEER 2016/01** *A Methodology for the Estimation of Kappa (κ) from Large Datasets: Example Application to Rock Sites in the NGA-East Database and Implications on Design Motions.* Olga-Joan Ktenidou, Norman A. Abrahamson, Robert B. Darragh, and Walter J. Silva. April 2016.
- PEER 2015/13** *Self-Centering Precast Concrete Dual-Steel-Shell Columns for Accelerated Bridge Construction: Seismic Performance, Analysis, and Design.* Gabriele Guerrini, José I. Restrepo, Athanassios Vervelidis, and Milena Massari. December 2015.
- PEER 2015/12** *Shear-Flexure Interaction Modeling for Reinforced Concrete Structural Walls and Columns under Reversed Cyclic Loading.* Kristijan Kolozvari, Kutay Orakcal, and John Wallace. December 2015.
- PEER 2015/11** *Selection and Scaling of Ground Motions for Nonlinear Response History Analysis of Buildings in Performance-Based Earthquake Engineering.* N. Simon Kwong and Anil K. Chopra. December 2015.
- PEER 2015/10** *Structural Behavior of Column-Bent Cap Beam-Box Girder Systems in Reinforced Concrete Bridges Subjected to Gravity and Seismic Loads. Part II: Hybrid Simulation and Post-Test Analysis.* Mohamed A. Moustafa and Khalid M. Mosalam. November 2015.
- PEER 2015/09** *Structural Behavior of Column-Bent Cap Beam-Box Girder Systems in Reinforced Concrete Bridges Subjected to Gravity and Seismic Loads. Part I: Pre-Test Analysis and Quasi-Static Experiments.* Mohamed A. Moustafa and Khalid M. Mosalam. September 2015.
- PEER 2015/08** *NGA-East: Adjustments to Median Ground-Motion Models for Center and Eastern North America.* August 2015.
- PEER 2015/07** *NGA-East: Ground-Motion Standard-Deviation Models for Central and Eastern North America.* Linda Al Atik. June 2015.
- PEER 2015/06** *Adjusting Ground-Motion Intensity Measures to a Reference Site for which $V_{S30} = 3000$ m/sec.* David M. Boore. May 2015.
- PEER 2015/05** *Hybrid Simulation of Seismic Isolation Systems Applied to an APR-1400 Nuclear Power Plant.* Andreas H. Schellenberg, Alireza Sarebanha, Matthew J. Schoettler, Gilberto Mosqueda, Gianmario Benzoni, and Stephen A. Mahin. April 2015.
- PEER 2015/04** *NGA-East: Median Ground-Motion Models for the Central and Eastern North America Region.* April 2015.
- PEER 2015/03** *Single Series Solution for the Rectangular Fiber-Reinforced Elastomeric Isolator Compression Modulus.* James M. Kelly and Niel C. Van Engelen. March 2015.
- PEER 2015/02** *A Full-Scale, Single-Column Bridge Bent Tested by Shake-Table Excitation.* Matthew J. Schoettler, José I. Restrepo, Gabriele Guerrini, David E. Duck, and Francesco Carrea. March 2015.
- PEER 2015/01** *Concrete Column Blind Prediction Contest 2010: Outcomes and Observations.* Vesna Terzic, Matthew J. Schoettler, José I. Restrepo, and Stephen A. Mahin. March 2015.
- PEER 2014/20** *Stochastic Modeling and Simulation of Near-Fault Ground Motions for Performance-Based Earthquake Engineering.* Mayssa Dabaghi and Armen Der Kiureghian. December 2014.
- PEER 2014/19** *Seismic Response of a Hybrid Fiber-Reinforced Concrete Bridge Column Detailed for Accelerated Bridge Construction.* Wilson Nguyen, William Trono, Marios Panagiotou, and Claudia P. Ostertag. December 2014.
- PEER 2014/18** *Three-Dimensional Beam-Truss Model for Reinforced Concrete Walls and Slabs Subjected to Cyclic Static or Dynamic Loading.* Yuan Lu, Marios Panagiotou, and Ioannis Koutromanos. December 2014.

- PEER 2014/17** *PEER NGA-East Database*. Christine A. Goulet, Tadahiro Kishida, Timothy D. Ancheta, Chris H. Cramer, Robert B. Darragh, Walter J. Silva, Youssef M.A. Hashash, Joseph Harmon, Jonathan P. Stewart, Katie E. Wooddell, and Robert R. Youngs. October 2014.
- PEER 2014/16** *Guidelines for Performing Hazard-Consistent One-Dimensional Ground Response Analysis for Ground Motion Prediction*. Jonathan P. Stewart, Kioumars Afshari, and Youssef M.A. Hashash. October 2014.
- PEER 2014/15** *NGA-East Regionalization Report: Comparison of Four Crustal Regions within Central and Eastern North America using Waveform Modeling and 5%-Damped Pseudo-Spectral Acceleration Response*. Jennifer Dreiling, Marius P. Isken, Walter D. Mooney, Martin C. Chapman, and Richard W. Godbee. October 2014.
- PEER 2014/14** *Scaling Relations between Seismic Moment and Rupture Area of Earthquakes in Stable Continental Regions*. Paul Somerville. August 2014.
- PEER 2014/13** *PEER Preliminary Notes and Observations on the August 24, 2014, South Napa Earthquake*. Grace S. Kang and Stephen A. Mahin, Editors. September 2014.
- PEER 2014/12** *Reference-Rock Site Conditions for Central and Eastern North America: Part II – Attenuation (Kappa) Definition*. Kenneth W. Campbell, Youssef M.A. Hashash, Byungmin Kim, Albert R. Kottke, Ellen M. Rathje, Walter J. Silva, and Jonathan P. Stewart. August 2014.
- PEER 2014/11** *Reference-Rock Site Conditions for Central and Eastern North America: Part I - Velocity Definition*. Youssef M.A. Hashash, Albert R. Kottke, Jonathan P. Stewart, Kenneth W. Campbell, Byungmin Kim, Ellen M. Rathje, Walter J. Silva, Sissy Nikolaou, and Cheryl Moss. August 2014.
- PEER 2014/10** *Evaluation of Collapse and Non-Collapse of Parallel Bridges Affected by Liquefaction and Lateral Spreading*. Benjamin Turner, Scott J. Brandenberg, and Jonathan P. Stewart. August 2014.
- PEER 2014/09** *PEER Arizona Strong-Motion Database and GMPEs Evaluation*. Tadahiro Kishida, Robert E. Kayen, Olga-Joan Ktenidou, Walter J. Silva, Robert B. Darragh, and Jennie Watson-Lamprey. June 2014.
- PEER 2014/08** *Unbonded Pretensioned Bridge Columns with Rocking Detail*. Jeffrey A. Schaefer, Bryan Kennedy, Marc O. Eberhard, and John F. Stanton. June 2014.
- PEER 2014/07** *Northridge 20 Symposium Summary Report: Impacts, Outcomes, and Next Steps*. May 2014.
- PEER 2014/06** *Report of the Tenth Planning Meeting of NEES/E-Defense Collaborative Research on Earthquake Engineering*. December 2013.
- PEER 2014/05** *Seismic Velocity Site Characterization of Thirty-One Chilean Seismometer Stations by Spectral Analysis of Surface Wave Dispersion*. Robert Kayen, Brad D. Carkin, Skye Corbet, Camilo Pinilla, Allan Ng, Edward Gorbis, and Christine Truong. April 2014.
- PEER 2014/04** *Effect of Vertical Acceleration on Shear Strength of Reinforced Concrete Columns*. Hyerin Lee and Khalid M. Mosalam. April 2014.
- PEER 2014/03** *Retest of Thirty-Year-Old Neoprene Isolation Bearings*. James M. Kelly and Niel C. Van Engelen. March 2014.
- PEER 2014/02** *Theoretical Development of Hybrid Simulation Applied to Plate Structures*. Ahmed A. Bakhaty, Khalid M. Mosalam, and Sanjay Govindjee. January 2014.
- PEER 2014/01** *Performance-Based Seismic Assessment of Skewed Bridges*. Peyman Kaviani, Farzin Zareian, and Ertugrul Taciroglu. January 2014.
- PEER 2013/26** *Urban Earthquake Engineering*. Proceedings of the U.S.-Iran Seismic Workshop. December 2013.
- PEER 2013/25** *Earthquake Engineering for Resilient Communities: 2013 PEER Internship Program Research Report Collection*. Heidi Tremayne (Editor), Stephen A. Mahin (Editor), Jorge Archbold Monterossa, Matt Brosman, Shelly Dean, Katherine deLaveaga, Curtis Fong, Donovan Holder, Rakeeb Khan, Elizabeth Jachens, David Lam, Daniela Martinez Lopez, Mara Minner, Geffen Oren, Julia Pavicic, Melissa Quinonez, Lorena Rodriguez, Sean Salazar, Kelli Slaven, Vivian Steyert, Jenny Taing, and Salvador Tena. December 2013.
- PEER 2013/24** *NGA-West2 Ground Motion Prediction Equations for Vertical Ground Motions*. September 2013.
- PEER 2013/23** *Coordinated Planning and Preparedness for Fire Following Major Earthquakes*. Charles Scawthorn. November 2013.
- PEER 2013/22** *GEM-PEER Task 3 Project: Selection of a Global Set of Ground Motion Prediction Equations*. Jonathan P. Stewart, John Douglas, Mohammad B. Javanbarg, Carola Di Alessandro, Yousef Bozorgnia, Norman A. Abrahamson, David M. Boore, Kenneth W. Campbell, Elise Delavaud, Mustafa Erdik, and Peter J. Stafford. December 2013.
- PEER 2013/21** *Seismic Design and Performance of Bridges with Columns on Rocking Foundations*. Grigorios Antonellis and Marios Panagiotou. September 2013.

- PEER 2013/20** *Experimental and Analytical Studies on the Seismic Behavior of Conventional and Hybrid Braced Frames.* Jiun-Wei Lai and Stephen A. Mahin. September 2013.
- PEER 2013/19** *Toward Resilient Communities: A Performance-Based Engineering Framework for Design and Evaluation of the Built Environment.* Michael William Mieler, Bozidar Stojadinovic, Robert J. Budnitz, Stephen A. Mahin, and Mary C. Comerio. September 2013.
- PEER 2013/18** *Identification of Site Parameters that Improve Predictions of Site Amplification.* Ellen M. Rathje and Sara Navidi. July 2013.
- PEER 2013/17** *Response Spectrum Analysis of Concrete Gravity Dams Including Dam-Water-Foundation Interaction.* Arnkjell Løkke and Anil K. Chopra. July 2013.
- PEER 2013/16** *Effect of Hoop Reinforcement Spacing on the Cyclic Response of Large Reinforced Concrete Special Moment Frame Beams.* Marios Panagiotou, Tea Visnjic, Grigorios Antonellis, Panagiotis Galanis, and Jack P. Moehle. June 2013.
- PEER 2013/15** *A Probabilistic Framework to Include the Effects of Near-Fault Directivity in Seismic Hazard Assessment.* Shrey Kumar Shahi, Jack W. Baker. October 2013.
- PEER 2013/14** *Hanging-Wall Scaling using Finite-Fault Simulations.* Jennifer L. Donahue and Norman A. Abrahamson. September 2013.
- PEER 2013/13** *Semi-Empirical Nonlinear Site Amplification and its Application in NEHRP Site Factors.* Jonathan P. Stewart and Emel Seyhan. November 2013.
- PEER 2013/12** *Nonlinear Horizontal Site Response for the NGA-West2 Project.* Ronnie Kamai, Norman A. Abramson, Walter J. Silva. May 2013.
- PEER 2013/11** *Epistemic Uncertainty for NGA-West2 Models.* Linda Al Atik and Robert R. Youngs. May 2013.
- PEER 2013/10** *NGA-West 2 Models for Ground-Motion Directionality.* Shrey K. Shahi and Jack W. Baker. May 2013.
- PEER 2013/09** *Final Report of the NGA-West2 Directivity Working Group.* Paul Spudich, Jeffrey R. Bayless, Jack W. Baker, Brian S.J. Chiou, Badie Rowshandel, Shrey Shahi, and Paul Somerville. May 2013.
- PEER 2013/08** *NGA-West2 Model for Estimating Average Horizontal Values of Pseudo-Absolute Spectral Accelerations Generated by Crustal Earthquakes.* I. M. Idriss. May 2013.
- PEER 2013/07** *Update of the Chiou and Youngs NGA Ground Motion Model for Average Horizontal Component of Peak Ground Motion and Response Spectra.* Brian Chiou and Robert Youngs. May 2013.
- PEER 2013/06** *NGA-West2 Campbell-Bozorgnia Ground Motion Model for the Horizontal Components of PGA, PGV, and 5%-Damped Elastic Pseudo-Acceleration Response Spectra for Periods Ranging from 0.01 to 10 sec.* Kenneth W. Campbell and Yousef Bozorgnia. May 2013.
- PEER 2013/05** *NGA-West 2 Equations for Predicting Response Spectral Accelerations for Shallow Crustal Earthquakes.* David M. Boore, Jonathan P. Stewart, Emel Seyhan, and Gail M. Atkinson. May 2013.
- PEER 2013/04** *Update of the AS08 Ground-Motion Prediction Equations Based on the NGA-West2 Data Set.* Norman Abrahamson, Walter Silva, and Ronnie Kamai. May 2013.
- PEER 2013/03** *PEER NGA-West2 Database.* Timothy D. Ancheta, Robert B. Darragh, Jonathan P. Stewart, Emel Seyhan, Walter J. Silva, Brian S.J. Chiou, Katie E. Wooddell, Robert W. Graves, Albert R. Kottke, David M. Boore, Tadahiro Kishida, and Jennifer L. Donahue. May 2013.
- PEER 2013/02** *Hybrid Simulation of the Seismic Response of Squat Reinforced Concrete Shear Walls.* Catherine A. Whyte and Bozidar Stojadinovic. May 2013.
- PEER 2013/01** *Housing Recovery in Chile: A Qualitative Mid-program Review.* Mary C. Comerio. February 2013.
- PEER 2012/08** *Guidelines for Estimation of Shear Wave Velocity.* Bernard R. Wair, Jason T. DeJong, and Thomas Shantz. December 2012.
- PEER 2012/07** *Earthquake Engineering for Resilient Communities: 2012 PEER Internship Program Research Report Collection.* Heidi Tremayne (Editor), Stephen A. Mahin (Editor), Collin Anderson, Dustin Cook, Michael Erceg, Carlos Esparza, Jose Jimenez, Dorian Krausz, Andrew Lo, Stephanie Lopez, Nicole McCurdy, Paul Shipman, Alexander Strum, Eduardo Vega. December 2012.
- PEER 2012/06** *Fragilities for Precarious Rocks at Yucca Mountain.* Matthew D. Purvance, Rasool Anooshehpour, and James N. Brune. December 2012.
- PEER 2012/05** *Development of Simplified Analysis Procedure for Piles in Laterally Spreading Layered Soils.* Christopher R. McGann, Pedro Arduino, and Peter Mackenzie-Helnwein. December 2012.

- PEER 2012/04** *Unbonded Pre-Tensioned Columns for Bridges in Seismic Regions.* Phillip M. Davis, Todd M. Janes, Marc O. Eberhard, and John F. Stanton. December 2012.
- PEER 2012/03** *Experimental and Analytical Studies on Reinforced Concrete Buildings with Seismically Vulnerable Beam-Column Joints.* Sangjoon Park and Khalid M. Mosalam. October 2012.
- PEER 2012/02** *Seismic Performance of Reinforced Concrete Bridges Allowed to Uplift during Multi-Directional Excitation.* Andres Oscar Espinoza and Stephen A. Mahin. July 2012.
- PEER 2012/01** *Spectral Damping Scaling Factors for Shallow Crustal Earthquakes in Active Tectonic Regions.* Sanaz Rezaeian, Yousef Bozorgnia, I. M. Idriss, Kenneth Campbell, Norman Abrahamson, and Walter Silva. July 2012.
- PEER 2011/10** *Earthquake Engineering for Resilient Communities: 2011 PEER Internship Program Research Report Collection.* Heidi Faison and Stephen A. Mahin, Editors. December 2011.
- PEER 2011/09** *Calibration of Semi-Stochastic Procedure for Simulating High-Frequency Ground Motions.* Jonathan P. Stewart, Emel Seyhan, and Robert W. Graves. December 2011.
- PEER 2011/08** *Water Supply in regard to Fire Following Earthquake.* Charles Scawthorn. November 2011.
- PEER 2011/07** *Seismic Risk Management in Urban Areas.* Proceedings of a U.S.-Iran-Turkey Seismic Workshop. September 2011.
- PEER 2011/06** *The Use of Base Isolation Systems to Achieve Complex Seismic Performance Objectives.* Troy A. Morgan and Stephen A. Mahin. July 2011.
- PEER 2011/05** *Case Studies of the Seismic Performance of Tall Buildings Designed by Alternative Means.* Task 12 Report for the Tall Buildings Initiative. Jack Moehle, Yousef Bozorgnia, Nirmal Jayaram, Pierson Jones, Mohsen Rahnama, Nilesh Shome, Zeynep Tuna, John Wallace, Tony Yang, and Farzin Zareian. July 2011.
- PEER 2011/04** *Recommended Design Practice for Pile Foundations in Laterally Spreading Ground.* Scott A. Ashford, Ross W. Boulanger, and Scott J. Brandenburg. June 2011.
- PEER 2011/03** *New Ground Motion Selection Procedures and Selected Motions for the PEER Transportation Research Program.* Jack W. Baker, Ting Lin, Shrey K. Shahi, and Nirmal Jayaram. March 2011.
- PEER 2011/02** *A Bayesian Network Methodology for Infrastructure Seismic Risk Assessment and Decision Support.* Michelle T. Bensi, Armen Der Kiureghian, and Daniel Straub. March 2011.
- PEER 2011/01** *Demand Fragility Surfaces for Bridges in Liquefied and Laterally Spreading Ground.* Scott J. Brandenburg, Jian Zhang, Pirooz Kashighandi, Yili Huo, and Minxing Zhao. March 2011.
- PEER 2010/05** *Guidelines for Performance-Based Seismic Design of Tall Buildings.* Developed by the Tall Buildings Initiative. November 2010.
- PEER 2010/04** *Application Guide for the Design of Flexible and Rigid Bus Connections between Substation Equipment Subjected to Earthquakes.* Jean-Bernard Dastous and Armen Der Kiureghian. September 2010.
- PEER 2010/03** *Shear Wave Velocity as a Statistical Function of Standard Penetration Test Resistance and Vertical Effective Stress at Caltrans Bridge Sites.* Scott J. Brandenburg, Naresh Bellana, and Thomas Shantz. June 2010.
- PEER 2010/02** *Stochastic Modeling and Simulation of Ground Motions for Performance-Based Earthquake Engineering.* Sanaz Rezaeian and Armen Der Kiureghian. June 2010.
- PEER 2010/01** *Structural Response and Cost Characterization of Bridge Construction Using Seismic Performance Enhancement Strategies.* Ady Aviram, Božidar Stojadinović, Gustavo J. Parra-Montesinos, and Kevin R. Mackie. March 2010.
- PEER 2009/03** *The Integration of Experimental and Simulation Data in the Study of Reinforced Concrete Bridge Systems Including Soil-Foundation-Structure Interaction.* Matthew Dryden and Gregory L. Fenves. November 2009.
- PEER 2009/02** *Improving Earthquake Mitigation through Innovations and Applications in Seismic Science, Engineering, Communication, and Response.* Proceedings of a U.S.-Iran Seismic Workshop. October 2009.
- PEER 2009/01** *Evaluation of Ground Motion Selection and Modification Methods: Predicting Median Interstory Drift Response of Buildings.* Curt B. Haselton, Editor. June 2009.
- PEER 2008/10** *Technical Manual for Strata.* Albert R. Kottke and Ellen M. Rathje. February 2009.
- PEER 2008/09** *NGA Model for Average Horizontal Component of Peak Ground Motion and Response Spectra.* Brian S.-J. Chiou and Robert R. Youngs. November 2008.
- PEER 2008/08** *Toward Earthquake-Resistant Design of Concentrically Braced Steel Structures.* Patxi Uriz and Stephen A. Mahin. November 2008.

- PEER 2008/07** *Using OpenSees for Performance-Based Evaluation of Bridges on Liquefiable Soils.* Stephen L. Kramer, Pedro Arduino, and HyungSuk Shin. November 2008.
- PEER 2008/06** *Shaking Table Tests and Numerical Investigation of Self-Centering Reinforced Concrete Bridge Columns.* Hyung IL Jeong, Junichi Sakai, and Stephen A. Mahin. September 2008.
- PEER 2008/05** *Performance-Based Earthquake Engineering Design Evaluation Procedure for Bridge Foundations Undergoing Liquefaction-Induced Lateral Ground Displacement.* Christian A. Ledezma and Jonathan D. Bray. August 2008.
- PEER 2008/04** *Benchmarking of Nonlinear Geotechnical Ground Response Analysis Procedures.* Jonathan P. Stewart, Annie On-Lei Kwok, Youssef M. A. Hashash, Neven Matasovic, Robert Pyke, Zhiliang Wang, and Zhaohui Yang. August 2008.
- PEER 2008/03** *Guidelines for Nonlinear Analysis of Bridge Structures in California.* Ady Aviram, Kevin R. Mackie, and Božidar Stojadinović. August 2008.
- PEER 2008/02** *Treatment of Uncertainties in Seismic-Risk Analysis of Transportation Systems.* Evangelos Stergiou and Anne S. Kiremidjian. July 2008.
- PEER 2008/01** *Seismic Performance Objectives for Tall Buildings.* William T. Holmes, Charles Kircher, William Petak, and Nabih Youssef. August 2008.
- PEER 2007/12** *An Assessment to Benchmark the Seismic Performance of a Code-Conforming Reinforced Concrete Moment-Frame Building.* Curt Haselton, Christine A. Goulet, Judith Mitrani-Reiser, James L. Beck, Gregory G. Deierlein, Keith A. Porter, Jonathan P. Stewart, and Ertugrul Taciroglu. August 2008.
- PEER 2007/11** *Bar Buckling in Reinforced Concrete Bridge Columns.* Wayne A. Brown, Dawn E. Lehman, and John F. Stanton. February 2008.
- PEER 2007/10** *Computational Modeling of Progressive Collapse in Reinforced Concrete Frame Structures.* Mohamed M. Talaat and Khalid M. Mosalam. May 2008.
- PEER 2007/09** *Integrated Probabilistic Performance-Based Evaluation of Benchmark Reinforced Concrete Bridges.* Kevin R. Mackie, John-Michael Wong, and Božidar Stojadinović. January 2008.
- PEER 2007/08** *Assessing Seismic Collapse Safety of Modern Reinforced Concrete Moment-Frame Buildings.* Curt B. Haselton and Gregory G. Deierlein. February 2008.
- PEER 2007/07** *Performance Modeling Strategies for Modern Reinforced Concrete Bridge Columns.* Michael P. Berry and Marc O. Eberhard. April 2008.
- PEER 2007/06** *Development of Improved Procedures for Seismic Design of Buried and Partially Buried Structures.* Linda Al Atik and Nicholas Sitar. June 2007.
- PEER 2007/05** *Uncertainty and Correlation in Seismic Risk Assessment of Transportation Systems.* Renee G. Lee and Anne S. Kiremidjian. July 2007.
- PEER 2007/04** *Numerical Models for Analysis and Performance-Based Design of Shallow Foundations Subjected to Seismic Loading.* Sivapalan Gajan, Tara C. Hutchinson, Bruce L. Kutter, Prishati Raychowdhury, José A. Ugalde, and Jonathan P. Stewart. May 2008.
- PEER 2007/03** *Beam-Column Element Model Calibrated for Predicting Flexural Response Leading to Global Collapse of RC Frame Buildings.* Curt B. Haselton, Abbie B. Liel, Sarah Taylor Lange, and Gregory G. Deierlein. May 2008.
- PEER 2007/02** *Campbell-Bozorgnia NGA Ground Motion Relations for the Geometric Mean Horizontal Component of Peak and Spectral Ground Motion Parameters.* Kenneth W. Campbell and Yousef Bozorgnia. May 2007.
- PEER 2007/01** *Boore-Atkinson NGA Ground Motion Relations for the Geometric Mean Horizontal Component of Peak and Spectral Ground Motion Parameters.* David M. Boore and Gail M. Atkinson. May 2007.
- PEER 2006/12** *Societal Implications of Performance-Based Earthquake Engineering.* Peter J. May. May 2007.
- PEER 2006/11** *Probabilistic Seismic Demand Analysis Using Advanced Ground Motion Intensity Measures, Attenuation Relationships, and Near-Fault Effects.* Polsak Tothong and C. Allin Cornell. March 2007.
- PEER 2006/10** *Application of the PEER PBEE Methodology to the I-880 Viaduct.* Sashi Kunnath. February 2007.
- PEER 2006/09** *Quantifying Economic Losses from Travel Forgone Following a Large Metropolitan Earthquake.* James Moore, Sungbin Cho, Yue Yue Fan, and Stuart Werner. November 2006.
- PEER 2006/08** *Vector-Valued Ground Motion Intensity Measures for Probabilistic Seismic Demand Analysis.* Jack W. Baker and C. Allin Cornell. October 2006.

- PEER 2006/07** *Analytical Modeling of Reinforced Concrete Walls for Predicting Flexural and Coupled–Shear-Flexural Responses.* Kutay Orakcal, Leonardo M. Massone, and John W. Wallace. October 2006.
- PEER 2006/06** *Nonlinear Analysis of a Soil-Drilled Pier System under Static and Dynamic Axial Loading.* Gang Wang and Nicholas Sitar. November 2006.
- PEER 2006/05** *Advanced Seismic Assessment Guidelines.* Paolo Bazzurro, C. Allin Cornell, Charles Menun, Maziar Motahari, and Nicolas Luco. September 2006.
- PEER 2006/04** *Probabilistic Seismic Evaluation of Reinforced Concrete Structural Components and Systems.* Tae Hyung Lee and Khalid M. Mosalam. August 2006.
- PEER 2006/03** *Performance of Lifelines Subjected to Lateral Spreading.* Scott A. Ashford and Teerawut Juirnarongrit. July 2006.
- PEER 2006/02** *Pacific Earthquake Engineering Research Center Highway Demonstration Project.* Anne Kiremidjian, James Moore, Yue Yue Fan, Nesrin Basoz, Ozgur Yazali, and Meredith Williams. April 2006.
- PEER 2006/01** *Bracing Berkeley. A Guide to Seismic Safety on the UC Berkeley Campus.* Mary C. Comerio, Stephen Tobriner, and Ariane Fehrenkamp. January 2006.
- PEER 2005/17** *Earthquake Simulation Tests on Reducing Residual Displacements of Reinforced Concrete Bridges.* Junichi Sakai, Stephen A Mahin, and Andres Espinoza. December 2005.
- PEER 2005/16** *Seismic Response and Reliability of Electrical Substation Equipment and Systems.* Junho Song, Armen Der Kiureghian, and Jerome L. Sackman. April 2006.
- PEER 2005/15** *CPT-Based Probabilistic Assessment of Seismic Soil Liquefaction Initiation.* R. E. S. Moss, R. B. Seed, R. E. Kayen, J. P. Stewart, and A. Der Kiureghian. April 2006.
- PEER 2005/14** *Workshop on Modeling of Nonlinear Cyclic Load-Deformation Behavior of Shallow Foundations.* Bruce L. Kutter, Geoffrey Martin, Tara Hutchinson, Chad Harden, Sivapalan Gajan, and Justin Phalen. March 2006.
- PEER 2005/13** *Stochastic Characterization and Decision Bases under Time-Dependent Aftershock Risk in Performance-Based Earthquake Engineering.* Gee Liek Yeo and C. Allin Cornell. July 2005.
- PEER 2005/12** *PEER Testbed Study on a Laboratory Building: Exercising Seismic Performance Assessment.* Mary C. Comerio, Editor. November 2005.
- PEER 2005/11** *Van Nuys Hotel Building Testbed Report: Exercising Seismic Performance Assessment.* Helmut Krawinkler, Editor. October 2005.
- PEER 2005/10** *First NEES/E-Defense Workshop on Collapse Simulation of Reinforced Concrete Building Structures.* September 2005.
- PEER 2005/09** *Test Applications of Advanced Seismic Assessment Guidelines.* Joe Maffei, Karl Telleen, Danya Mohr, William Holmes, and Yuki Nakayama. August 2006.
- PEER 2005/08** *Damage Accumulation in Lightly Confined Reinforced Concrete Bridge Columns.* R. Tyler Ranf, Jared M. Nelson, Zach Price, Marc O. Eberhard, and John F. Stanton. April 2006.
- PEER 2005/07** *Experimental and Analytical Studies on the Seismic Response of Freestanding and Anchored Laboratory Equipment.* Dimitrios Konstantinidis and Nicos Makris. January 2005.
- PEER 2005/06** *Global Collapse of Frame Structures under Seismic Excitations.* Luis F. Ibarra and Helmut Krawinkler. September 2005.
- PEER 2005/05** *Performance Characterization of Bench- and Shelf-Mounted Equipment.* Samit Ray Chaudhuri and Tara C. Hutchinson. May 2006.
- PEER 2005/04** *Numerical Modeling of the Nonlinear Cyclic Response of Shallow Foundations.* Chad Harden, Tara Hutchinson, Geoffrey R. Martin, and Bruce L. Kutter. August 2005.
- PEER 2005/03** *A Taxonomy of Building Components for Performance-Based Earthquake Engineering.* Keith A. Porter. September 2005.
- PEER 2005/02** *Fragility Basis for California Highway Overpass Bridge Seismic Decision Making.* Kevin R. Mackie and Božidar Stojadinović. June 2005.
- PEER 2005/01** *Empirical Characterization of Site Conditions on Strong Ground Motion.* Jonathan P. Stewart, Yoojoong Choi, and Robert W. Graves. June 2005.
- PEER 2004/09** *Electrical Substation Equipment Interaction: Experimental Rigid Conductor Studies.* Christopher Stearns and André Filiatrault. February 2005.

- PEER 2004/08** *Seismic Qualification and Fragility Testing of Line Break 550-kV Disconnect Switches.* Shakhzod M. Takhirov, Gregory L. Fenves, and Eric Fujisaki. January 2005.
- PEER 2004/07** *Ground Motions for Earthquake Simulator Qualification of Electrical Substation Equipment.* Shakhzod M. Takhirov, Gregory L. Fenves, Eric Fujisaki, and Don Clyde. January 2005.
- PEER 2004/06** *Performance-Based Regulation and Regulatory Regimes.* Peter J. May and Chris Koski. September 2004.
- PEER 2004/05** *Performance-Based Seismic Design Concepts and Implementation: Proceedings of an International Workshop.* Peter Fajfar and Helmut Krawinkler, Editors. September 2004.
- PEER 2004/04** *Seismic Performance of an Instrumented Tilt-up Wall Building.* James C. Anderson and Vitelmo V. Bertero. July 2004.
- PEER 2004/03** *Evaluation and Application of Concrete Tilt-up Assessment Methodologies.* Timothy Graf and James O. Malley. October 2004.
- PEER 2004/02** *Analytical Investigations of New Methods for Reducing Residual Displacements of Reinforced Concrete Bridge Columns.* Junichi Sakai and Stephen A. Mahin. August 2004.
- PEER 2004/01** *Seismic Performance of Masonry Buildings and Design Implications.* Kerri Anne Taeko Tokoro, James C. Anderson, and Vitelmo V. Bertero. February 2004.
- PEER 2003/18** *Performance Models for Flexural Damage in Reinforced Concrete Columns.* Michael Berry and Marc Eberhard. August 2003.
- PEER 2003/17** *Predicting Earthquake Damage in Older Reinforced Concrete Beam-Column Joints.* Catherine Pagni and Laura Lowes. October 2004.
- PEER 2003/16** *Seismic Demands for Performance-Based Design of Bridges.* Kevin Mackie and Božidar Stojadinović. August 2003.
- PEER 2003/15** *Seismic Demands for Nondeteriorating Frame Structures and Their Dependence on Ground Motions.* Ricardo Antonio Medina and Helmut Krawinkler. May 2004.
- PEER 2003/14** *Finite Element Reliability and Sensitivity Methods for Performance-Based Earthquake Engineering.* Terje Haukaas and Armen Der Kiureghian. April 2004.
- PEER 2003/13** *Effects of Connection Hysteretic Degradation on the Seismic Behavior of Steel Moment-Resisting Frames.* Janise E. Rodgers and Stephen A. Mahin. March 2004.
- PEER 2003/12** *Implementation Manual for the Seismic Protection of Laboratory Contents: Format and Case Studies.* William T. Holmes and Mary C. Comerio. October 2003.
- PEER 2003/11** *Fifth U.S.-Japan Workshop on Performance-Based Earthquake Engineering Methodology for Reinforced Concrete Building Structures.* February 2004.
- PEER 2003/10** *A Beam-Column Joint Model for Simulating the Earthquake Response of Reinforced Concrete Frames.* Laura N. Lowes, Nilanjan Mitra, and Arash Altoontash. February 2004.
- PEER 2003/09** *Sequencing Repairs after an Earthquake: An Economic Approach.* Marco Casari and Simon J. Wilkie. April 2004.
- PEER 2003/08** *A Technical Framework for Probability-Based Demand and Capacity Factor Design (DCFD) Seismic Formats.* Fatemeh Jalayer and C. Allin Cornell. November 2003.
- PEER 2003/07** *Uncertainty Specification and Propagation for Loss Estimation Using FOSM Methods.* Jack W. Baker and C. Allin Cornell. September 2003.
- PEER 2003/06** *Performance of Circular Reinforced Concrete Bridge Columns under Bidirectional Earthquake Loading.* Mahmoud M. Hachem, Stephen A. Mahin, and Jack P. Moehle. February 2003.
- PEER 2003/05** *Response Assessment for Building-Specific Loss Estimation.* Eduardo Miranda and Shahram Taghavi. September 2003.
- PEER 2003/04** *Experimental Assessment of Columns with Short Lap Splices Subjected to Cyclic Loads.* Murat Melek, John W. Wallace, and Joel Conte. April 2003.
- PEER 2003/03** *Probabilistic Response Assessment for Building-Specific Loss Estimation.* Eduardo Miranda and Hesameddin Aslani. September 2003.
- PEER 2003/02** *Software Framework for Collaborative Development of Nonlinear Dynamic Analysis Program.* Jun Peng and Kincho H. Law. September 2003.
- PEER 2003/01** *Shake Table Tests and Analytical Studies on the Gravity Load Collapse of Reinforced Concrete Frames.* Kenneth John Elwood and Jack P. Moehle. November 2003.

- PEER 2002/24** *Performance of Beam to Column Bridge Joints Subjected to a Large Velocity Pulse.* Natalie Gibson, André Filiatrault, and Scott A. Ashford. April 2002.
- PEER 2002/23** *Effects of Large Velocity Pulses on Reinforced Concrete Bridge Columns.* Greg L. Orozco and Scott A. Ashford. April 2002.
- PEER 2002/22** *Characterization of Large Velocity Pulses for Laboratory Testing.* Kenneth E. Cox and Scott A. Ashford. April 2002.
- PEER 2002/21** *Fourth U.S.-Japan Workshop on Performance-Based Earthquake Engineering Methodology for Reinforced Concrete Building Structures.* December 2002.
- PEER 2002/20** *Barriers to Adoption and Implementation of PBEE Innovations.* Peter J. May. August 2002.
- PEER 2002/19** *Economic-Engineered Integrated Models for Earthquakes: Socioeconomic Impacts.* Peter Gordon, James E. Moore II, and Harry W. Richardson. July 2002.
- PEER 2002/18** *Assessment of Reinforced Concrete Building Exterior Joints with Substandard Details.* Chris P. Pantelides, Jon Hansen, Justin Nadauld, and Lawrence D. Reaveley. May 2002.
- PEER 2002/17** *Structural Characterization and Seismic Response Analysis of a Highway Overcrossing Equipped with Elastomeric Bearings and Fluid Dampers: A Case Study.* Nicos Makris and Jian Zhang. November 2002.
- PEER 2002/16** *Estimation of Uncertainty in Geotechnical Properties for Performance-Based Earthquake Engineering.* Allen L. Jones, Steven L. Kramer, and Pedro Arduino. December 2002.
- PEER 2002/15** *Seismic Behavior of Bridge Columns Subjected to Various Loading Patterns.* Asadollah Esmaeily-Gh. and Yan Xiao. December 2002.
- PEER 2002/14** *Inelastic Seismic Response of Extended Pile Shaft Supported Bridge Structures.* T.C. Hutchinson, R.W. Boulanger, Y.H. Chai, and I.M. Idriss. December 2002.
- PEER 2002/13** *Probabilistic Models and Fragility Estimates for Bridge Components and Systems.* Paolo Gardoni, Armen Der Kiureghian, and Khalid M. Mosalam. June 2002.
- PEER 2002/12** *Effects of Fault Dip and Slip Rake on Near-Source Ground Motions: Why Chi-Chi Was a Relatively Mild M7.6 Earthquake.* Brad T. Aagaard, John F. Hall, and Thomas H. Heaton. December 2002.
- PEER 2002/11** *Analytical and Experimental Study of Fiber-Reinforced Strip Isolators.* James M. Kelly and Shakhzod M. Takhirov. September 2002.
- PEER 2002/10** *Centrifuge Modeling of Settlement and Lateral Spreading with Comparisons to Numerical Analyses.* Sivapalan Gajan and Bruce L. Kutter. January 2003.
- PEER 2002/09** *Documentation and Analysis of Field Case Histories of Seismic Compression during the 1994 Northridge, California, Earthquake.* Jonathan P. Stewart, Patrick M. Smith, Daniel H. Whang, and Jonathan D. Bray. October 2002.
- PEER 2002/08** *Component Testing, Stability Analysis and Characterization of Buckling-Restrained Unbonded Braces™.* Cameron Black, Nicos Makris, and Ian Aiken. September 2002.
- PEER 2002/07** *Seismic Performance of Pile-Wharf Connections.* Charles W. Roeder, Robert Graff, Jennifer Soderstrom, and Jun Han Yoo. December 2001.
- PEER 2002/06** *The Use of Benefit-Cost Analysis for Evaluation of Performance-Based Earthquake Engineering Decisions.* Richard O. Zerbe and Anthony Falit-Baiaumont. September 2001.
- PEER 2002/05** *Guidelines, Specifications, and Seismic Performance Characterization of Nonstructural Building Components and Equipment.* André Filiatrault, Constantin Christopoulos, and Christopher Stearns. September 2001.
- PEER 2002/04** *Consortium of Organizations for Strong-Motion Observation Systems and the Pacific Earthquake Engineering Research Center Lifelines Program: Invited Workshop on Archiving and Web Dissemination of Geotechnical Data, 4-5 October 2001.* September 2002.
- PEER 2002/03** *Investigation of Sensitivity of Building Loss Estimates to Major Uncertain Variables for the Van Nuys Testbed.* Keith A. Porter, James L. Beck, and Rustem V. Shaikhutdinov. August 2002.
- PEER 2002/02** *The Third U.S.-Japan Workshop on Performance-Based Earthquake Engineering Methodology for Reinforced Concrete Building Structures.* July 2002.
- PEER 2002/01** *Nonstructural Loss Estimation: The UC Berkeley Case Study.* Mary C. Comerio and John C. Stallmeyer. December 2001.
- PEER 2001/16** *Statistics of SDF-System Estimate of Roof Displacement for Pushover Analysis of Buildings.* Anil K. Chopra, Rakesh K. Goel, and Chatpan Chintanapakdee. December 2001.

- PEER 2001/15** *Damage to Bridges during the 2001 Nisqually Earthquake.* R. Tyler Ranf, Marc O. Eberhard, and Michael P. Berry. November 2001.
- PEER 2001/14** *Rocking Response of Equipment Anchored to a Base Foundation.* Nicos Makris and Cameron J. Black. September 2001.
- PEER 2001/13** *Modeling Soil Liquefaction Hazards for Performance-Based Earthquake Engineering.* Steven L. Kramer and Ahmed-W. Elgamel. February 2001.
- PEER 2001/12** *Development of Geotechnical Capabilities in OpenSees.* Boris Jeremić. September 2001.
- PEER 2001/11** *Analytical and Experimental Study of Fiber-Reinforced Elastomeric Isolators.* James M. Kelly and Shakhzod M. Takhirov. September 2001.
- PEER 2001/10** *Amplification Factors for Spectral Acceleration in Active Regions.* Jonathan P. Stewart, Andrew H. Liu, Yoojoong Choi, and Mehmet B. Baturay. December 2001.
- PEER 2001/09** *Ground Motion Evaluation Procedures for Performance-Based Design.* Jonathan P. Stewart, Shyh-Jeng Chiou, Jonathan D. Bray, Robert W. Graves, Paul G. Somerville, and Norman A. Abrahamson. September 2001.
- PEER 2001/08** *Experimental and Computational Evaluation of Reinforced Concrete Bridge Beam-Column Connections for Seismic Performance.* Clay J. Naito, Jack P. Moehle, and Khalid M. Mosalam. November 2001.
- PEER 2001/07** *The Rocking Spectrum and the Shortcomings of Design Guidelines.* Nicos Makris and Dimitrios Konstantinidis. August 2001.
- PEER 2001/06** *Development of an Electrical Substation Equipment Performance Database for Evaluation of Equipment Fragilities.* Thalia Agnamos. April 1999.
- PEER 2001/05** *Stiffness Analysis of Fiber-Reinforced Elastomeric Isolators.* Hsiang-Chuan Tsai and James M. Kelly. May 2001.
- PEER 2001/04** *Organizational and Societal Considerations for Performance-Based Earthquake Engineering.* Peter J. May. April 2001.
- PEER 2001/03** *A Modal Pushover Analysis Procedure to Estimate Seismic Demands for Buildings: Theory and Preliminary Evaluation.* Anil K. Chopra and Rakesh K. Goel. January 2001.
- PEER 2001/02** *Seismic Response Analysis of Highway Overcrossings Including Soil-Structure Interaction.* Jian Zhang and Nicos Makris. March 2001.
- PEER 2001/01** *Experimental Study of Large Seismic Steel Beam-to-Column Connections.* Egor P. Popov and Shakhzod M. Takhirov. November 2000.
- PEER 2000/10** *The Second U.S.-Japan Workshop on Performance-Based Earthquake Engineering Methodology for Reinforced Concrete Building Structures.* March 2000.
- PEER 2000/09** *Structural Engineering Reconnaissance of the August 17, 1999 Earthquake: Kocaeli (Izmit), Turkey.* Halil Sezen, Kenneth J. Elwood, Andrew S. Whittaker, Khalid Mosalam, John J. Wallace, and John F. Stanton. December 2000.
- PEER 2000/08** *Behavior of Reinforced Concrete Bridge Columns Having Varying Aspect Ratios and Varying Lengths of Confinement.* Anthony J. Calderone, Dawn E. Lehman, and Jack P. Moehle. January 2001.
- PEER 2000/07** *Cover-Plate and Flange-Plate Reinforced Steel Moment-Resisting Connections.* Taejin Kim, Andrew S. Whittaker, Amir S. Gilani, Vitelmo V. Bertero, and Shakhzod M. Takhirov. September 2000.
- PEER 2000/06** *Seismic Evaluation and Analysis of 230-kV Disconnect Switches.* Amir S. J. Gilani, Andrew S. Whittaker, Gregory L. Fenves, Chun-Hao Chen, Henry Ho, and Eric Fujisaki. July 2000.
- PEER 2000/05** *Performance-Based Evaluation of Exterior Reinforced Concrete Building Joints for Seismic Excitation.* Chandra Clyde, Chris P. Pantelides, and Lawrence D. Reaveley. July 2000.
- PEER 2000/04** *An Evaluation of Seismic Energy Demand: An Attenuation Approach.* Chung-Che Chou and Chia-Ming Uang. July 1999.
- PEER 2000/03** *Framing Earthquake Retrofitting Decisions: The Case of Hillside Homes in Los Angeles.* Detlof von Winterfeldt, Nels Roselund, and Alicia Kitsuse. March 2000.
- PEER 2000/02** *U.S.-Japan Workshop on the Effects of Near-Field Earthquake Shaking.* Andrew Whittaker, Editor. July 2000.
- PEER 2000/01** *Further Studies on Seismic Interaction in Interconnected Electrical Substation Equipment.* Armen Der Kiureghian, Kee-Jeung Hong, and Jerome L. Sackman. November 1999.
- PEER 1999/14** *Seismic Evaluation and Retrofit of 230-kV Porcelain Transformer Bushings.* Amir S. Gilani, Andrew S. Whittaker, Gregory L. Fenves, and Eric Fujisaki. December 1999.

- PEER 1999/13** *Building Vulnerability Studies: Modeling and Evaluation of Tilt-up and Steel Reinforced Concrete Buildings.* John W. Wallace, Jonathan P. Stewart, and Andrew S. Whittaker, Editors. December 1999.
- PEER 1999/12** *Rehabilitation of Nonductile RC Frame Building Using Encasement Plates and Energy-Dissipating Devices.* Mehrdad Sasani, Vitelmo V. Bertero, James C. Anderson. December 1999.
- PEER 1999/11** *Performance Evaluation Database for Concrete Bridge Components and Systems under Simulated Seismic Loads.* Yael D. Hose and Frieder Seible. November 1999.
- PEER 1999/10** *U.S.-Japan Workshop on Performance-Based Earthquake Engineering Methodology for Reinforced Concrete Building Structures.* December 1999.
- PEER 1999/09** *Performance Improvement of Long Period Building Structures Subjected to Severe Pulse-Type Ground Motions.* James C. Anderson, Vitelmo V. Bertero, and Raul Bertero. October 1999.
- PEER 1999/08** *Envelopes for Seismic Response Vectors.* Charles Menun and Armen Der Kiureghian. July 1999.
- PEER 1999/07** *Documentation of Strengths and Weaknesses of Current Computer Analysis Methods for Seismic Performance of Reinforced Concrete Members.* William F. Cofer. November 1999.
- PEER 1999/06** *Rocking Response and Overturning of Anchored Equipment under Seismic Excitations.* Nicos Makris and Jian Zhang. November 1999.
- PEER 1999/05** *Seismic Evaluation of 550 kV Porcelain Transformer Bushings.* Amir S. Gilani, Andrew S. Whittaker, Gregory L. Fenves, and Eric Fujisaki. October 1999.
- PEER 1999/04** *Adoption and Enforcement of Earthquake Risk-Reduction Measures.* Peter J. May, Raymond J. Burby, T. Jens Feeley, and Robert Wood. August 1999.
- PEER 1999/03** *Task 3 Characterization of Site Response General Site Categories.* Adrian Rodriguez-Marek, Jonathan D. Bray and Norman Abrahamson. February 1999.
- PEER 1999/02** *Capacity-Demand-Diagram Methods for Estimating Seismic Deformation of Inelastic Structures: SDF Systems.* Anil K. Chopra and Rakesh Goel. April 1999.
- PEER 1999/01** *Interaction in Interconnected Electrical Substation Equipment Subjected to Earthquake Ground Motions.* Armen Der Kiureghian, Jerome L. Sackman, and Kee-Jeung Hong. February 1999.
- PEER 1998/08** *Behavior and Failure Analysis of a Multiple-Frame Highway Bridge in the 1994 Northridge Earthquake.* Gregory L. Fenves and Michael Ellery. December 1998.
- PEER 1998/07** *Empirical Evaluation of Inertial Soil-Structure Interaction Effects.* Jonathan P. Stewart, Raymond B. Seed, and Gregory L. Fenves. November 1998.
- PEER 1998/06** *Effect of Damping Mechanisms on the Response of Seismic Isolated Structures.* Nicos Makris and Shih-Po Chang. November 1998.
- PEER 1998/05** *Rocking Response and Overturning of Equipment under Horizontal Pulse-Type Motions.* Nicos Makris and Yiannis Roussos. October 1998.
- PEER 1998/04** *Pacific Earthquake Engineering Research Invitational Workshop Proceedings, May 14–15, 1998: Defining the Links between Planning, Policy Analysis, Economics and Earthquake Engineering.* Mary Comerio and Peter Gordon. September 1998.
- PEER 1998/03** *Repair/Upgrade Procedures for Welded Beam to Column Connections.* James C. Anderson and Xiaojing Duan. May 1998.
- PEER 1998/02** *Seismic Evaluation of 196 kV Porcelain Transformer Bushings.* Amir S. Gilani, Juan W. Chavez, Gregory L. Fenves, and Andrew S. Whittaker. May 1998.
- PEER 1998/01** *Seismic Performance of Well-Confined Concrete Bridge Columns.* Dawn E. Lehman and Jack P. Moehle. December 2000.

PEER REPORTS: ONE HUNDRED SERIES

- PEER 2012/103** *Performance-Based Seismic Demand Assessment of Concentrically Braced Steel Frame Buildings.* Chui-Hsin Chen and Stephen A. Mahin. December 2012.
- PEER 2012/102** *Procedure to Restart an Interrupted Hybrid Simulation: Addendum to PEER Report 2010/103.* Vesna Terzic and Božidar Stojadinovic. October 2012.
- PEER 2012/101** *Mechanics of Fiber Reinforced Bearings.* James M. Kelly and Andrea Calabrese. February 2012.
- PEER 2011/107** *Nonlinear Site Response and Seismic Compression at Vertical Array Strongly Shaken by 2007 Niigata-ken Chuetsu-oki Earthquake.* Eric Yee, Jonathan P. Stewart, and Kohji Tokimatsu. December 2011.
- PEER 2011/106** *Self Compacting Hybrid Fiber Reinforced Concrete Composites for Bridge Columns.* Pardeep Kumar, Gabriel Jen, William Trono, Marios Panagiotou, and Claudia Ostertag. September 2011.
- PEER 2011/105** *Stochastic Dynamic Analysis of Bridges Subjected to Spatially Varying Ground Motions.* Katerina Konakli and Armen Der Kiureghian. August 2011.
- PEER 2011/104** *Design and Instrumentation of the 2010 E-Defense Four-Story Reinforced Concrete and Post-Tensioned Concrete Buildings.* Takuya Nagae, Kenichi Tahara, Taizo Matsumori, Hitoshi Shiohara, Toshimi Kabeyasawa, Susumu Kono, Minehiro Nishiyama (Japanese Research Team) and John Wallace, Wassim Ghannoum, Jack Moehle, Richard Sause, Wesley Keller, Zeynep Tuna (U.S. Research Team). June 2011.
- PEER 2011/103** *In-Situ Monitoring of the Force Output of Fluid Dampers: Experimental Investigation.* Dimitrios Konstantinidis, James M. Kelly, and Nicos Makris. April 2011.
- PEER 2011/102** *Ground-Motion Prediction Equations 1964–2010.* John Douglas. April 2011.
- PEER 2011/101** *Report of the Eighth Planning Meeting of NEES/E-Defense Collaborative Research on Earthquake Engineering.* Convened by the Hyogo Earthquake Engineering Research Center (NIED), NEES Consortium, Inc. February 2011.
- PEER 2010/111** *Modeling and Acceptance Criteria for Seismic Design and Analysis of Tall Buildings.* Task 7 Report for the Tall Buildings Initiative - Published jointly by the Applied Technology Council. October 2010.
- PEER 2010/110** *Seismic Performance Assessment and Probabilistic Repair Cost Analysis of Precast Concrete Cladding Systems for Multistory Buildings.* Jeffrey P. Hunt and Božidar Stojadinovic. November 2010.
- PEER 2010/109** *Report of the Seventh Joint Planning Meeting of NEES/E-Defense Collaboration on Earthquake Engineering. Held at the E-Defense, Miki, and Shin-Kobe, Japan, September 18–19, 2009.* August 2010.
- PEER 2010/108** *Probabilistic Tsunami Hazard in California.* Hong Kie Thio, Paul Somerville, and Jascha Polet, preparers. October 2010.
- PEER 2010/107** *Performance and Reliability of Exposed Column Base Plate Connections for Steel Moment-Resisting Frames.* Ady Aviram, Božidar Stojadinovic, and Armen Der Kiureghian. August 2010.
- PEER 2010/106** *Verification of Probabilistic Seismic Hazard Analysis Computer Programs.* Patricia Thomas, Ivan Wong, and Norman Abrahamson. May 2010.
- PEER 2010/105** *Structural Engineering Reconnaissance of the April 6, 2009, Abruzzo, Italy, Earthquake, and Lessons Learned.* M. Selim Günay and Khalid M. Mosalam. April 2010.
- PEER 2010/104** *Simulating the Inelastic Seismic Behavior of Steel Braced Frames, Including the Effects of Low-Cycle Fatigue.* Yuli Huang and Stephen A. Mahin. April 2010.
- PEER 2010/103** *Post-Earthquake Traffic Capacity of Modern Bridges in California.* Vesna Terzic and Božidar Stojadinović. March 2010.
- PEER 2010/102** *Analysis of Cumulative Absolute Velocity (CAV) and JMA Instrumental Seismic Intensity (I_{JMA}) Using the PEER–NGA Strong Motion Database.* Kenneth W. Campbell and Yousef Bozorgnia. February 2010.
- PEER 2010/101** *Rocking Response of Bridges on Shallow Foundations.* Jose A. Ugalde, Bruce L. Kutter, and Boris Jeremic. April 2010.
- PEER 2009/109** *Simulation and Performance-Based Earthquake Engineering Assessment of Self-Centering Post-Tensioned Concrete Bridge Systems.* Won K. Lee and Sarah L. Billington. December 2009.
- PEER 2009/108** *PEER Lifelines Geotechnical Virtual Data Center.* J. Carl Stepp, Daniel J. Ponti, Loren L. Turner, Jennifer N. Swift, Sean Devlin, Yang Zhu, Jean Benoit, and John Bobbitt. September 2009.

- PEER 2009/107** *Experimental and Computational Evaluation of Current and Innovative In-Span Hinge Details in Reinforced Concrete Box-Girder Bridges: Part 2: Post-Test Analysis and Design Recommendations.* Matias A. Hube and Khalid M. Mosalam. December 2009.
- PEER 2009/106** *Shear Strength Models of Exterior Beam-Column Joints without Transverse Reinforcement.* Sangjoon Park and Khalid M. Mosalam. November 2009.
- PEER 2009/105** *Reduced Uncertainty of Ground Motion Prediction Equations through Bayesian Variance Analysis.* Robb Eric S. Moss. November 2009.
- PEER 2009/104** *Advanced Implementation of Hybrid Simulation.* Andreas H. Schellenberg, Stephen A. Mahin, Gregory L. Fenves. November 2009.
- PEER 2009/103** *Performance Evaluation of Innovative Steel Braced Frames.* T. Y. Yang, Jack P. Moehle, and Božidar Stojadinovic. August 2009.
- PEER 2009/102** *Reinvestigation of Liquefaction and Nonliquefaction Case Histories from the 1976 Tangshan Earthquake.* Robb Eric Moss, Robert E. Kayen, Liyuan Tong, Songyu Liu, Guojun Cai, and Jiaer Wu. August 2009.
- PEER 2009/101** *Report of the First Joint Planning Meeting for the Second Phase of NEES/E-Defense Collaborative Research on Earthquake Engineering.* Stephen A. Mahin et al. July 2009.
- PEER 2008/104** *Experimental and Analytical Study of the Seismic Performance of Retaining Structures.* Linda Al Atik and Nicholas Sitar. January 2009.
- PEER 2008/103** *Experimental and Computational Evaluation of Current and Innovative In-Span Hinge Details in Reinforced Concrete Box-Girder Bridges. Part 1: Experimental Findings and Pre-Test Analysis.* Matias A. Hube and Khalid M. Mosalam. January 2009.
- PEER 2008/102** *Modeling of Unreinforced Masonry Infill Walls Considering In-Plane and Out-of-Plane Interaction.* Stephen Kadsiewiczski and Khalid M. Mosalam. January 2009.
- PEER 2008/101** *Seismic Performance Objectives for Tall Buildings.* William T. Holmes, Charles Kircher, William Petak, and Nabih Youssef. August 2008.
- PEER 2007/101** *Generalized Hybrid Simulation Framework for Structural Systems Subjected to Seismic Loading.* Tarek Elkhoraibi and Khalid M. Mosalam. July 2007.
- PEER 2007/100** *Seismic Evaluation of Reinforced Concrete Buildings Including Effects of Masonry Infill Walls.* Alidad Hashemi and Khalid M. Mosalam. July 2007.

The Pacific Earthquake Engineering Research Center (PEER) is a multi-institutional research and education center with headquarters at the University of California, Berkeley. Investigators from over 20 universities, several consulting companies, and researchers at various state and federal government agencies contribute to research programs focused on performance-based earthquake engineering.

These research programs aim to identify and reduce the risks from major earthquakes to life safety and to the economy by including research in a wide variety of disciplines including structural and geotechnical engineering, geology/seismology, lifelines, transportation, architecture, economics, risk management, and public policy.

PEER is supported by federal, state, local, and regional agencies, together with industry partners.



PEER Core Institutions

University of California, Berkeley (Lead Institution)
California Institute of Technology
Oregon State University
Stanford University
University of California, Davis
University of California, Irvine
University of California, Los Angeles
University of California, San Diego
University of Nevada, Reno
University of Southern California
University of Washington

PEER reports can be ordered at <https://peer.berkeley.edu/peer-reports> or by contacting

Pacific Earthquake Engineering Research Center
University of California, Berkeley
325 Davis Hall, Mail Code 1792
Berkeley, CA 94720-1792
Tel: 510-642-3437
Email: peer_center@berkeley.edu

ISSN 2770-8314
<https://doi.org/10.55461/ZISP3722>